Extended Narrow Line Region in Seyfert Galaxies: Photoionization by Thick Accretion Disk Emission

Thesis submitted for the degree of

"Doctor Philosophiae"

Astrophysics Sector

Candidate:

José Acosta–Pulido

Supervisor:

Prof. Massimo Calvani

Academic Year 1990

Extended Narrow Line Region in Seyfert Galaxies: Photoionization by Thick Accretion Disk Emission

Thesis submitted for the degree of

"Doctor Philosophiae"

Astrophysics Sector

Candidate:

José Acosta–Pulido

Supervisor:

Prof. Massimo Calvani

Academic Year 1990

ABSTRACT

Very extended regions of highly ionized gas have been observed in many active galaxies. In most cases the emission aligns with the radio structure. However morphological differences in the spatial distribution of the emitting gas are found depending on the AGN type. The line emitting gas around radio galaxies and QSO's appears to very extended and luminous but very filamentary. On the contrary the extended emission around the radio-quiet Seyfert galaxies is distributed generally into two cones, the axis is aligned with the radio structure and the apices point to the nucleus. Such emission extends well beyond the classical narrow line region. In this work we will concentrate in the latter class of objects, namely those showing the ionization cones.

The physical conditions of the emitting gas can be estimated from the line spectrum, and it results to be a low density gas $n_H \sim 10^2 - 10^3\ cm^{-3}$, with temperature $T \sim 10^4\ K$. There is evidence that photoionization by the active nucleus is the most likely excitation mechanism. The emission line spectrum is very similar to that observed for the Narrow Line Region, we will consider the current models for this region and present its problems. We will use simple ionizing continua (black body, power law and accretion disk spectra) to make predictions and discuss the agreement of these predictions with the observed emission line spectrum. Black body emission with $T \sim 130000\ K$, a power law continuum with spectral index $\alpha = -1.5$ and thin accretion disk spectra around black holes of masses $10^7 - 10^8\ M_\odot$ produce good agreement with the observed line emission.

The conical shape of line emitting gas suggests collimation or anisotropy of the ionizing continuum. There are several ways in which the nuclear continuum can be collimated: extrinsic mechanisms which block the radiation to escape in certain directions or intrinsic mechanisms where the radiation is emitted anisotropically, like a relativistic jet or a geometrically thick accretion disk. We shortly review a unification scheme for Seyfert galaxies, based on the existence of a large obscuring torus located at distances farther than the Broad Line Region. If the axis of this torus is very inclined with respect to our line of sight we will observe Seyfert 2 galaxies, instead when the axis of this torus is close to our line of sight those objects will be observed as Seyfert 1 galaxies.

We investigate the possibility that photoionization by a geometrically thick (radiation–pressure supported) accretion disk can reproduce the emission line spectra. Such a torus naturally provides the apparent collimation of the ionizing radiation field, because the hot funnel of the torus is occulted when viewing at large angles from the disk axis. We have considered the physical conditions on the emitting surface of these torus and how variations of the opacity and configuration, due to different angular momentum distributions will affect the emitted radiation. We conclude that the characteristics (effective temperature) of the emission are not strongly affected by the variation of the angular momentum distribution. However the angular dependence of the continuum emission will be affected by the geometrical change of the configuration.

We use a simple model for a thick accretion disk around a supermassive black hole and a photoionization code to make theoretical predictions of the line ratios. The sensitivity of the predicted line ratios to variations in ionization parameter, black hole mass and accretion disk size is discussed in detail. The majority of line ratios are most sensitive to the ionization parameter but some are also functions of the accretion disk size at fixed ionization parameter. Our results are compared with observational data

(for Seyfert galaxies), in order to constrain the disk parameters and the properties of the emission-line clouds. Typical model fits involve an ionization parameter of several times 10^{-2} and an accretion disk of radius $\simeq$ 500 (150) gravitational radii around a $10^6 M_\odot$ ($10^7 M_\odot$) black hole. The spectral shape of the ionizing continuum is briefly discussed. The inclusion of additional effects, such as a hard X–ray component and photoelectric absorption of soft X–rays by gas between the nucleus and the extended emission–line regions, may improve the agreement between observed and predicted line ratios.

The predicted angular variation of the emission lines is studied in the frame of a geometrically thick accretion disk model. We have assumed that the gas is distributed uniformly in a disk, which contains the rotation axis of the torus. The disk emission is calculated at different separation angles θ from the rotation axis and the variation of the line emission is considered at a fixed distance to the disk. We have considered different accretion disk configurations and make predictions for the different cases. The value of the ionization parameter at the rotation axis is fixed from the best fit with the observed emission line spectrum. Our predictions can not be tested directly with the observations, because the data are lacking at this moment. We only make a qualitative discussion of our predictions. We will ask the prediction for the [OIII] λ5007 emission to decrease at large θ, and this is the figure of merit of the model. We have found that the variation of the emission lines as predicted by the disk emission with $M \sim 10^6\ M_\odot$ is not consistent with the expected decrease at large θ. However models with $M \sim 10^8\ M_\odot$ are more appropriate. In the latter models the variation of the line emission shows a plateau at small θ and then a sudden decrease at θ larger than the opening angle of the funnel. This different behaviour with M is due to the hardening of the disk emission with decreasing M. We have arbitrarily tried a different opacity source in the disk surface, namely free-free absorption, which softens the emitted continuum to a sum of blackbodies. We have found that the angular variation of the emission line for $M \geq 10^6\ M_\odot$ is consistent in this case with the observed behaviour.

Contents

ACKNOWLEDGEMENTS

I am really indebted to Prof. Ismael Pérez–Fournon who proposed me to do the main topic of this Thesis. He has offered me, apart from many valuable suggestions and discussions, the occasion to have a closer view of the hardness of the observational work. I also thank the Instituto de Astrofisica de Canarias for hospitality during the first period of this work.

I also thank Prof. Andrew S. Wilson for many enlightening comments in the elaboration of some contents of this Thesis. I also thank him for his hospitality at the Astronomy Program at the University of Maryland, where the first pages of this manuscript were written.

I would also like to thank my supervisor Prof. Massimo Calvani for reading the manuscript of this thesis and constant encouragement.

My thanks are also due to Prof. Sciama who allowed for several travels abroad.

Luc Binette deserves a particular acknowledgement for supplying a so beautiful and user–friendly Photoionization code and also for his constant interest on the applications of his code.

I will give the largest acknowledgement to all SISSA people, in particular my colleagues of the same year and/or the same room with whom I shared many worries and happiness.

Mauro Orlandini helped me many times with technical problems, I am indebt to his patience for teaching me SuperMongo (la putenza).

Armando Pisani, Antonio Lanza and Hugo Morales-Tecotl were crucial to keep me on my feet the last hours of this work. Alessandretto Romeo was a good friend in the bad hours in front of the terminal.

INTRODUCTION

The optical/UV spectrum of Active Galactic Nuclei shows two distinct types of emission lines: 1) very broad lines with FWZI $\sim$ 10000 $km\,s^{-1}$, which are seen only in the permitted and semiforbidden lines, and 2) narrow lines with FWZI $\sim$ 1000 $km\,s^{-1}$, which are seen in both permitted and forbidden lines. Seyfert 1 galaxies show both types of emission lines, while Seyfert 2 galaxies show only narrow lines. Optical QSO's show mostly broad lines, although narrow lines have been ocassionally detected.

The *standard* picture of the line emission assumes that there exist two different spatial regions where the two types of emission lines are generated:

- The Broad Line Region (BLR) which is located at a distance of $\sim$ 0.1 pc for the low luminosity objects (Seyfert 1 galaxies), or $\sim$ 1 pc for the high luminosity objects (distant QSO's) from the nucleus. The gas density is in the range from 10^9 to 10^{10} cm^{-3}.

- The Narrow Line Region (NLR) is located at distances ranging from 0.1 kpc to 1 kpc from the nucleus. The gas density is in the range 10^3 to 10^6 cm^{-3}.

A pictorial description of the spatial scales corresponding to the major features present in a generic AGN is given in Figure 0.1. The positions of the BLR and the NLR are indicated.

In the last decade the investigation of the NLR has advanced considerably. This region is like a bridge connecting the inner BLR where the physical conditions are poorly known, with the external and more familiar interstellar medium conditions of the host galaxy. The spatial extent of the NLR is approximately coincident with the arcsecond radio emission. Apart from the similar spatial scale there are a few other features which suggest a close relation between the NLR and the radio emission, such as the well established correlation between the narrow line and the total radio luminosity (Meurs and Wilson, 1984) and the correlation between total radio power and the FWHM of the line [OIII] λ5007 (Whittle, 1985). Moreover in some cases the outer part of the NLR can be spatially resolved with ground observations, in the optical band. In those cases the NLR shows an elongated structure, which is found to be aligned with the radio structure (Wilson and Heckman, 1985).

On the other hand the tremendous energy output produced in the Active Nucleus must affect the environment of the host galaxy. It is therefore very reasonable to look for the imprint of the nuclear activity at distances far from the center of activity. The development in this area has been mostly possible due to a great technological improvement of optical detectors. The study of extranuclear activity is very costly because in most cases the structures we are interested to observe have very low surface brightness, in contrast with the bizarre nucleus. Therefore these observations demand

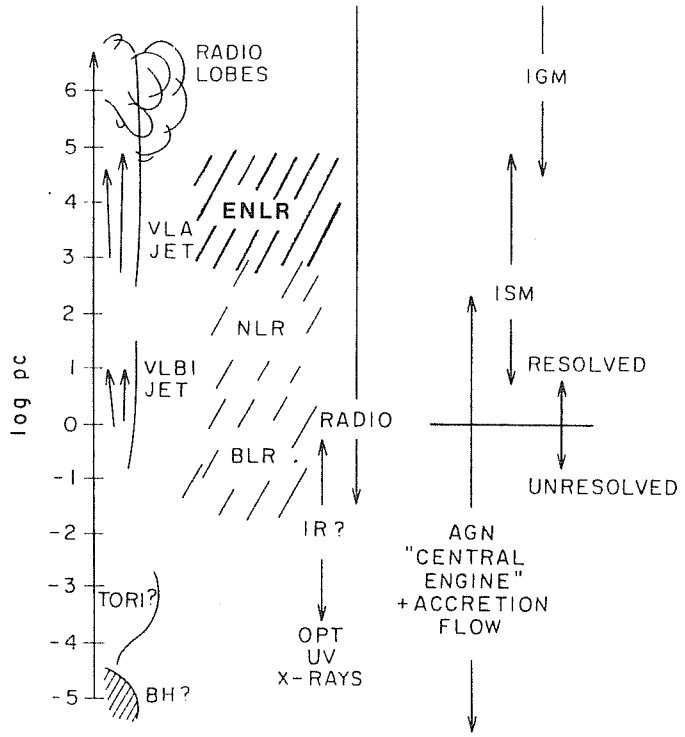

Figure 0.1: Spatial scales of the major features observed in a generic AGN. The NLR spatial scale is close to arcsecond radio emission (VLA scale) and the ENLR scale corresponds to the one of the ISM in the host galaxy, far from the nuclear environment. The distinction between resolved and unresolved refers to the highest spatial resolution 1 *pc* which can be achieved with radio interferometry techniques. The limit of the optical spatial resolution is of the order of 1 *kpc*, or somewhat lower for the nearby objects. This picture is adapted from Begelman (1989).

high dynamical range detectors. Fortunately, the search for extranuclear activity has provided very exciting results and it is becoming a very fascinating area of work.

Extended conical zones where high ionization emission lines are produced have been discovered around many nearby Seyfert galaxies. The opening angles of the observed cones are of the order of several tens of degrees. The emission line spectrum resembles that of the NLR, and is commonly referred to as the Extended NLR (ENLR). The observed line profiles are generally very narrow. The conical shape region is very often present at both sides of the nucleus and extends along the radio emission structure. The radio emission in many objects is confined to distances nearer the nucleus than the extended line emission gas, with no signs of interaction between both components. It seems therefore that the most plausible excitation mechanism of the gas is photoionization by the nuclear emission.

Extended line emission is also found around radio galaxies and low redshift QSO's (Fosbury, 1986; Stockton and MacKenty, 1987). In these objects the gas extends even to larger distances from the nucleus (100 *kpc*) than those observed in Seyferts, although the emission is more patchy and does not clearly show a conical structure.

The occurrence of the extended emission line gas is linked to the combination of two factors: the availability of photons to ionize the gas and the presence of the gas itself. The latter factor might be responsible for the different structures seen in Seyferts on one side and radio galaxies and QSO's on the other side. Generally the host galaxies for the Seyfert nuclei (spirals) tend to be richer in gas than the ones for powerful radio galaxies (ellipticals, or lenticulars). Kinematical studies show that the line emitting gas present in the cones shares the rotational motion of the galaxy disk, and most probably it is kinematically undisturbed gas sitting on it. Therefore it seems that the conical shape of the line emission observed around the Seyfert galaxies does not depend on the distribution of gas, but on the availability of photons. This leads to the conclusion that the ionizing continuum that emerges from the nuclear region ($\lesssim 10$ *pc*) is anisotropic and most probably concentrated in two cones which are oriented in the same direction as the radio emission.

Another confirmation for the anisotropy of the nuclear emission comes from the energy requirements of the emission line regions. Using the luminosity from the NLR (Wilson, Ward and Haniff, 1988), and the extended NLR (Pérez-Fournon and Wilson, 1990; Penston *et al.*, 1990) it is shown that there is a deficit of photons as inferred from the observed nuclear continuum, which suggests that the gas is exposed to a higher flux of ionizing photons than that received at the Earth.

Therefore if we believe that photoionization is the excitation mechanism of the gas, the spatial distribution of the line emission is reflecting the angular variation of the nuclear radiation. The imaging of the line emission becomes a powerful tool (*a spectrophotometer*) to investigate the polar diagram of the nuclear emission.

A striking discovery was the finding of a typical Seyfert 1 spectrum in the polarized light of the Seyfert 2 galaxy NGC 1068 (Antonucci and Miller, 1985). Similar features have been found in a number of Seyfert 2 galaxies (Miller and Goodrich, 1990). Separately, Shields and Filippenko (1988) detected broad Hα emission in a conical region offside the nucleus in the Seyfert 2 galaxy NGC 4388. Antonucci and Miller (1985) proposed a plausible interpretation of these findings. Their model consists in a very thick absorbing torus which surrounds the nucleus. Such a thick torus will block the radiation from the nucleus when looking at the system at inclination angles far from the symmetry axis of the torus. The height scale of the torus should be large enough

to hide the nucleus and the BLR, as well. A scattering medium which pervades the hole of the torus and extends over its top, is invoked to scatter those photons coming from the interior of the torus in directions far from the torus axis. According to this interpretation the only difference between Seyfert 1 and 2 galaxies resides in the orientation of such tori relative to the sky plane. Although this unified scheme seems to work reasonably well, some problems have arisen with this scenario (Miller, 1989).

The obscuring torus provides an extrinsic way to collimate the nuclear radiation. There are however other plausible mechanisms which intrinsically depend on the way the radiation is produced. The proposed mechanisms of the latter class are mainly two: the polar diagram of a radiation pressure supported geometrically thick accretion disk (Madau, 1988), and the beaming produced by a relativistic jet (Königl, 1981; Ghisellini, Maraschi and Treves, 1985). The latter possibility seems to be more appropriate for powerful radio sources. Moreover in this model the radiation will be collimated in a fairly narrow beam, which is difficult to reconcile with the rather wide observed cones. This model has been proposed to explain the case of the radio galaxy Pks 2152-69 (Tadhunter, Fosbury and di Serego Alighieri, 1988): a high ionization cloud is found at large distance from the galaxy nucleus in the radio emission direction, the opening angle of the ionizing beam is very narrow $\sim 10°$. However the geometrically thick disk could be more adequate for those cases in which a wide cone of ionizing radiation is observed. Thick accretion disks are characterized by the formation of a funnel in the inner parts, where most of the radiation is produced. The radiation will be concentrated in the direction of the funnels and therefore it will be highly anisotropic. The subject of this thesis work is precisely to explore the possibility that the continuum produced by a geometrically thick accretion disk may reproduce the emission line cones. We have adopted a very simple model to calculate the disk emission and with the aid of a photoionization code we have computed the different emission lines at the expected conditions in the ENLR location.

The plan of this Thesis is as follows:

In Chapter 1 we will shortly review the observations of extended emission line gas around Seyfert galaxies. A description of individual sources will be followed for several cases in which the presence of an ionization cone is well confirmed. We will also be concerned with estimation of the number of photons needed to produce the observed line luminosity. In several cases the number of ionizing photons present in the observed nuclear continuum is not sufficient to produce the line luminosity: this is commonly referred to as the photon deficit problem. We will also sketch the differences between the extended emission line around Seyfert, and around radio galaxies and QSOs. Several trends have been found between the line luminosity, the extent of the emitting region and the nuclear luminosity. We will discuss the significance and implications of these relations.

In Chapter 2 we will review and discuss a unified scheme, in which the Seyfert 2 galaxies possess a hidden Seyfert 1 nucleus, due to the presence of a thick torus blocking our sight of the nucleus and the BLR.

In Chapter 3 we will discuss the physical conditions and the excitation mechanisms of the gas which are expected to prevail in the extended line emitting regions. We will further justify the assessment that the excitation mechanism of the gas is photoionization by the nuclear emission. We will point out the similarity of the Extended NLR line spectrum with the Nuclear one, and we will present different photoionization models developed for the Nuclear NLR. We will also try different ionizing continua (namely:

black body, power law and thin accretion disk spectra) and compare the predictions for the different emission lines with the observed values for the ENLR around Seyfert and emission line radio galaxies.

In Chapter 4 the thick accretion disk theory will be shortly reviewed. Special emphasis will be given to the way to calculate the emission from such structures, as well as the variation of the continuum emission with the inclination angle, and with the parameters governing the disk configuration. We will also investigate how the continuum emission depends on the adopted disk model. We will make a qualitative discussion about opacity sources which have not been considered in our modelling. We have also investigated the influence of changing the angular momentum distribution on the emitted radiation, *i.e.* its polar diagram and its spectral shape.

The photoionization of a low density gas by the thick accretion disk emission (using the Madau [1988] model) is discussed in detail in Chapter 5. We are very concerned in this Chapter with the ability of the disk emission as ionizing continuum for the ENLR line spectrum. Most of the disk emission is produced in the inner part where a steep funnel is formed, it is due to this geometrical configuration that the more energetic radiation is collimated into two cones along the rotation axis. The disk emission will be considered along the disk axis only, since it is reasonable to assume that the place where the line emission is detected (or equivalently it is most intense) corresponds to the maximum of the ionizing flux. We will compare the predictions for the emission lines with the observed values for several ENLRs around Seyfert galaxies, and explore the parameter space available to the accretion disk model. The possible modifications of the ionizing continuum relative to the disk emission, are then considered in order to improve the agreement of the predicted emission lines with the observed values.

The expected angular dependence of the emission lines such as induced by the angular variation of the disk emission is studied in detail in Chapter 6. The angular dependence of the thick accretion disk emission will be governed by the occultation of the inner parts of the disk, *i.e.* the absolute flux will decrease at large inclination angles. In addition the emission will change its energy distribution, *i.e.* at small separation angles from the disk axis the radiation will be dominated by the hotter parts whereas at large separation angles the radiation will be dominated by emission from cooler zones. Firstly we will consider separately the effects of decreasing the number of ionizing photons and changing the spectral shape of the ionizing continuum with the inclination angle, and how both results are affected by the variation of the disk model parameters. Once we have understood these effects, we will adopt a disk geometry for the ENLR and then calculate the angular dependence of the emission line spectrum due to the actual change of the disk emission, *i.e.* combining consistently the two mentioned effects. This is done for different disk parameters. The comparison with the observations is not possible at this stage, due to the lack of spectroscopic data varying the inclination angles through the ENLR. We will make a qualitative discussion in order to accept or reject certain regions of the disk model parameters space which are compatible or not with the observations of ionization cones. A final discussion will follow, describing some of the problems with this thick disk model, and some suggestions are proposed to alleviate them.

Chapter 1

EXTENDED NARROW LINE REGIONS AROUND SEYFERT GALAXIES

1.1 DETECTION OF EXTRANUCLEAR ACTIVITY

The presence of extranuclear emission line nebulosities in many AGNs has been amply confirmed during the last decade. The observational work in extranuclear activity is relatively expensive due to the low surface brightness of the observed features. The first discoveries were made by using long–slit techniques which led to the impression that extranuclear activity was a rare phenomenon, due to the low spatial coverage. It has been only with the increase of sensitivity in the modern bidimensional detectors and using narrow band imaging that extranuclear activity is becoming a commonly observed feature.

In the following we will concentrate on the structures observed around Seyfert galaxies, although extended regions of line emitting gas are also commonly found around QSOs and radio galaxies. It is important to mention that we refer here to extranuclear activity as that directly related to the presence of the active nucleus. Any other extranuclear phenomena such as starbursts or giant H II regions which are sometimes observed in galaxies containing a Seyfert nucleus are not of our interest in this Thesis, although their occurrence may be related to its presence. In Chapter 3 we will mention how these phenomena can be distinguished spectroscopically.

The existence of a correlation between the radio power and the luminosity of the emission line [OIII] λ5007 (de Bruyn and Wilson, 1978; Wilson and Willis, 1980; Meurs and Wilson, 1984) suggests that a physical relationship should exist between the NLR and the radio structure. In many cases where the NLR has been spatially resolved, the line emitting gas appears to be elongated in the same direction as the radio emission (Wilson and Heckman, 1985; Haniff, Wilson and Ward, 1988). Furthermore the physical extent of the NLR and the radio emission are comparable: in some cases where high spectral resolution is available, substructures in the [OIII] λ5007 line profiles can be separated and very often associated with individual radio components (Whittle *et al.*, 1986; Whittle *et al.*, 1988). Whittle *et al.* (1986) and later on Wilson, Haniff and Ward (1988) proposed a scenario in which the distribution of the gas in the NLR is affected by the presence of the radio components via shocks, compression and acceleration, although the source of ionization is the nuclear emission.

High excitation gas has been found at distances from the nucleus larger than those of the NLR, this gas emits a similar line spectrum to that observed from the NLR. The distribution of the gas tends to be aligned with the radio emission, although it usually extends to large distances (Unger *et al.*, 1987). It is natural to ask if the radio emission can be here as relevant as in the NLR case. It was noticed by Heckman *et al.* (1981) and later by Unger *et al.* (1987) and Schulz (1988) that the gas in these regions does not exhibit large line width as in the NLR. Meanwhile it has been found some shift from the systemic velocity which is consistent with normal rotational motions in the galaxy plane. This fact suggests that radio emission is not affecting kinematically the gas emission in the ENLR, and it makes sense to separate the emission into two components: an NLR emission and an Extended NLR. The way to separate them is based primarily on the spatial extension and the different line width. This separation might be artificial and a smooth transition will likely occur between the two regions.

The apparent no influence of the radio emission in the ENLR leaves photoionization by the nuclear UV emission as the only viable excitation mechanism of the gas. Furthermore, the fact that the ENLR is found preferentially in the direction of the radio emission leads to the conclusion that the ionizing radiation should be also collimated in that direction. Hence the nuclear radiation field will be highly anisotropic.

A more impressive evidence that gas in the ENLR is ionized by an anisotropic source comes from direct narrow band imaging of the line emitting gas. These images are usually taken in the light of the [OIII] λ5007 and $H\alpha$ lines, and they reveal a conical structure whose axis approximately coincides with the radio axis, and whose vertex points directly to the nucleus (Baldwin, Wilson and Whittle, 1987; Pérez *et al.*, 1989; Pérez-Fournon and Wilson, 1990; Pogge, 1988a; Pogge, 1988b; Pogge, 1989a; Pogge, 1989b; Tadhunter and Tsvetanov, 1989). In most cases a biconical structure is present, although in few cases only a one side conical structure is observed, reflecting perhaps the obscuration due to the inclination of the galaxy disk. Given the large amount of obscuring material that may be present in the host galaxy plane, only the sides of the cone which are emerging towards us from the near side of the galaxy will be visible (see discussion below on NGC 1068). The opening angle of these cones are fairly large, up to values of 90° from edge to edge (Pogge, 1989b).

The interpretation that the origin of the ionized gas in the ENLRs is unperturbed gas from the galaxy disk[1], together with the fact that the nuclear radiation field is collimated into a certain solid angle arises a natural question about the orientation of the nuclear axis with respect to the plane of the galaxy (Meurs, 1989) and the distribution of the gas inside the galaxy. The necessary condition to intersect a plane and a cone whose vertex lies on this plane requires that the angle formed by the axis of the cone and the plane should be less than the opening angle of such cone. This implies in some cases that the axis of the nuclear emission should be highly inclined with respect to the galaxy rotation axis, unless the aperture of the cone is fairly large. The tipping of the nuclear axis with respect to the rotation axis of the galaxy seems to be contrary to the principle of conservation of angular momentum. In this respect Tohline and Osterbrock (1982) have suggested, based on simple dynamical considerations, that the axis of the nuclear structure can be tilted relative to the host galaxy plane. This feature is also consistent with the observation that radio axis and kinematical axis are

[1] There is a relevant counterexample: the galaxy NGC 4388 shows a cone of line emitting gas which is oriented perpendicularly to the galaxy plane. The galaxy NGC 5252 could be another case in which most of the emission is outside the galaxy plane.

not aligned necessarily in radio galaxies and Seyferts (Wilson and Heckman, 1985).

The orientation of the nuclear radiation beam with respect to our line of sight may influence the appearance of the ionized regions. If the distribution of the gas inside the radiation cone is uniform then the opening angle of the cone projected in the sky plane is an increasing function of the inclination of the radiation beam relative to our line of sight. In such case, the probability of observing line emission distributed in a conical region will be a decreasing function of the opening angle of the cone. However if the gas is distributed in the galaxy disk, the probability to observe a cone projected on the sky depends only on the inclination of the galaxy disk, assuming that the cone of ionizing radiation intersects the plane of the galaxy. In order to discriminate what are the actual effects governing the appearance of the ionization cones statistical studies should be envisaged concerning the morphological type of the host galaxy and the orientation of the ionization cone relative to the kinematical axis of the galaxy.

Several authors (Lawrence and Elvis, 1982; Antonucci and Miller, 1985) have proposed that Seyfert 2 and Seyfert 1 galaxies are the same class of objects, the difference being merely an orientation effect. Seyfert 2 galaxies might have a Seyfert 1 nucleus which is hidden from our line of sight, as inferred from the observations of broad emission lines in the polarized nuclear emission of the classical Seyfert 2 NGC 1068 (Antonucci and Miller, 1985). In Chapter 2 we will review a model which tries to unify classes 1 and 2 of Seyfert galaxies. It is interesting to investigate how the finding of the cones of ionizing radiation is compatible with such an unifying picture. As we mentioned above the conical appearance of the ionized gas will depend mostly on the relative inclination between the nuclear cone of radiation and the plane of the host galaxy and perhaps for a more isotropic gas distribution on the orientation of the cone in the plane of the sky. In the frame of the unified scheme, we could ask if there is any relation with the presence of ionizing cones and the Seyfert class. Pogge (1989b) carried out a search for spatially extended ionized gas using narrow band imaging (in the light of [OIII] λ5007 and Hα), and therefore complete coverage of the surroundings of the nucleus. His results show that radiation cones are found more frequently in class 2 (eight out of eleven) than in class 1 (three out of nine) objects, which is in good agreement with the unified scheme. Pogge (1989b) concluded that Seyfert 2 are probably hidden Seyfert 1, but not all Seyfert 1 will appear as Seyfert 2 when seen from a line of sight perpendicular to the present one, because they could be intrinsically different. In this respect we believe that his arguments are not conclusive. It is possible to imagine a situation in which, allowing for the presence of an obscuring torus, we have still direct view of the active nucleus and at the same time the distribution of the emitting lines will resemble a cone. Let us suppose the gas is limited to the galaxy disk. If the axis of the torus is inclined with respect to the galaxy disk axis but the cone of ionizing radiation still intersects such plane, then the line emission gas will appear as in a conical distribution. In addition the inclination of the torus axis would be high enough to allow us look at its interior. To achieve this situation the opening angle of the cone should be as large as the angle formed between the galaxy plane and our line of sight.

1.2 A SHORT CATALOGUE OF GALAXIES WITH CONES OF IONIZING RADIATION

In this section we will present information about individual Seyfert galaxies which could exhibit cones of ionizing radiation. This compilation is by no means complete, it is only indicative and we have included only the cases where to our knowledge the cones seem to be present[2]. We will mention meanwhile the most salient and relevant features for the presence of the ENLR in each case.

1.2.1 Mkn 6

This SOa Hubble type galaxy hosts a Seyfert 1.5 nucleus. Unger *et al.* (1987) detected line emitting gas with signs of high ionization, along the radio axis up to a distance[3] of 19 *kpc* but only at one side of the nucleus.

Meaburn, Whitehead and Pedlar (1989) detected two lobes of [OIII] λ5007 aligned with the radio components up to distances of the order of 30 *kpc*. The observed structure is rather filamentary. The widths of the line profile of [OIII] λ5007 is only $\sim 30 - 70\ km\ s^{-1}$.

1.2.2 Mkn 34

This is a Seyfert 2 galaxy. Unger *et al.* (1987) detected the line emitting gas along the radio axis up to a distance of $\sim$ 12 kpc at both sides of the nucleus. Haniff, Wilson and Ward (1988) showed both the [OIII] λ5007 and Hα images to be elongated in the same direction as the radio emission, and to be remarkably coincident.

1.2.3 Mkn 78

This is a Seyfert 2 galaxy. The extended line emission was detected by Unger *et al.* (1987) to extend along the radio structure up to a distance of 16 *kpc*. Haniff, Wilson, and Ward (1988) detected a different structure in the two lines [OIII] λ5007 and Hα. The [OIII] λ5007 image is indicative of a double-lobed structure aligned with the triple radio source. Pedlar *et al.* (1989) presented both [OIII] λ5007 imaging and long–slit spectroscopy, their results show evidences for an extended resolved NLR with non–orbital motions, confirming the results of Haniff, Wilson and Ward (1988). At distances over 30 *kpc* the profiles of [OIII] λ5007 are narrow indicating that the gas is kinematically unperturbed ambient gas, although there is no evidence for rotation with the underlying galaxy gas. The gas is predominantly extended in one direction and aligned with the radio emission. A striking feature is the fan shape of the ENLR, with a noticeable decrease of surface brightness in the center of the fan, resembling a hollow cone.

[2] In some cases the line emission is rather elongated in the radio axis, although they could be good candidates to detect cones, with some observational effort.

[3] We will adopt $H_0 = 50\ km\ s^{-1}\ Mpc^{-1}$ in this work.

1.2.4 Mkn 573

This SO Hubble type galaxy harbours a Seyfert 2 nucleus. Haniff, Wilson and Ward (1987) found the NLR elongated along the triple radio source up to distances of ~ 2 *kpc*. Unger *et al.* (1987) found line emitting gas extending up to $\sim$ 6 *kpc* in both sides of the nucleus along the radio axis direction. Unger *et al.* (1987) also found good evidences for galactic rotation of the gas. Tsvetanov *et al.* (1989) confirmed the presence of such gas. Furthermore Tsvetanov *et al.* (1989) presented kinematic evidences suggesting that the gas shares the rotation of the galaxy and in addition presents some radial motion component. These authors suggested a picture in which the cone is viewed from its edge.

1.2.5 NGC 1068

This Sb galaxy is the archetypical Seyfert 2 galaxy and it is one of the most luminous and nearest Seyferts. This galaxy is seen at a low inclination and a good mapping of the galaxy is then possible. In the first studies (Walker, 1968) it was found that the central parts of this galaxy contained several high ionization clouds moving with velocity differences $\sim$ 600 $km\ s^{-1}$, from the systemic velocity. The external gas was found to be in rotation consistent with the motion of gas in the disk galaxy. A very detailed study of the kinematics of the nucleus was carried out by Cecil(1989) and Cecil, Bland and Tully (1990). Balick and Heckman (1985) presented direct images in the [OIII] λ5007 and Hα emission. Those images revealed a highly structured emission region extending several *kpc* from the nucleus.

Baldwin, Wilson and Whittle (1987) made an exhaustive study of both kinematics and ionization of this galaxy. They found that the observed ionization of the gas may be understood as a mixture of two components projected on top of each other: one component, rather diffuse which is of low ionization, excited by hot stars and the other less extended, which is of high ionization probably excited by the nuclear continuum. The two components are distinguished kinematically. The [OIII] λ5007 emission exhibits a plateau which extends 10" to 30" (1 – 3 *kpc*) from the nucleus along the direction of the radio axis, at the North East. The ratio [OIII] λ5007/Hβ is constant up to distances of 45" (4.5 *kpc*). The velocity field over the [OIII] plateau seems to be consistent with the ordered rotation field of the galaxy. The emission in the opposite direction to the nucleus is weaker and more patchy. Pogge (1988a) presented [OIII] and Hα images and in addition an ionization map ([OIII]/Hα)[see Fig. 1.1] in which this high ionization zone is revealed with a clearly delineated conical shape (the opening angle is 40°). No clear evidence for such cone was found in the SW direction along the radio emission. The fact that only one side of the cone is observed suggests that the axis of the biconical structure is tilted with respect to the galactic disk, the North-East part of the cone is tilted towards us, although this may be in conflict with the idea of the high ionization gas sitting in the galaxy disk.

Perhaps the most exciting feature concerning NGC 1068 is the discovery of broad emission lines in its polarized nuclear light (Antonucci and Miller, 1985). The interpretation given by Antonucci and Miller (1985), and later on theoretically developed by Krolik and Begelman (1986, 1988) is that a huge molecular torus (inner edge $\sim$ 1 *pc*) is blocking our view of the BLR, we only see the fraction of the radiation which is scattered. This torus may be also collimating the radiation that produces the extended [OIII] λ5007 emission. We will discuss this model with more detail in Chapter 2.

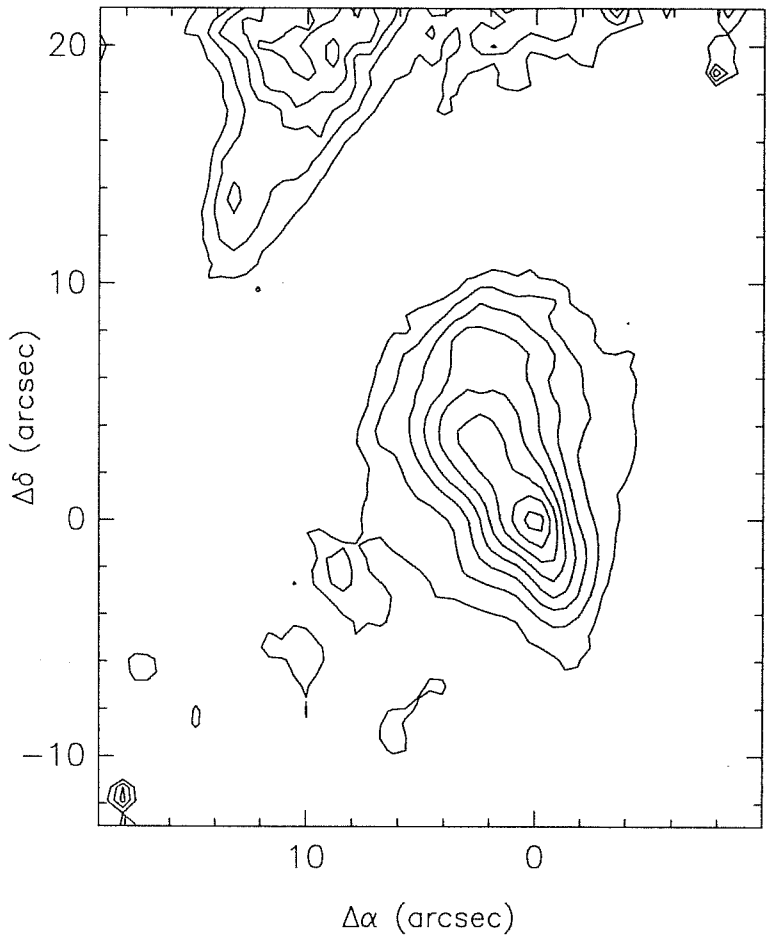

Figure 1.1: The Seyfert 2 galaxy NGC 1068. Contours of constant [OIII] $\lambda 5007/(H\alpha+[NII]\ \lambda\lambda 6548, 6584)$ ratio. The orientation is North up, East to the left. The nucleus is located at the origin. Notice the conical structure extending North–East to the nucleus. Adapted from Pogge (1988a).

Evans and Dopita (1986) and recently Bergeron, Petitjean and Durret (1989) detected extended strong emission from high excitation lines, such as [NeV] λ3426 and HeII λ4686. The emission in such lines is concentrated in a cone about 80° wide which resembles that found by Pogge (1988a), although in the latter case appears only to open for 40°. The [NeV] λ3426 emission is constrained to a narrow angular zone, and the ratio [NeV] λ3426/Hβ is anomalously high. Evans and Dopita (1986) and Bergeron, Petitjean and Durret (1989) proposed that a superposition of low and high ionized gas is observed. Moreover they propose that the high ionization gas can be only produced by a continuum which is absorbed at low energies, from 1 ryd up to energies of 350 eV and 500 eV. The existence of both high and low ionization lines is explained with the combination of ordinary H II region plus a power law ionized gas.

Appenzeller and Wagner (1990) showed that the infrared emission is dominated by emission lines. Their line free continuum images show an unresolved central nucleus, but no extended circumnuclear region. Instead the image in the line Brγ shows an elongation similar to that observed in [OIII] emission.

1.2.6 NGC 2110

This is a Seyfert 2 galaxy, which was originally classified as a Narrow–Line X–ray galaxy by Shuder (1980). Morphologically, it may be classified as SO Hubble type.

Wilson, Baldwin and Ulvestad (1985) found an elongated distribution up to 5" of the line emission [OIII] λ4959 aligned with the radio structure, instead the Hα emission is distributed rather symmetrically around the nucleus. This result was confirmed by Pogge (1989b); an ionization map was also presented although the images had not sufficient resolution for any recognizable structure to emerge.

1.2.7 NGC 3081

This galaxy of Hubble type Sa/SBa harbours a Seyfert 2 nucleus. The stellar disk of this galaxy is seen nearly face–on. The extended emission in Hα was first detected by Durret and Bergeron (1986), and they confirmed that the circumnuclear gas is ionized by the nuclear continuum, as derived from the high ionization observed. The outermost part corresponding to the ring–like structure are H II regions. Pogge (1989b) confirmed these results. The narrow band image in the light of [OIII] λ5007 shows a rather compact circumnuclear emission.

1.2.8 NGC 3516

This Hubble type SB0 galaxy shows in the nucleus a Seyfert 1 spectrum. This Seyfert nucleus is highly variable in the continuum light and emission lines. The UV lines CIV λ1550, NV λ1240 and SiIV λ1400 contain a variable absorption component, which is blueshifted with respect to the narrow lines and the peaks of the broad lines (Voit, Shull and Begelman, 1987). They suggested that the absorbing material will be contained in either optically thin clouds in the BLR or very dense clouds in the NLR, which share an outwards flow. The first indications of the presence of extended ionized gas comes from Adams (1977). Later spectrographic and spectrophotometric observations were carried out by Ulrich and Péquignot (1980). They found several condensations and zones of extended emission lines up to distances 30" (7.5 *kpc*) to the North East of the nucleus. A complete spatial coverage was presented by Pogge (1989a): the subtracted

continuum images of Hα + [NII] $\lambda\lambda$6548, 6584 and [OIII] λ5007 show a similarly wide but elongated structure, with a reminiscent spiral trail in the circumnuclear parts. The emission in the [OIII] line is more extended than the Hα emission. The [OIII] λ5007 emission is observed up to distances $\sim$ 12", also a small knot at 20" North of the nucleus is also detected, which may coincides with the farthest feature detected by Ulrich and Péquignot (1980). The extended line emission aligns quite well with the radio one, although an exact correspondence is not observed. On the contrary, the emission line images do not show any similarity with the stellar light distribution, furthermore the spiral trail is well contained in the stellar bar which indicates that both structures should be independent.

Pogge (1989a) reported also long–slit spectrophotometry coincident with the elongation of the emission line image, confirming the high ionization degree of the extended line emitting gas where the lines [NeV] λ3426 and HeII λ4686 are detected.

1.2.9 NGC 4151

This SBab galaxy is a famous Seyfert 1.5 nucleus which has been studied many times, mainly because its proximity and brightness. Heckman and Balick (1983) detected first extended emission line gas. This work appears simultaneously with another work reporting the finding of extended X–ray emission whose size scale was comparable to that of the radio–emission (Elvis, Briel and Henry, 1983). Both X–ray and emission line are asymmetrically extended to the SW of the nucleus up to distances of 18" ($\sim$ 3.2 *kpc*). The emission line extension appears like a chain of narrow knots.

Schulz (1988) presented high resolution spectra of the extended regions of emission lines. Those spectra reveal two important features: 1) the line widths are in the range of $20 - 40$ $km\ s^{-1}$ which are close to the typical values of H II regions; 2) the high ionization observed suggests ionization by the nuclear continuum.

More recently, Pérez *et al.* (1989) and Pérez–Fournon and Wilson (1990) presented [OIII] λ5007 and Hα continuum subtracted images which reveal two components of the line emitting gas:

- A linear structure of high ionization knots which extends to the SW (which can be identified with that found by previous workers), with a much less extended structure to the NE of the nucleus.

- A low ionization component detected around the nucleus, and to the NE at a distance of 16" in the form of a shell of Hα emission, which can be the North East component of the SW chain, emerging from the galaxy disk. It is spatially associated with a dust lane detected as reddening in a color map (namely a blue image divided by a red image, Pérez–Fournon and Wilson [1990]).

Assuming that the ENLR is confined to the disk of the galaxy, it is possible to estimate the inclination of the linear structure with respect to our line of sight. The angle A between the axis of the linear structure and our line of sight is given by the expression:

$$sinA = (1 + sin^2\Psi\, tan^2 i)^{-1/2},$$

where Ψ is the angle projected onto the plane of the sky between the major axis of the galaxy and the structure axis. For NGC 4151 $i = 21°$ and $\Psi = 22°$. Based on kinematical arguments the orientation of the galaxy disk can be derived and it is

concluded that the South East is the part closest to us. The value obtained for the angle A is 82°, therefore the cone will be almost in the plane of the sky and slightly pointing towards us. Assuming that there is a blocking structure which is responsible for both the collimation of the radiation field, and as in the case of NGC 1068, hiding the BLR, the opening angle should be larger than 82° to allow us to observe NGC 4151 as a Seyfert 1 nucleus and simultaneously produce the collimation of the ionizing radiation. Therefore if a blocking structure is present we will be looking at the edge of the structure, and probably the same will be occurring with the gas in the galaxy disk, since a narrow cone of ionized gas is observed. The axis of the obscuring torus should be very tilted with respect to the galaxy disk.

The results of a high S/N spectrophotometric study made along the extended linear structure were recently reported by Penston *et al.* (1990). The values of the intensity for the usually observed lines and several other weak lines are measured accurately. The nuclear continuum is confirmed as the ionization mechanism. The density and temperature of the emitting gas were determined using emission line diagnostics.

Similarly to the collimation observed in the lines in the optical band, Bruhweiler and Smith (1988) reported spatially resolved extended emission in the light of the lines CIII] λ1909 and CIV λ1549. The observed structure resembles the one observed in the optical lines. Furthermore they estimate a rather high ionization parameter U_t (we refer to Sect. 3.2 for the definition of U_t) from comparison with the predictions from current photoionization models for the Nuclear NLR.

1.2.10 NGC 4235

This is a Sa Hubble type galaxy, which is seen nearly edge–on. Its nucleus shows a Seyfert 1.5 spectrum. Images of the emission lines Hα + [NII] and [OIII] are presented by Pogge (1989b). The [OIII] λ5007 image is only slightly extended $\sim$ 4", unlike the stubbier Hα image.

1.2.11 NGC 4388

This galaxy is highly inclined which makes difficult its morphological classification, although it has been classified as Hubble type Sab by Sandage and Tamann (1981). It is located in the core of the Virgo cluster, although its membership has been discussed (Phillips and Malin, 1982). The nucleus shows a Seyfert 2 spectrum, with substantial obscuration by a prominent dust lane crossing the disk and the bulge of the galaxy.

Colina *et al.* (1987) presented high resolution spectra in a range of frequencies containing the line [OIII] λ5007. They found that the line profiles can be decomposed into several kinematically distinct components. A similar study was done by Ayani and Ike (1989).

Pogge (1988b) reported the results of imaging in the lines [OIII] λ5007 and Hα, together with long–slit spectroscopy. The [OIII] λ5007 image is richly structured: a complex of emission clouds lies above the galaxy disk towards the North East up to a distance of 25", 38" (1.7 – 6.5 *kpc*); in the opposite direction against the nucleus a less extended structure is present. An ionization map [OIII]/Hα reveals a biconical morphology with a highly structured system of clouds (see Fig. 1.2). This structure is approximately aligned with the radio emission which reveals itself rather complex (Stone, Wilson and Ward, 1988). The South cone is well defined and it emerges directly from the nucleus; however the North cone is evident only outside the galaxy disk. A

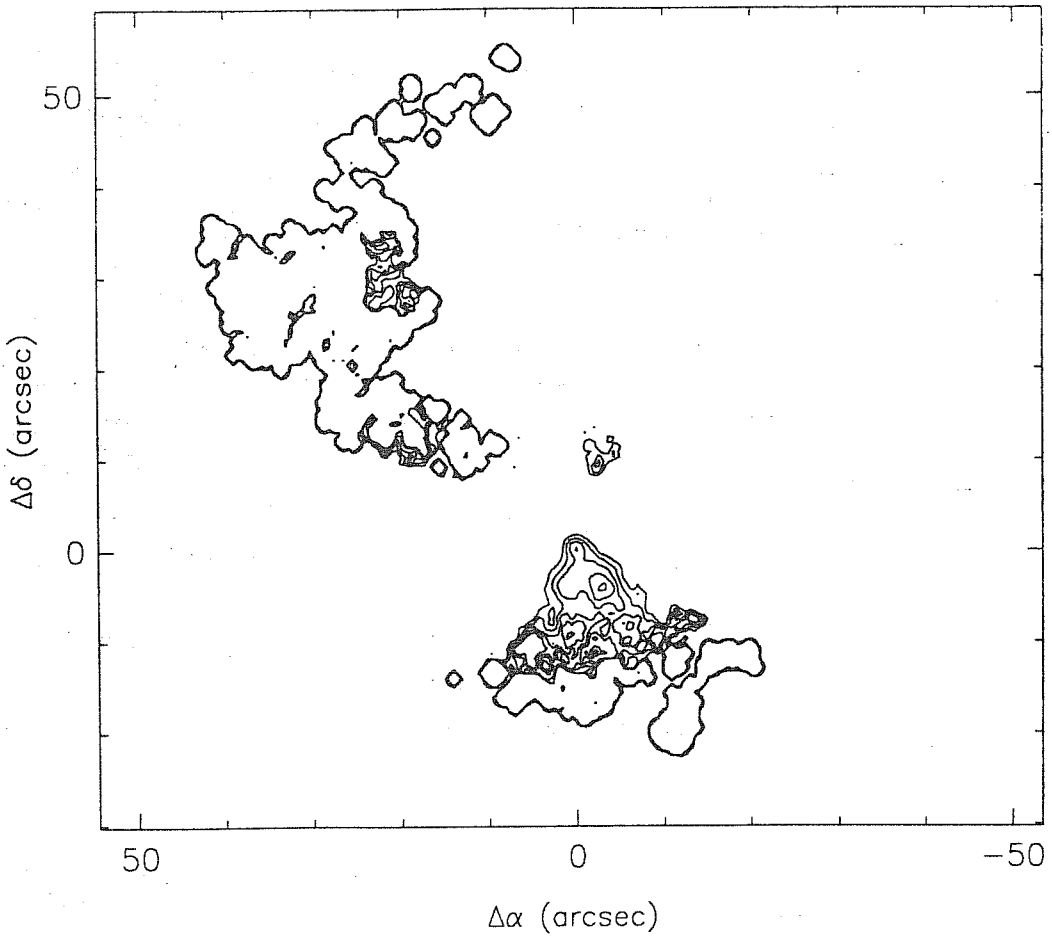

Figure 1.2: The Seyfert 2 galaxy NGC 4388. Contours of constant [OIII] λ5007/(Hα+[NII] $\lambda\lambda$6548, 6584) ratio. Regions outlined by the heavy contour indicate regions where the line [OIII] λ5007 was detected but Hα was not. The orientation is North up and East to the left, with the nucleus located at the origin. This figure is adopted from Pogge (1988b).

simple explanation for this feature is that the axis of the bi-cone is tilted: the South side is slightly tilted towards us, whereas the North one is directed away from us, with the North side of the disk galaxy, which is the nearest to us, obscuring the vertex of the cone. The emission line spectra corresponding to the observed clouds indicate a high ionization level and hence this suggests photoionization by the nuclear emission as the excitation mechanism.

Similar results were obtained by Corbin, Baldwin and Wilson (1988). They discussed the kinematical properties of the material outside the galaxy disk; the velocity field is rather complex and rotational motion is restricted to the stellar disk. Several origins for the gas outside the galaxy disk were discussed, among others the most favored was ram pressure from the intracluster medium which strips gas from the galaxy disk.

1.2.12 NGC 5252

This is a SO Hubble type galaxy and its nucleus shows a Seyfert 2 spectrum. Unger *et al.* (1987) found line emitting gas at both sides of the nucleus in the radio emission direction, up to a distance of 11 *kpc*. Tadhunter and Tsvetanov (1989) reported [OIII] and Hα images (see Fig. 1.3). The [OIII] image shows a very impressive biconical structure (the opening angle is $\sim 75°$) up to distances of 50" ($\sim$ 30 *kpc*). The stellar continuum image of this galaxy presents a completely different aspect than the emission line images. The major axis of the galaxy disk is misaligned relative to the cone axis by $\sim 30°$. An additional ionization map is presented where the biconical structure is still present, indicating the high ionization level of the [OIII] emitting gas. *This is by now the most striking evidence that the nuclear ionizing continuum should be collimated in a limited solid angle.*

1.2.13 NGC 5548

This is a Seyfert 1 galaxy which has been very often studied, especially for its variability in the broad emission lines and the continuum. The morphology of this galaxy is rather particular: It contains an inner disk plus an outer ring (Su and Simkin, 1980). Wilson *et al.* (1989) showed the existence of extended emission in the [OIII] line up to a distance $\sim$ 3.5 *kpc* from the nucleus. The extended emission is elongated in the direction very close to the axis of the radio emission. On the contrary the Hα image is highly symmetric.

1.2.14 NGC 5728

This is a Seyfert 2 nucleus in a SBb galaxy. Schommer *et al.* (1988) found the nucleus surrounded by an arc of blue light and emission lines, with a rather complex velocity field. The presence of non rotational motions has been interpreted as evidence for inflow motions, due to the presence of the stellar bar. Gas in the inner regions is highly ionized, suggesting that the nonthermal emission is the ionizing source.

Pogge (1989b) presented [OIII] and Hα images. The [OIII] image shows two diffuse emission regions extending farther than the H II regions ring. An ionization map allows to separate the low ionization regions from the high ones. This map shows a lobe extending to the South East up to 3", in the North West part the line emission is less extended. An [OIII] image was also presented by Appenzeller and Wagner (1990) and their results agree with the structure observed by Pogge (1989b).

1.3 THE PHOTON DEFICIT PROBLEM

Apart from the morphological evidence from the extended line emission that the ionizing continuum should be collimated in two opposite cones, there is a very conspicuous argument favouring the anisotropy of the nuclear radiation field in Seyfert galaxies, which is based on energetics considerations. It is possible to estimate the number of ionizing photons which is needed to produce the observed luminosity in recombination lines, with the assumption that only photoionization is the responsible for the excitation of the line emitting gas and we are in the low density limit. From the radiative equilibrium we require that the total number of absorptions is balanced by the number

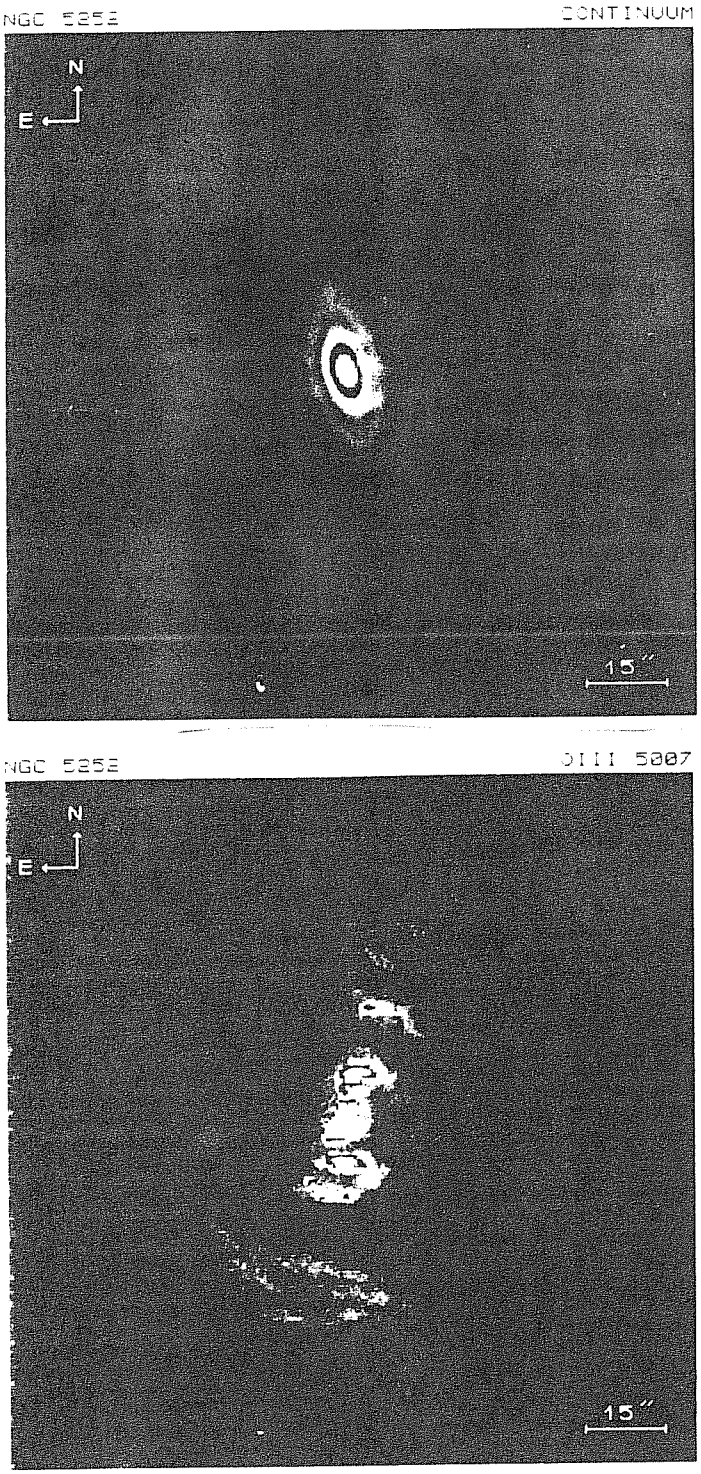

Figure 1.3: Top panel: The Seyfert 2 galaxy NGC 5252 appears in the line free continuum light as an SO galaxy.
Bottom panel: Continuum subtracted [OIII] λ5007 image of NGC 5252. North is up and East to the left. Note the impressive biconical distribution of the emission. The axis of this structure is missaligned with respect to the major axis as defined in the continuum image.
This Figure is adopted from Tadhunter and Tsvetanov (1989).

of recombinations per unit time. Adopting case B conditions (Osterbrock [1974], p. 63) we then write:

$$\frac{\epsilon\omega}{4\pi}\int_{\nu_0}^{\infty}\frac{L_\nu}{h\nu}d\nu = n_e^2\alpha_B\ f\ V,$$

where f is the filling factor, V is the total emitting volume, ω is the solid angle covered by the nebula as seen from the nucleus, ν_0 is the ionization potential of the hydrogen and n_e is the electronic density. ϵ measures the efficiency of the gas absorbing the photons reaching there, it is equal to unity in the case that all the photons are absorbed (optically thick nebula).

The luminosity of any recombination line (*e.g.* Hα) is given by the expression:

$$L(\mathrm{H}\alpha) = n_e^2\alpha_{\mathrm{H}\alpha}^{eff}h\nu_{\mathrm{H}\alpha}fV.$$

Combining then the two above expressions we obtain:

$$\frac{1}{4\pi}\int_{\nu_0}^{\infty}\frac{L_\nu}{h\nu}d\nu = \frac{\alpha_B}{\alpha_{\mathrm{H}\alpha}^{eff}}\frac{1}{\epsilon\omega}\frac{1}{h\nu_{\mathrm{H}\alpha}}L(H\alpha),$$

where α_B and $\alpha_{\mathrm{H}\alpha}^{eff}$ depend on the temperature and the values are tabulated for case B recombination (Osterbrock, 1974). The left hand side of the expression denotes the number of photons emitted by the ionizing source per solid angle, and we denote by N_l, whereas the right hand side is directly calculated from the observations.

Wilson, Ward and Haniff (1988) evaluated the number of photons which is necessary to produce the total observed luminosity in Hβ from the NLR, which is estimated from the pure emission line images. On the other hand they estimated the number of ionizing photons present in the continuum, extrapolating from the optical and the X–ray when available, the continuum as a power law energy distribution. The number of ionizing photons present in the nuclear emission should be sufficient to produce the observed line luminosity. However there are several uncertainties in these estimations: 1) Most of the ionizing photons in the continuum are emitted into a range of frequencies unobserved from the Earth. Moreover reddening and absorption by intervening material in our galaxy or the host galaxy will affect the estimates. 2) The nuclear continuum is strongly contaminated by the stellar emission and it is particularly difficult to estimate the actual non stellar contribution. This problem is particularly relevant in Seyfert 2 which are the cases where discrepancies between both estimates are expected. 3) The covering fraction of the gas is unknown.

Despite these difficulties the results confirm that the number of ionizing photons present in the continuum as received on Earth is not enough to produce the observed luminosity in the recombination lines. In some cases (*e.g.* Mkn 3, Mkn 78) the discrepancy is larger than a factor of 10, although affected by many uncertainties this discrepancy seems to be real.

The same kind of estimations can be carried out using the spatially resolved emission from the ENLR, in such case the spatial coverage is known. Pérez–Fournon and Wilson (1990) found that the number of photons present in the continuum of NGC 4151 is marginally enough to produce the observed Hβ luminosity. These authors considered a large covering of the nucleus by the BLR clouds (Ferland and Mushotzky, 1982), in such case they found that the photons present in the continuum are insufficient to ionize the extended line emitting gas by a factor of 10. Penston *et al.* (1990) used a slightly different method, based on the value of ionization parameter U_t (we refer to

Section 3.2 for a definition) derived from the emission lines in the extended emission, to compute the number of photons reaching the clouds. Comparing this value with the one derived from direct observation of the continuum, they reached the conclusion that the ENLR sees a number of photons a factor of 10 larger than what we observe from the Earth.

Tadhunter (1987) made a similar study in several emission line radio galaxies which presented extended emission line nebulosities. The results indicate that differences in the character of the nuclear emission lines affect the conclusions on the counting of photons. The Broad Line radio galaxies seem to have enough flux to ionize the emission line gas, whereas the Narrow Line radio galaxies do not satisfy the requirements.

In the above estimations for N_l it was always assumed that the gas absorbs all the photons emitted in the fraction of solid angle (*i.e.* $\epsilon = 1$), however the actual collecting area of the gas may be largely reduced if the material is arranged in small unresolved clouds. Equivalently the factor ϵ will take values less than unity. It is possible to estimate the value of ϵ from the expression:

$$\epsilon = \frac{\alpha_B}{\alpha_{\mathrm{H}\alpha}^{eff}} \frac{1}{h\nu_{\mathrm{H}\alpha}} \frac{L(H\alpha)}{A_S U_l n_H c},$$

where A_S is the area of the emitting region facing to the nucleus ($\omega = A_S/D^2$). The value of U_l is determined from the emission line spectrum. Using the typical values for the intervening quantities we obtain:

$$\epsilon \approx 0.26 \frac{L_{40}(H\alpha)}{U_{l_{-3}}\ A_{S_1} n_2} \quad (T \approx 15000\ K),$$

A_{S_1} is given in kpc^2. Therefore one must conclude that the collecting area of the clouds in the nebulosities is smaller than the global area and consequently not all the ionizing photons reaching the clouds will be absorbed. This fact implies even a larger discrepancy when the counting of photons needed to produce the line luminosities is done and compared with those directly observed from the Earth.

The arrangement of the emitting gas into clouds is further suggested by the small values of the filling factor f which are estimated from the line luminosity if an independent measure of the density is available, *e.g.* from the line ratios. From the expression above for the line luminosity we obtain:

$$f = \frac{L(\mathrm{H}\alpha)}{n_e^2 \alpha_{\mathrm{H}\alpha}^{eff} h\nu \mathrm{H}\alpha V}.$$

1.4 ENLR AROUND RADIO-GALAXIES AND QSO'S: DIFFERENCES AND SIMILARITIES

Extensive regions of highly ionized gas have also been observed around low-redshift quasars with extended steep–spectrum radio lobes (Stockton and MacKenty, 1987; Macchetto *et al.*, 1990) and around emission line radio galaxies (Fosbury, 1986; Baum *et al.*, 1988; Tadhunter, 1987).

Stockton and MacKenty (1987) found evidences linking the presence of the extended line emission with extended steep spectrum radio emission and strong nuclear line

emission, although the vice versa was not found. The observed structures are very filamentary and probably this fact reflects the lack of condensed gas rather than the shadowing by the nuclear emission. The origin of the gas may be related to mergers with neighbouring galaxies or to cooling of the hot intracluster gas like the cooling flows observed in rich galaxy clusters (Fabian, Nulsen and Canizares, 1984). This gas will be highly ionized by the nuclear radiation field. Macchetto *et al.* (1990) found in the case of MR 2251-178 that the distribution of the gas emitting [OIII] λ5007 and [OII] λ3727 is elongated in the direction of the radio structure, similarly as observed around Seyfert galaxies. The high ionization level of the gas indicates photoionization by the nuclear continuum.

The extended line emission detected around powerful radio galaxies (Fosbury, 1986; Baum and Heckman, 1988a; Hansen, 1989) shows a large variety of morphologies, although many objects show the gas preferentially along the axis of the double radio sources. The kinematical studies suggest that the most likely origin of the gas is accretion from an external source (Tadhunter, Fosbury and Quinn, 1989). Some of the objects which have been studied are: Pks 2158-38 (Fosbury *et al.*, 1982); Pks 0349-27 (Danziger *et al.*, 1984); Pks 0634-20 (Fosbury *et al.*, 1984). Tadhunter (1987) and Robinson *et al.* (1987) remark that the line spectra of the extended nebulosities observed around powerful radio galaxies resemble those observed in the associated Nuclear Narrow Line Region. These studies suggest larger extension (up to distances of 100 *kpc*) and higher luminosity of the line emitting gas in radio galaxies as compared to the ones observed in Seyfert galaxies. In Figure 1.4 the number of photons which is needed to produce the observed line luminosity is presented vs. the maximum distance at which line emission is detected for both Seyfert and radio galaxies. From the inspection of this figure it can be noticed that the data for radio galaxies are tendentiously shifted to larger distances and present slightly higher energetic requirements than those for Seyferts do.

One of the best studied emission line radio galaxies with extended emission is Pks 2152-69 (di Serego Alighieri *et al.*, 1988; Tadhunter *et al.*, 1988; Tadhunter, Fosbury and di Serego Alighieri, 1988). A very luminous high ionization cloud is found at a distance 8 *kpc* along the radio axis. This cloud shows in addition to very high ionization emission lines (*e.g.* [NeV] λ3426, [FeVII] $\lambda\lambda$6087,5721 and [FeX] λ6374) a blue continuum with a rising spectrum $F_\nu \propto \nu^{-3}$, and a degree of polarization of 10%. Tadhunter, Fosbury and di Serego–Alighieri (1988) proposed a scenario for this source consisting of a blazar beam from the nucleus which ionizes the cloud and the nearby medium. Then scattering of the incoming radiation off dust or free electrons associated with the cloud accounts for the blue continuum and the polarization. The spatial distribution of the line emission within the cloud has been resolved, and spatial gradients of ionization are found in both the radial and transversal directions.

In particular Baum and Heckman (1988b) found that small extent radio sources exhibit emission line gas which is cospatial with the radio emitting plasma. On the contrary they found that in the large extent radio sources the emission line gas is found to be not coincident with the radio component, and sometimes deviates from the radio axis direction. This fact reflects the relative importance of the radio interaction with the surrounding medium in the former case, and the minor effect of that interaction in the latter one. It has been shown by Baum and Heckman (1988a) that there exists a correlation between the number of ionizing photons present in the nuclear non-stellar continuum and the number of photons needed to produce the observed line luminosity,

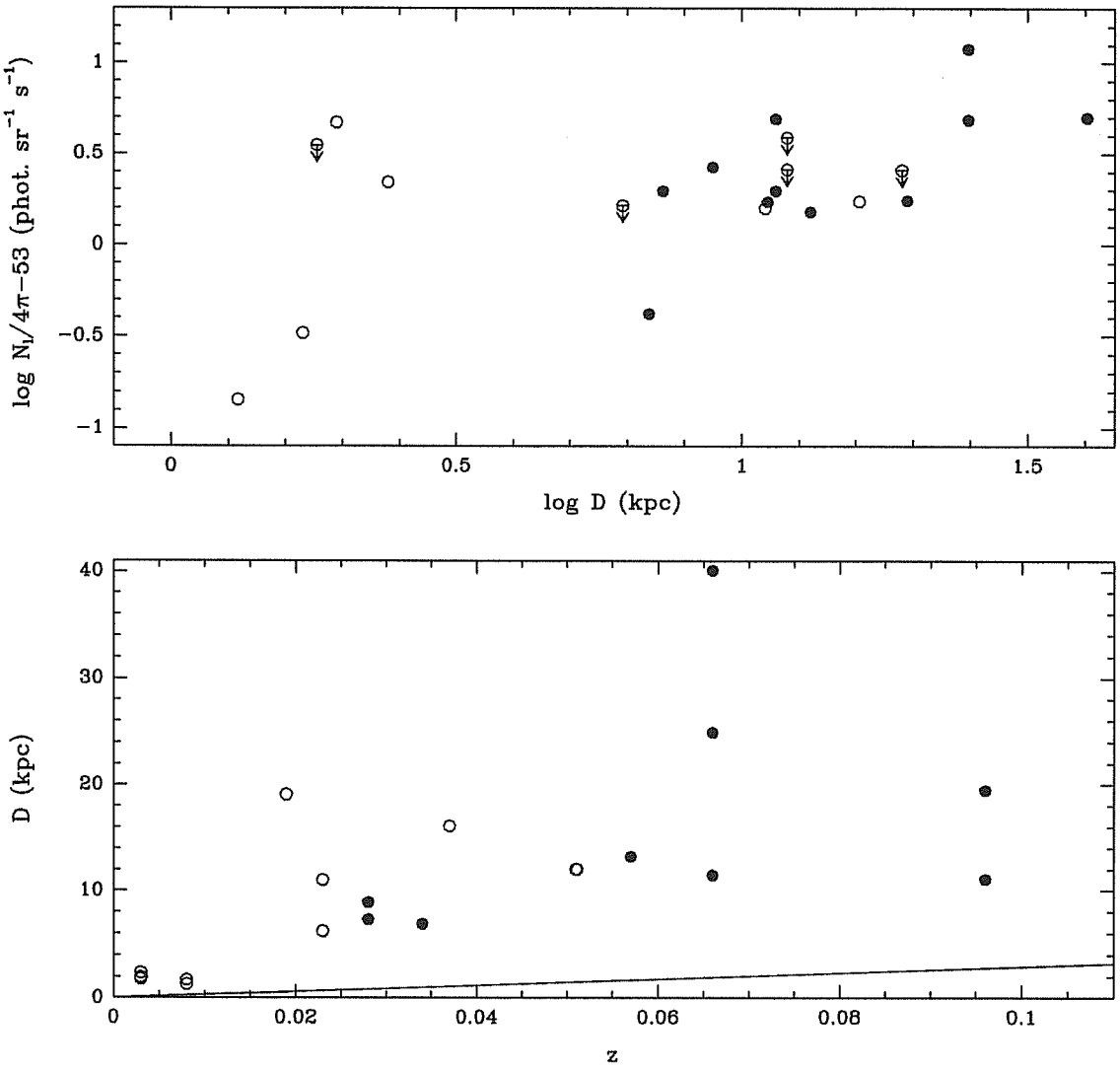

Figure 1.4: Upper panel: Number of ionizing photons per solid angle needed to produce the observed Hα luminosity in the ENLR. Filled circles correspond to radio galaxies, open circles correspond to Seyfert galaxies. A trend of increasing the number of photons with maximum distance could be present. There is no clear differences between the two sets of data, although there is a trend for radio galaxies to show more extended emission line nebulosity than Seyferts do.

Bottom panel: Maximum distance to the extended line nebulosities vs. the redshift of the host galaxy. The solid line indicates the resolution limit (1 arcsecond in angular separation) at the distance indicates by the redshift. The meaning of the symbols is the same as in the above panel.

Table 1.1: $N_l/4\pi$ AND D FOR ENLR'S

Source		Distance	$N_l/4\pi \times 10^{-53}$	Ref.
Mkn 6	N	19.	$\lesssim 2.6$	1
Mkn 34	NW	12.	$\lesssim 3.9$	1
	SE	12.	$\lesssim 2.6$	1
Mkn 78	W	16.	1.7	1
NGC 3516	NE	1.7	0.33	1
	SW	1.3	0.14	1
		2.1	0.23	2
NGC 4151	NE	1.8	$\lesssim 3.5$	1
	SW	2.0	4.7	1
	SW	2.2	2.2	3
NGC 5252	NE	6.2	$\lesssim 1.6$	1
	SW	11.	1.6	1
NGC 1068	NE	2.2	1.0	4
Pks 2356-61	A	20.	1.7	5
	B	11.	1.7	5
Pks 2152-69	A	8.9	2.7	5
	B	7.3	2.0	5
Pks 0349-27	A	11.	2.0	5
	B	11.	4.9	5
	C	40.	5.0	5
	D	25.	12.	5
	E	25.	4.9	5
Pictor A		6.9	0.42	5
3C445	A	13.	1.5	5
Pks 2014-55	A	17.	0.67	5
Pks 2300-18	A	37.	4.9	5
Pks 0634-20	A	8.1	0.82	5
	B	13.	1.3	5
Pks 1404-26	A	3.7	0.30	5
Pks 2158-38	A	8.6	3.9	5
	B	8.6	2.2	5

Table 1.1: Observational data for ENLR found in Seyfert and radio galaxies. The distance measures the maximum extension at which the clouds are found. $N_l/4\pi$ is the number of ionizing photons per steradian needed to produce the observed line luminosity, it is calculated dividing the total number of ionizing photons observed in the emission line nebulosities by its covering fraction. References: [1] Unger *et al.* (1987); [2] Pogge (1989a); [3] Pérez–Fournon and Wilson (1990); [4] Baldwin, Wilson, and Whittle (1987); [5] Tadhunter (1987).

thus confirming that photoionization by the nuclear continuum plays an important role in the excitation of line emitting gas, even in objects with strong radio emission. In particular they claim that this correlation extends to high luminosities but from their Figure 6 (Baum and Heckman 1988a) it seems that the dispersion of the values for N_l is large with the same nuclear luminosity at the high end, which implies that extended line emission in those cases may also be affected by environmental effects. In addition, Baum and Heckman (1988b) found a relationship between the line luminosity and the total radio luminosity, which is a sign of a close relation for both phenomena. The same correlation is not valid for Seyfert galaxies, in such case the emission line to radio luminosity ratio is much higher than found for radio galaxies.

1.5 SOME OBSERVED TRENDS

In this Section we examine the evidences for common properties or trends in the ENLRs. We will consider together the ENLRs observed around Seyfert galaxies and those around powerful radio galaxies, although in the latter objects the interaction with the radio emission could be relevant.

The first correlation that should be noticed is with the radio properties, although it could be not indicative of radio interaction in ENLRs observed around Seyfert galaxies, apart from the coincidence of the orientation of both the ENLR and the radio structure. As we mentioned in Section 1.4, Baum and Heckman (1988b) found a correlation between the total radio luminosity and the line luminosity for a sample of powerful radio galaxies. Wilson, Ward, and Haniff (1988) established a similar relationship for Seyfert galaxies, although the ratio of radio to lines luminosity is lower than in the radio galaxy case. Concerning uniquely the ENLR, Durret (1990) found a correlation between the maximum distance where line emission is present and the radio power at 6 cm, for a large sample of active nuclei. This correlation is not firmly established and selection effects may be acting. Nevertheless, most objects in Durret's sample where radio loud, which is not the case for Seyfert galaxies and we will consider this correlation irrelevant in our problem.

A more interesting feature for our problem of photoionization is the correlation between the UV luminosity of the nuclear source and the maximum distance where line emission is found (Durret, 1990). This correlation strongly suggests that the extended ionized gas is a strong function of the UV continuum, *i.e.* of the reservoir of ionizing photons and rather independent of the gas distribution. However Durret's sample is rather heterogeneous and comprises different classes of objects which differ by orders of magnitude in luminosity. This sample may not be free of bias effects, *e.g.* the most luminous objects will be systematically more distant and therefore the nebulosities, if detected detached from the nucleus, will have to be largely extended, strengthening this correlation if any exists. This correlation will be certainly weakened if anisotropy is present in the nuclear emission. If the beam of nuclear emission is directed close to the plane of the sky the nuclear UV continuum we observe will be only a fraction of that observed by the clouds (even in the case of a scattering medium deviating some nuclear emission into our line of sight). Whereas in the case of the nuclear beam intersecting our line of sight we will observe the same nuclear emission as emission line clouds do. This feature will introduce some dispersion in the mentioned correlation. Moreover the maximum distance will be affected by projection effects. In this respect we propose to search for a correlation between the actual ionizing flux which is really seen by the

clouds and the maximum distance, in order to confirm this correlation. The absolute ionizing flux per unit solid angle in the direction of the clouds can be derived from the energetic requirements to produce the observed luminosity (we refer to Section 1.3). We present (see Table 1.1) the results for a small sample including most Seyferts with well defined conical ENLR, including also the data for radio galaxies from Tadhunter (1987) (see also Robinson *et al.* [1987]), which is plausible because of the similarities of the emission line spectra. We have not found any evident correlation between $N_l/4\pi$ and D (Fig. 1.4), although a trend for $N_l/4\pi$ increasing with D may be present. These data may be affected by undetermined errors (*e.g.* covering fractions of the clouds, projection effects). We believe it will be hard to find any correlation with the data available at this moment. In order to look for a selection effect related to the distance of the galaxy, we have plotted the redshift vs. the maximum distance at which emission line is detected. An apparent trend for more distant objects to have more extended nebulosities is observed for both types of objects, although it is perhaps more evident for the radio galaxies than for the Seyfert ones.

Fosbury (1989) and Prieto, di Serego–Alighieri and Fosbury (1989) present a diagram with the line ratio [OIII] λ5007/Hβ vs. Hα surface brightness, using data across the extended line emission region for the radio galaxy 3C 227. They found a positive correlation between the line surface brightness and the ionization stage, which is an additional evidence indicating that the distribution of line emission follows the distribution of the ionizing flux rather than the distribution of gas density. This result has some implications concerning the structure of the emission line region. For a slab of ionized gas the emissivity is proportional to n_e^2, and its surface brightness should increase with the density, however for a constant flux of ionizing photons when the density is increased U_t decreases and the ratio [OIII] λ5007/Hβ should decrease. However in the case that the emission we are observing comes from a number of unresolved optically thick clouds, the surface brightness is given by the expression (Robinson, 1989):

$$S_{\mathrm{H}\alpha} = \frac{\alpha_{\mathrm{H}\alpha}}{\alpha_B} h\nu_{\mathrm{H}\alpha} A_c \sigma \frac{\int_{\nu_0}^{\infty} L_\nu / h\nu d\nu}{4\pi D^2} = \frac{\alpha_{\mathrm{H}\alpha}}{\alpha_B} h\nu_{\mathrm{H}\alpha} A_c \sigma c n_H U_t,$$

where σ is the column density of the clouds, A_c is the cloud face area, $\alpha_{\mathrm{H}\alpha}$ and α_B are recombination coefficients (Osterbrock, 1974), and n_H is the hydrogen density. In this case the surface brightness is directly proportional to the ionizing flux. This is a further confirmation that the emitting gas is clumpy and arranged in small unresolved clouds.

The clumpiness of the medium rises the problem of confinement of the clouds (Robinson, 1989). The clouds will tend to expand and finally dissipate if there is no medium which can confine them. The timescale on which they expand will be of the order of the sound crossing time. The sound crossing time is estimated from the expression $t_{sc} \sim l_{cloud}/c_s$, where l_{cloud} is the extent of the cloud and $c_s = \sqrt{kT/m_p\mu}$ the sound speed. Using the common values $T \sim$ and $l_{cloud} \sim 10^{19}\ cm$ it results $t_{sc} \sim 10^5 yr$. This time scale seems to be rather short if extended emission line regions are common phenomena. Hence the existence of a hot and tenuous medium which confine the clouds is necessary. Evidence for the presence of hot gas can be extracted from the extended X–ray emission detected around a few Seyfert galaxies (Elvis, Briel and Henry, 1983; Elvis *et al.*, 1990). It is concluded that the origin of the extended X–ray emission is probably thermal emission from an optically thin plasma at $T \sim 10^6 - 10^7\ K$. X–ray haloes are also found in bright clusters of galaxies and nearby ellipticals (Fabian, Nulsen

and Canizares, 1984; Forman, Jones and Tucker, 1985). Nevertheless an outstanding problem is the heating of the gas at the relatively high temperatures $10^7 - 10^8$ K which is required to confine the cold dense clouds and at the same time avoid strong soft X–ray absorption (Krolik and Vrtilek, 1984; Fabian *et al.*, 1986; Mathews and Ferland, 1987).

On the other hand, the fact that the surface brightness and the ionization degree depend on the ionizing flux, supports the hypothesis of an anisotropic ionizing continuum: at a given radial distance from the nucleus the highest ionization, largest luminosity clouds are simply those that fall in the most intense part of the radiation field. According to the above expression for the surface brightness, the ENLR will be constrained to a relatively narrow range in radial distance due to the geometrical dilution of the ionizing flux. However this is in apparent contradiction with the large spatial extension of the ENLR and the fairly constant value of U_t through it. An alternative solution to this problem can be envisaged from the model recently proposed by Binette and Raga (1990) [more details in Sect. 3.6]

Chapter 2

UNIFIED SCHEME FOR SEYFERT GALAXIES

In Chapter 1 we have described a set of observations which suggest the existence of a collimated UV radiation field that emerges from the nuclear region ($\lesssim 1\ pc$) in many AGNs. Such a conclusion was reached according to morphological and energetic considerations concerning the extended line emitting gas.

We also mentioned the remarkable discovery of a Seyfert 1 spectrum in the polarized nuclear emission of the typical Seyfert 2 galaxy NGC 1068 (Antonucci and Miller, 1985). The same authors proposed a model in which a geometrically and optically thick torus surrounds the nucleus and the Broad Line Region. On the contrary the Narrow Line Region should not be occulted by the torus. The spatial scale of the blocking structure will be therefore limited to the range between 1 *pc* to few tens of *pc*. Krolik and Begelman (1986) limited the torus size to few parsecs from the maximum inferred nuclear size as measured with Speckle images in the nucleus of NGC 1068 (Meaburn *et al.*, 1982). The only way to observe the nuclear and BLR emission is by means of scattering by a warm medium, which should be present along the torus axis and at some distance above it. In this Chapter we will shortly review the observations and the theoretical developments related with the torus scenario.

2.1 OBSERVATIONAL EVIDENCE FOR THE EXISTENCE OF THE MOLECULAR TORUS

The study of the polarization of the nonstellar emission in Seyfert galaxies has revealed considerable information about the nuclear structure (Miller, 1989). Most Seyferts do not have significant optical polarization. However among those objects showing the largest polarization it has been found that (Antonucci, 1983): type 1 Seyferts tend to have low polarization ($\sim 1\%$) with the polarization position angle aligned with the radio structure, whereas type 2 Seyferts tend to show relatively high polarization (up to 20%) and the polarization angle is oriented perpendicular to the radio structure. Later on Antonucci and Miller (1985) and more recently Miller and Goodrich (1990) presented spectropolarimetry of several high polarization Seyfert 2 galaxies. Spectropolarimetric studies are important because they can provide information about the featureless continuum and the emission lines separately. The very salient result from these studies was the finding of broad emission lines with the same high polarization degree as the continuum in the polarized light of classical Seyfert 2 galaxies. Let us examine in

some detail these observations. The emission observed from the nucleus of Seyfert 2 galaxies is generally strongly contaminated by the stellar emission, which is basically unpolarized. Therefore a careful subtraction of this component should be carried out before any measurements of the polarization could be done. The measurements of the degree of polarization P_λ are very dependent on the estimation of the stellar contribution, which itself is plagued by uncertainties. However the product $P_\lambda \times F_\lambda$, where F_λ is the total flux, is relatively free of possible errors in the estimation of the stellar component. The plots of $P_\lambda \times F_\lambda$ presented by Antonucci and Miller for NGC 1068 and by Miller and Goodrich for Mkn 3, Mkn 348, Mkn 463E and NGC 7674 show broad Balmer emission lines and in some cases the FeII multiplets. On the contrary the narrow emission lines show a low degree of polarization ($\sim$ 1%). The resulting polarized continuum is remarkably flat indicating that the polarization mechanism is largely wavelength independent, and likely associated with electron scattering. Nevertheless Miller and Goodrich (1990) found P_λ decreasing with the wavelength in these cases, what may indicate either some improper correction for the stellar component or some contribution to the polarization coming from dust particles. A related observation is presented by Shields and Filippenko (1988), who detected broad Hα emission in a conical region outside the nucleus in the Seyfert 2 galaxy NGC 4388.

The only plausible model which has been proposed to explain these observations is the already mentioned thick torus by Antonucci and Miller (1985). According to this model, in Seyfert 2 galaxies the axis of the torus will be oriented close to the sky plane. The photons arising in the nucleus and BLR and travelling along the torus axis will be scattered by electrons into our line of sight. The high polarization degree ($\sim$ 15%), which is observed leads to think that the nucleus and the BLR are hidden deep inside the torus, or equivalently the inner walls of the torus will be very steep.

The presence of the obscuring torus is well related to the cones of ionizing radiation presented in Chapter 1. This torus provides an extrinsic way to collimate the emerging nuclear radiation along the torus axis. Miller (1989) reported the discovery of a highly polarized knot with the polarization vector perpendicular to the nuclear direction, at a distance of 5" North East from the nucleus of NGC 1068, the location of this knot being close to the [OIII] λ5007 plume found by Baldwin, Wilson and Whittle (1987). Furthermore the polarization in this knot was found to increase rapidly towards the blue, indicating that the nuclear light is being scattered by dust grains in these offnuclear regions.

The low detection of Seyfert 2 galaxies in X–ray surveys is consistent with the heavy obscuration provided by the torus. Recently, Elvis and Lawrence (1988) and Koyama *et al.* (1989) reported detection of hard X–ray emission from NGC 1068, using EXOSAT and Ginga satellites, respectively. Elvis and Lawrence (1988) failed to detect soft X–ray absorption and Koyama *et al.* (1989) detected a low column density. The detected hard X–ray emission is consistent with the one observed in Seyfert 1 galaxies. All this seems to be consistent with the idea that we are not seeing directly the X–ray emission but in scattered light. Moreover, the scattering medium should be mostly composed of electrons because dust will produce strong soft X–ray absorption. Warwick *et al.* (1989) detected hard X–ray emission from the Seyfert 2 Mkn 348, although in this case strong absorption was at low energies. According to their interpretation this fact may indicate that unlike the previous cases, we are looking directly to the nucleus through a certain column density. A similar discovery was made for NGC 4388 by Hanson *et al.* (1990).

It seems unquestionable that those Seyfert 2 galaxies showing broad emission lines

in polarized light would be classified as Seyfert 1 galaxies if they were seen from the appropriate direction in the sky plane. However it is not clear if all Seyfert galaxies are of the same class, and their classification as type 1 or 2 will be uniquely a viewing aspect. There is some controversy on this point, an ample statement of the possible problems with the unification scheme is given by Miller (1989) and Miller and Goodrich (1990). Among the difficulties with this scheme, perhaps the most severe is the lack of the expected infrared reradiation of the absorbed fraction of the nuclear luminosity by the torus (Penston *et al.*, 1990).

In the following we will present some observations which are related to the presence of the obscuring torus. If we assume that all Seyfert galaxies are characterized by the presence of the thick obscuring torus with a characteristic opening angle θ_c, then it will be possible to predict for a sample of randomly oriented objects the fraction of obscured and unobscured objects. However this fraction is difficult to estimate observationally because selection effects can be operating in the choice of the sample. Perhaps the best opportunities will be offered by spectroscopic search techniques (Wasilewski, 1983; Osterbrock and Shaw, 1988) and by *no pre–selected objects*[1] infrared surveys, *e.g.* the complete, flux-limited IRAS survey of Lawrence *et al.* (1986) (for discussion see Lawrence [1987], and Miller and Goodrich [1990]).

The radio properties of Seyfert 1 and 2 galaxies could be used as a good indicator of the orientation effects which will differentiate both types of galaxies. If Seyfert 2 were predominantly oriented with their radio axis in the sky plane their radio sizes will be larger than the one observed in Seyfert 1 whose structure should be foreshortened due to the projection in our line of sight. Ulvestad and Wilson (1984) noticed such an effect and in addition they found that type 2 Seyferts are generally more powerful radio emitters. However, in a more recent paper the same authors (Ulvestad and Wilson, 1989) found the previous result to be a selection effect and only marginal differences are found in the two classes of objects for both radio luminosities and sizes.

2.2 THE MOLECULAR TORUS

The theoretical development of the idea of the thick obscuring torus suggested by Antonucci and Miller (1985) was rapidly undertaken by Krolik and Begelman (1986, 1988). In the present section we will review the major features of their model. A graphic impression of the model is given in Fig. 2.1. Other reference papers were published by Krolik where different aspects of the theory of the obscuring torus and the relation with the the Interstellar Medium in Seyfert galaxies are presented (Krolik, 1988; Krolik, 1989a; Krolik, 1989b). The material presented in this section is largely based on these works.

2.2.1 Location and Geometry of the Obscuring Material

The location of the obscuring torus was well constrained by the requirement to hide the BLR and leaving unocculted the NLR. Thus a likely distance from the nucleus for the inner edge of the torus will be of several parsecs. This distance results to be an interesting one, since at this location the gravitational potential due to the stars becomes comparable with the gravitational potential due to the central object.

[1] We mean by *pre–selected objects* those that are strong emitters in other bands.

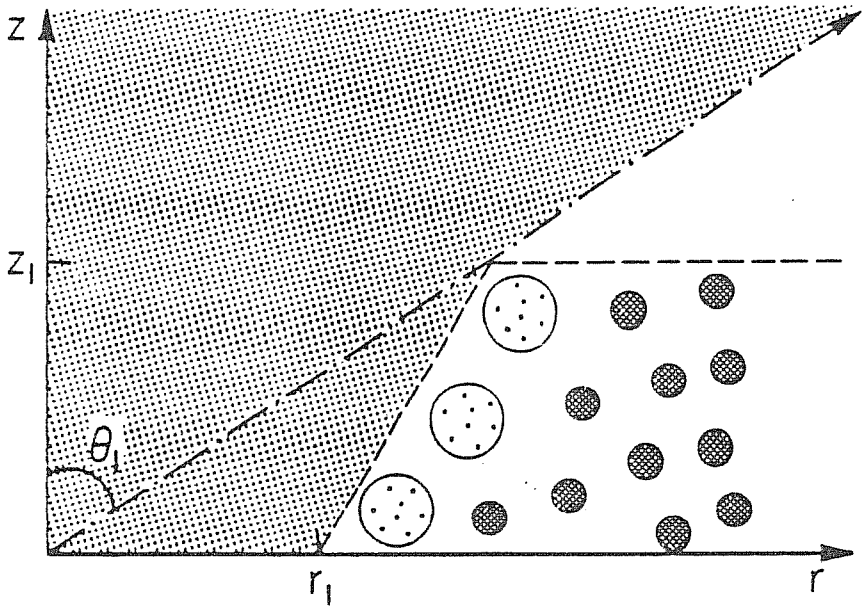

Figure 2.1: A schematic representation of the molecular torus. The obscuring torus is formed by optically thick molecular clouds (cross–hatched), which are orbiting around the nucleus and moving with high dispersion velocities. The nuclear continuum is located in the origin. The clouds directly exposed to the continuum light are strongly ionized and heated. These clouds (stippled) will expand until they reach the equilibrium with the external medium. However the physical conditions are such that the gas will be heated continuously by the radiation flux, and will tend to escape the region. This heated gas will flow away forming a wind (shaded area). This wind will be the scattering medium which allows to observe the inner of the torus at viewing angles close to the equatorial plane. Adopted from Krolik and Begelman (1986).

The material make up the torus is probably dusty, since dust is a very efficient absorber at the optical and ultraviolet frequencies. Krolik and Begelman (1988) assumed that all the galaxies with infrared excess possess a molecular torus. They used the fraction of Seyfert 2 present in the sample of Edelson, Malkan and Rieke (1987) to estimate the opening angle of the torus. The obtained value is $\sim 40°$, which indicates a geometrically rather thick torus.

In order to maintain the torus geometrically thick we must require that the material forming it has a large velocity dispersion, at least of the order of the stellar orbital velocity ($\sim 200 km\, s^{-1}$) at the location of the torus. If the random velocities correspond to the thermal motion of a gas, the temperature will be $\sim 10^6\, K$, and at such high temperatures the dust grains can not survive. Therefore the material will be likely clumped into small clouds with temperatures low enough to allow dust to survive. These clouds will move with the required random velocities. Krolik and Begelman (1986) further suggest that these clouds may be molecular clouds because there is a prominent starburst region extending up to distances of ~ 1 *kpc* from the nucleus in NGC 1068, and large quantities of molecular gas has been found associated with it (Scoville, Young and Lucy, 1983).

The clouds are confined by the external interstellar pressure present in the region, which can be inferred from the presence of the starburst region and scaled to the appropriate distance. The balance between cloud merging and the tidal shearing determines the shape of the cloud size distribution and at the same time produces a covering factor in the equatorial plane which is unity.

These clouds orbiting around the nucleus will receive the nuclear ionizing continuum. The inner face of the clouds will be photoionized and the temperature will be of the order of $10^4\ K$. Deeper in the clouds, when the ultraviolet photons have been absorbed the gas will receive only the X–ray photons which are those capable of penetrating farthest. The interior of the clouds therefore will be heated up to values of the order of $10^3\ K$ and the electron fractions will be relatively high for a molecular gas. The molecules will not be dissociated at this temperature and molecular emission lines will come from the torus. Krolik and Lepp (1989) investigated the internal state of the clouds. They found that a substantial fraction of the hard X–ray luminosity is deposited in the molecular clouds and the local reradiation is about half in molecular lines. However the emission lines are expected to be weak mainly due to the amount of dust which reabsorbs the line emission and to the large number of lines over which the energy is spread.

2.2.2 Dynamics of the Clouds

As we asserted above, to maintain the torus geometrically thick the clouds forming it should be moving with large dispersion velocities. The origin of these velocities is rather speculative. Krolik and Begelman (1988) showed that stirring by stellar processes is largely inefficient to compete with the losses by cloud collisions. Cloud-cloud collisions dissipate orbital energy producing a cloud inflow which may help to fuel the central object. Krolik and Begelman (1988) proposed viscous heating arising in the cloud collisions when shear stresses are present as a plausible mechanism. Such a mechanism is similar to that producing the velocity dispersion of dust particles in Saturn's rings (Goldreich and Tremaine, 1978). The heating rate by viscosity is proportional to $(d\,ln\Omega/d\,lnr)^2$ and hence it may change sharply when the gravitational potential

becomes dominated by the central black hole rather than by the stellar potential[2].

A balance between the viscous heating and the cooling by the cloud collisions is difficult to obtain because the quantities which are involved in both the heating and cooling are determined by independent processes. Therefore if there is net viscous heating the torus will inflate until the rotational reservoir of energy is exhausted, *i.e.* the velocity dispersion can not exceed the orbital velocity; when cooling by cloud collisions is dominant the clouds will be confined to the disk.

Since the viscous heating works to maintain the torus thick only under particular circumstances, then it is plausible to expect that the formation of a thick torus will be a difficult event, which may explain why some Seyfert 1 do not posses a thick torus.

2.2.3 The Electron Scattering Medium: An X–ray heated wind

The optical depth of the scattering medium should be less than 1 in order to account for the high observed polarization in the broad lines, but meanwhile the density of scatterers should be sufficient to reflect the nuclear continuum at the level we observe it. Krolik and Begelman (1986) estimated $\tau \sim 0.01$. On the other hand the maximum observed width of the polarized broad emission line puts an upper limit on the temperature of the scattering medium of the order of $10^6\ K$. Krolik and Begelman (1986) found that, using this value of τ and the common values for the luminosity the resulting ionization parameter[3] indicates that for $T \leq 10^6$ the gas will be in a state of net radiative heating (Krolik, MacKee and Tarter, 1981). If the gas were in hydrostatic equilibrium then the temperature would rise to the effective Compton temperature which is of the order of $10^7\ K$ for the observed continuum in Seyfert 1 (Mathews and Ferland, 1987). This temperature is in conflict with the maximum permitted value from the line width. On the other hand the virial temperature is lower than the Compton value. Therefore the most likely situation will be the formation of a radiation heated wind. The temperature will be determined by the balance between the heating by the nuclear radiation field and the adiabatic cooling due to the expansion. Krolik and Begelman (1986) estimated the temperature to be $\sim 10^6\ K$ at the base of the wind, close to the edge of the torus and then to decrease outwards.

Once the ionization parameter and the temperature in the wind have been determined the ionization level of the elements can be estimated assuming ionization equilibrium. It results that all the elements are stripped of the electrons, the exceptions are Fe and some fraction of Si and S which keep a few electrons. Therefore considerable Fe Kα emission is expected. Krolik and Kallman (1987) correctly predicted the Equivalent

[2] In the Galaxy $(d\,ln\Omega/d\,lnr) = 9/4$ at $r \leq 10\ pc$ and $(d\,ln\Omega/d\,lnr) \lesssim 1$ at $r > 10\ pc$.

[3] The ionization parameter used by Krolik, MacKee and Tarter (1981) is defined as the ratio between the radiation pressure and the gas pressure. The expression is:

$$\Xi = \frac{\int_{\nu_0}^{\infty} L_\nu/h\nu\, d\nu}{4\pi D^2 N_H c k T}$$

It differs from that used in the rest of this thesis, by a constant and the inclusion of the temperature in the denominator. The expression used here is:

$$U_t = \frac{\int_{\nu_0}^{\infty} L_\nu/h\nu\, d\nu}{4\pi D^2 N_H c}.$$

Width of this line as confirmed by Ginga observations (Koyama *et al.*, 1989).

2.2.4 Self–Regulating Mechanisms

The clouds making up the torus will loose orbital energy due to cloud collision losses, and hence a net inflow of clouds will be driven. This mass inflow is approximately matched by the total mass flux which is expected to be flowing out in the form of X–ray heated wind (Krolik and Begelman, 1988). When these inflowing clouds reach the inner edge of the torus, they will be strongly ionized and heated, as a consequence they will expand until the pressure equilibrates the external one in that region. When the external pressure is reached the value of the ionization parameter will have increased so much that the gas will be no more in equilibrium and will heat and expand more, forming the wind (Krolik and Begelman, 1986).

Furthermore an important mechanism of self–regulation of the accretion may be taking place here. The cloud–cloud collisions continuously drive matter inward, but some part of this matter will not be blown up contributing to the radiation heated wind, but will be accreted by the central object. The mechanism of accretion has not been mentioned here, but it should be any kind of accretion disk because the inflowing matter may have sufficient angular momentum. If more matter is accreted the radiative flux produced by the nucleus (*e.g.* accretion disk) will be increased, and consequently the evaporation of the clouds will be increased in the inner edge of the torus. Hence the supply of matter to the inner accretion disk will decrease and equally the radiation flux, establishing a feed–back mechanism. (Krolik and Begelman, 1988).

Chapter 3

PHYSICAL CONDITIONS AND IONIZATION MECHANISMS IN THE ENLR

3.1 INTRODUCTION

In Chapter 1 we discussed the morphology of the extended line emitting gas around Seyfert galaxies. The emission spectrum presents high ionization lines and photoionization by the nuclear continuum seems to be the only efficient excitation mechanism: heating and compression by the radio component can be ruled out since no direct spatial relationship is observed; local ionization is unlikely because the spatial distribution of the continuum emission differs largely from that of the lines. In this respect an anisotropic nuclear radiation field can account for the peculiar conical shape of the line emitting region.

In this Chapter we investigate in more detail the physical conditions (namely, density and temperature) present in the extended nebulosities, confirming that photoionization is the main excitation mechanism for the line emission. We will also discuss the similarities of the emission line spectrum from the Extended Narrow Line Region (ENLR) with the inner and only marginally resolved Nuclear Narrow Line Region (NNLR, or simply NLR). We recall that the distinction between both regions is based purely on the kinematics of the gas: NLR gas will be affected by radial motions instead ENLR will be kinematically undisturbed gas reflecting the motions of the underlying galactic gas. Different ionizing continua will be proposed and their ability to reproduce the emission line spectrum will be discussed.

3.2 PHYSICAL CONDITIONS OF THE LINE EMITTING GAS

The emission line spectrum observed from the ENLRs is characterized in the optical band by the presence of the Balmer lines, Hα (λ6563) and Hβ (λ4861), the recombination line HeII λ4686 and several forbidden lines, combining both high ionization, such as [OIII] λ5007 (the most intense line), [NeIII] λ3869 and [NeV] λ3426, with low ionization lines, such as [OI] λ6300, [SII] $\lambda\lambda$6716, 6731, [NII] $\lambda\lambda$6548, 6584 and [OII] λ3727. This line spectrum resembles that of a planetary nebula, although a larger range of ionization is now present. Consequently similar procedures to those applied in low density

gaseous nebulae can be used to determine the physical conditions in the emitting gas.

3.2.1 Density

The presence of the forbidden lines places upper limits on the density. The density should be lower than the critical density for collisional deexcitation starts to be relevant. Among the observed lines, [OII] λ3727 has the lowest critical density, which is around $10^3\ cm^{-3}$. The low surface brightness of the nebulosities and the low resolution of the spectra do no allow to use in all cases the doublet ratios [SII] λ6716/λ6731 and [OII] λ3729/λ3726, to determine the density (Osterbrock 1974). Nevertheless in the cases where it has been possible to measure directly the density from the doublet ratios the values range from $10^2 cm^{-3}$ for NGC 4151 (Penston *et al.*, 1990) to $10^3 cm^{-3}$ for NGC 1068 (Baldwin, Wilson and Whittle, 1987). Therefore the observed values confirm that we are below the critical density limit for all the observed transitions, and collisional deexcitations will not be relevant for the ionization equilibrium.

3.2.2 Temperature

The temperature of the gas is an important parameter which allows to identify the excitation mechanism. The typical electronic temperatures T_e reached by photoionization are in the range 10000 - 15000 K, higher values than these are only attained either by collisional ionization or by additional heating sources, such as shock compression, or energetic particles.

The strength of the line [OIII] λ4363 with respect to the lines [OIII] $\lambda\lambda$4959, 5007 is an increasing function of T_e. This line is generally difficult to detect however it has been measured for several ENLRs: Penston *et al.* (1990) found a value of 14000 K for NGC 4151, in the case of NGC 3516 the values $T_e \sim$ 13500 and $\sim$ 19000 K are found (Pogge, 1989a). Tadhunter, Robinson and Morganti (1989) estimated T_e from the [OIII] ratio in several ENLRs, using data for emission line radio galaxies (Tadhunter, 1987) including also the Seyfert galaxies NGC 5252, NGC 4151 and NGC 3516. They found that the derived temperatures are relatively high ($T_e \sim$ 10000 – 20000 K), when compared to the values predicted by photoionization models ($T_e \leq$ 11000 K), which are otherwise successful explaining the emission lines. The most plausible explanation for this discrepancy considers heating sources others than photoionization or alternatively a much lower ratio O/H than the assumed solar value, since in this case the effective cooling line [OIII] λ5007 will not be able to maintain the temperature in the H^+ region. The values of T_e predicted when using our ionizing continua (thick accretion disk emission) are in the range of observed values (see Table A.1), and they are usually higher than those predicted by the models considered by Tadhunter, Robinson and Morganti (1989), although our ionizing continua seems to be rather hard when the predicted emission lines are compared with the observations. (this point will be further discussed in Chapter 5). We believe that the "space" of the possible ionizing continua has not been completely explored and the inclusion of hard components would be helpful to overcome this difficulty. A similar problem was found by Stasińska (1984) modelling the NLR, the proposed solution was to consider a two densities system, high density gas shows a high value of the line [OIII] λ4363, although this may be not appropriate for the ENLR where rather low densities are observed. We can conclude that the temperature of the ionized gas is consistent with photoionization being the main excitation mechanism.

Assuming ionization equilibrium and the limit of low density gas, the ionization level of the elements will be uniquely determined by the number of photons with energy larger than the corresponding ionization potential per atom. The ionization equilibrium condition for any ionic specie and its contiguous can be written as:

$$n(X^i)\int_{\nu_i}^{\infty}\frac{4\pi J_\nu}{h\nu}a_\nu(X^i)d\nu = n(X^{i+1})n_e\alpha(X^{i+1},T_e),$$

where $a_\nu(X^i)$ and $\alpha(X^{i+1},T)$ are absorption and recombination coefficients, respectively. Then doing some approximations (see Osterbrock [1974]) for justifications) it results:

$$n(X^i)a(X^i)\int_{\nu_i}^{\infty}\frac{4\pi J_\nu}{h\nu}d\nu = n(X^{i+1})n_e\alpha(X^{i+1},T_e).$$

An arrangement of this expression leads to:

$$\frac{n(X^{i+1})}{n(X^i)} = \frac{a(X^i)}{\alpha(X^{i+1},T_e)}\frac{1}{n_e}\int_{\nu_i}^{\infty}\frac{4\pi J_\nu}{h\nu}d\nu$$

Neglecting the diffuse radiation field we can take $4\pi J_\nu = L_\nu/4\pi D^2$ and therefore we may write:

$$\frac{n(X^{i+1})}{n(X^i)} = \frac{a(X^i)}{\alpha(X^{i+1},T_e)}\frac{1}{n_e}\int_{\nu_i}^{\infty}\frac{L_\nu}{4\pi D^2 h\nu}d\nu$$

Equivalently, the above expression can be rewritten as a function of the ionization parameter U_t, which is defined by:

$$U_t = \frac{\int_{\nu_0}^{\infty} L_\nu/h\nu\ d\nu}{4\pi D^2 n_H c},$$

where L_ν is the monochromatic luminosity, ν_0 is the frequency corresponding to 1 ryd, n_H is the hydrogen density of the ionized clouds, D is the distance from the ionizing source. The final expression is:

$$\frac{n(X^{i+1})}{n(X^i)} = \frac{a(X^i)}{\alpha(X^{i+1},T_e)}\frac{\int_{\nu_i}^{\infty} L_\nu/h\nu d\nu}{\int_{\nu_0}^{\infty} L_\nu/h\nu d\nu}\,c\,U_t,$$

from which we may extract the fact that the ionization level is proportional to the value of U_t. In the derivation of this formula we have assumed that the gas is optically thin, but most likely in a real situation the photons will be absorbed through the nebula and the ionization level of any element will depend also on the radiation transfer inside it. Nevertheless, the relative intensity of the different emission lines will be directly related to the number of photons which is available to excite each ionic specie.

3.3 SPECTROSCOPIC EVIDENCES FOR PHOTOIONIZATION BY THE NUCLEAR EMISSION

A first guess about the characteristics of the ionizing continuum can be obtained from the classification method proposed by Baldwin, Phillips and Terlevich (1981), and more recently refined by Veilleux and Osterbrock (1987). They looked for a single line ratio which is able to separate objects photoionized by different continua, but without

success. Instead the successful method combines the values of two line ratios in a bidimensional diagram, which effectively divide the area into two zones corresponding to: gas ionized by stellar continuum as corresponding to H II regions, and gas ionized by a *power law* continuum as corresponding to Active Galactic Nuclei. The involved line ratios are [OIII] $\lambda 5007/\mathrm{H}\beta$, [NII] $\lambda 6584/\mathrm{H}\alpha$, [SII] $\lambda\lambda 6716, 6731/\mathrm{H}\alpha$ and [OI] $\lambda 6300/\mathrm{H}\alpha$. These line ratios are chosen on the basis of several requirements: they should be strong lines and not widely separated in wavelength to avoid reddening and flux calibration errors. The above line ratios are combined in the following way: the ratio [OIII] $\lambda 5007/\mathrm{H}\beta$ is presented in one axis, whereas any of the other ratios is presented in the other.

It is not difficult to understand how these diagrams are constructed. The feature which differentiates the ionizing continuum in the two classes of objects mentioned above is the extension to the X–ray energies, which is not present in the stellar continua but is important for power laws. The ratio [OIII] $\lambda 5007/\mathrm{H}\beta$ is not sensitive to the details at X–ray energies whereas the rest of mentioned ratios are primarily dependent on that part of continuum. It is shown empirically that the H II regions line emission presents weaker low ionization lines, especially [OI] $\lambda 6300$, than *power law* ionized objects do. This difference derives from the extension to X–ray energies in the *power law*, as we mentioned above. Since the absorption cross–section of H^0, He^0, He^+ and other ions decrease rapidly with increasing energy, the X–ray photons can penetrate deeply in the region where H is mostly neutral. Eventually these X–ray photons can be absorbed in the neutral region producing energetic electrons. These electrons has sufficient energy to ionize H^0, creating in this way an extended partially ionized region. In this zone the dominant forms of O, S and N are O^0, S^+ and N^0, and some fraction of N^+ and O^+ is also present, since N^0 and O^0 have similar ionization potential to H they can be also collisionally ionized. Hence the low ionization lines are produced in this region when the ionizing continuum has an X–ray component. However the partly ionized region is not present when the stellar emission is the ionizing continuum. In this case the low ionization lines can only be produced in the inner part (the opposite to that facing the nucleus) of the full ionized region, depending on the degree of ionization.

In the cases where spectroscopical data are available for the line ratios in the ENLRs, they are mostly located in the *power law* ionized region in the diagnostic diagrams: NGC 4388 (Pogge, 1988b); NGC 3516 (Pogge, 1989a); and several other objects (Pogge, 1989b). Although in some cases according to the location in the diagrams, the line emission can be interpreted as originated with a composite mechanism: NGC 1068 (Baldwin, Wilson and Whittle, 1987); NGC 5728 (Pogge, 1989b). In the latter cases the line emission can be interpreted as a superposition of H II regions emission plus the high excitation emission, *i.e.* we will observe different emitting regions which are physically separated, but appear to be coincident due to projection effects.

On the other hand the line ratio observed in the ENLR around Seyfert galaxies and low-z radio galaxies lies in the same region of the diagnostic diagrams (a similar result was found by Cohen and Osterbrock [1981] for the Nuclear NLRs), which indicates that the relevant excitation mechanism does not depend on the radio properties (*e.g.* see Fig. 3.2).

TABLE 3.1: OBSERVED EMISSION LINES IN ENLRS

Object	[OIII]/Hβ	[OII]/Hβ	[OI]/Hβ	[NII]/Hβ	[SII]/Hβ	HeII/Hβ	[NeIII]/Hβ	[NeV]/Hβ	[OIII] λ4363/Hβ	Hα/Hβ	Ref.
Seyfert 2	11. (3.)	3.2 (1.7)	0.57 (0.2)	2.9 (1.0)	1.5 (0.5)	0.29 (0.1)	1.4 (0.4)	1.2 (0.2)	0.21 (0.1)	3.1 (0.1)	□
NGC 1068	6.7	5.1	0.85	3.0	0.84	0.39	2.3	...	0.22	3.01	◇
NGC 1068 1	3.7	2.4	0.15	2.1	0.87	0.28	0.83	2.2	0.11	3.1	⋆
NGC 1068 2	6.2	3.1	0.29	2.5	1.3	0.35	1.4	1.9	0.21	3.1	⋆
NGC 1068 3	2.9	3.1	0.15	0.65	1.1	0.15	0.86	0.82	0.27	3.1	⋆
NGC 2110	7.3	...	1.0	6.0	4.4	...	...	...	...	3.1	•
NGC 3516	10.	2.6	0.45	4.0	2.3	0.30	0.80	1.2	0.12	3.5	△
NGC 3516 (NE)	10.	3.5	0.23	3.8	2.1	0.26	1.2	0.25	0.33	3.8	♣
NGC 3516 (SW)	9.2	3.5	0.25	4.5	2.2	0.35	0.92	0.21	0.14	3.8	♣
NGC 4151	13.	2.4	0.25	1.2	1.0	0.38	1.0	0.60	0.24	2.8	♠
NGC 4388 a[i]	8.7	...	0.30	2.2	1.7	...	...	...	...	2.7	♡
NGC 4388 c[i]	16.	...	0.03	2.1	0.75	...	...	...	...	2.9	♡
NGC 4388 d[i]	9.7	...	0.58	1.8	1.9	0.31	...	...	...	2.9	♡

The symbols of the references correpond to: □ Ferland and Osterbrock (1986); ◇ Baldwin, Wilson and Whittle (1987); ⋆ Bergeron, Petitjean and Durret (1989); • Pogge (1989b); △ Ulrich and Péquignot (1980); ♣ Pogge (1989a); ♠ Penston *et al.* (1990); ♡ Pogge (1988b).
[i] a,c and d refer to Table 1 in Pogge (1988b).

3.4 COMPARISON WITH THE NUCLEAR NLR SPECTRUM

The emission line spectra observed in the ENLRs closely resembles that observed in the inner nuclear NLR. In Table 3.1 (also in Fig. 3.1) we present the line intensities relative to Hβ, for comparison we present the same values for the mean Seyfert 2 spectrum as derived by Ferland and Osterbrock (1986). The main differences of the ENLR spectrum which are noticed with respect to the nuclear one (represented by the mean Seyfert 2), are summarized in the following:

- [OII] λ3727/Hβ and HeII λ4686/Hβ show similar values in both cases.
- The values of [OIII] λ5007/Hβ , [NII] λ6584/Hβ, [SII] $\lambda\lambda$6716,6731/Hβ and [NeV] λ3426/Hβ are spread in a wide range including the mean value for the nuclear region.
- The line ratios [OI] λ6300/Hβ and [NeIII] λ3869/Hβ tend to be lower than observed in the nuclear zones.

These differences are mostly apparent and far for being established. Moreover the values of the line ratios for different objects, instead of being clustered around an average value could tend to form a sequence of values corresponding to variations of physical conditions in the various objects. This feature was noticed by Robinson *et al.* (1987) for the ENLRs around emission line radio galaxies. Moreover it was found in their sample that ENLRs show usually lower [OI] λ6300/[OIII] λ5007 coincident with lower [OI] λ6300/Hα , [NII] λ6584/Hα and [SII] $\lambda\lambda$6716,6731/Hα and higher [OIII] λ5007/Hβ , relative to the nuclear value corresponding to the same object. Their interpretation is that ENLRs are probably characterized by a higher value of the ionization parameter than Nuclear NLRs.

It is striking that such similar emission line spectra from two regions which are spatially separated by at least one order of magnitude in distance from the ionizing source[1]. There should be a dilution of the radiation field by a factor of $\gtrsim 10^2$ which will be reflected in a decreasing degree of ionization level of the emitting gas, contrary to the observed constancy. This will imply that the density will decrease as $1/D^2$ to either keep constant U_i or increasing its value. This is not confirmed observationally, although NNLR models require often densities $\sim 10^4 cm^{-3}$, whereas ENLR estimates do not exceed much $10^3 cm^{-3}$. We discuss below an alternative to this solution (Sect. 3.6) .

Since the emission line spectra of ENLR and NNLR are so similar, it will be worth to mention the attempts which has been made to model the NLR emission. The spatial structure of the NLR models can be divided into three groups:

[1] The NNLR is located at $\sim$ 100 *pc*, whereas the ENLR is at $\sim$ 10 *kpc*. Probably both regions are smoothly connected and are parts of the same region, but the present observations do not allow to confirm this point and the spectra are taken from separated spatial regions. The high spatial resolution of the Hubble Space Telescope would make to disappear the distinction between the two zones. Actually the ground based telescopes has a resolution limit about $\sim$ 1" which corresponds to distances $\sim$ 100 *pc* for the nearby objects, *e.g.* at the distance of NGC 4151 ($z = 0.0033$). The Space Telescope will lower this limit in one order of magnitude and up to objects distant such as $z = 0.03$ it will resolve $\sim$ 100 *pc*. This estimates are done being a little bit pessimistic about the current focusing problems.

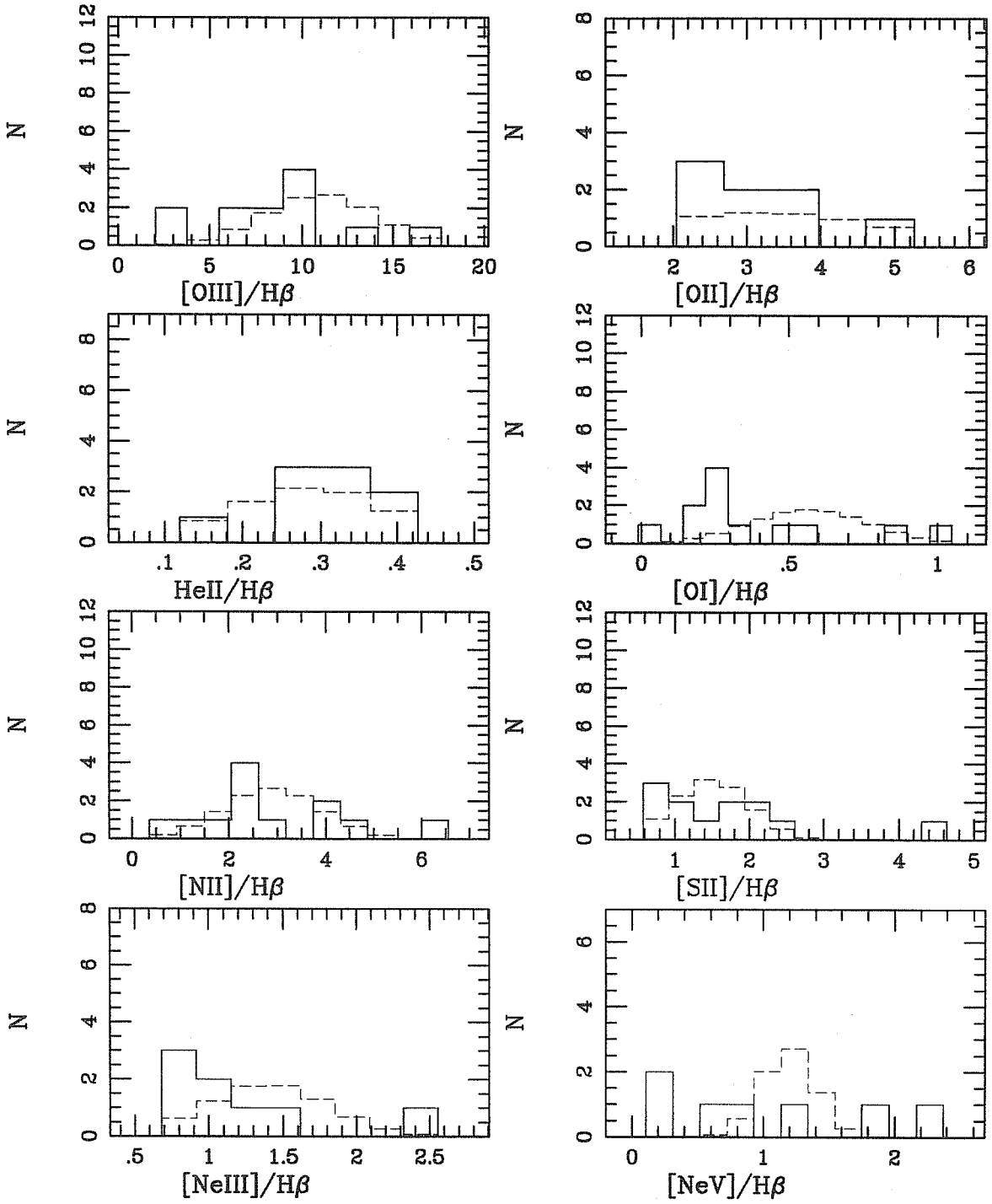

Figure 3.1: Histogram of the line ratios observed in the ENLR around Seyfert galaxies. The base of the histogram bars corresponds to a relative error of the emission line of 20 %. In spite of the small sample, note the large dispersion of the data.

- The simplest consists of a single density cloud located at a certain distance from the ionizing source (Ferland and Netzer, 1983; Halpern and Steiner, 1983; Stasińska, 1984). The existence of inhomogeneities and possible stratification of the density may rule out this model, although it can be taken as a first approximation when the range of distance from the ionizing source is relatively narrow.

- A more realistic approach will allow for stratification of the density $N(r)$ and a range of ionization which comes from a certain range of distance from the nucleus. The gas will be condensed in small filaments, which are individually optically thin (this is modelled by a volume filling factor), although cumulatively they may become optically thick (MacAlpine, 1972).

- The most likely situation will consist of small clouds which are individually optically thick and the whole system will extend over a large range in distance from the ionizing source (Osterbrock, 1984). This approach is the most sophisticated and the dimensions of the clouds and shadowing effects would be considered.

Ferland and Mushotzky (1982) modelled the NLR in NGC 4151 using an ionizing continuum (the low frequencies are dominated by a power law with index 1.5 whereas the X–ray part has an index 0.5) in which the radiation of energies $\leq$ 3 keV was absorbed by the Broad Line Region material. The NLR is modelled as an uniform plane parallel slab ($N_H = 10^{3.5}\ cm^{-3}$), the thickness of the slab is determined by the strength of the line [OI] λ6300 relative to Hβ. The results do not agree simultaneously with the observed values of [OIII] λ5007 and [OII] λ3727. Moreover the temperature seems to be underestimated and the ratio [OIII] λ5007/Hβ is large for most values of U_l. However if the abundances of the heavy elements are lowered these problems will be alleviated, and in fact the agreement with the observed values is improved. This occurs because [OIII] λ5007 is an important cooling of the H^+ region, therefore reducing the presence of O the temperature will increase.

Stasińska (1984) made a very detailed comparison of the observed emission lines for a sample of Seyfert and narrow-line radio galaxies with the predictions of photoionization models. The clouds are assumed to be plane parallel slab with constant density and located at a fixed distance to the nucleus. In this work a wide range of ionizing continua was explored together with the variation of U_l, gas density and element abundances. Among the most interesting results it is worth to mention:

- Black bodies with T_{eff} in the range $10^4 - 10^5$ K are able to reproduce well the line ratios, besides the standard power law continua.

- The theoretical curves in the diagram [OIII] λ5007/Hβ vs. [OII] λ3727/Hβ are insensitivity to the spectral shape of the continuum.

- The predicted values of [OII] λ3727/Hβ are found to be below the observed ones.

- The observed values of the ratio [OIII] λ4363/$\lambda\lambda$4959, 5007 are higher than those predicted by the models. This ratio is sensitive to the temperature, although it becomes also sensitive to the density, increasing with it when $N_H \gtrsim 10^5\ cm^{-3}$. Furthermore this ratio tends to decrease with the ratio [OIII] λ5007/[OII] λ3727 increasing.

- The line ratios [SII] $\lambda 6716/\lambda 6731$ and [SII] $\lambda 4070/\lambda\lambda 6716, 6731$ are both sensitive to the density. However the observed values for the latter ratio are higher than the predicted values, requiring to increase the density to agree with observations. In addition, the second ratio shows a trend to increase with the ratio [OIII] $\lambda 5007$/[OII] $\lambda 3727$ increasing.

It was proposed that a way to reconcile the model predictions with the observed ratios is to have a gas with two densities: a high density ($N_e \geq 10^6 cm^{-3}$) with similar value of U_t for all the objects, and then a low density ($N_e \leq 10^4 cm^{-3}$) for which U_t varies from object to object, which accounts for the different observed ionization as measured by the ratio [OIII] $\lambda 5007$/[OII] $\lambda 3727$. In this way the high density clouds produce high values for the ratios [SII] $\lambda 4070/\lambda\lambda 6716, 6731$ and [OIII] $\lambda 4363/\lambda\lambda 4959, 5007$, then the low density component will tend to lower the value of the latter ratio when U_t increases, whereas the former ratio will tend to decrease in the low density component when U_t decreases. The interesting idea emerging from this work is that the emission line region is composed of a system of clouds rather than a homogeneous model. This idea is also supported by the kinematical studies of line profiles (Filippenko, 1986; DeRobertis and Osterbrock, 1984).

Ferland and Osterbrock (1986) derived a mean NLR spectrum (see Table 3.1) using both optical and ultraviolet observations of Seyfert 2 galaxies. Photoionization by a power law continuum ($F_\nu \propto \nu^{-1.4}$) whose index is inferred directly from the observations of the continua, can reproduce the emission line spectrum. The geometry of the NLR is assumed to be spherical, with a power law density distribution and an uniform filling factor. The density at the inner radius is fixed in order to allow for the presence of very high ionized species, like FeX, moreover certain values of the density are required to have values lower than the critical in the zones of emission of relevant lines such as [OIII] $\lambda 5007$ ($N_e \sim 10^5 cm^{-3}$) or [SII] $\lambda\lambda 6716, 6731$ ($N_e \sim 10^3 cm^{-3}$). The filling factor f is determined from the whole extension of the emitting region. Since low values of f will lead to very extended regions and large production of emission in the low ionization lines [OI] $\lambda 6300$ and [OII] $\lambda 3727$. Hence the extension of the zone is limited by the value of f which reproduces the observed values of the ratio between the two mentioned lines.

Binette, Robinson and Courvoisier (1988) adopted the same geometry as Ferland and Osterbrock (1986) but they concentrated in the analysis of the ionizing continuum variation. The main result from this work is the establishment that black bodies with T_{eff} in the range $1.2 - 1.6 \times 10^5$ K are as good candidates for the ionizing continuum of the NLR as the conventional power law with index 1.5. The main inconveniences for the black bodies model concern the weakness of the [SII] $\lambda\lambda 6716, 6731/\mathrm{H}\beta$ and an overestimation of the ratio [OI] $\lambda 6300/\mathrm{H}\beta$. The former ratio can be increased with the addition of an X–ray component, which makes to increase the latter ratio, and then leading to a bigger problem for it. A noticeable characteristic of the black body as ionizing continuum is the sensitivity of the ratio HeII $\lambda 4686/\mathrm{H}\beta$ to the value of T_{eff}, and furthermore with high values of T_{eff} such ratio can reach the observed values which are not possible to reach with power law models. The results show that a reasonable fit to the NLR spectrum can be obtained independently of the slope of the ionizing continuum at the Lyman limit, it depends mainly on the mean ionizing energy $\bar{\varepsilon}$ of the photons. The continua which have $\bar{\varepsilon} < 50$ eV produce a good agreement with the observed values; instead those which have $\bar{\varepsilon} > 50$ eV predict very strong low ionization lines arising from the partially ionized region. These authors found also that the geometry adopted for the NLR affects predominantly the lines produced in the

partially ionized region. Differences between the line spectra predicted by black body and power law are larger in the case of a plane parallel slab than in a spherical geometry, and affect predominantly the lines produced in the partially ionized region. The reason for such behaviour can be envisaged by looking at the fraction of the continuum which is absorbed in the whole emitting region. In a spherical geometry the X–ray part is less absorbed than in the plane parallel slab because the optical depth is smaller due to the decreasing density distribution by the geometrical dilution.

Based on the variation of HeII $\lambda 4686/\mathrm{H}\beta$ with T_{eff}, Binette, Courvisier, and Robinson (1988) derived constraints on the shape of the extreme UV/soft X–ray ionizing continuum for the NLR. This portion of the continuum can not be directly observed due to the galactic absorption by neutral H. No values of HeII $\lambda 4686/\mathrm{H}\beta$ larger than 0.5 are observed in Seyfert 2 galaxies. Limiting the value of the ratio HeII $\lambda 4686/\mathrm{H}\beta$ to this maximum and using black body as ionizing continuum they derived an upper limit to T_{eff}. The results show that to be consistent with the observations the flux at 105 eV can not exceed 15 % of the flux at the Lyman limit. This fact limits the amount of energy which is conveyed in the nuclear continuum combining the values either at far UV or soft X–rays. These energies represent respectively, the low and high energy end of the "big blue bump" (see Section 4.2.2), where rising slopes into the unobserved region are present in some cases.

Viegas–Aldrovandi (1988) considered the case in which NLR clouds are not completely thick, this is suggested by an anticorrelation observed between the ratio HeII $\lambda 4686/\mathrm{H}\beta$ and the low ionization lines [OI] $\lambda 6300/\mathrm{H}\beta$ and [NI] $\lambda 5200/\mathrm{H}\beta$. The observed values of these ratios can be explained if the NLR is formed by a combination of optically thin and thick clouds.

The effect of relativistic electrons in the ionization and heating of the gas in the NLR clouds has been considered by Ferland and Mushotzky (1984) and Viegas–Aldrovandi and Gruenwald (1988). The main effect of relativistic electrons is to increase the temperature, consequently a better agreement with the observations is attained for the temperature sensitive ratio [OIII] $\lambda 4363/\lambda\lambda 4959, 5007$ and the low ionization lines. The effect of shock heating combined with the photoionization by a power law has been studied by Viegas–Aldrovandi and Contini (1989) showing that shock heating is comparable to photoionization when the ionization parameter is low.

3.5 PHOTOIONIZATION OF THE ENLR

The geometry of the emitting gas in the Extended NLR is not as complex as in the case of the Nuclear NLR. The basic difference arises from the fact that the Extended NLR are well resolved spatially and therefore the range in distance from the central source is limited locally by the resolution of the observations. Furthermore the presence of strong [OI] $\lambda 6300$ and other low ionization lines such as [SII] $\lambda\lambda 6716, 6731$ and [NII] $\lambda 6584$ indicates that the emitting structures are optically thick. In such case the extension of the clouds can be estimated from the Strömgren radius which is of the order of 10^{18} cm, ($10^{18} - 10^{19}$ cm as can be read from Table A.1 for the most likely value of U_l derived from the observed line ratios, see below). The distance of the emitting gas from the ionizing source is of the order of 1 kpc, which makes a plane parallel slab a good approximation to the geometry of the Extended NLR clouds. In addition, no clear evidence for strong density gradients is found. Therefore the most appropriate description for the ENLR will consist of a number of unresolved optically thick clouds

at a given distance from the nucleus, which is confirmed by the derived values of the filling factor.

Ulrich and Péquignot (1890) calculated the photoionization by an power law continuum ($F_\nu \propto \nu^{-1}$) for the extended line emission they found around NGC 3516, in two cases: optically thin and thick slab. Their results confirm that an optically thick cloud model can well reproduce the relative line intensities of OI, OII and OIII for a certain range of the hydrogen density ($N_H = 10 - 100 cm^{-3}$). The only drawback of this model is the slightly high value of the OIII lines; an alternative model with lower oxygen abundance was then proposed, and was in better agreement with the observed lines. Moreover they found that an extension of the clouds of the order 10^{19} cm gives reasonable line ratios.

Robinson *et al.* (1987) noticed that the line ratios observed in the ENLR of line–emission radio galaxies (Tadhunter, 1987) are consistent with photoionization by a continuum with $\bar{\varepsilon}$ in the range of 30-40 eV. A plane parallel geometry and constant density $N_H = 100$ cm^{-3} is assumed, moreover the clouds will be optically thick, *i.e.* radiation bounded. Photoionization by hot stars is clearly insufficient to produce the observed [OIII] λ5007/Hβ and [OI] λ6300/Hα ratios. The spectral shapes of the continuum which are examined by these authors are single power laws and black bodies with relatively high T_{eff} ($\sim$ 100000 K). The best agreement with the observations is found using a power law $F_\nu \propto \nu^{-1.5}$ and a black body with $T_{eff} = 130000$ K. We have repeated their calculations, and present diagnostic diagrams including several additional line ratios in Figure 3.2, with the observed line ratios for ENLR in both Seyfert and radio galaxies. The models are calculated using the photoionization code MAPPINGS, a brief description of which is given at the end of this section. The diagnostic diagrams are adopted from Baldwin, Phillips and Terlevich (1981) and Veilleux and Osterbrock (1987), except that the abscissa is now the ratio [OI] λ6300/[OIII]λ5007. This ratio is very effective in separating the NLR and ENLR ratios from the normal H II and planetary nebula: the latter objects have usually values of this ratio ≤ 0.01 and will lie beyond the left edge of these diagrams (Robinson *et al.*, 1987). Moreover [OI] λ6300 and [OIII] λ5007 are insensitive to the density up to $N_e \simeq 10^6 cm^{-3}$, instead the line [OII] λ3727 is sensitive to values $N_e \simeq 10^3 cm^{-3}$. The line [OII] λ3727 lies in a frequency range where CCD detectors are less sensitive and therefore it is difficult to measure it.

A striking feature which emerges from a first inspection of Fig. 3.2 is the distribution of the line ratios along a sequence, particularly evident for [OIII] λ5007/Hβ , [OI] λ6300/Hα , [NII] λ6584/Hα and [SII] $\lambda\lambda$6716,6731/Hα . As it is evident from the model calculations, this sequence corresponds to a variation of the ionization parameter. The ratio HeII λ4686/Hβ remains almost constant, which is consistent with this explanation, since this ratio does not depend essentially on the value of U_t (Binette, Courvoisier and Robinson, 1988). The absence of any trend in the other ratios [OII] λ3727/Hβ and [NeIII] λ3869/Hβ can not be interpreted in the same terms but it is probably an effect of the scarcity of data.

The predictions for the black body and power law run almost parallel for several line ratios (*e.g.* [OIII] λ5007/Hβ , [OI] λ6300/Hα , [SII] $\lambda\lambda$6716,6731/Hα and HeII λ4686/Hβ), although for a given value of [OI] λ6300/[OIII] λ5007 the corresponding value of U_t is much smaller in the black body than in the power law case. This is because the black body continuum is more effective ionizing O^+ than the power law, which on the contrary carries much energy in the X–ray part favoring the exis-

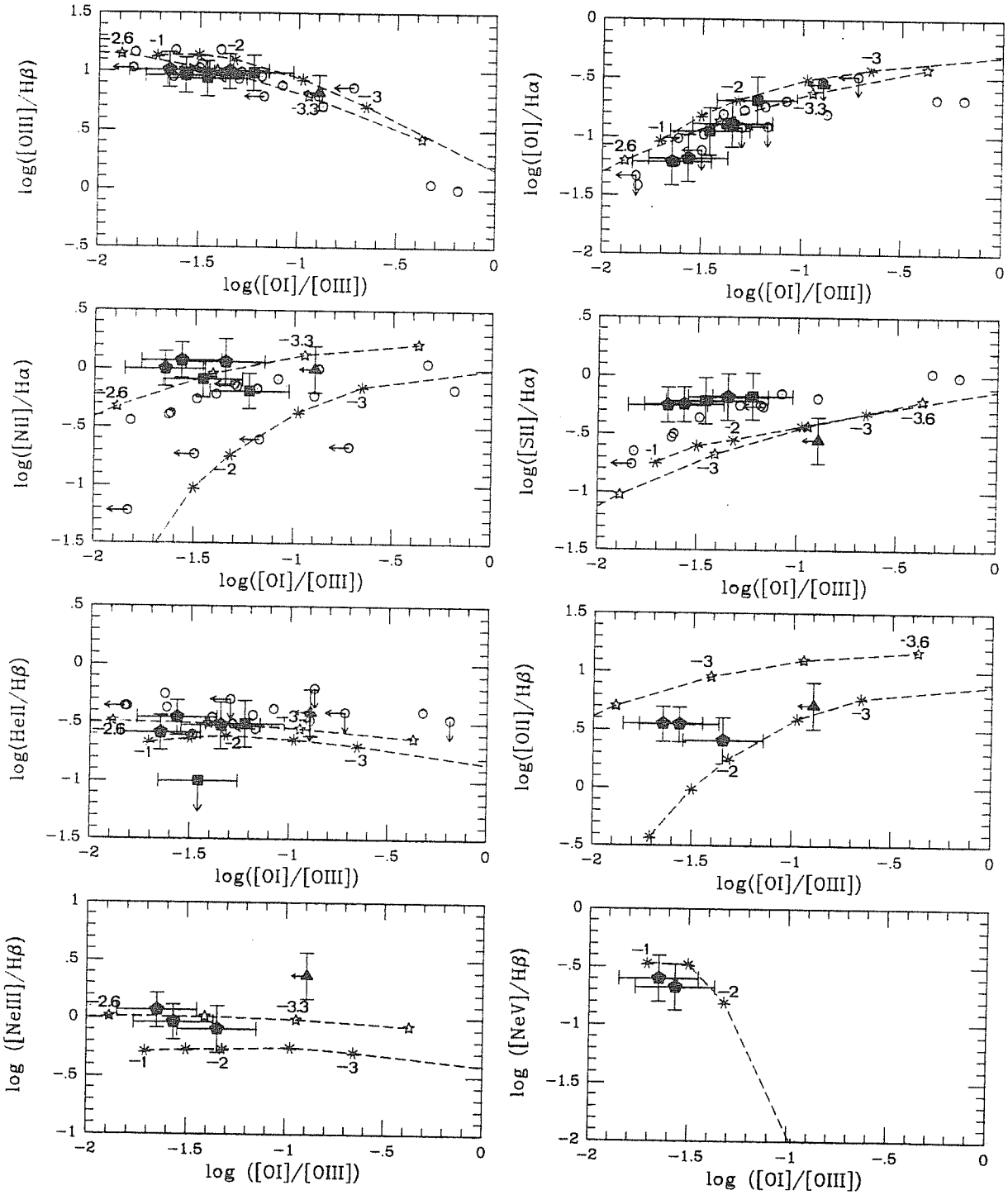

Figure 3.2: Black body and power law predictions for several important line ratios. The curves join theoretical points corresponding to the variation of U_t (log U_t is indicated). The black body predictions are represented by stars, whereas the power law by asterisks. The observational data are indicated by the following symbols: filled triangles for NGC 1068 (Baldwin, Wilson, and Whittle 1987), filled pentagons for NGC 3516 (Ulrich and Péquinot 1980; Pogge 1989a), filled squares for NGC 4388 (Pogge 1988b) and open circles for line–emission radio galaxies (Tadhunter 1987). Notice the good agreement for most of the observed line ratios with the predicted ratios. The observed ratios apparently define a sequence in the diagnostic diagrams, which can be associated with the variations of U_t along the theoretical curves.

tence of the partly ionized H^0 region, where most of the line [OI] λ6300 is produced. Most of the observed values are well predicted for these ratios, except for the ratio [SII] $\lambda\lambda 6716, 6731/H\alpha$ which lies well above the predictions for both ionizing continua.

The predicted curves using black body and power law for [OII] $\lambda 3727/H\beta$ and [NII] $\lambda 6584/H\alpha$ are well separated in the diagnostic diagrams. The separation is merely an effect of the different value of the ratio [OI] $\lambda 6300/$[OIII] $\lambda 5007$. The values predicted for [OII] $\lambda 3727/H\beta$ and [NII] $\lambda 6584/H\alpha$ are similar for both ionizing continua. The insensitivity of both line ratios to the continuum shape arises from the fact that they are mainly produced in the inner parts of the H^+ region and their strength depends on the number of photons with energies close to $1ryd$.

The predictions using the black body continuum for [NeIII] $\lambda 3869/H\beta$ are above the power law predictions. This ratio does not vary with U_t. This line is also produced in the inner part of the H^+ region. At low value of U_t the black body is more effective producing Ne^{2+}, and at high U_t the power law is more effective ionizing higher than Ne^{2+} ionization stages and then the region where this line is produced is largely restricted.

A drawback of the blackbody model is the low value of the ratio [NeV] $\lambda 3426/H\beta$ for the adequate [OI] $\lambda 6300/$[OIII] $\lambda 5007$, whereas the power law model is able to reproduce the observed values simultaneously. This is because the observed value of the ratio [NeV] $\lambda 3426/H\beta$ is obtained for $U_t \gtrsim 10^{-2}$, whereas black body models produce good fits to the observed ratios for $U_t \sim 10^{-3}$.

Summarizing a black body with $T_{eff} = 130000$ K as well as a power law with $\alpha = -1.5$ and for a range of U_t, respectively from 5×10^{-4} to 2.5×10^{-3} and from 2.5×10^{-3} to 10^{-1} can reproduce the overall features of the ENLR emission line spectrum, with the problems mentioned above.

3.5.1 Photoionization by Thin Accretion Disk Emission

In the previous section, we have shown that black bodies are as good candidates as power laws for ionizing ENLRs, then we may guess that standard accretion disk emission, similar to black body emission, can be considered as well an appropriate candidate.

For a thin disk the surface is assumed to emit locally as a black body and the total emission is calculated as the sum of black bodies over a certain range of temperatures (Frank, King and Raine, 1985). We have computed the disk emission using the expression

$$F_\nu = \int_{r_{in}}^{r_{out}} I_\nu(r) 2\pi r dr \quad (ergs\, s^{-1}\, Hz^{-1}\, sr^{-1}),$$

where $r_{in} = 3r_g$ ($r_g = 2GM/c^2$) and r_{out} are respectively, the inner and outer edge, of the disk. $I_\nu(r)$ is the specific intensity and is given by the Planck function:

$$I_\nu(r) = B_\nu[T(r)] = \frac{2h\nu^3}{c^2\left(e^{h\nu/kT(r)} - 1\right)} \quad (ergs\, s^{-1}\, cm^{-2}\, Hz^{-1}\, sr^{-1})$$

and $T(r)$ is computed by equating the dissipation rate per unit area $D(r)$ to the black body flux,

$$\sigma T^4(r) = \frac{3GM\dot{M}}{8\pi r^3}\left[1 - \left(\frac{r_{in}}{r}\right)^{1/2}\right]$$

The distribution of T with r shows a maximum at $r \sim 4r_g$ and then decreases at large r as $T \propto r^{-3/4}$. The accretion rate is calculated according to $\dot{M} = L/\eta c^2$, (η is the

efficiency and it is taken to be 0.06 as appropriate for a Schwarzschild case) In our case we have fixed $L = 0.1L_E$, where L_E is the Eddington luminosity (see Chapter 4).

We have calculated the predictions for different black hole masses and r_{out}. The increase of the black hole mass produces a shift towards low frequencies of the emission, whereas variation of r_{out} affects the low energy part of the emission. The line ratios are calculated with the same assumptions as in the power law and black body continua concerning the density and geometry of the ENLR clouds. The results are presented in Figures 3.3 and Table 3.2. From direct inspection of Figs. 3.3.b and 3.3.c we notice that predictions do not depend on the value of r_{out}, when $M \gtrsim 10^7 M_\odot$ since the continua do not change at energies higher than 1 ryd, however as it can be seen from Fig. 3.3.a this is not valid for $M = 10^6\ M_\odot$. As we said above the continuum softens when M increases, thus we obtain at a given value of U_t, lower values of [OI] $\lambda 6300/\mathrm{H}\alpha$, [SII] $\lambda\lambda 6716,6731/\mathrm{H}\alpha$, [OII] $\lambda 3727/\mathrm{H}\beta$ (close to a factor of 10) and a less extend [NII] $\lambda 6584/\mathrm{H}\alpha$, for $M = 10^8\ M_\odot$ than for $M = 10^6\ M_\odot$. The ratio [OIII] $\lambda 5007/\mathrm{H}\beta$ has similar values using different values of M, except when $U_t \gtrsim 10^{-2}$ models with $M \lesssim 10^7\ M_\odot$ predicts low values of [OIII] $\lambda 5007/\mathrm{H}\beta$ because the continuum is so hard to ionize rapidly O to higher levels of O than O^{2+}, which is not the case for models with $M \gtrsim 10^7\ M_\odot$. A similar effect is present due to the changes in r_{out} whenever $M \lesssim 10^7\ M_\odot$, the continuum is harder for low r_{out} (we will discuss an analogous effect for the thick disk continua in Chapter 5, and we will defer a more detailed discussion for that moment). The observed values agree well with the predictions of the models when $U_t \sim\ 10^{-3} - 10^{-2}$. The predictions for the ratio HeII $\lambda 4686/\mathrm{H}\beta$, which is primarily sensitive to the hardness of the ionizing continua, are above the observed values for $M \lesssim 10^7\ M_\odot$, but they are adequate for $M = 10^8\ M_\odot$. The line ratio [NeV] $\lambda 3426/\mathrm{H}\beta$, which is sensitive to the value of U_t and to the extension of the continuum at high energies, reaches values similar to those observed for $U_t \gtrsim 10^{-2}$. The predictions for the other line ratio involving Ne, [NeIII] $\lambda 3869/\mathrm{H}\beta$ are rather insensitive to variations of either the continuum shape or the value of U_t.

We can conclude that an ionizing continuum like the one corresponding to a thin disk model for M in the range $10^7 - 10^8\ M_\odot$ and $L/L_E \sim 0.1$ is an excellent compromise to explain the emission line ratios of ENLRs. Aldrovandi (1981) similarly concluded that thin accretion disk emission is a good ionizing continuum capable of reproducing the observed line ratios in a large range of AGNs. Furthermore this author proposed that by looking at the luminosity of the lines and the hardness of the spectrum as determined by the ratio HeII $\lambda 4686/\mathrm{H}\beta$ the two critical parameters M and $\dot{M}$ can be estimated.

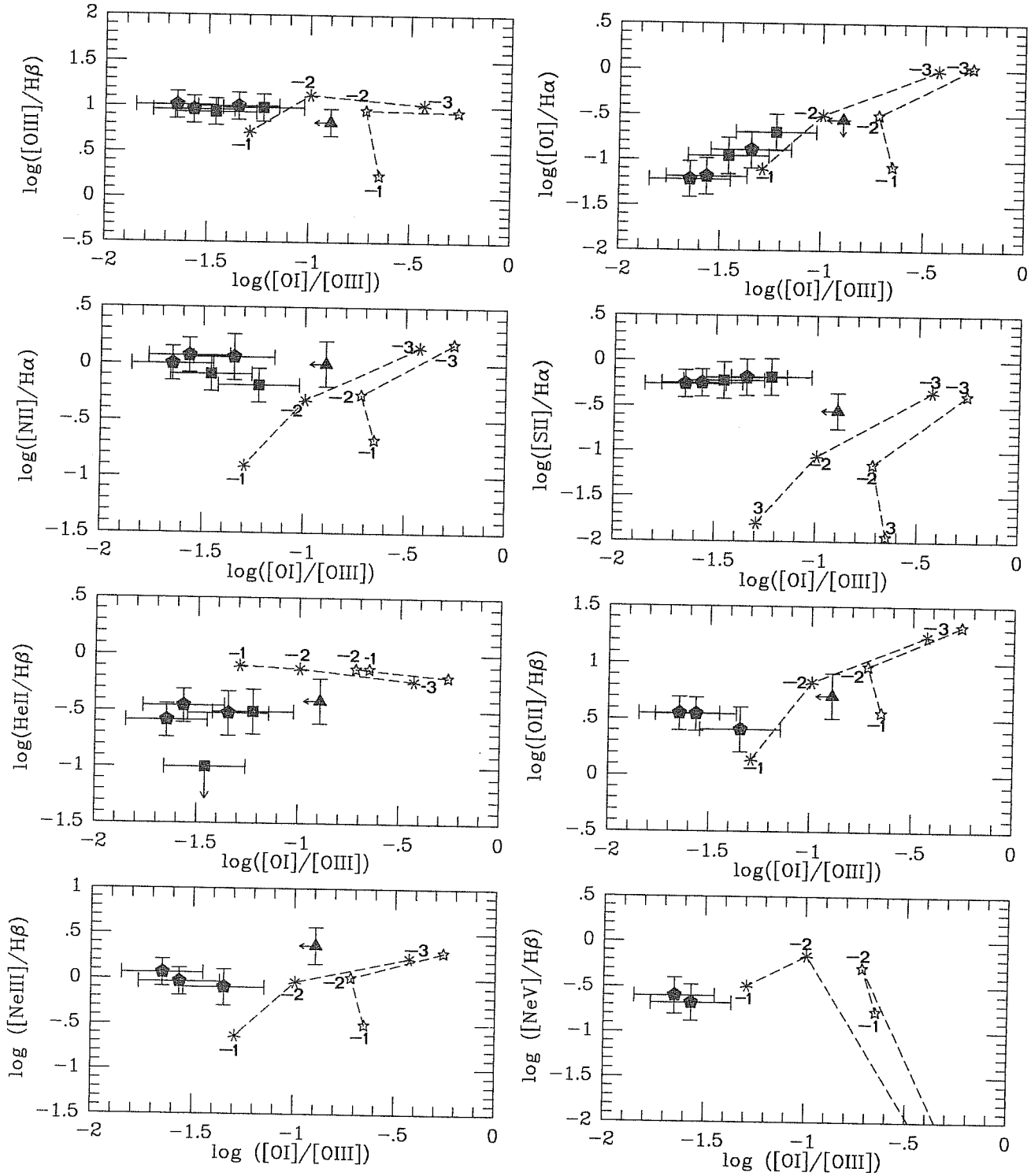

Figure 3.3: Diagnostic diagrams using the thin accretion disk emission as ionizing continuum. Predictions are presented for different values of M and r_{out} all models are calculated with $L/L_E = 0.1$. The lines join theoretical points corresponding to the variation of U_l (its logarithm is indicated). The meaning of the symbols, which are joined by lines is as follows: stars for models with $r_{out} = 50\, r_g$ and asterisks for $r_{out} = 1000\, r_g$. The different figures *a*, *b* and *c* correspond to models with $M = 10^6, 10^7$ and $10^8\ M_\odot$, respectively. The observational data are indicated by the following symbols: triangles for NGC 1068 (Baldwin, Wilson, and Whittle 1987), pentagons for NGC 3516 (Ulrich and Péquinot 1980; Pogge 1989a) and squares for NGC 4388 (Pogge 1988b).

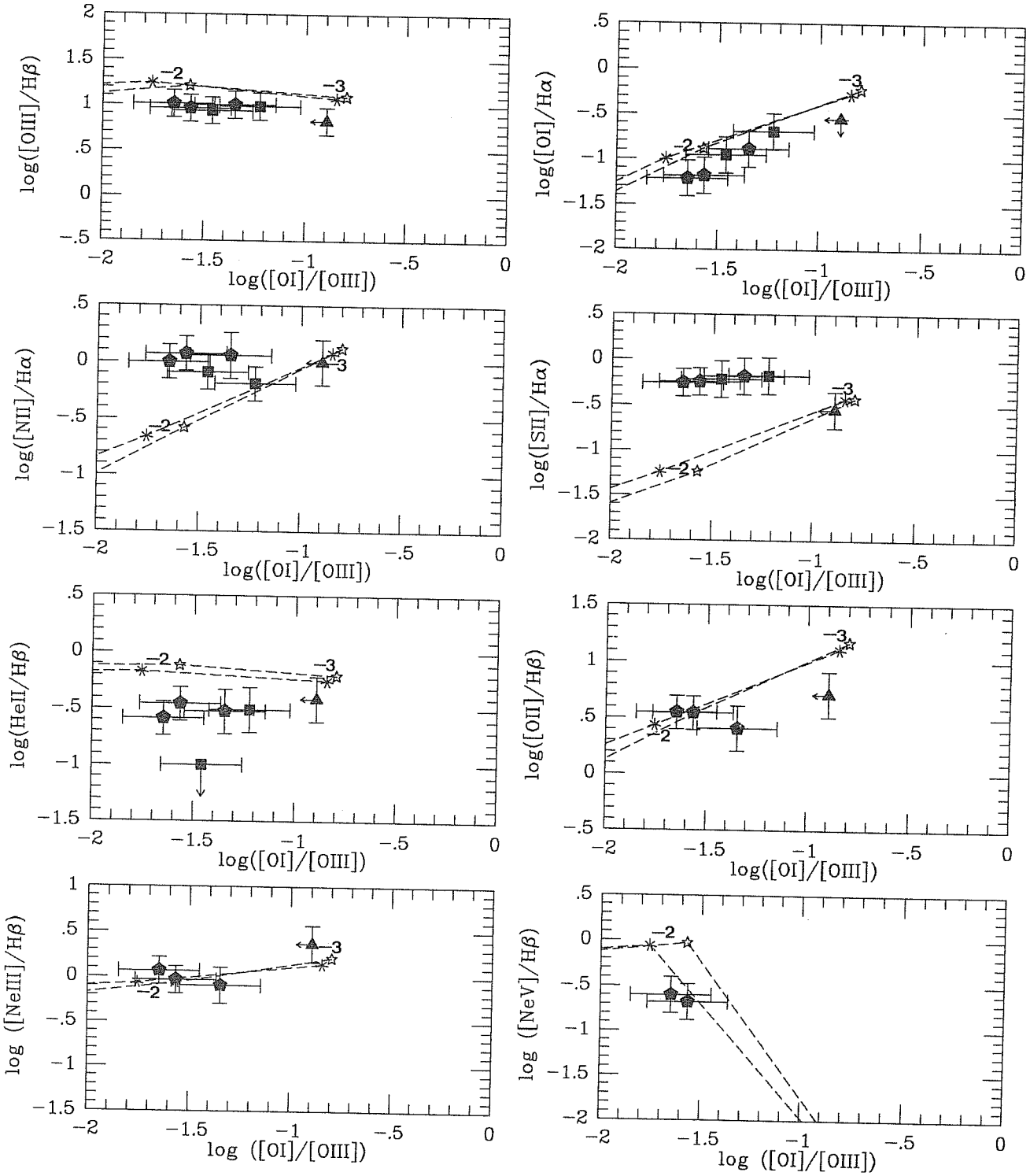
log([OIII]/Hβ)
log([OI]/[OIII])
log([OI]/Hα)
log([NII]/Hα)
log([SII]/Hα)
log(HeII/Hβ)
log([OII]/Hβ)
log ([NeIII]/Hβ)
log ([NeV]/Hβ)
−2
−3

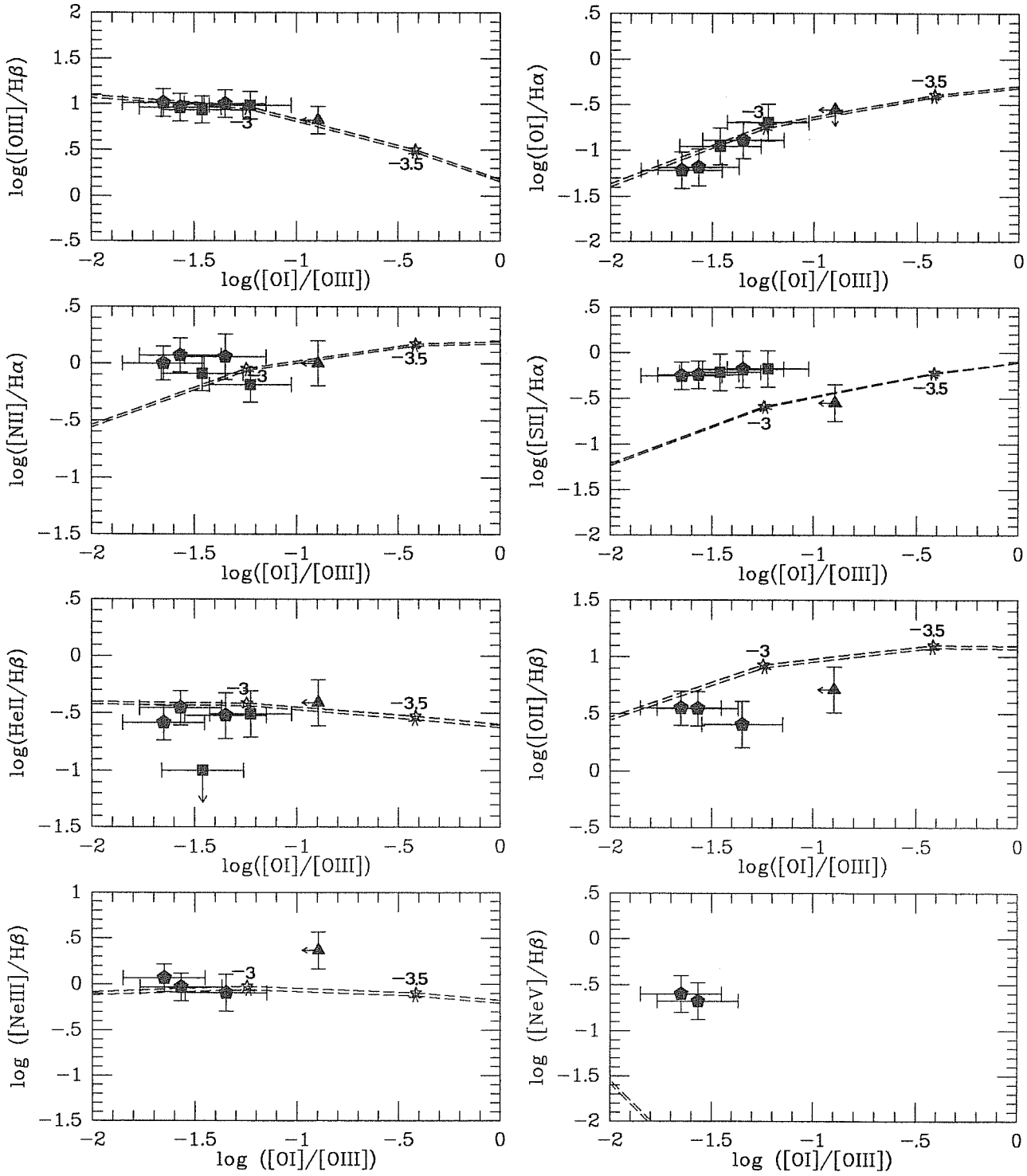
log([OIII]/Hβ)
log([OI]/[OIII])
log([OI]/Hα)
log([NII]/Hα)
log([SII]/Hα)
log(HeII/Hβ)
log([OII]/Hβ)
log ([NeIII]/Hβ)
log ([NeV]/Hβ)
−3
−3.5

TABLE 3.2: PREDICTED LINE RATIOS

RATIO	$U_t = 10^{-3}$		$U_t = 10^{-2}$		$U_t = 10^{-1}$	
	$50r_g$	$1000r_g$	$50r_g$	$1000r_g$	$50r_g$	$1000r_g$
			$M = 10^6\ M_\odot$			
[OIII] λ5007/Hβ	8.8	11.	9.0	13.	1.7	5.2
[OII] λ3727/Hβ	21.	17.	9.3	6.8	3.6	1.4
[OI] λ6300/Hα	1.1	0.98	0.31	0.31	0.09	0.08
[NII] λ6584/Hα	1.5	1.4	0.53	0.48	0.21	0.12
[SII] $\lambda\lambda$6716,6731/Hα	0.42	0.46	0.07	0.09	0.01	0.02
HeII λ4686/Hβ	0.64	0.59	0.75	0.75	0.75	0.80
[NeIII] λ3869/Hβ	2.0	1.7	1.0	0.93	0.31	0.23
[NeV] λ3426/Hβ	0.00	0.01	0.51	0.70	0.17	0.33
			$M = 10^7\ M_\odot$			
[OIII] λ5007/Hβ	13.	12.	16.	18.	9.7	12.
[OII] λ3727/Hβ	15.	13.	3.4	2.7	0.30	0.27
[OI] λ6300/Hα	0.59	0.52	0.13	0.10	0.01	0.00
[NII] λ6584/Hα	1.3	1.2	0.26	0.22	0.02	0.02
[SII] $\lambda\lambda$6716,6731/Hα	0.37	0.37	0.06	0.06	0.01	0.00
HeII λ4686/Hβ	0.63	0.57	0.76	0.68	0.75	0.64
[NeIII] λ3869/Hβ	1.6	1.4	0.86	0.85	0.45	0.59
[NeV] λ3426/Hβ	0.01	0.00	0.93	0.86	0.54	0.52
			$M = 10^8\ M_\odot$			
[OIII] λ5007/Hβ	9.6	8.9	15.	14.	14.	14.
[OII] λ3727/Hβ	8.5	7.9	1.6	1.6	0.23	0.23
[OI] λ6300/Hα	0.19	0.18	0.02	0.02	0.00	0.00
[NII] λ6584/Hα	0.90	0.86	0.15	0.14	0.02	0.02
[SII] $\lambda\lambda$6716,6731/Hα	0.26	0.25	0.03	0.03	0.00	0.00
HeII λ4686/Hβ	0.39	0.37	0.40	0.39	0.34	0.32
[NeIII] λ3869/Hβ	0.95	0.87	0.77	0.71	0.82	0.77
[NeV] λ3426/Hβ	0.00	0.00	0.27	0.22	0.70	0.64

Table 3.2: Predicted line ratios for a thin disk model calculated for $M = 10^6$, 10^7, and $10^8\ M_\odot$ with $r_{out} = 50$, and $1000\ r_g$. All the models are computed with $L/L_E = 0.1$.

The Photoionization Code MAPPINGS

The calculations of the line spectrum have been carried out using the photoionization code MAPPINGS (Binette, Dopita and Tuohy, 1985), which we briefly describe. The equations of photoionization and thermal equilibrium are solved by standard methods. The atomic database has been updated to include the more recent compilation of Mendoza (1983). The major cooling mechanisms are the collisional excitation of forbidden lines, of neutral hydrogen and due to recombination lines. Forbidden lines are calculated for several ions of the elements O, N, S, Ne, Ar and Cl ($\sim$ 150 lines). Equally the intensities for $\sim$ 60 resonances lines and $\sim$ 50 intercombination lines are computed. The effects of heating and ionization by supra-thermal electrons are considered. The coverage of photon energy extends from 7.6 eV to 5 keV, which makes this code suitable to deal with the energetic ionizing continua observed in AGNs. The diffuse ionizing radiation field is treated in the outward only approximation.

Péquinot (1986) presented a comparison between different photoionization codes. His results shows that the observed differences between the compared codes are usually in the range $10-25\%$. An important "defect" of this code is the absence of Iron lines, which are effective coolants, although it was shown that in the NLR case the results for the other lines do not differ greatly.

3.6 CONSTANCY OF U_t

We have seen above that the emission line spectra from Nuclear and the Extended Narrow Line Regions can be explained as photoionization by similar continua and with similar values of U_t. If the ionizing continuum is emitted by the active nucleus there will be a dilution of the radiation from the NNLR ($D \sim 0.01-0.1\ kpc$) location to the ENLR ($D \sim 1-10\ kpc$) by a factor of $\sim 10^2 - 10^6$. In order to keep U_t constant the density will have to decrease by the same factor, which does not seem to be confirmed by the observations. This problem will not be present if there exits a locally ionizing source. Although there is no evidence for continuum emission in the optical band associated with the line emitting gas, it could exist an emission whose spectrum rises at extreme UV/soft X–ray (Tadhunter *et al.*, 1988; Elvis *et al.*, 1990).

An alternative and attractive solution to this problem has been proposed recently by Binette and Raga (1990). They propose that the outer layers of the clouds (those facing the ionizing source) are stratified in density, which is increasing inwards. In such circumstances, when the radiation field is increased the region H^+ extends innerwards in the cloud, however it will find a larger value of the density and then the number of ionizing photons per atom is decreasing. The location of the ionization front can be computed as the Strömgren distance in the adopted plane slab geometry, this distance will be given by the integral equation (eq. 1 in Binette and Raga [1990]):

$$\frac{Q_t}{4\pi D^2} = \int_{x_S}^{L} [n(x)]^2 \alpha_B dx,$$

where $n(x)$ is the density at the position x inside the cloud, x increases from inner to outer parts in the cloud. If an average ionization parameter is defined using an average density over the H^+ region, it will result a value which depends weakly on the absolute ionizing photon flux, for the appropriate density stratification. The most critical limitation of this model is the arbitrariness of the density distribution. In spite of this, the model presents several advantageous with respect to the homogeneous one. Perhaps the most noticeable feature, apart from the fact that the average value of U

does not depend strongly on the flux of ionizing photons is the increase of the ionization range due to the intra–cloud stratification of density. Thus the strength of the UV lines, associated with high U_l in the homogeneous models, is increased and to a certain extend the agreement with the observed values is improved.

Chapter 4

THICK ACCRETION DISK EMISSION

4.1 MOTIVATION OF THE CHAPTER

This Chapter will be devoted to a general description of the accretion radiation supported tori with preferential interest on the radiation they emit. Geometrically thick disks have a desirable feature to explain the cones of ionizing radiation: since most of the radiation emitted by this sort of toroidal star will come from the inner parts, the self-occultation of the torus hole at viewing angles far from the torus axis provides an anisotropic source of radiation.

Contrarily to what happens with the thin disks models, very little work has been devoted to calculate the emission from such configurations in a suitable fashion for observational inspection. The only model known to us, which has been developed to investigate this problem is described in Madau (1988). We will largely base our discussion in this chapter on Madau's work. On the contrary, much more work has been done to investigate the self–consistency of the models based on general theoretical arguments, although still a wide range of possible configurations is allowed. The thick disks theory is still in a primary stage (Treves, Maraschi and Abramowicz, 1988). The main difficulties to be solved, besides those shared with the thin disk theory (understanding of viscosity and dissipative processes), are inherent to the bi–dimensional structure and hence the diversity of transport processes taking place inside the torus. The viability of the thick disk models has been put in question by the discovery of a violent dynamical non-axisymmetric instability, acting in nonaccreting constant angular momentum tori (Papaloizou and Pringle, 1984). At present several mechanisms capable of stabilizing such structures have been found and the instability could be not relevant in real astrophysical situations (see Blaes [1987] and references in Madau [1988] and Treves, Maraschi and Abramowicz [1988]).

The plan of this Chapter is as follows: in Section 4.2 we will mention some of the evidences supporting accretion disks as the central engine for AGNs. We will give more importance to those arguments requiring thick radiation supported disks rather than thin disks; in Section 4.3 we will describe how the physical conditions in the interior of these tori can be estimated, this section is largely based in a review paper by Blandford (1985b); in Section 4.4 the surface properties and the emission from the disk are discussed; in Section 4.5 the possible modifications of the disk emission induced by changing the surface properties and the angular momentum distribution are considered.

4.2 OBSERVATIONAL EVIDENCES FOR (THICK) ACCRETION DISKS

4.2.1 When are Thick Disks formed?

It is widely accepted that accretion of matter with angular momentum around supermassive black holes is the powerhouse for Active Galactic Nuclei. Different modes of accretion are found depending on the ratio between the accretion rate $\dot{M}$ and the Eddington rate $\dot{M}_E$ [1] (for a review see Blandford [1985a]). When $0.1 \lesssim \dot{M}/\dot{M}_E \lesssim 10$ a thin disk is formed (Pringle, 1981), however when $\dot{M}/\dot{M}_E \gtrsim 10$ the thin disk approximation is not longer valid, if mechanical equilibrium is to be maintained. Super–Eddington luminosities do not imply the breaking of equilibrium and the arising of strong winds if accretion with differential rotation is considered (Abramowicz, Calvani and Nobili, 1980). Luminosities larger than the Eddington value can be achieved naturally in any geometry of thick disks thanks to the rotation of the gas. For an illustrative description see Chapter 10 in Frank, King and Raine (1985). Hence the most likely situation is that the inner part of the disk will puff up forming a radiation pressure supported torus, when $\dot{M}/\dot{M}_E \gtrsim 10$.

4.2.2 The Big Blue Bump

The $10 - 0.1\mu$ continuum of most QSO's and Seyfert 1 galaxies can be decomposed into a single power law ($F_\nu \propto \nu^{-1}$) plus a superimposed bump in the optical/UV part (for a review see Elvis [1989]). This optical/UV component has been attributed by Shields (1978) and later on by Malkan and Sargent (1982) to *thermal* emission which peaks at UV frequencies and is well described by a single–temperature blackbody of $T \sim 20000 - 30000$K. Malkan (1983) discovered in IUE data for QSO with $z \approx 2$ a broad excess at short wavelengths which can not be fitted with a single–temperature blackbody, instead an accretion disk spectrum seems to improve considerably the fits. Nowadays it has been realized that this optical/UV excess comprises a "small blue bump" which peaks at 3000Å plus a more extended hump which may reach up to X–ray energies and it is called "the big blue bump" (Bechtold *et al.*, 1987). The "small blue bump" is actually well explained as the blending of the Balmer lines plus the Balmer continuum plus the FeII UV multiplets (Wills, Netzer and Wills, 1985). The presence of this component certainly influenced the earliest fits to the continua, leading to a conspicuous constancy of the blackbody temperature. Once this component is removed from the continuum, the "big blue bump" becomes evident. The "big blue bump" is too broad to be fitted by a blackbody and its spectral shape resembles rather a power law than a blackbody. However X–ray observations require that a cutoff is present in such power law before 120Å ($\sim 100eV$), implying the presence of a peak at intermediate energies, but this result yields only to an upper limit on its temperature. It has been found that some QSO's have a large excess of soft X–ray emission (Elvis, Wilkes and Tananbaum, 1985; Singh, Garmire and Nousek, 1985; Pounds *et al.*, 1986). If this excess is thermal and connected with the UV bump the required temperatures are very high ($T \sim 10^5 - 10^6$K). Concluding the spectral shape of the UV/soft X–ray

[1] For any accreting system the Eddington rate can be defined as: $\dot{M}_E = L_E/c^2 = 4\pi GM/k_T c$, where L_E is the Eddington luminosity, M is the mass of the accreting object and k_T is the Thomson scattering cross–section; G and c have the usual meanings. The Eddington luminosity represents the maximum of luminosity for which the radiation pressure allows a free electron to be accreted.

continuum is actually uncertain and there is no determination of any characteristic temperature.

The energy range between 912 and 120Å, where most of the radiation seems to be emitted, is unobserved because of the absorption by interstellar hydrogen in our Galaxy. There are two ways to look at this energy gap: using the emission lines from the BLR or the NLR, which are supposed to be generated via photoionization by the nuclear continuum, or alternatively using the most distant QSO's in which the extreme UV continuum is shifted into the observable optical region. The physics of the line emission in the BLR is rather complex and uncertain which makes difficult to determine the strength of the continuum at the various line producing energies (Krolik and Kallman, 1988). In spite of this some authors have tried to put constraints on the shape of the continuum using broad UV lines: Clavel and Santos-Lléo (1990) and Binette *et al.* (1989) modelled the UV/soft X–ray continuum of the luminous Seyfert 1 galaxy Fairall 9. They reached the conclusion that the ionizing continuum should peak at energies close to or below 1 ryd to be in agreement with the observations of several UV lines ratios. The processes of line emission in the ENLR and the NLR are certainly not as complex as those operating in the BLR, and the use of the lines coming from the former regions may allow us to have a cleaner diagnostic of the ionizing continuum and in fact this is one the goals of this thesis.

4.2.3 Black Hole Mass and the Ratio L/L_E

The simple thin disk models fits to observations of the UV/soft X-ray continuum require very often that $L/L_E \gg 1$ (Bechtold *et al.*, 1987; Sun and Malkan, 1989). The inclusion of opacity effects on real disks are very important in particular for the inner regions of the disk and they imply higher temperatures to radiate the same luminosity than in the blackbody approximation. More sophisticated models with finite opacity and Comptonization (Czerny and Elvis, 1987) decrease the required $\dot{M}/\dot{M}_E$ but they still yield to values $\gtrsim 10$. In the latter cases it appears more consistent with the observations to consider geometrically thick than thin disks, as it is referred in Section 4.2.1. These fits to thin disk models seem to imply that the largest values of L/L_E are required for the more luminous objects. In particular it is found that the most luminous quasars are radiating near, or even above the Eddington value, instead Seyfert galaxies are normally radiating only a few percent of the Eddington luminosity, (Padovani and Rafanelli, 1988; Sun and Malkan, 1989). We are conscious of the fact that Seyferts galaxies are not the objects in which super–Eddington rates are expected, and in spite of this we apply thick disks models to objects of this class (the cones of ionizing radiation are commonly observed around Seyfert nuclei). We rely on the inconclusive results about the determination of the ratio L/L_E to propose thick disk models for Seyfert galaxies.

Observational determinations of the black hole masses needed to compute L/L_E are very uncertain (Netzer, 1989; Halpern, 1990). Most of them are based on measurements of the width of broad emission–lines and several assumptions concerning the motions of the clouds: keplerian motions (Joly *et al.*, 1985; Wandel and Yahil, 1985); gravitational infall (Padovani and Rafanelli, 1988). The ratio L/L_E derived in these cases are mostly sub-Eddington for low luminosity objects. However smaller central masses and consequently larger L/L_E ratios are allowed in the case of outward radiatively accelerated clouds (Mathews and Capriotti, 1985). On the other hand the unobserved UV/soft X–ray continuum may contribute to the bolometric luminosity,

especially when the continuum raises in both extremes, in the far UV ($\sim$ 1200Å) and in the soft X-ray ($\sim$ 120Å). It is tentative to assume that they are the ends of the same physical component: in such a case the bolometric luminosity is underestimated (but see Binette, Courvoisier and Robinson [1988]).

Certainly, very promising methods to weight black holes come from X–ray observations. The X–ray continuum is most likely emitted close to the inner edge of accretion disk as confirmed by the short variability timescale (hundreds seconds to 3 days) detected in several Seyfert galaxies (for a review see McHardy 1989). Such short timescales may place upper limits to the size of the emitting region and consequently to the black hole mass. Kunieda *et al.* [1990] found variations of the X–ray continuum from NGC 6814 in timescales $\leq 200\ s$ (using GINGA satellite), which requires $M \lesssim 10^6\ M_\odot$. Kaastra and Barr (1989) also found variability in the soft and hard emission from NGC 5548 on timescales of few hours (using EXOSAT). Furthermore the discovery of an iron K-fluorescence line at 6.4 keV in the spectra of several Seyfert 1 (Pounds, 1989) opens a new and exciting possibility to determine the black hole mass. This iron line is probably produced by cold material sitting down close to the center of the disk, perhaps in the disk itself. The line appears to be broad and redshifted although still unresolved, the broadening will be likely dominated by Doppler and gravitational redshift in the rotating disk (Kallman and White, 1989; Fabian *et al.*, 1989). Stella (1990) has proposed a method to weight the black hole which makes use of the variability of the line profiles. This method could be applied to the iron line when the next generation of X-ray satellites will fly and provide the sufficient spectroscopic resolution.

It is worth to mention also the great effort which is currently undertaken to determine the structure of the BLR by means of simultaneous measurements of variability of the lines and the continuum (Clavel *et al.*, 1990; Netzer *et al.*, 1990). If the structure of the BLR is well determined, modelling of that region will allow to discern the cause of the motions expected in its clouds.

Summarizing, a lot of work has been done in order to determine the ratio L/L_E, or equivalently $\dot{M}/\dot{M}_E$. Although some constraints can be imposed to these ratios we believe that there is no firm ground yet on which the models should be based.

4.2.4 Polarization from Disk Emission

The thermal emission from a thin accretion disk should be highly polarized since most of the radiation comes from regions where electron scattering is the dominant opacity source (Webb and Malkan, 1986). The polarization for a pure scattering, planar atmosphere, ranges from zero when looking directly down on the surface of the disk to values $\geq 10\%$ when observing perpendicularly to the surface of the disk. The observed values of the optical polarization are crowded into two groups: high polarization ($p \sim 10 - 30\%$) and low polarization ($p \leq 2\%$) values. High polarization is observed in optically violent variable objects (OVV's), and it is explained in terms of the non-thermal processes, with the same origin as the strong-core radio emission. Instead low polarization is observed in quiescent quasars and Seyferts 1; and the electric vector appears to be parallel to the radio axis (Stockman, Moore and Angel, 1984). In the latter class of objects the optical emission is expected to come from an accretion disk and therefore it should be polarized and the electric vector should be oriented perpendicular to the radio axis. The conflict between the observed and the predicted polarization degree and orientation is a problem for the thin accretion disk model (Antonucci, 1988).

However very recently it has been suggested that a geometrically thick disk can be responsible for the low degree of polarization observed in optically quiescent quasars (Coleman and Shields, 1990) and X-ray selected BL Lac objects (Kartje and Königl, 1990).

We conclude therefore that radiation supported thick accretion disks are potentially good candidates for being the central engine at least in some classes of AGN's, although much more work both theoretical and observational needs to be done (see for a general description Abramowicz, Calvani and Madau [1987]).

4.3 STRUCTURE OF RADIATION TORI

Radiation tori can be considered similar to massive OB stars. However tori are geometrically more complicated and the microphysics is rather different, the opacity is dominated by electron scattering and the energy generation relies on the viscous dissipation. We intend to sketch in this section the basic physical properties of the interior of such structures.

The geometrically thick disk is maintained in hydrostatic equilibrium in the gravitational potential of the black hole, by the radiation pressure and by the centrifugal force. In the thin disk approximation the vertical and horizontal structure can be separated and then the structure equations can be solved exactly in the stationary case (Shakura and Sunyaev, 1973; Frank, King and Raine, 1985). However the interior of a thick disk is an extended region, and vertical and horizontal structure can not be separated. The differential equations to be solved become very complex, and they can be integrated only with simplifying assumptions. This complexity is caused mostly by the poor knowledge of the angular momentum transport and energy generation mechanisms. The angular momentum distribution can not be keplerian because the horizontal pressure gradient is now comparable with the vertical one and therefore it will contribute to the dynamical equilibrium. The heat produced at a given place in the disk is not immediately radiated away as it happens in the thin disk, but it travels a long distance inside the disk. If the structure must be in steady state at each point inside the disk the radiative flux must balance the effective gravity (gravity plus centrifugal force), but in the case that the heat flux exceeds the radiative flux convection will take place, although in the outer parts of the atmosphere the role of convection may be neglected (Blandford, 1985b).

A common way to avoid the above difficulties is to assume an *ad hoc* free function (namely, the angular momentum distribution), which contains all the unknown processes and then the resulting structure can be computed. The structure of thick accretion disks have been computed in the Kerr metric (Jaroszynski, Abramowicz and Paczynski, 1980), in a newtonian approximation to the Schwarzschild geometry (Paczynski and Wiita, 1980; Abramowicz, Calvani and Nobili, 1980; Wiita, 1982). More sophisticated approaches have been undertaken by several authors in order to reduce this bidimensional problem to a one–dimensional one: Begelman and Meier (1982), assumed a self-similarity flow. Paczyński (1980) assumed that the accretion flow is confined to the surface of the disk. Paczyński and Abramowicz (1982) assumed an accretion flow which is constrained to the equatorial plane, this approach is somehow complementary to previous one.

In the rest of this section we will present how the interior properties of a thick disk can be derived from an assumed angular momentum distribution and a barotropic equation of state. A newtonian approximation will be followed and general relativity effects are included in the use of a pseudo-newtonian potential, $\Phi(r,z) = -GM/(R-r_g)$, where R is the distance from the black hole and $r_g = 2GM/c^2$ the gravitational radius. It has been noticed by Paczyński and Wiita (1980) that this potential mimics the essential features of a Schwarzschild spacetime, as far as accretion properties are concerned The dynamical equilibrium should be maintained at any point inside the disk. In steady state the equations to be solved are, in cylindrical coordinates:

$$\frac{1}{\rho}\frac{\partial p}{\partial r} = -\frac{\partial \Phi}{\partial r} + \frac{l^2}{r^3}$$

$$\frac{1}{\rho}\frac{\partial p}{\partial z} = -\frac{\partial \Phi}{\partial z},$$

where l is the specific angular momentum. The radial and vertical velocities are neglected against the orbital velocity and the convective terms are not considered. The ratio between the gas to total pressure is considered constant in the whole disk. The assumption of a barotropic equation of state $p = p(\rho)$ for a rotating fluid requires that the specific angular momentum is only a function of the distance to the rotation axis (von Zeipel theorem). In this case the above equations can be integrated to yield:

$$\int \frac{dp}{\rho} = \Phi_{eff}(r,z) = -\frac{GM}{R-r_g} + \int \frac{l^2}{r^3} dr$$

The equipotential surfaces can be determined when the function $l(r)$ is specified. Furthermore the requirement of vanishing pressure at the surface of the torus allows to compute the shape of the disk. The geometrical shape of the disk resembles a torus, in which interior a characteristic funnel is formed (see Fig. 4.1). It has been shown by Kozlowski, Jaroszyński and Abramowicz (1978) and Abramowicz, Jaroszyński and Sikora (1978) that the existence of a cusp where an equipotential surface crosses itself occurs for any value of l between the keplerian values of l at the marginally bound (l_{mb}) and marginally stable (l_{ms}) orbits. This cusp is located where the angular momentum equates the keplerian value. The existence of such cusp is a very important feature. If material fills this critical equipotential surface (the one which crosses itself) accretion will occur in a similar way as Roche–Lobe overflow causes mass loss in a binary system. The location of the inner edge of the disk affects the efficiency of the accretion process. The efficiency is given by the binding energy at the inner radius (Paczynski and Wiita, 1980):

$$e = \frac{-GM}{2r}\frac{(r-2r_g)r}{(r-r_g)^2},$$

which is equal to zero at the marginally bound radius ($r_{mb} = 2r_g$) and has a maximum at the marginally stable radius ($r_{mb} = 3r_g$).

The distribution of the density, pressure and temperature inside the torus are given by the expressions (Madau, 1987):

$$\rho(r,z) = 4.82 \times 10^{12}\beta^4/(1-\beta)\,\Phi_{eff}^3(r,z)\ gr\,cm^{-3}$$

$$T(r,z) = 6.81 \times 10^{11}\beta\,\Phi_{eff}(r,z)\ \mathrm{K}$$

$$p(r,z) = 5.42 \times 10^{32}\beta^4/(1-\beta)\,\Phi_{eff}^4(r,z)\ dyn\,cm^{-2},$$

where $\Phi_{eff} = \Psi + \int l^2/r^3\,dr$ is dimensionless, and $\Psi = -1/(r-1)$, r is measured in units of r_g.

With the above expressions and the boundary conditions that p, ρ, and $T = 0$ at the surface of the disk, the conditions at the interior of the torus can be computed for any angular momentum distribution. In the derivation of the above equations, radiation and matter are described by a simple fluid description and the equation of state is that corresponding to a relativistic gas ($p = k\rho^{4/3}$). This assumption is valid under the conditions of quasi-stationary azimuthal motion. It is found that the time to achieve radiative equilibrium is always shorter than the inflow time, therefore the gas will be heated or cooled to the Compton temperature of the radiation field (Blandford, 1985a).

Self–consistency constraints should be imposed to the models constructed in this way. The constraint that the total mass of the disk should not exceed the mass of the hole was found to be very stringent, even more than the onset of self–gravity instabilities (Abramowicz, Calvani and Nobili, 1980). Other constraints (*e.g.* onset of nuclear reactions, viscosity becoming very large and dynamical equilibrium no longer valid, the surface density exceeding the central value) may play a role and the model will not be valid for a certain range of parameters. Wiita (1982) studied the physical conditions in the interior of thick disks under two approaches: 1) constant ratio between gaseous and total pressure, and 2) constant viscosity prescription. He found very stringent limits to build self–consistent models. However some of the constraints can be relaxed and different models incorporating those effects should be considered. In spite of all these constraints the range of allowed configurations is quite large. The models we have considered in Chapters 5 and 6 are in the range of self–consistency models according to Blandford (1985b).

At this point we know how to estimate the physical properties in the interior of the disk and therefore the opacity can also be computed. It is found that electron scattering dominates the opacity everywhere in the disk [2]. In the innermost part the photons are generated via free–free transitions and are thermalized inside the surface where the effective absorption depth $\tau = [\tau_{ff}(\tau_{ff} + \tau_T)]^{1/2}$ is unity. For sufficiently high frequencies the photosphere is found to be situated well below the last scattering surface and therefore the photons suffer multiple scatterings before escaping to infinity. The constant radiation flux through the atmosphere must be at the Eddington value if the torus is radiation supported. This implies that if the pressure scale height is much smaller than the disk thickness the opacity must be constant to maintain hydrostatic equilibrium (Blandford, 1985a). The last scattering surface is therefore located very close to the surface of the disk to have the opacity constant through the whole atmosphere. The location of the equipressure surfaces depends critically on the value

[2] The free-free and electron scattering opacities are given by the expressions:

$$k_{ff}^{\nu} = 1.5 \times 10^{25}\rho T^{-7/2}\frac{\left(1-e^{-h\nu/kT}\right)}{(h\nu/kT)^3},$$

$$k_{es} = 0.4\ cm^2 g^{-1},$$

The free-free opacity independent of the frequency can be computed by the Rosseland mean, valid for large optical depths:

$$k_{ff} = 6.6 \times 10^{22}\rho T^{-7/2}\ cm^2 g^{-1}$$

all the quantities are in *cgs* units.

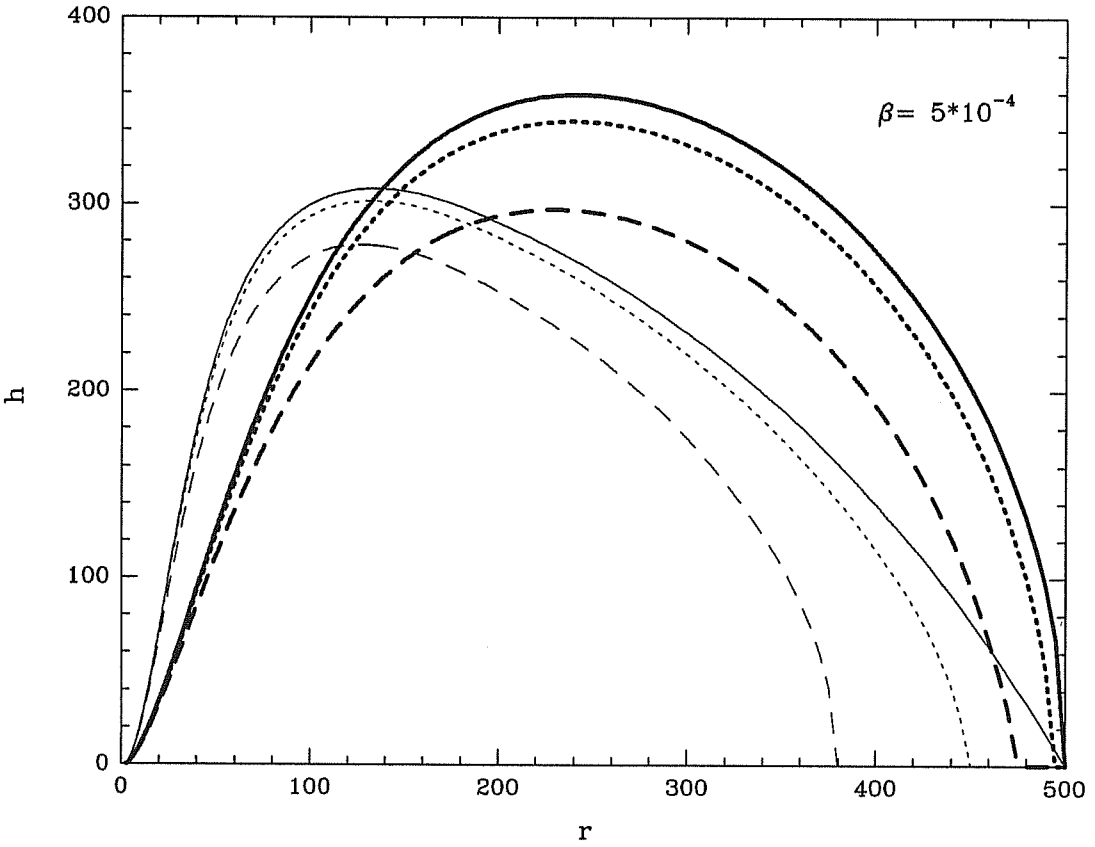

Figure 4.1: Meridional cross sections of a radiation torus for $M = 10^8\, M_\odot$, with $r_{in} = 2.7\, r_g$ and $r_{out} = 500\, r_g$. The geometry of the disk is determined by the angular momentum distribution, which is fixed *a priori* in these models. The two shapes (continuous lines) are computed using the single power law (thick line) and the Jaroszyński (thin line) *amd*, respectively (see Section 4.5.2). The dotted and dashed lines indicates the location of the last scattering and thermalization surfaces, respectively. The thick lines are for the power law *amd* and the thin lines for the Jaroszyński one. We have adopted a value $\beta = 5 \times 10^{-4}$ to have a thin atmosphere.

adopted for β (see the expressions above for p, ρ, T). Hence the location of the last scattering and thermalization surfaces will depend on β, and a such value should be chosen to be in accordance with the previous requirements [3]. However as we will describe later on, in the case of electron scattering the spectrum emitted by the surface of the disk will not depend on the precise value of β (see Section 4.4). We present in Figure 4.1 the location of the thermalization and last scattering surface for $\beta = 5 \times 10^{-4}$, and for two angular momentum distributions (more details in Section 4.5.2). This particular value of β verifies the requirements of an optically thick atmosphere where electron scattering dominates the opacity.

[3] In most models β is taken to be constant although this is a crude approximation. A more sophisticated model will include a variation of β in the interior of the disk.

4.4 SURFACE AND EMISSION PROPERTIES

Up to now we have considered properties of the disk which can be estimated without considering the character of the radiation and the gas temperature. However the surface properties depend essentially on the radiation temperature, and probably non-LTE effects should be included in the calculation of the radiation transfer through the atmosphere to have a continuum emission which can be compared to the one observed in AGNs. The flux emitted by the surface of an accretion disk can be calculated by assuming that it is emitting at the maximum value to be in hydrostatic equilibrium. In that case the total flux is given by the expression:

$$\boldsymbol{F}_r = -\frac{c}{k_T}(1-\beta)\boldsymbol{g}_{eff} = -\frac{c}{k_T}(1-\beta)\left(-\nabla\phi + \Omega^2\boldsymbol{r}\right)$$

Taking the module the following expression is obtained:

$$F = -\frac{c}{k_T}(1-\beta)\left[\frac{(GM)^2}{(R-r_g)^4} + \frac{l^4}{r^6} - \frac{2GMl^2}{R(R-r_g)^2r^2}\right]^{1/2} \tag{4.1}$$

The total luminosity emitted by the disk is then calculated by integrating this expression over the whole disk surface:

$$L = \int_{\Sigma_{disk}} F(r,h)d\Sigma$$

The total luminosity can be approximated asymptotically by an expression like:

$$L/L_E = A \times \log(r_{out}/r_{in}) - B, \tag{4.2}$$

where A and B depend on the angular momentum distribution (Abramowicz, Calvani and Nobili, 1980; Madau, 1988). Hence the outer radius of the disk governs the value of the ratio of the total luminosity to the Eddington value, therefore for larger disks the disk will be more luminous and consequently in an equilibrium configuration the disk will inflate more.

In order to calculate the actual shape of the spectrum we must make assumptions about the temperature structure in the atmosphere where the radiation is processed. Considering that electron scattering dominates, the specific intensity is given by the expression (eq. 3.2 from Shakura and Sunyaev [1973]), for an uniform and isothermal atmosphere:

$$I_\nu = 3.2 \times 10^{-15} T_s^{11/4} \left[\beta/(1-\beta)\right]^{1/2} x^{3/2} e^{-x}(1-e^{-x})^{-1/2}, \tag{4.3}$$

where $x = h\nu/kT_s$. The total flux integrated over all the frequencies is given by the expression:

$$F = 3.2 \times 10^{-4} T_s^{5/4} \left[\beta/(1-\beta)\right]^{1/2} \tag{4.4}$$

The surface temperature T_s can be derived from the condition of equilibrium (eq. 4.1) and the modified blackbody emission (eq. 4.4). Once the surface temperature is determined, then the specific intensity will be computed from eq. 4.3. The derived surface temperature is appreciably higher than the effective temperature derived in the blackbody approximation for the total flux (see Fig. 2 from Madau [1988]), and therefore the spectrum will be harder than a simple sum of blackbodies. Furthermore

the surface temperature depends weakly on β and on M: $T_s \propto M^{-4/15}\beta^{-2/15}$. Hence the change of β will modify the physical conditions in the interior of the disk, but it will not affect substantially the surface emission.

The effective temperature shows a similar behaviour as in the thin disk models. It has a sharp peak at a radius close to the inner edge of the disk and situated well inside the funnel. Beyond that radius it decreases roughly as $T_{eff} \propto l^2/r^{3/4}$ in the region where the centrifugal force dominates upon gravity and then becomes constant in the outer parts where the shape of the disk becomes spherical.

The funnel will be the place where most of the radiation is emitted, since the effective temperature reaches its maximum there. The radiation produced will be collimated because of the geometry of the emitting region and the self–shadowing of the funnel walls at large viewing angles from the disk axis. This is one of the most exciting feature of the thick accretion disk emission. Let us now calculate what is the continuum observed at any viewing angle with respect to the disk axis, including the occultation of the inner parts. The flux per steradian seen at an angle θ is given by: $F_\nu = \int_\Sigma I_\nu(\mathbf{n})(\mathbf{n}\cdot\mathbf{N})d\Sigma/D^2$, where $\mathbf{n}$ and $\mathbf{N}$ are the direction of the line of sight and the outward normal to the surface of the disk, respectively, and $d\Sigma$ is an element of surface area. Furthermore it is assumed that the surface of the disk radiates isotropically: I_ν is independent of $\mathbf{n}$ whenever $\mathbf{n}\cdot\mathbf{N} > 0$, otherwise it is assumed to be zero. The treatment of the self–shadowing of the disk will be now presented. Let us consider a line of sight in the plane YZ, which forms an angle θ_0 with the disk axis. The center of the disk coincides with the origin of coordinates (we are considering cartesian coordinates). Consider a point P_0 $(0, r_0, z_0)$ on the surface of the funnel, whose outward normal $\mathbf{N_0}(0, -cos\theta_0, sin\theta_0)$ is perpendicular to the line of sight, and a generic point P on the funnel walls, the vector $\mathbf{R}$ joins P_0 with P. The condition $\mathbf{R}\cdot\mathbf{N}_0 \geq 0$ establishes the region where the emission from the element of area on P is not shadowed by other parts of the disks. The continuum calculated in this way will strongly depend on the viewing angle. The highest frequencies of the continuum will be the most affected by the occultations of the funnel, since the hottest parts of the disk are situated well inside the funnel. The enhancement of the luminosity with increasing r_{out} (equation 4.2) over the Eddington limit occurs in the inner regions of the disk, whereas the effective temperature in the outer regions decreases as $\propto r_{out}^{-1/2}$. Consequently the most dramatic changes of the emission with the viewing angle will be achieved for large disks rather than for small ones, since the range of surface temperature is larger.

The spectral characteristics of the disk emission depends upon the size of the disk and the black hole mass. Let us consider for simplicity the spectrum seen by an observer situated along the rotation axis, in order to study this dependence. The angular momentum distribution is given by the function: $l(r) = l_{kep}(r_{in})(r/r_{in})^{2-q}$, and $0 \leq q \leq 2$. For small tori and not very massive black holes ($r_{out} = 50r_g$ and $M = 10^6 M_\odot$), the flux is peaked around 100Å (soft X–rays), the inner parts of the disk contributing most at this wavelength. The flux in the low frequency tail of the spectrum increases with increasing disk size, producing a broader and flatter spectrum. For very large disks ($r_{out} \gtrsim 1000r_g$) and $M = 10^6 M_\odot$, the outer parts emit most radiation at energies below $1ryd$ and so have a minor effect on the photoionization of the emission line regions and will not be considered in the following. An increase of the black hole mass produces a shift of the spectrum towards lower frequencies. For small tori and more massive black holes ($r_{out} = 50\ r_g$ and $M = 10^8\ M_\odot$) the spectrum has a maximum located close to 300 Å (40 eV). An increase in the disk radius beyond

$\sim 300\ r_g$ produces a significant increase in the flux only at frequencies lower than 1 ryd, and does not affect greatly the photoionization of the emission lines (this topic will be discussed further in Chapter 5).

We will now consider how the flux varies with the viewing angle. As the angle between the direction of view and the rotation axis increases, the funnel walls become progressively occulted by the torus, resulting in a drastic decrease in the high frequency radiation. This effect has important consequences for the photoionization problem, because the spectrum is modified in just the important energy range of tens of eV to a few keV. This range includes the ionization potentials of the most abundant elements and therefore is relevant to the ionization structure of the nebula (ENLR). When we change drastically the number and energy distributions of the photons reaching the nebula, we expect to change its ionization level appreciably. From the above described angular dependence of the ionizing continuum, we predict a high ionization spectrum from clouds close to the disk axis and a lower ionization spectrum from clouds far from the axis, since the value of the ionization parameter decreases with increasing angle from the disk axis and, in addition the ionizing continuum becomes less energetic (a more quantitative discussion is given in Chapter 6).

4.4.1 The Reflection Effect

In the model described so far we have not considered, at a given location, photons impinging from different parts of the funnel. However, since most of the radiation in a thick disk is produced in the funnel, the radiation energy density is large and thus reflection of photons in the funnel walls will affect the net radiative flux which is necessary to counteract the effective gravity (Sikora, 1981). Each photon within the funnel will scatter many times before escaping and as a result the surface brightness will be noticeably increased. In order to simplify the calculations, the photons are assumed to be scattered isotropically off the walls. This is a good approximation since the electron scattering dominates at frequencies where most radiation is conveyed. The balance of forces at the surface of the disk is given by the expression:

$$\mathbf{F}_e - \mathbf{F}_{in} = \frac{c}{k_T}\mathbf{g}_{eff},$$

where $\mathbf{F}_e$ includes the flux which is locally generated plus the flux which is scattered isotropically. $\mathbf{F}_{in}$ is the incoming flux from different parts of the funnel. The balance is only required to the normal component of the forces. The normal component of the incident flux is given by the integral over the whole funnel of the normal flux coming from the other zones:

$$F_{in} = \frac{1}{\pi}\int F_e(\mathbf{R}\cdot\mathbf{N})d\Omega,$$

where $\mathbf{R}$ and $\mathbf{N}$ have the usual meaning and $d\Omega$ is the element of solid angle in the direction of $\mathbf{R}$.

To compute the flux emitted by each region one must solve an equation containing an integral of the unknown flux, which is hard to solve. The way proposed by Sikora (1981) to solve this problem consist in dividing the funnel in a large but finite number of rings and then the problem will reduce to solve a system of linear algebraic equations:

$$F_{e,i} - \frac{1}{\pi}\sum_j B_{ij}F_{e,j} = \frac{c}{k_T}g_{eff,i}$$

The matrix B_{ij} represents the fraction of the radiation emitted from the j–th ring which reaches the i–th ring:

$$B_{ij} = \int_{\Omega_{ij}} \frac{\mathbf{N}_i \cdot \mathbf{R}}{\mid R \mid} d\Omega,$$

and $d\Omega = \mathbf{N_j} \cdot \mathbf{R} / \mid R \mid^3 \; d\Sigma_j$

Once the flux at each ring is known the new surface temperature is calculated from the modified blackbody assumption, and then the specific intensity can be computed. The resulting continuum shows an increasing of the surface brightness from the funnel due to the multiple reflections. On the other hand the highest frequency part of the spectrum will be less collimated than without considering multiple reflections, since the photons produced in the innermost funnel are scattered into viewing angles outside the opening angle of the funnel. It is expected that for very narrow funnels the photons produced very deep in the funnel can escape at large angles, instead when the funnel is very wide the reflection does not affect the collimation. This implies the existence of a sort of limit for the narrowest angle in which the radiation is collimated.

4.5 INFLUENCE OF THE DISK MODEL ON THE EMISSION

4.5.1 Surface properties and Opacity Sources

The model we are describing here (Madau, 1988) assumes a constant value of β everywhere in the disk, which is a very crude approximation; real disks will be more complex than this. In the previous section we found that the precise value of β does not affect the quality of the emission, although it determines the location of the photosphere. However the insensitivity of the continuum to the value of β breaks down when the variation of the interior physical properties affects what is the main source of opacity in the atmosphere. Let us imagine a situation in which β is very low in the interior but becomes large close to the surface, *i.e.* the interior of the torus is supported by radiation pressure, instead in the outer parts the gaseous pressure dominates. In such case the opacity in the atmosphere will be most likely dominated by free–free absorption. In this case the temperature of the emitting surfaces will be lower than the one derived using the modified blackbody approximation. Consequently the emission will be softer than the one calculated above, and it is approximated by the sum of blackbodies (see Fig. 8 from Madau [1988]). In Chapter 6 we further discuss this possibility and its effects on the photoionization of the ENLR.

Once the temperature of the atmosphere has been determined a consistency analysis can be done to check if the assumed source of opacity is really dominant. At low frequencies the free-free absorption dominates upon electron scattering as can be seen from the expressions for k_{es} and k^{ν}_{abs} (Section 4.3). The value of the frequency ν_o which separates the two regimes can be calculated by equating the expressions for both opacities:

$$\frac{h\nu_o}{kT_s} \approx 6.2 \times 10^{12} T_s^{-7/4} \rho^{1/2}.$$

Using the maximum value for T_s, ν_o results to be around 10^{13}Hz, however the emission at those frequencies is rather irrelevant. The photons are scattered many times before they leave the surface of the disk if the thermalization surface lies well below the last

scattering surface. In such a way they will be able to maintain the temperature of the electrons at the Compton value. However the high temperature of the electrons may cause some Comptonization of the low energy photons. The frequency at which Compton scattering becomes important can be computed and corresponds to make the $y(\nu)$ parameter equals to unity (Rybicki and Lightman, 1979). The frequency dependent Compton parameter is defined by:

$$y(\nu) = \frac{4kT_s}{mc^2}\tau_T^2(\nu),$$

where $\tau_T(\nu)$ is the electron scattering optical depth corresponding to an effective optical depth ($\tau_{eff} = [\tau_{ff}(\tau_{ff} + \tau_T)]^{1/2}$=1). The resulting expression for the y parameter is:

$$y(\nu_c) = \frac{4kT_s}{mc^2}\frac{k_{es}}{k_{ff}^{\nu}} = 1.$$

Comptonization will affect frequencies $\nu \geq \nu_c$ and a Wien peak will appear in the emission at these frequencies. For the adequate value of the parameters in this disk model it results $h\nu_c \geq kT_s$. Therefore the inverse Compton may be neglected in this case, although it should be included when calculating the continuum at very high frequencies. The effect of Comptonization has been included in the calculation of the disk emission by several authors (Czerny and Elvis, 1987; Wandel and Petrosian, 1988), and in a very detailed paper by Maraschi and Molendi (1990). These calculations have the attractive feature that they can explain at the same time the UV bump and the power law observed in hard X–rays.

In the same fashion than thin disks, radiation tori can have a hot optically thin corona. Several mechanisms can contribute to the heating of this corona either by X–rays irradiation from the central parts of the disk or by mechanical processes (see Czerny and Elvis [1987] and references therein). The high temperature electrons will suffer inverse Compton cooling and the emission at X–ray frequencies will be increased. The radiative properties of the gas in the corona can be analyzed in a similar way as those surrounding thin disks (Begelman, 1985).

Some attempts have been done to include radiative transfer effects as is done in stellar atmospheres (Kolykhalov and Sunyaev, 1984). All these effects could modify the emission from an accretion disk and should be taken into account if a "realistic model" of the continuum is going to be built. However the comparison with the observed continuum or the use of the accretion disk emission as a photoinizing continuum are not still precise enough to allow a good discrimination among the different models and make necessary such detailed modelling.

4.5.2 Angular Momentum Distribution

The shape of the accretion disk is determined once the angular momentum distribution (hereafter *amd*) is fixed (Jaroszynski, Abramowicz and Paczynski, 1980; Abramowicz, Calvani and Nobili, 1980). The choice of this function is restricted by the following requirements: first, the specific angular momentum should not decrease outwards (Seguin, 1975), for rotation to be dynamically stable; second, the angular velocity should not increase outwards in order to have inward accretion. In addition, boundary conditions should be given at the inner and outer radius of the disk. At the inner radius the

specific angular momentum should be Keplerian because the existence of the cusp (Kozlowski, Jaroszyński and Abramowicz, 1978; Abramowicz, and Sikora, 1978). At the outer boundary the disk should be thin, in particular a geometrically thin disk can be matched if the specific angular momentum is required to be keplerian (Paczynski and Wiita, 1980).

We have chosen two *amd* which are close to be extreme cases as concerning with the disk shape (Jaroszynski, Abramowicz and Paczynski, 1980). These two distributions can be described as follows (see Fig. 4.2):

- The first distribution is a single power law, whose index fixes the value of the radius where the disk becomes thin again but the specific angular momentum is not keplerian at that radius. Conversely once the outer radius of the disk is fixed the index of the power law can be determined. Stability constraints require that the index is in the range 0. to 0.25 (Abramowicz, Henderson and Ghosh, 1983). The value of this index spans from 0.18 to 0.21 for $r_{out} = 50, 1000\, r_g$, respectively.

- The second distribution is more complex, and is commonly called Jaroszyński *amd*. In the innermost part of the disk the angular velocity is assumed to be constant, then the specific angular momentum increases as r^2. An intermediate region in which the angular momentum is kept constant and it equates the keplerian value at the center of the disk. In the outer part the angular velocity is again constant and the specific angular momentum is keplerian in the outer edge of the disk. It has been shown that this *amd* maximizes the luminosity emitted by the disk (Abramowicz, Calvani and Nobili, 1980).

We now analyze how the shape of the disk and the emitted flux depends on the adopted *amd*. The centrifugal force acting on the funnel walls is larger in the case of the Jaroszyński *amd* than in the single power law. Therefore the radiation pressure needed to support the disk in equilibrium should be larger in the former case (see Fig. 4.1). A large radiation pressure will inflate more the disk, which will result in a steepening of the funnel. In the intermediate part of the disk the Jaroszyński *amd* is lower than the single power law and the disk profile is more inflated in the latter case, at these radii (see again Fig. 4.1). The flux coming from these intermediate radii is larger for the single power law *amd* because the emitting surface is enlarged and so is the absolute flux. However in the outer parts of the disk when no keplerian value for the specific angular momentum is required the radiation pressure helps to balance gravity. Instead when the specific angular momentum is required to be keplerian in the outer edge, gravity is balanced uniquely by the centrifugal force, and then at that radius the effective temperature should be calculated from the local generation of energy, as in the thin disk case. Therefore differences on the surface temperature may arise depending on the adopted *amd*; however the very outer regions do not contribute substantially to the emission and differences on the disk emission are not seen.

We have computed the flux using the two *amd* mentioned above, with the same assumptions about the surface properties of the disk (the opacity is dominated by electron scattering and the emitted radiation corresponds to a modified blackbody) [4]. Let us now compare the fluxes computed using the two *amd* when the disk is observed

[4] Ocasionally when we refer to the continuum computed with these two *amd* – power law and Jaroszyński – they will be identified as Madau's and Abramowicz, Calvani and Nobili's (ACN) models, respectively.

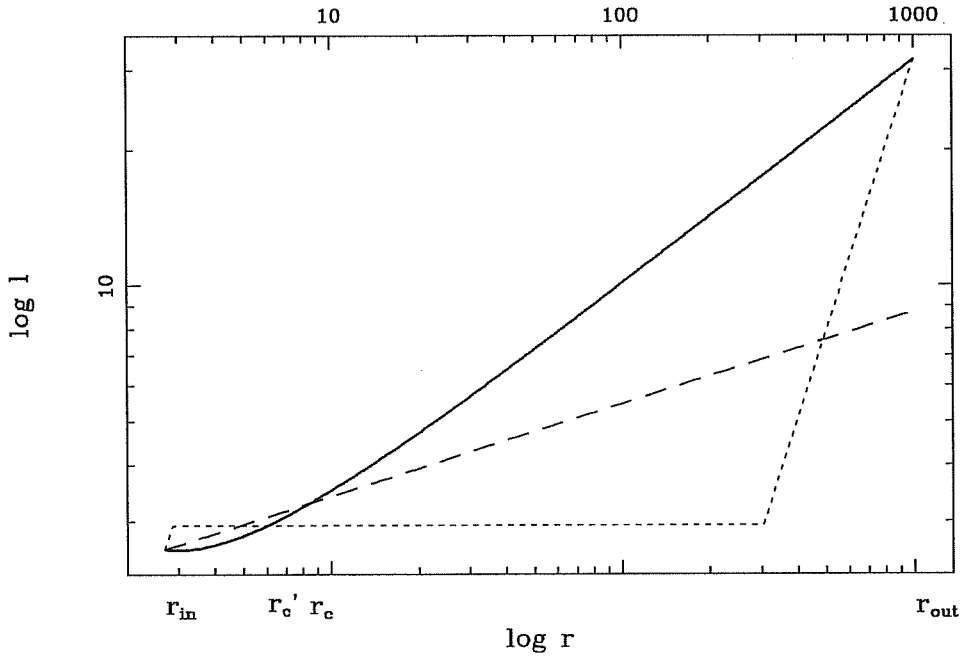

Figure 4.2: Different angular momentum distributions for a disk configuration with $r_{in} = 2.7r_g$ and $r_{out} = 1000r_g$. The centre of the disk is indicated by r_c, which is the point where the non-keplerian amd crosses the keplerian one. The continuous, dotted and dashed curves represent the keplerian, Jaroszyński and single power law *amd*, respectively.

along the rotation axis. When the disk size is $\lesssim 100r_g$ the flux computed using the Jaroszyński's *amd* is larger at the highest frequencies than when the single power law one is used. When the disk size is $\gtrsim 200r_g$ the high energy part of the spectrum is still above in the Jaroszynski *amd*, whereas the low energy part of the spectrum is larger for the single power law *amd*. The reason for this behaviour arises from the different contribution at a particular frequency which comes from a certain zone of the disk. The funnel calculated with the Jaroszyński *amd* emits at a higher surface temperature than the single power law, thus the high energy part is larger in the former case. When the disk is large enough the radiation at low energies is mainly dominated by the regions outside the funnel, and the absolute flux will depend on the extension of the surface which is emitting. The fluxes and their difference computed with the two *amd* are presented in Figure 4.3[5]. The number of ionizing photons is presented in table 4.1 for both *amd's* and the ratio between the two cases is also given.

From direct inspection of the Figures 4.3 the largest differences are found at the high energy tail of the spectrum, when the disk is seen along the rotation axis. The largest variation in the number of photons with energies $\gtrsim 1$ ryd is found for large disks

[5]We use the difference between the logarithm of the fluxes because it can be loosely related with the relative error of the emission line intensities. This is valid only if the emission line intensity is nearly proportional to the ionization parameter (U_t). In such case we can write: $I_\lambda \approx AU_t^c$, where c ~ 1. The relative error of the emission line intensity is the absolute error of its logarithm, taking logarithm in the previous expression and calculating the variation we obtain: $\Delta log I_\lambda = c\Delta log U_t$. The variation of $logU_t$ is proportional to the variation of the logarithm of the number of photons with energies ≥ 1 ryd, which can be equated to the variation of the monochromatic flux for a power law continuum, in other cases it will be a crude approximation.

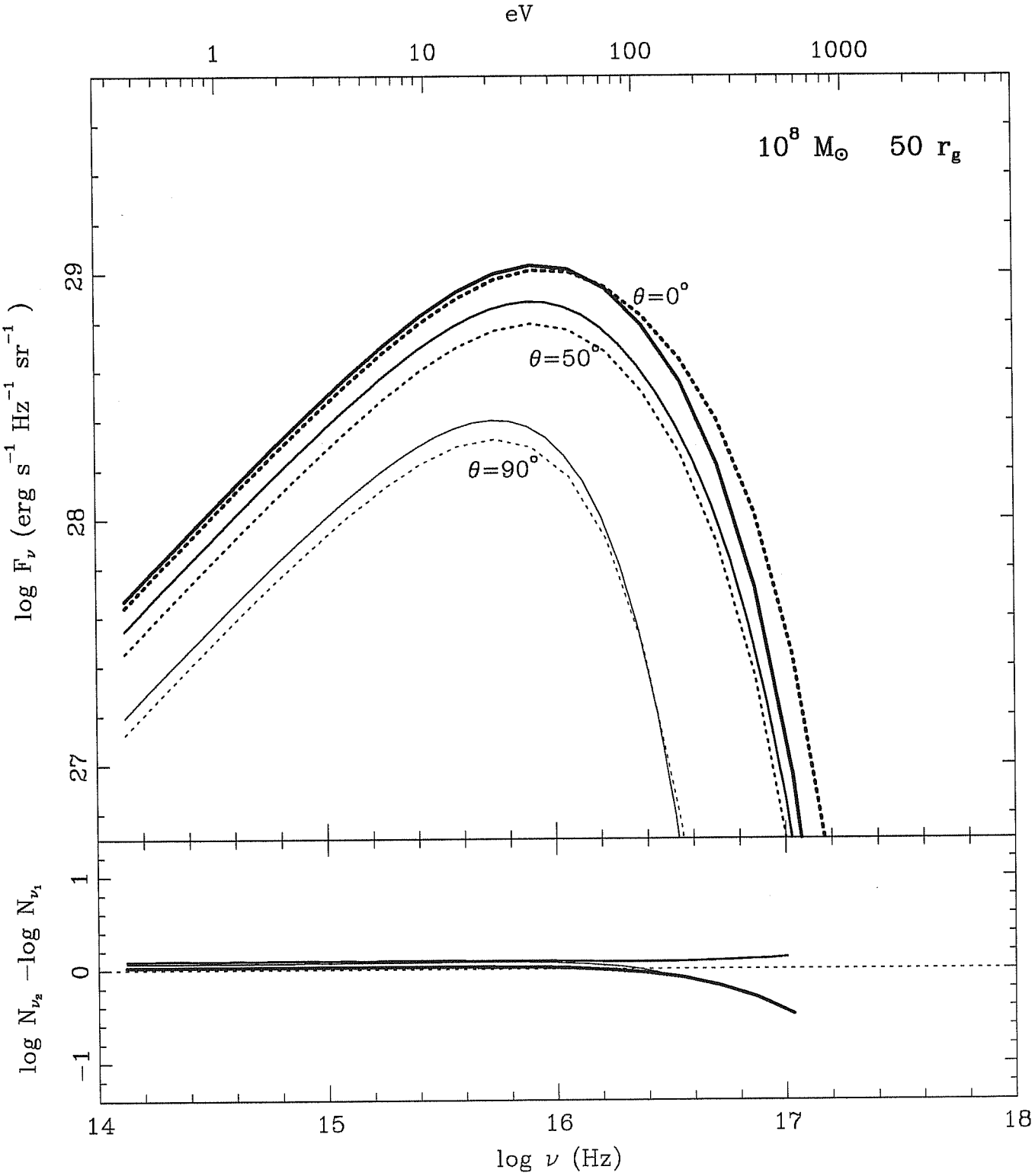

Figure 4.3: Flux emitted by a thick accretion disk at various viewing angles and for several values of M and r_{out}, assuming two different *amd's*. The continuous and dotted curves correspond to the Madau's and ACN models[4], respectively. The difference between the two fluxes is presented as the subtraction between their logarithmic values (continuous minus dotted). Lines of different weight represent different viewing angles.

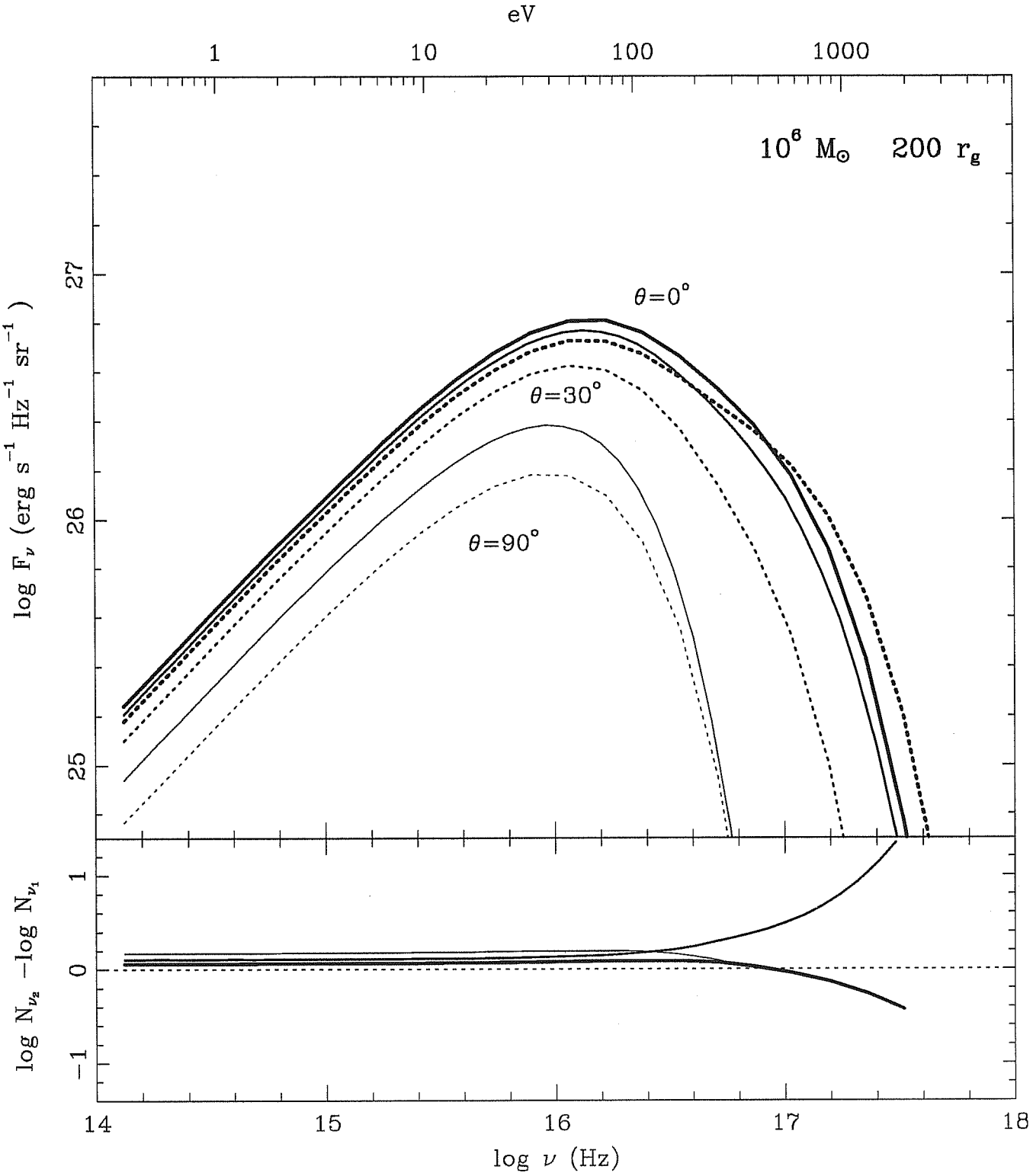
eV
1
10
100
1000
10^6 $M_\odot$ 200 r_g
θ=0°
θ=30°
θ=90°
log F_ν (erg s^{-1} Hz^{-1} sr^{-1})
27
26
25
log N_{ν_2} −log N_{ν_1}
1
0
−1
14
15
16
17
18
log ν (Hz)

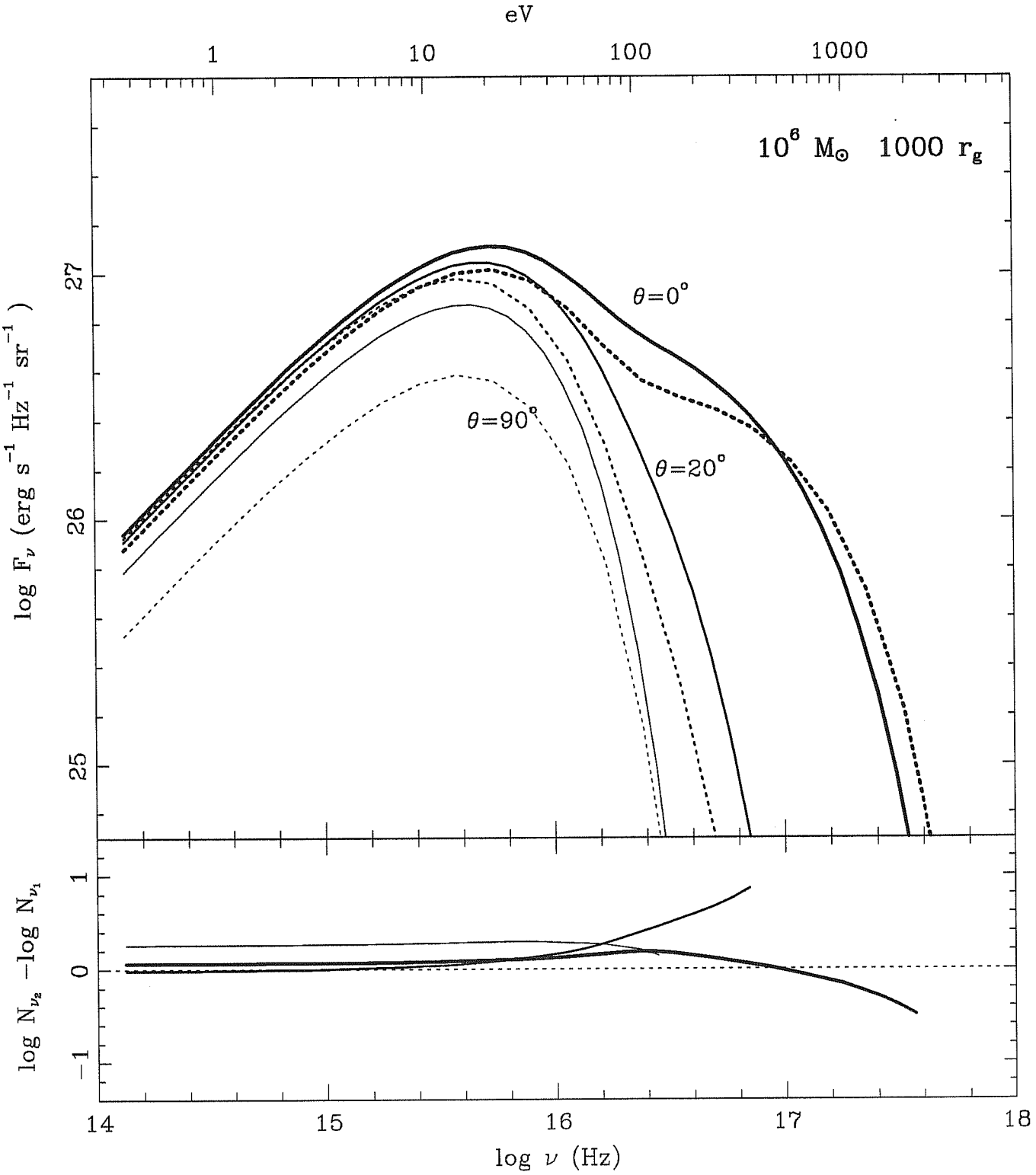
eV
1
10
100
1000
10^6 $M_\odot$ 1000 r_g
θ=0°
θ=20°
θ=90°
log F_ν (erg s^{-1} Hz^{-1} sr^{-1})
27
26
25
log N_{ν_2} −log N_{ν_1}
1
0
−1
14
15
16
17
18
log ν (Hz)

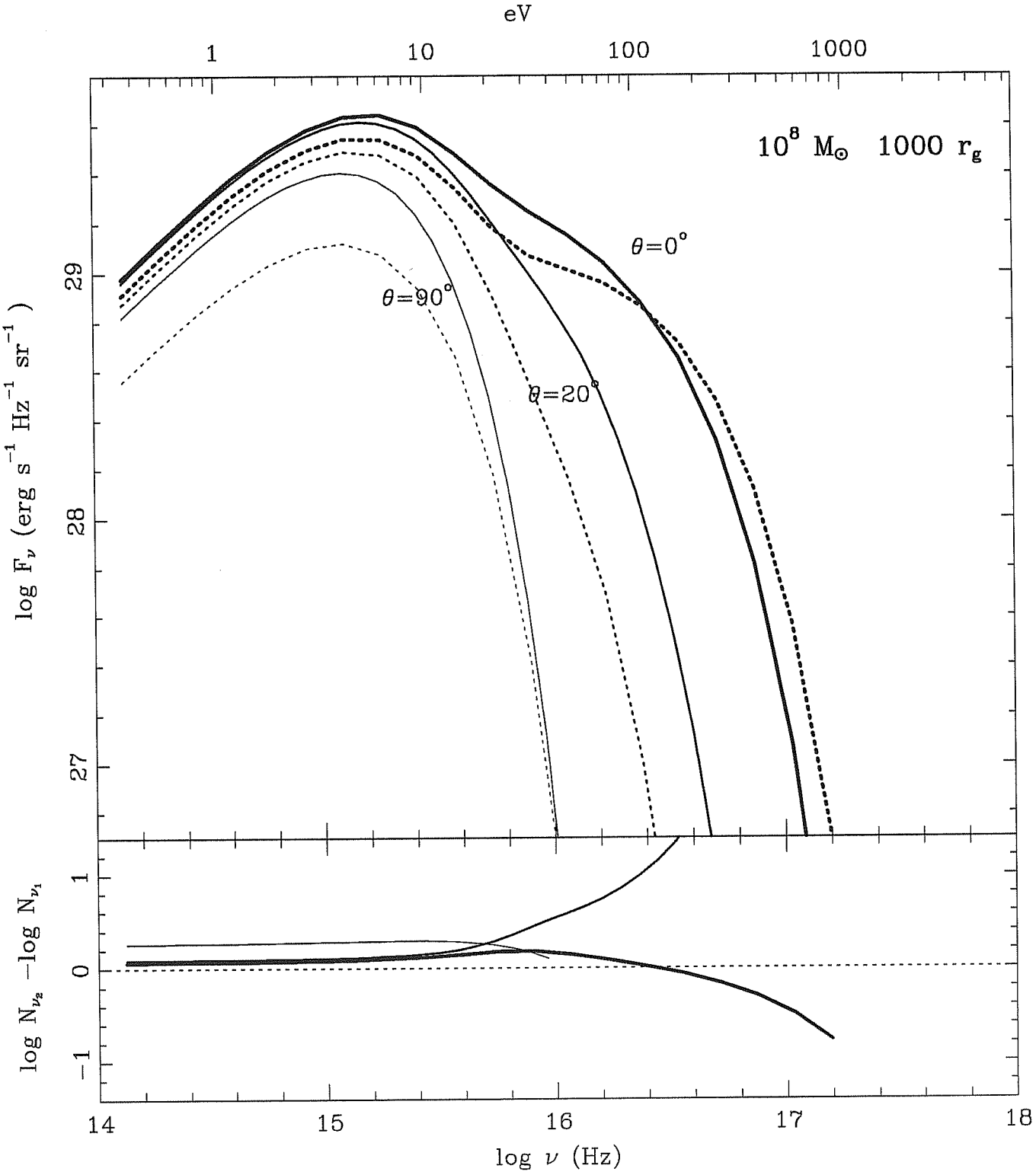
eV
1
10
100
1000
10^8 $M_\odot$ 1000 r_g
θ=0°
θ=90°
θ=20°
log F_ν (erg s^{-1} Hz^{-1} sr^{-1})
29
28
27
log N_{ν_2} − log N_{ν_1}
1
0
−1
14
15
16
17
18
log ν (Hz)

TABLE 4.1: IONIZING PHOTONS

	$N_i/4\pi \times 10^{-53}$					
r_{out}	$10^6\ M_\odot$			$10^8\ M_\odot$		
(r_g)	MADAU	ACN	Ratio	MADAU	ACN	Ratio
50	1.3	1.3	1.00	333.	341.	0.98
200	2.6	2.2	1.15	555.	488.	1.14
1000	4.0	3.2	1.27	604.	466.	1.30

Table 4.1: Number of ionizing photons for different values of r_{out} and two thick accretion disk models. The labels MADAU and ACN refer respectively to the models calculated with the single power law and the Jaroszyński *amd's*

around high black hole masses, *e.g.* in the case of a hole with $10^8 M_\odot$ and $r_{out} = 1000 r_g$ the difference is almost 20% at 1 ryd, in the other cases it is not larger than 10% at that range of energies. The larger variations found in the value of N_i (see Table 4.1), or equivalently in U_t, are induced by the differences in the high energy extension.

The differences between the computed spectra with the two *amd* reveal very important at viewing angles far from the rotation axis. The funnel is very steep when the Jaroszyński *amd* is adopted and therefore the angular variation of the emitted flux will be very pronounced in this case. This is clearly seen from the Figures 4.3. The continua calculated at the same value of the separation angle from the disk axis differ always in the high energy part, which is the part affected by the occultation of the funnel. The differences between the computed fluxes is large when the disk sizes are fairly large and affects more the range of ionizing photons for large black hole masses. Finally when the disk is seen from angles close to the equatorial plane the main difference is found because the emitting surface varies. In this case the single power law *amd* predicts a larger flux than the Jaroszyński one, at any frequency, although in both cases the continuum emission extends up to roughly the same frequencies.

Summarizing, the choice of the *amd* reveals not very critical at small separation angles from the disk axis, regarding the total amount and the distribution of energy which is emitted by the disk. However the choice of the *amd* affects very much the geometry of the funnel and consequently the occultation of its walls will vary considerably from case to case. The angular dependence of the emitted continuum is then conditioned by the chosen *amd*. Nevertheless, the Jaroszyński *amd* is very unlikely to be physically correct: the actual *amd* will be rather flat when the accretion rate is largely super–Eddington (Abramowicz *et al.*, 1988). Therefore the formation of such steep funnels is not expected and the opening angle will be much closer to the values derived using the single power law *amd* (values of the opening angle of the funnel are presented in Table 6.1).

There are several effects not considered here, which may reduce the relevance of the choice of the *amd* and the geometry of the funnel regarding the collimation of the continuum emission. The inclusion of the reflection effect will introduce differences even when the disk is seen along the rotation axis. When the funnel is very steep the reflection in the walls will be large and the absolute flux which escapes outside is effectively increased (Sikora, 1981). On the other hand, the reflection effect will decrease the collimation of the radiation. These two effects will operate in opposite senses and the expectation will be that the differences on the angular dependence of the emission are smoothed.

Chapter 5

PHOTOIONIZATION OF THE ENLR BY THE THICK ACCRETION DISK EMISSION: SENSITIVITY TO VARIATIONS OF THE DISK PARAMETERS

5.1 OVERVIEW OF THE CHAPTER

In this chapter we investigate the photoionization of the ENLR by the continuum emitted by an accreting radiation supported torus. We are mainly concerned with the ability of such continuum to reproduce the emission line spectra observed in ELNRs. Good quality observations of emission lines at positions far from the axes of the high excitation cones are not yet available. For this reason we have considered the emission lines only at small angles from the rotation axis of the torus. In the next chapter we will investigate the angular behavior of the lines. We use a simple model to compute the emission from the thick accretion disk, as we described in Chap. 4 (Madau, 1988). The continuum emission for two black hole masses $M = 10^6$ and 10^8 $M_\odot$ and various values of the accretion disk size are presented in Fig. 5.1. When calculating the emission from the disk, we have assumed a constant ratio between the gaseous and the total pressure $\beta = 10^{-4}$ and that the inner edge of the disk is at the intermediate value $2.7 r_g$ (r_{in} should be located between $r_{mb} = 2\,r_g$ and $r_{ms} = 3\,r_g$, see Sect. 4.3). A photoionization code is used to make theoretical predictions of the emission lines. The parameter space available to this model is explored by varying the size of the accretion disk, the mass of the accreting black hole and the ionization parameter. The majority of line ratios are most sensitive to the ionization parameter but some are also functions of the accretion disk size at fixed ionization parameter. Our results are compared with observational data (for Seyfert galaxies), in order to constrain the disk parameters and the properties of the emission–line clouds. Typical model fits involve an ionization parameter of several times 10^{-2} and an accretion disk of radius $\simeq$ 500 (150) gravitational radii around a $10^6 M_\odot$ ($10^7 M_\odot$) black hole.

We discuss the variation of the spectral shape of the ionizing continuum. The inclusion of an additional hard X–ray component may change the predictions of the emission lines. We study how those effects influence the agreement between observed and predicted line ratios. We have not included in the computation of the disk emission the

reflection effect considered in Madau's model. This effect is related to the multiple scattering of photons in the funnel walls (Sikora, 1981), and produces a substantial increase in the surface brightness, especially in the highest frequency parts of the spectrum (see Section 4.4.1). However a reliable treatment of this effect is difficult and we feel that it is beyond the scope of the present work. Anyway we briefly discuss the modifications operated on the emission lines due to the inclusion of the reflection effect.

The plan of this chapter is as follows: Section 2 is devoted to a discussion of the photoionization of the ENLR by the torus continuum and the dependence of the emission lines on the model parameters (black hole mass, accretion disk size and ionization parameter). In Section 3 the predictions for several line ratios are compared with those observed in the ENLR of three Seyfert galaxies (NGC 1068, NGC 3516 and NGC 4388). Section 4 is devoted to a discussion of the results from Sect. 3. In Section 5 we present conclusions and closing remarks.

5.2 PHOTOIONIZATION OF THE ENLR: VARIATION OF MODEL PARAMETERS

We now calculate the emission line spectrum from a gas ionized by the UV/soft X-ray spectrum produced in the radiation supported torus. In this section we study the dependence of the line emission on the parameters (mass of the black hole and size of the disk) which model the accretion disk spectrum, and also on the ionization parameter. The ionization parameter, U_t, is defined by:

$$U_t = \frac{\int_{\nu_0}^{\infty} L_\nu / h\nu \; d\nu}{4\pi D^2 n_H c} = \frac{N_i}{4\pi D^2 n_H c},$$

where L_ν is the monochromatic luminosity, ν_0 is the frequency corresponding to 1 ryd, n_H is the hydrogen density of the ENLR clouds, D is the distance of these clouds from the nucleus and N_i is the total number of ionizing photons emitted per second. We construct a grid of models for three values of $M - 10^6, 10^7$ and $10^8 M_\odot$. This grid is built by varying the size of the accretion disk and the ionization parameter (see Fig. 5.2 and Table 5.1).

The ionization level of the emitting gas is primarily dependent on the ionization parameter. Variation of the ionization parameter (for a given black hole mass and accretion disk size) is equivalent to varying one or both of the values D and n_H. In practice we have taken a constant density ($n_H = 100 cm^{-3}$), so changes of the ionization parameter correspond to changes in D. There is no loss of generality in using a constant density since, at the low density assumed, collisional de–excitation effects are unimportant. Models with equal U_t, but different n_H and D, are then equivalent.

Variations in the size of the accretion disk (for a given M, D and n_H) will change both the ionization parameter and the shape of the ionizing spectrum. In the discussion below (Sect. 5.2.3), we hold the ionization parameter constant as the disk size is varied, which implies an associated change in D (for fixed M and n_H). Thus variations of the disk size correspond to variations in the spectral shape of the ionizing continuum at constant ionization parameter.

The photoionization code MAPPINGS (Binette, Dopita and Tuohy, 1985) was used to obtain the line intensities. The extended narrow line region is assumed to be a plane parallel slab; the calculations of the ionization structure are terminated when the ratio

TABLE 5.1: PREDICTED LINE RATIOS

RATIO	$U_i = 10^{-3.5}$			$U_i = 10^{-2}$			$U_i = 10^{-1}$		
	$50r_g$	$200r_g$	$1000r_g$	$50r_g$	$200r_g$	$1000r_g$	$50r_g$	$200r_g$	$1000r_g$
				$M = 10^6\ M_\odot$					
[OIII] λ5007/Hβ	0.68	1.44	2.01	6.48	10.00	20.89	2.50	2.21	19.16
[OII] λ3727/Hβ	16.98	16.80	14.59	14.78	10.22	6.60	6.47	4.70	1.03
[OI] λ6300/Hα	2.03	1.87	1.61	0.48	0.51	0.51	0.13	0.18	0.14
[NII] λ6584/Hα	1.54	1.57	1.47	0.68	0.65	0.57	0.22	0.27	0.12
[SII] $\lambda\lambda$6716,6731/Hα	1.49	1.50	1.46	0.22	0.26	0.33	0.06	0.08	0.12
HeII λ4686/Hβ	0.30	0.34	0.28	0.52	0.61	0.55	0.57	0.66	0.63
[NeIII] λ3869/Hβ	1.12	1.09	0.89	1.39	1.13	1.16	0.58	0.42	0.68
[NeV] λ3426/Hβ	0.00	0.00	0.00	0.29	0.53	0.74	0.12	0.22	0.81
				$M = 10^7\ M_\odot$					
[OIII] λ5007/Hβ	1.88	2.56	2.41	10.51	18.27	22.05	1.86	14.32	17.90
[OII] λ3727/Hβ	18.78	16.68	14.09	8.90	5.53	3.95	3.61	0.63	0.35
[OI] λ6300/Hα	1.66	1.40	1.21	0.39	0.36	0.31	0.12	0.06	0.03
[NII] λ6584/Hα	1.69	1.63	1.50	0.58	0.47	0.38	0.23	0.07	0.03
[SII] $\lambda\lambda$6716,6731/Hα	1.09	1.08	1.06	0.13	0.15	0.16	0.03	0.03	0.03
HeII λ4686/Hβ	0.43	0.38	0.30	0.71	0.67	0.56	0.74	0.72	0.59
[NeIII] λ3869/Hβ	1.30	1.11	0.88	1.03	1.02	0.98	0.32	0.51	0.61
[NeV] λ3426/Hβ	0.00	0.00	0.00	0.58	0.78	0.76	0.21	0.56	0.60
				$M = 10^8\ M_\odot$					
[OIII] λ5007/Hβ	3.12	2.95	2.76	18.15	18.37	18.62	12.56	13.28	14.11
[OII] λ3727/Hβ	17.22	15.17	13.09	3.66	2.99	2.36	0.32	0.28	0.25
[OI] λ6300/Hα	1.07	0.94	0.81	0.19	0.16	0.12	0.01	0.01	0.00
[NII] λ6584/Hα	1.73	1.62	1.49	0.30	0.25	0.21	0.02	0.02	0.02
[SII] $\lambda\lambda$6716,6731/Hα	0.86	0.84	0.82	0.08	0.08	0.08	0.01	0.01	0.01
HeII λ4686/Hβ	0.43	0.38	0.32	0.71	0.62	0.53	0.71	0.60	0.49
[NeIII] λ3869/Hβ	1.18	1.00	0.83	0.92	0.86	0.80	0.53	0.56	0.61
[NeV] λ3426/Hβ	0.00	0.00	0.00	0.85	0.74	0.64	0.51	0.48	0.43

Table 5.1: Predicted line ratios for a disk model with $M = 10^6, 10^7, 10^8\,M_\odot$ and $r_{out} = 50, 200, 1000\,r_g$.

of ionized hydrogen to neutral hydrogen is lower than 1% (radiation bounded nebula), and solar abundances were assumed throughout. The intensity of any given line is computed by adding the contributions to the line at each location in the cloud and hence is proportional to the column density [$N(X^i) = \int n(X^i)dl$, X^i is the element emitting the line, $n(X^i)$ the number density of this element and l is the distance along the cloud].

Generally we are more concerned with relative, than with absolute, line intensities, since the predictions about absolute values involve assumptions about the geometry and filling factor of the clouds, which are poorly known. We discuss our calculations by means of diagnostic diagrams (Baldwin, Phillips and Terlevich, 1981; Veilleux and Osterbrock, 1987). Gas photoionized by hot stars and power law spectra occupy different regions in these diagrams. We use the line ratios proposed by those authors as a measure of the agreement or disagreement between the predictions of our models and the observational data (Fig. 5.2). However, we take as abscissa in Fig. 5.2 the line ratio [OI] λ6300/[OIII] λ5007, which cleanly delineates the range where ENLR and NLR are located, separating them from normal HII regions and planetary nebulae ($\log$[OI]/[OIII] $\gtrsim -2$; Robinson *et al.* 1987).

As discussed above, we expect to find that the most drastic changes in the emission line spectrum result from variations of the ionization parameter. This fact has been pointed out by Tarter, Tucker and Salpeter (1969), who concluded that any attempts to distinguish between different shapes of the ionizing continua by looking at the emission line ratios are futile. A similar conclusion was reached by Krolik and Kallman (1988), although they did find several line ratios which are sensitive to variations in the spectral shape. Our aim is to find emission line ratios sensitive not only to the ionization parameter but also to the different spectral shapes produced by different black hole masses and disk sizes.

5.2.1 Variation of the Ionization Parameter

The range of ionization parameters spanned by our calculations allows us to cover a wide range of ionization levels (see Fig. 5.3). For a value of the ionization parameter of order $10^{-3.5}$ the line ratio [OI] λ6300/Hα is on average of the order of unity, while for a value $U_l \sim 10^{-1}$ this ratio ranges between 10^{-1} and 10^{-2}. The line ratio [OIII] λ5007/Hβ increases from the values $2-3$ to 20, for U_l in the range $10^{-3.5} - 10^{-2}$. At larger values of U_l this line ratio tends to decrease since the dominant ionization level of oxygen becomes O^{3+}. The line ratio HeII λ4686/Hβ increases slowly with increasing U_l at low values of U_l ($10^{-3.5} - 10^{-2.5}$), and then remains almost constant. The line ratio [NeIII] λ3869/Hβ increases with increasing the ionization parameter up to $U_l \approx 10^{-2.5}$ and then starts to decrease, as higher ionization species dominate. The line ratio [NeV] λ3426/Hβ reaches a maximum (~ 0.8) at U_l in the range $10^{-1.5} - 10^{-2}$ and then decreases again at higher U_l.

The low ionization lines, such as [SII] $\lambda\lambda$6716, 6731, [OI] $\lambda\lambda$6300, 6363 and a significant fraction of [NII] $\lambda\lambda$6548, 6584 are produced in the partially ionized H^0 region. In this region the dominant forms of O, S and N are O^0, S^+ and N^0, while smaller fractions of N^+ and O^+ are also present. If the ionization parameter increases, the intensity of the hydrogen recombination lines increases proportionally (the column density of ionized hydrogen increases linearly with U_l), but the intensity of the lines emitted in the partly ionized region does not increase so fast because the relative size of this region is

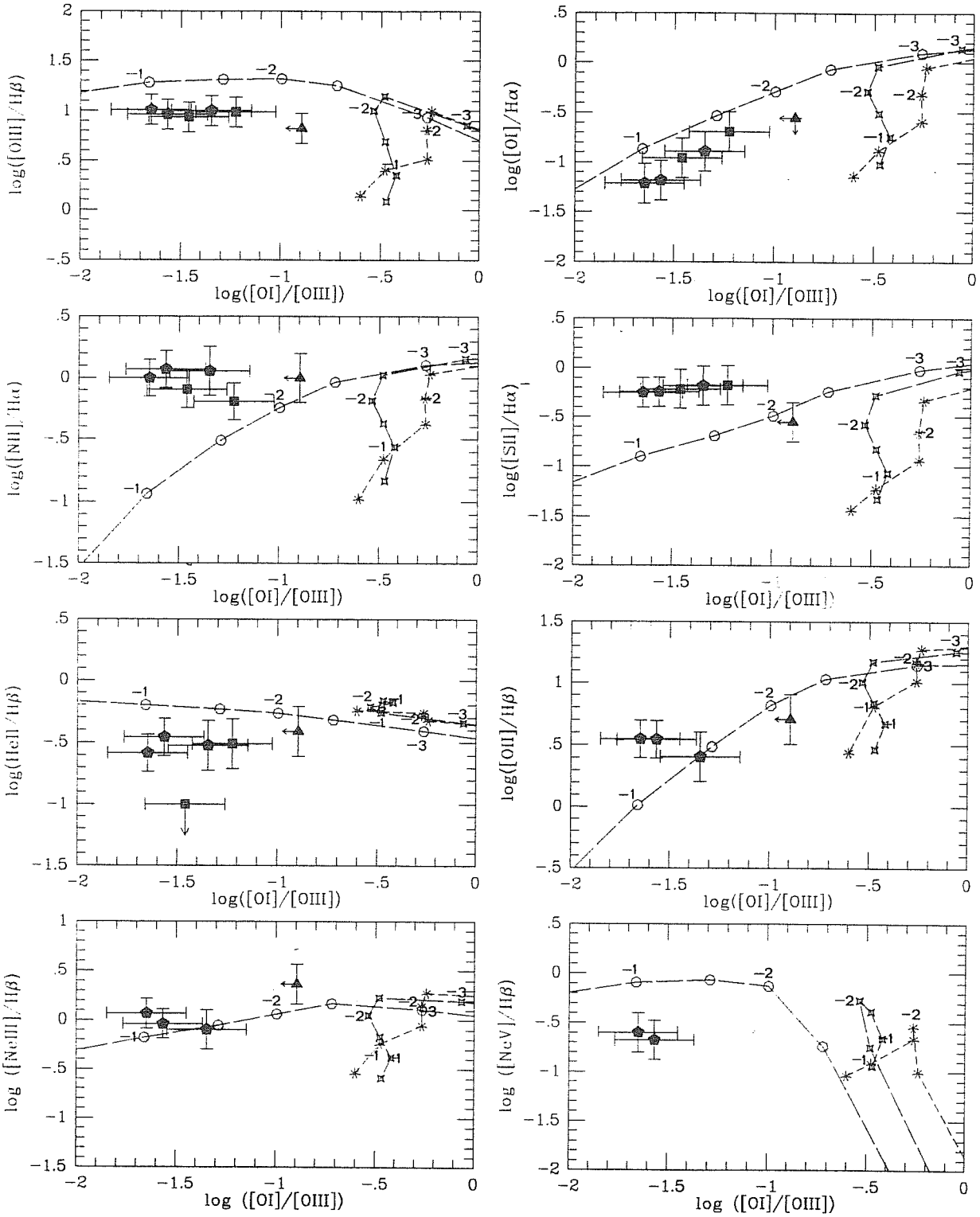

Figure 5.2: Diagnostic diagrams for different black hole masses and accretion disk sizes. The presented line ratios correspond to those in Table 5.1, for simplicity we omit the wavelength in the labelling of the figures. The lines join theoretical points corresponding to variation of the ionization parameter (which is indicated in logarithmic value) for each model with a given r_{out}; conceptually each line may be thought of as indicating the dependence of the line ratios on the distance of a line–emitting cloud from the accretion disk for a given black hole mass, disk size and density of the cloud. The different figures a, b and c correspond to models with black hole masses $10^6, 10^7$ and 10^8 $M_\odot$, respectively. The meaning of the symbols, which are joined by lines is as follows: asterisks correspond to a model with an accretion disk size $r_{out} = 50r_g$, stars to $r_{out} = 200r_g$ and open circles to $r_{out} = 1000r_g$. The observational data are indicated by the following filled symbols: triangles for NGC 1068 (BWW), pentagons for NGC 3516 (UP; Pogge, 1989a) and squares for NGC 4388 (Pogge, 1988b).

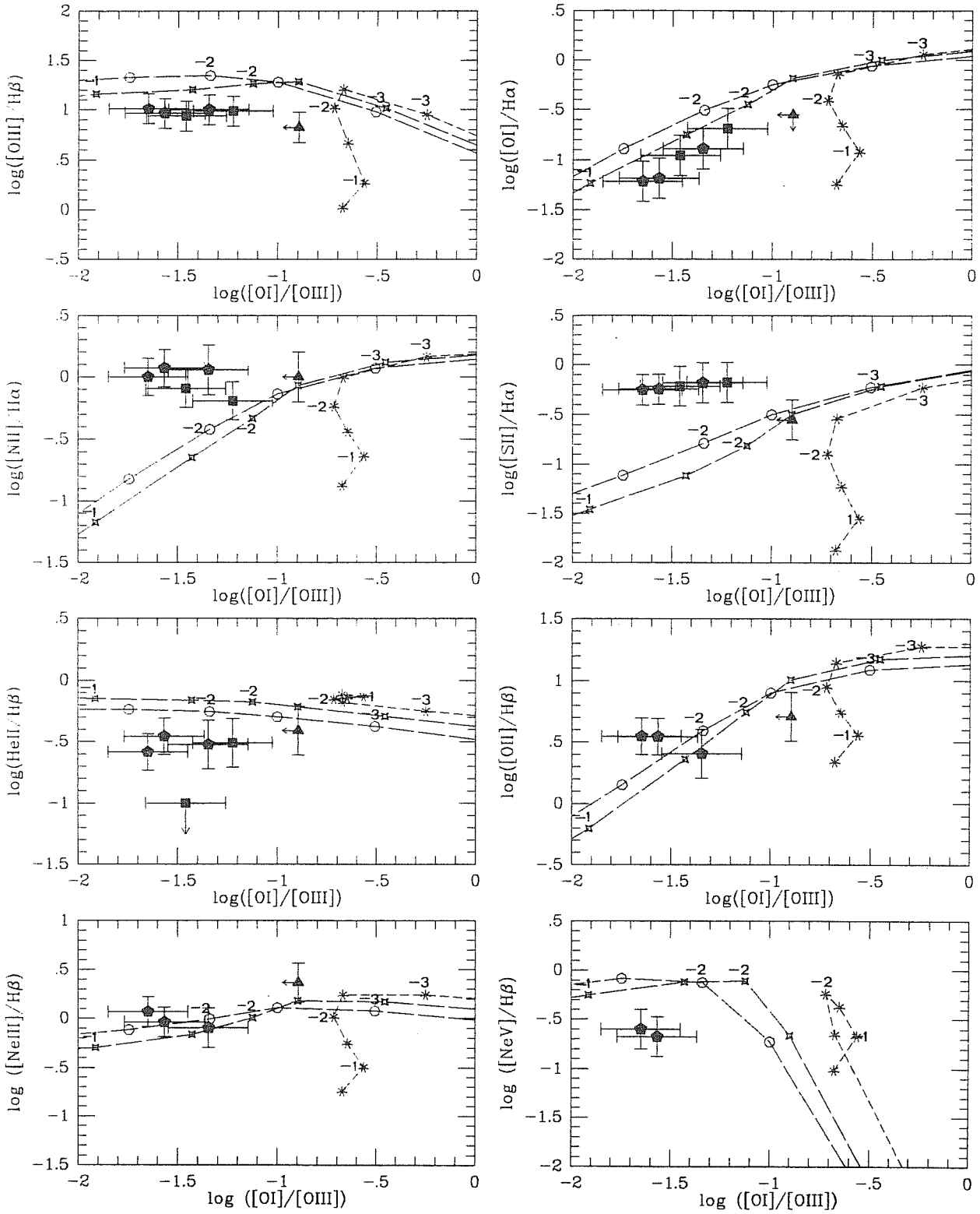
log([OIII]/Hβ)
log([OI]/[OIII])
log([OI]/Hα)
log([NII]/Hα)
log([SII]/Hα)
log(HeII/Hβ)
log([OII]/Hβ)
log ([NeIII]/Hβ)
log ([NeV]/Hβ)
log ([OI]/[OIII])

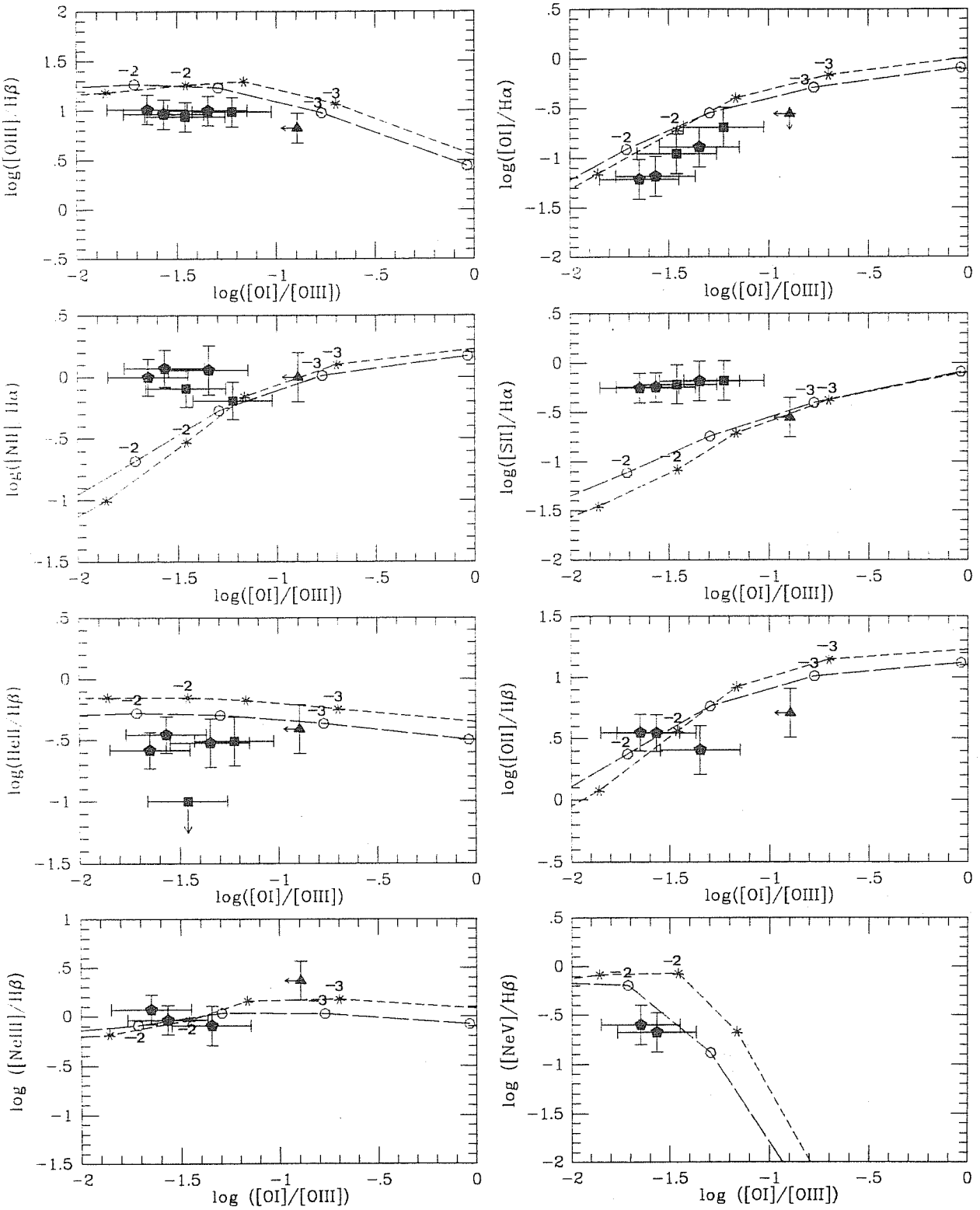
log([OIII] Hβ)
log([OI]/[OIII])
log([OI]/Hα)
log([NII] Hα)
log([SII]/Hα)
log(HeII/Hβ)
log([OII]/Hβ)
log ([NeIII]/Hβ)
log ([NeV]/Hβ)
−2
−3

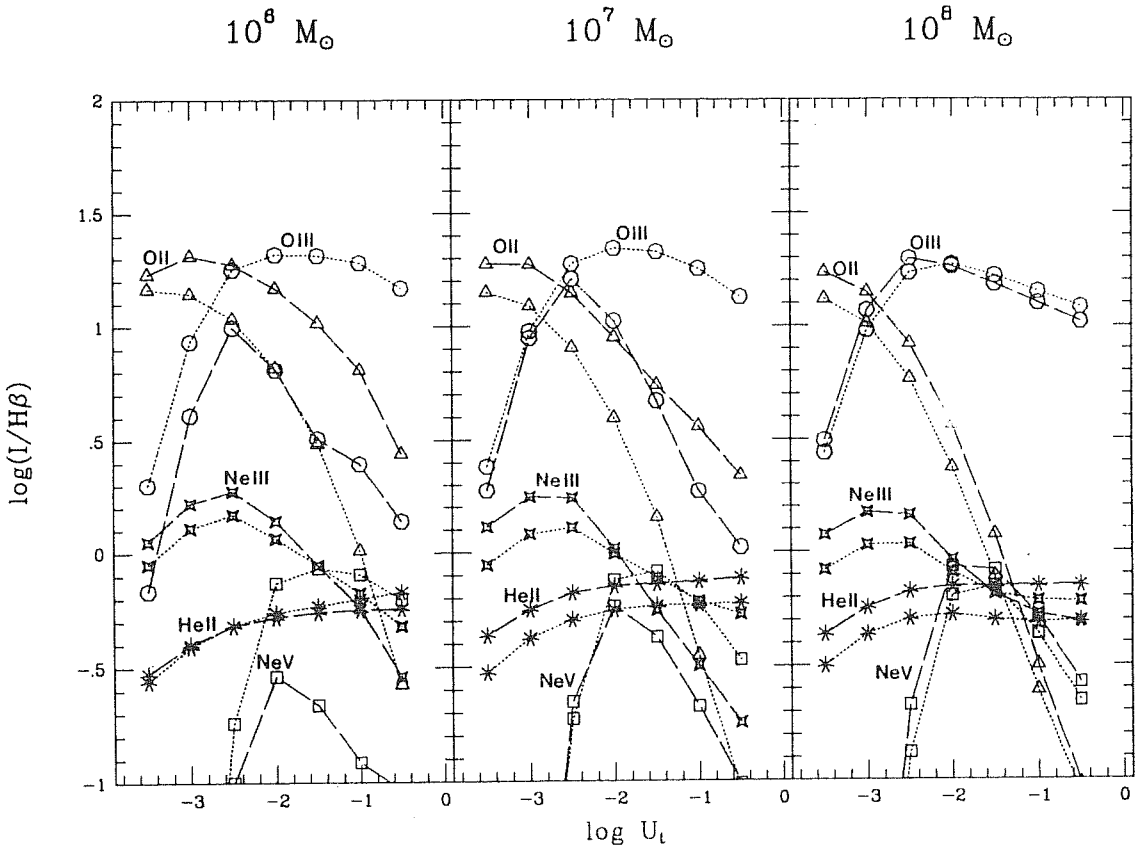

Figure 5.3: Line intensities relative to Hβ versus ionization parameter for different values of the black hole mass and accretion disk size. The symbols are as follows: open circles correspond to [OIII]λ5007, triangles to [OII]λ3727, stars to [NeIII]λ3869, squares to [NeV]λ3426 and asterisks to HeIIλ4686. The dashed and dotted lines correspond to $r_{out} = 50$ and $1000 r_g$, respectively. It is worth noting that for most of the considered line ratios, different values are obtained for the same U_t due to changes in the disk size.

not proportional to U_t (Tarter and Salpeter 1969). Therefore the strength of the low ionization lines relative to recombination lines decreases with increasing U_t.

5.2.2 Variation of the Black Hole Mass

The main effect of increasing the mass of the black hole from 10^6 to 10^8 $M_\odot$ is to increase the number of ionizing photons from $N_i/4\pi \sim 10^{53-54}$ to $10^{55-56} photons\ sr^{-1}\ s^{-1}$ (see Table 4.1). The result is to increase U_t by the same factor for clouds of given n_H and D. The predictions for line ratios at a given ionization parameter and disk size vary little with the black hole mass, for most values of U_t. However for $U_t \gtrsim 10^{-2.5}$ variations of the line ratios with M are significant for the following line ratios: [OII] λ3727/Hβ , [OIII] λ5007/Hβ and [NeV] λ3426/Hβ , using small disk sizes (see Fig. 5.3). This is because the *shape* of the spectrum is not critically dependent on the black hole mass, although the slight shift of the spectrum to lower frequencies with increasing M becomes important for large values of U_t, as we discuss in Sect. 5.2.3.

5.2.3 Variation of the Accretion Disk Size

We now consider the sensitivity of the different models to changes in the size of the accretion disk. When we increase the size of the accretion disk, the continuum increases at low frequencies. This effect is important for the line ratios [OIII] λ5007/Hβ and [OII] λ3727/Hβ because the ionization level of oxygen is changing between O^+ and O^{2+} in the range $U_t \sim 10^{-3.5} - 10^{-2}$ (the ionization potential of O^+ is $\simeq 35.1eV$). The result is that larger accretion disks tend to produce stronger [OIII] lines and weaker [OII] lines for a given ionization parameter. In this case the models corresponding to smaller disk sizes have a lower number of photons with energy $\geq 35.1eV$ than do models with larger disks and hence produce less O^{2+}.

More in detail we have found that, for a given U_t and $M = 10^6 M_\odot$, the [OIII] λ5007/Hβ and [OII] λ3727/Hβ line ratios depend critically on the accretion disk size (see Figs. 5.2.a and 5.3). For models with $M = 10^7 M_\odot$ we find that these two line ratios are only slightly dependent on accretion disk size as long as $U_t \lesssim 10^{-2}$ (see Figs. 5.2.b and 5.3). On the contrary, the dependence is very strong for $U_t \gtrsim 10^{-2}$. Models with $M = 10^8 M_\odot$ predict line ratios which are largely independent of the accretion disk size (see Fig 5.2.c). The explanation of these features lies in the following. When the ionization parameter increases, the ionization level of oxygen also increases. In particular, for $U_t \gtrsim 10^{-2.5}$ the ratio $n(O^{3+})/n(O^{2+})$ increases rapidly. Furthermore, for an ionizing spectrum peaked at frequencies close to the ionization potential of $O^{2+}(\sim 54.9eV)$, this ratio increases faster with the ionization parameter than for other spectra. Hence the line ratio [OIII] λ5007/Hβ decreases with increasing U_t because O^{3+} soon becomes the dominant ionization level of oxygen. This precise situation is found for the different spectra corresponding to different accretion disk sizes and $M \lesssim 10^7\ M_\odot$. For example, the spectrum produced by a disk of size $r_{out} \sim 50 r_g$ with $M = 10^7 M_\odot$ is peaked around 65 eV, whereas for $r_{out} \sim 1000 r_g$ the spectrum is peaked around 13 eV; note that the relative contributions to the ionization of O^{2+} and H are very different for these two values of r_{out}, causing the different dependences of the line ratio [OIII] λ5007/Hβ on ionization parameter.

The line ratio HeII λ4686/Hβ , which is usually taken as a clean diagnostic for the shape of the ionizing spectrum , is found to change slightly for the range of accretion disk sizes. It becomes somewhat more sensitive to variations in the size of the accretion

disk when $M \sim 10^8 M_\odot$ (see Fig. 5.3), and the trend is for this ratio to decrease for larger disk sizes since the number of photons capable of ionizing He^+ (energies between 4 and 6 ryd) relative to the number of photons capable of ionizing hydrogen decreases.

The line ratio [NeIII] $\lambda 3869/H\beta$ is also sensitive to the hardness of the spectrum in the UV region (the ionization potential of Ne^+ is $40.9eV$). At low values of the ionization parameter ($\leq 10^{-2}$) this ratio is lower for larger disks, but at larger values of the ionization parameter this trend is reversed.

The line ratio [NeV] $\lambda 3426/H\beta$ is very low for $U_t \approx 10^{-3}$ but reaches a peak for $10^{-2} \lesssim U_t \lesssim 10^{-1.5}$, at which values of U_t it may exceed the range of observed values. This line ratio tends to increase somewhat with the disk size (at $U_t \gtrsim 10^{-2}$), except for a black hole mass of $10^8 M_\odot$ in which case it is fairly independent of disk size.

The low ionization line ratios [OI] $\lambda 6300/H\alpha$, [SII] $\lambda\lambda 6716, 6731/H\alpha$ and [NII] $\lambda 6584/H\alpha$ are almost independent of the disk size, instead they depend mainly on the ionization parameter and geometrical factors, *e.g.* the thickness of the clouds (see Table 5.1).

An important feature which arises from our calculations is that models with black hole mass of order $10^7 M_\odot$ for relatively low values of the ionization parameter ($U_t \lesssim 10^{-2}$), and with mass of order $10^8 M_\odot$ for essentially all values of U_t, are degenerate, in the sense that models with different accretion disk sizes produce almost the same values of the line ratios. The application of line ratios as definitive discriminant between different accretion disk sizes is then restricted to $M \sim 10^6 M_\odot$; for $M \sim 10^7 M_\odot$, line ratios still provide some discrimination as long as $U_t \gtrsim 10^{-2}$ and $r_{out} \lesssim 200 r_g$. The reason for such behavior lies in the relatively small changes in the continuum at energies larger than $1ryd$ when we vary r_{out} for $M \gtrsim 10^7 M_\odot$ (*cf.* Fig. 5.1).

5.2.4 Sensitivity of the Predictions to β and r_{in}

We have tested the sensitivity of the predictions to changes in the ratio of gas to total pressure, β, and in the inner radius of the disk, r_{in}. The value of β must be larger than $\sim 10^{-6}$ because the thickness of the flow at the inner edge must be small (Abramowicz, 1985), whereas should not exceed $\sim 10^{-4}$ because the onset of a dynamical instability (Blandford, 1985a). Notice that in this model the value of β is assumed to be constant in the whole disk, however if β is allowed to vary these constraints can be relaxed. The decrease of β implies that the radiation pressure increases more and this leads to higher temperatures to be able to support the structure of the torus with the same total pressure (see eqs. 4.1 and 4.4). Hence the continuum emitted by the disk will tend to harden when β is very low. Changes of β are important for the predicted line ratios in the case of $M \sim 10^6 M_\odot$; for $\beta \simeq 10^{-6}$ the low ionization lines increase notably and the lines produced in the fully ionized region decrease slightly in comparison with the above models, for which $\beta = 10^{-4}$ (see Fig. 5.4.a). However, in the case of $M \sim 10^8 M_\odot$, only the luminosity of the lines produced in the partially ionized region changes appreciably: it increases relative to the previous model. Instead the luminosity of the lines coming from the H^+ region does not change appreciably (see Fig. 5.4.b). The variation of r_{in} leads to a change of the surface temperature in the innermost part of the disk since the flux which is generated at each radius is approximately proportional to r^{-3}. Thus the values of r_{in} close to $r_{mb} = 2r_g$ lead to a higher value of the maximum effective temperature than those close to $r_{ms} = 3r_g$. We have found that variations of r_{in} do not affect the predictions of the line intensities by more than a factor of 2, for any value of M. Anyhow the lines which are more affected are those produced in the partially

ionized zone (see Fig. 5.4.a,.b).

5.3 COMPARISON OF PREDICTED AND OBSERVED EMISSION LINE SPECTRA

In this section we fit the models described above to the observations of particular extended emission line nebulosities in Seyfert galaxies. Throughout this discussion we assume that the clouds lie along the rotation axis of the accretion disk. Some of the best quality spectroscopic data on ENLRs in Seyfert galaxies have been obtained along the radio axis, which is known to be close to the axis of the ionizing cones in all objects studied.

The models are parameterized in terms of the ionization parameter, the mass of the black hole and the outer radius of the accretion disk. We shall see that the mass of the black hole may be constrained by measuring the line luminosity from the ENLR and then, for a given black hole mass, we can place constraints on the size of the disk and the ionization parameter using the observed line ratios.

5.3.1 Number of Ionizing Photons

The study of extended emission line regions has several advantages over spatially unresolved emission line regions. One such advantage is that, since the projected distance from the active nucleus is known, we can estimate the number of ionizing photons reaching the cloud from the central source, using the observed line luminosities and ionization parameter (see below). However, uncertainties arise from the uncertain covering factor of the clouds and the insensitivity of the observations to weak lines.

One method of determining the absolute luminosity of the ionizing continuum is to count the number of Hβ photons emitted and then, assuming case B recombination (Osterbrock, 1974, p. 63), determine the number of photons in the ionizing continuum which are needed to produce such $H\beta$ luminosity. Then we can compare the number of photons required to produce a given observed line luminosity (N_l) with the number of photons available in the ionizing continuum (N_i) from a given accretion disk model. In Table 4.1 we present the number of ionizing photons per unit solid angle ($N_i/4\pi$) produced by the models we have used. The major variation in the number of ionizing photons for our models is produced by changing M, whereas changes in the disk size produce smaller variations. We have calculated N_l for two objects, NGC 1068 and NGC 3516, and the results are presented below in Sects. 5.3.3 and 5.3.3. These accretion disk models produce sufficient ionizing photons for both galaxies, even for the lowest value of the black hole mass we have considered.

A second method of constraining N_i is by means of the equation $N_i/4\pi = U_l n_H D^2 c$. U_l and n_H can often be estimated from the observed emission line spectrum and D can be measured directly, apart from projection effects. The best constraints on U_l result from ratios of lines produced in the fully ionized region (see Fig. 5.3), *e.g.* [OIII] λ5007/Hβ , [OII] λ3727/Hβ . The ratio [OII] λ3727/[OIII] λ5007 is found to be almost independent of the ionizing continuum for a variety of spectral shapes and only it is dependent on the value of U_l (Penston *et al.*, 1990).

Conversely, we may estimate the density from the expression $n_H = N_i/4\pi U_l D^2 c$;

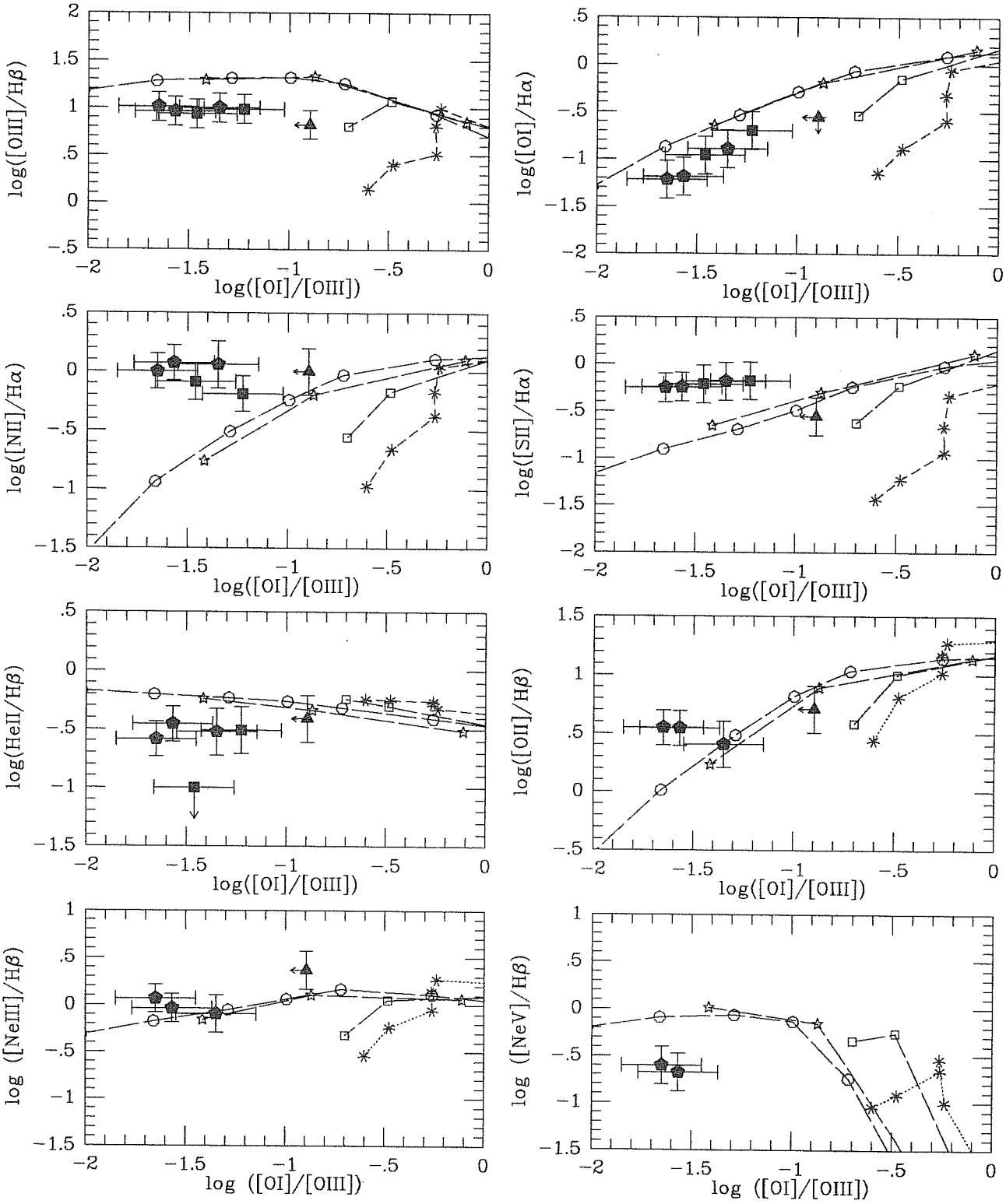

Figure 5.4: Diagnostic diagrams for $M = 10^6$, $10^8\,M_\odot$ and $r_{out} = 1000\,r_g$, changing the value of β and r_{in}. The meaning of the symbols is as follows: empty circles correspond to $r_{in} = 2.7r_g$ and $\beta = 10^{-4}$; open squares correspond to the same value of r_{in} and $\beta = 10^{-6}$: stars correspond to $r_{in} = 2.1r_g$ and $\beta = 10^{-4}$. For comparison the predicted line ratios for the corresponding M and $r_{out} = 50r_g$ (asterisks) are also presented. Note that the sequence of joined points correspond to values of U_t separated by an interval of 0.5 in logarithmic value for the usual values of β and r_{in} (they can be read from Fig. 5.2). Instead the sequence of joined points correspond to the values $logU_t = -1, -2, -3$ when the modified values of β and r_{in} are used. The observed line ratios are the same as in Fig. 5.2.

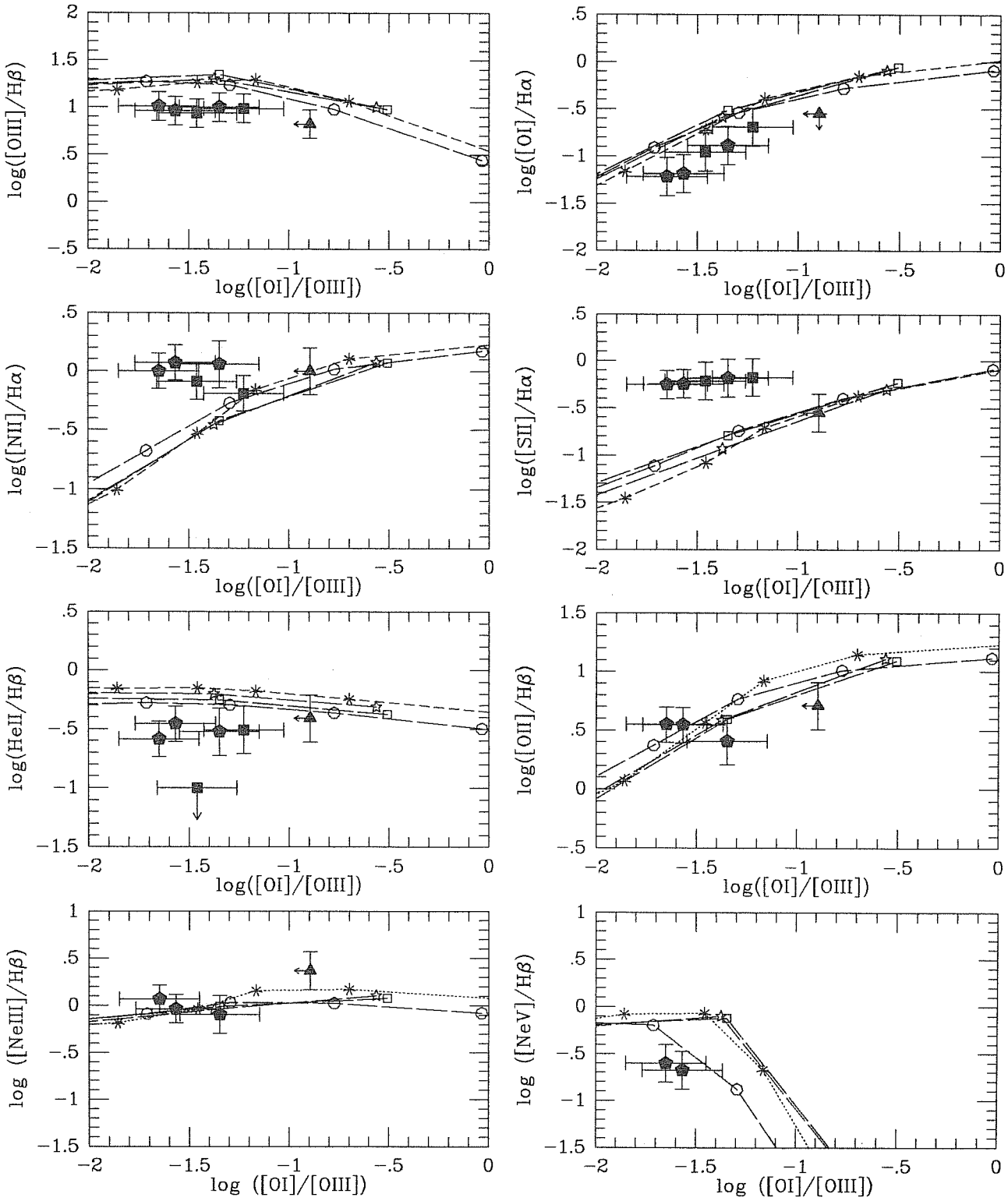
log([OIII]/Hβ)
log([OI]/[OIII])
log([OI]/Hα)
log([OI]/[OIII])
log([NII]/Hα)
log([OI]/[OIII])
log([SII]/Hα)
log([OI]/[OIII])
log(HeII/Hβ)
log([OI]/[OIII])
log([OII]/Hβ)
log([OI]/[OIII])
log ([NeIII]/Hβ)
log ([OI]/[OIII])
log ([NeV]/Hβ)
log ([OI]/[OIII])

the ionization parameter is taken from the best fit to the observed line ratios, the total number of ionizing photons is known (for a particular model) and the distance to the clouds is directly inferred from the observations. Subsequently this estimated value for the density is compared with that obtained for n_e from the observed [SII] $\lambda\lambda 6716, 6731$ or [OII] $\lambda\lambda 3726, 3729$ doublet ratios.

5.3.2 Line Ratios

In this section we fit the predicted line ratios to those observed in particular ENLRs. For three values of the mass of the black hole ($10^6, 10^7$ and $10^8 M_\odot$) we have looked for the most suitable values of two quantities – the ionization parameter and the size of the disk. The fitting is done for all the line ratios given in Table 5.3, when the lines involved are detected. In order to perform such fitting, we have to minimize some measure of the difference between the observed and predicted line ratios. We have tried to do the fitting with the help of a distribution function similar to that introduced by Krolik and Kallman (1988). However, such a function does not produce good discrimination for the different models, because some of the predicted ratios for any of the models considered are grossly different from their observational values. This is evident from direct inspection of the diagnostic diagrams presented in Fig. 5.2 (*e.g.* [SII] $\lambda\lambda 6716, 6731/\mathrm{H}\alpha$, [NII] $\lambda 6584/\mathrm{H}\alpha$). The figure of merit we have used is similar to a χ^2 distribution but includes a weighting function. It is defined as follows:

$$\chi^2 = \sum_{i=1}^{N} w_i \frac{(f_i - F_i)^2}{\sigma_i^2},$$

where f_i, F_i are the observed and predicted line ratios, respectively, σ_i is the observational error of the line ratios, N is the number of lines used in the fit and w_i is a weighting function which is assumed to be equal to unity for those line ratios in which any of the oxygen lines ([OIII] $\lambda 5007$, [OII] $\lambda 3727$ and [OI] $\lambda 6300$) are involved and equal to 0.2 for the remaining line ratios. Variation of these weighting factors within a factor of 2 gives similar results, compatible with the errors of the observed line ratios. This weighting function ensures a correct ionization level of the nebula, because it considers line ratios of the same element but at different ionization levels. Line ratios such as [NII] $\lambda 6584/\mathrm{H}\alpha$ and [SII] $\lambda\lambda 6716, 6731/\mathrm{H}\alpha$ are very sensitive to the column density and geometrical factors. The line ratio [OI] $\lambda 6300/\mathrm{H}\alpha$ has the same drawback, but we include it because it gives an indication about the extension of the continuum to high energies in the optically thick case we are considering. The line ratios HeII $\lambda 4686/\mathrm{H}\beta$, [NeIII] $\lambda 3869/\mathrm{H}\beta$ and [NeV] $\lambda 3426/\mathrm{H}\beta$ are sensitive to the shape of the spectrum for energies larger than a few rydbergs and they should be useful in determining the hardness of the continuum, although these lines are normally weak and thus difficult to measure.

The sensitivity of the quality of the fit to variations in U_l and r_{out} is also presented (see Fig. 5.5). We represent the confidence interval which contains 90% of the probability distribution, assuming that measurement errors are normally distributed, although this may be not statistically meaningful. Our best fit parameters for individual emission line regions in three Seyfert galaxies are given in Table 5.2 and discussed in detail below. We present the observed and predicted line ratios for each of the considered ENLRs in Table 5.3.

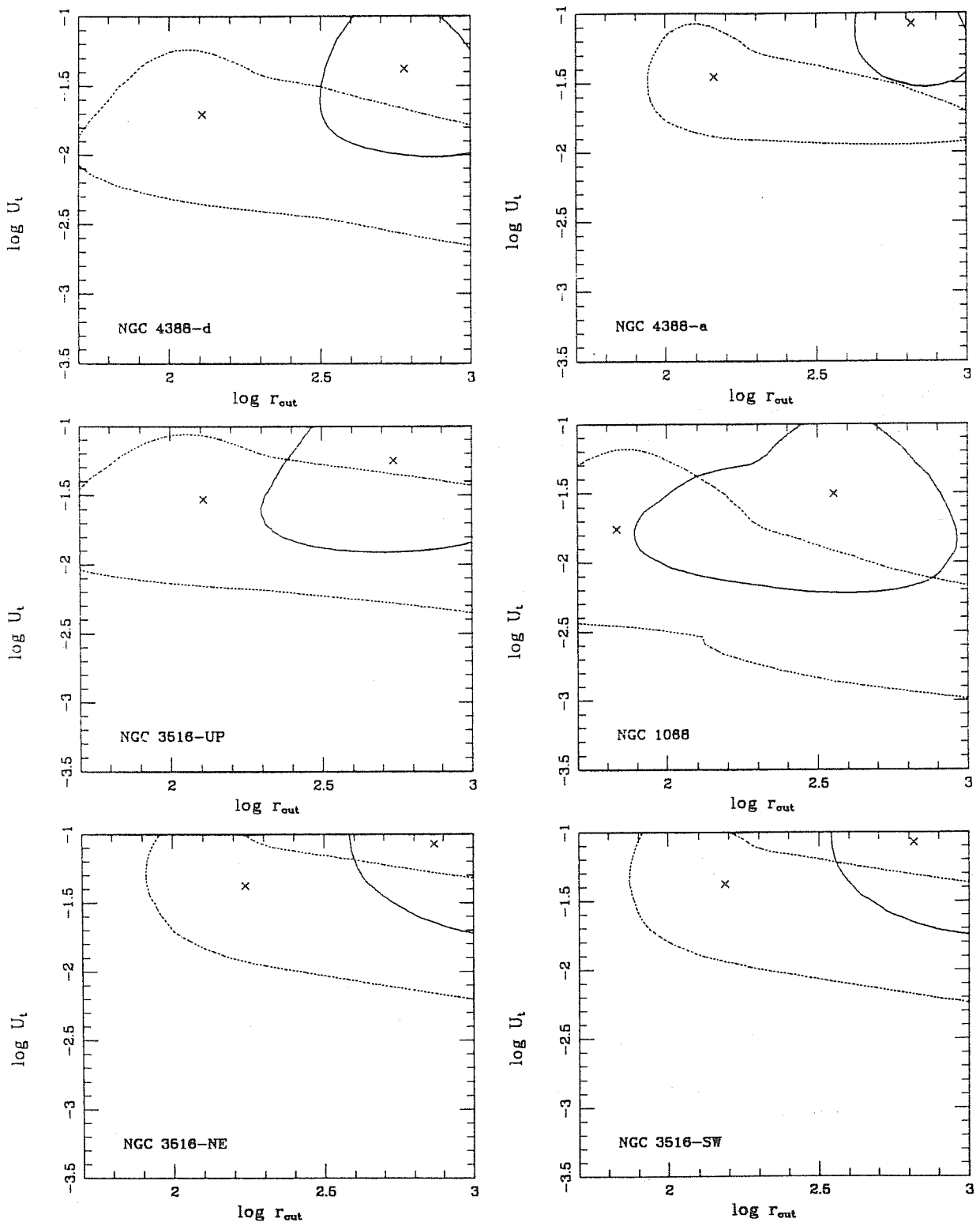

Figure 5.5: Plots of the probability distributions from our fitting function. The different panels represent different emission line regions, as indicated. The crosses denotes the maxima of the fitting function. The contours represent the 90% confidence intervals as for a χ^2 fit. The continuous lines are for models with $M = 10^6 M_\odot$, the dotted lines are for $M = 10^7 M_\odot$.

5.3.3 Individual Objects

NGC 1068

BWW have presented line ratios for a number of regions with high, medium and low excitation gas in NGC 1068. One of these regions, labelled "high 1" (see Fig 10a of BWW[1]), lies close to the axis of the "jet–like" radio source (Wilson and Ulvestad, 1987) and the cone of highly excited gas (Pogge, 1988a) and is therefore plausibly close to the axis of the accretion torus. We have taken the line ratios given by BWW for this off–nuclear high excitation region after applying a reddening correction, assuming an intrinsic $H\alpha/H\beta$ ratio of 3.1 (Veilleux and Osterbrock, 1987) .

For $M = 10^6 M_\odot$ the best fit to the observed line ratios is obtained for an accretion disk with $r_{out} = 360 r_g$ and $U_t = 3.1 \times 10^{-2}$. Assuming that the clouds are located at a distance of 2 kpc from the nucleus ($H_0 = 50\ km\ s^{-1}\ Mpc^{-1}$), the hydrogen density, as derived from $n_H = N_i/4\pi U_t D^2 c$ is $\sim 9\ cm^{-3}$. Instead, for $M = 10^7 M_\odot$ the best fit is obtained for an accretion disk with $r_{out} = 70 r_g$ and $U_t = 1.7 \times 10^{-2}$, and correspondingly we obtain $n_H \sim 130 cm^{-3}$. The best fit is for $M = 10^6 M_\odot$, but the two fits only differ in the minimum of the figure of merit by $\sim 20\%$. All models with $M = 10^8 M_\odot$ give similar predictions for the line ratios and the fit is equally good for any value of the disk size. The best fit is obtained for $U_t \sim 1.4 \times 10^{-3}$. The estimated hydrogen density is $\sim 10000 cm^{-3}$. This value is one order of magnitude higher than the one derived from the line ratio [SII]λ6716/[SII]λ6731 in BWW.

The number of ionizing photons may also be estimated from the observed Hβ luminosity, as discussed in section III-a. The covering fraction of the clouds is assumed to be 0.5% and the Hβ luminosity is $5 \times 10^{38}\ ergs\ s^{-1}$, from BWW. The resulting required number of ionizing photons per unit solid angle is $N_l/4\pi = 2.4 \times 10^{52}\ photons\ sr^{-1}\ s^{-1}$. A model with $M = 10^6 M_\odot$ and $r_{out} \sim 50 r_g$ produces $N_i/4\pi = 1.3 \times 10^{53}\ photons\ sr^{-1}\ s^{-1}$, a factor of 5 too large (see Table 4.1). A situation with such an excess of photons may still be viable if we allow for some extinction or photo-electric absorption along the path of the photons between the accretion disk and the emission line clouds (Bergeron, Petitjean and Durret, 1989). Alternatively, if the clouds are optically thin they may not absorb the whole budget of ionizing photons coming from the nucleus.

NGC 4388

The extended emission line gas in the Seyfert 2 galaxy NGC 4388 has been studied recently by several authors (Colina *et al.*, 1987; Corbin, Baldwin and Wilson, 1988; Pogge, 1988b). The Hα + [NII] $\lambda\lambda$6548, 6584 emission is dominated by HII regions in the almost edge-on galaxy disk. These HII regions are weak emitters of [OIII] λ5007. High ionization gas, best seen in [OIII]λ5007, extends above and below the galaxy disk to projected heights of 44″ (4.2 kpc for a distance to the Virgo cluster of 19.7 Mpc [Sandage and Tammann 1984]) to the North–East and 21″ to the South–West. The distribution of this high ionization gas, resembles two cones each with apex at the nucleus (Corbin, Baldwin and Wilson, 1988; Pogge, 1988b). The axis of each cone is close to that of the "linear" radio source (Stone, Wilson and Ward, 1988). For comparison with our models, we use Pogge's (1988b) spectra of the regions he terms

[1] Note that the diagrams of Figures 9 and 10 in BWW are interchanged. Their captions are, however, in the correct location.

$\underline{a}$ and $\underline{d}$ in his Table 1 (these are the outermost observed and should thus be less contaminated by the emission from the disk of the galaxy than regions farther in).

We have fitted models with $M = 10^6$, 10^7 and $10^8 M_\odot$ to the observations of each of the two regions. Obviously, the parameters of the accretion disk should be the same for both regions, if there is no extinction between the nucleus and each region. *A priori*, one notices that the line ratios are quite similar for the two regions and so a similar ionizing continuum is required.

For region $\underline{d}$ the best fit parameters for $M = 10^6 M_\odot$ are $r_{out} = 560 r_g$ and $U_t = 4.2 \times 10^{-2}$. This gives $n_H \sim 3\ cm^{-3}$, at the distance assumed for this cloud (3.3 *kpc*). The model for $M = 10^7 M_\odot$ gives the best fit for $r_{out} = 130 r_g$ and $U_t = 2.0 \times 10^{-2}$. The hydrogen density derived in this case is $\sim 55\ cm^{-3}$. The model for $M = 10^8 M_\odot$ produces the best fit at $U_t \sim 2 \times 10^{-3}$, independent of the disk size. The value derived for n_H is $\sim 8500\ cm^{-3}$.

The fits for region $\underline{a}$ give the following results: for $M = 10^6 M_\odot$, the best parameter values are $r_{out} = 655 r_g$ and $U_t = 8.4 \times 10^{-2}$; for $M = 10^7 M_\odot$, the respective values are $r_{out} = 145 r_g$ and $U_t = 3.5 \times 10^{-2}$; and for $M = 10^8 M_\odot$, r_{out} is not determined and $U_t \sim 4 \times 10^{-3}$. The estimations for the hydrogen densities, assuming a distance to the cloud of 5 *kpc*, are 0.6, 15 and 1900 cm^{-3}, respectively.

The best fit is obtained for region $\underline{d}$ ($\chi^2 = 4.6$) whereas the fit in region $\underline{a}$ ($\chi^2 = 8.7$) is significantly worse. There is no substantial difference in the quality of the fits for any of the black hole masses.

An encouraging result is that the best fits for the two regions are obtained with very similar values of the accretion disk size, in spite of the fact that the ionization parameter changes significantly from one region to another. Furthermore, region $\underline{a}$, which is located farther from the nucleus, is fitted with a higher value of the ionization parameter. However the statistical significance of this result is not clearly established. Anyhow, if the difference between the ionization parameters is significant, a steep density gradient must be present between regions $\underline{d}$ and $\underline{a}$ with the density decreasing faster than D^{-2}, D being the distance from the nucleus.

NGC 3516

UP found indications of the presence of highly ionized gas around the nucleus in the Seyfert 1 galaxy NGC 3516. They made spectroscopic observations of different regions outside the nucleus and reported the line ratios for a *typical* nebulosity. More recently Pogge (1989a) reported observations of the extended ionized gas, combining direct imaging with long-slit observations at $P.A. = 35°$. He gave line ratios for two regions located to the North East and South West at a distance of $8''$ from the nucleus. The position angles of these clouds from the nucleus are similar to that of the radio axis (Wrobel and Heeschen, 1988). The region located to the SW is close to the one described in UP. We have fitted our models to these three sets of line ratios.

As for the previous objects the fits have been done for the models with $M = 10^6$, 10^7 and $10^8 M_\odot$. Let us first consider the fit for the line ratios reported by UP. The best fit for $M = 10^6 M_\odot$ is obtained for $r_{out} = 655 r_g$ and $U_t = 6.3 \times 10^{-2}$. Assuming that the distance of the clouds is 2 *kpc* the estimated n_H is $\sim 5 cm^{-3}$. The best fit for $M = 10^7 M_\odot$ is accomplished for $r_{out} = 155 r_g$ and $U_t = 3.1 \times 10^{-2}$. The estimated n_H is $\sim 100 cm^{-3}$. For $M = 10^8 M_\odot$ the best fit is obtained for $U_t \sim 5 \times 10^{-3}$ and then the estimated n_H is $\sim 10000\ cm^{-3}$. We now consider the set of line ratios given by

TABLE 5.2: BEST FIT PARAMETERS

	NGC 1068		NGC 4388 (d)$^\diamond$		NGC 4388 (a)$^\diamond$		NGC 3516-UP		NGC 3516-NE		NGC 3516-SW	
Parameter	$10^6 M_\odot$	$10^7 M_\odot$	$10^6 M_\odot$	$10^7 M_\odot$	$10^6 M_\odot$	$10^7 M_\odot$	$10^6 M_\odot$	$10^7 M_\odot$	$10^6 M_\odot$	$10^7 M_\odot$	$10^6 M_\odot$	$10^7 M_\odot$
r_{out}	360	70	560	130	655	145	655	155	740	175	655	155
U_t	3.1×10^{-2}	1.7×10^{-2}	4.2×10^{-2}	2.0×10^{-2}	8.4×10^{-2}	3.5×10^{-2}	6.3×10^{-2}	3.1×10^{-2}	8.4×10^{-2}	4.2×10^{-2}	5.6×10^{-2}	3.1×10^{-2}
χ^2_{min}	3.3	4.2	4.6	6.0	8.7	9.8	7.2	8.7	16.9	16.1	21.0	21.6

Table 5.2: Best fit to the observed line ratios for the thick disk model with $M = 10^6$ and $10^7\,M_\odot$. For $M = 10^8\,M_\odot$ only the value of U_t is well constrained, but the value of r_{out} is not.

$^\diamond$ Letters in parentheses refer to regions defined in Table 1 of Pogge (1988b).

TABLE 5.3: OBSERVED AND PREDICTED LINE RATIOS

	NGC 1068			NGC 4388 (d)$^\diamond$			NGC 4388 (a)$^\diamond$			NGC 3516-UP			NGC 3516-NE			NGC 3516-SW		
		Predicted			Predicted			Predicted			Predicted			Predicted			Predicted	
Line Ratio	Obs.	$10^6 M_\odot$	$10^7 M_\odot$	Obs.	$10^6 M_\odot$	$10^7 M_\odot$	Obs.	$10^6 M_\odot$	$10^7 M_\odot$	Obs.	$10^6 M_\odot$	$10^7 M_\odot$	Obs.	$10^6 M_\odot$	$10^7 M_\odot$	Obs.	$10^6 M_\odot$	$10^7 M_\odot$
[OIII] λ5007/Hβ	6.67	8.26	8.63	9.7	11.32	12.45	8.67	11.30	11.70	10.0	12.07	12.65	10.27	13.20	13.42	9.21	12.39	12.65
[OII] λ3727/Hβ	5.12	5.16	6.07	...	3.35	4.15	...	1.75	2.54	2.55	2.21	2.73	3.54	1.58	1.87	3.50	2.42	2.73
[OI] λ6300/Hα	< 0.28	0.30	0.23	0.20	0.25	0.25	0.11	0.16	0.17	0.13	0.20	0.19	0.06	0.16	0.14	0.07	0.21	0.19
[NII] λ6584/Hα	1.0	0.38	0.43	0.65	0.29	0.34	0.81	0.17	0.23	1.14	0.20	0.25	1.00	0.16	0.18	1.18	0.22	0.25
[SII] $\lambda\lambda$6716, 6731/Hα	0.28	0.17	0.10	0.67	0.16	0.10	0.61	0.12	0.07	0.66	0.15	0.08	0.56	0.13	0.06	0.57	0.15	0.07
HeII λ4686/Hβ	0.39	0.62	0.71	0.31	0.62	0.69	< 0.1	0.63	0.70	0.30	0.62	0.70	0.26	0.63	0.70	0.35	0.62	0.70
[NeIII] λ3869/Hβ	2.33	0.75	0.78	...	0.74	0.78	...	0.62	0.63	0.80	0.68	0.66	1.17	0.64	0.62	0.92	0.70	0.66
[NeV] λ3426/Hβ	...	0.54	0.55	...	0.62	0.66	...	0.59	0.64	...	0.62	0.68	0.25	0.65	0.66	0.21	0.64	0.68

Table 5.3: Predicted line ratios for the best fit values of the disk model. The data are taken from the references in the text (Section 5.3.3). The errors of the data are assumed to be: 15% for the more intense lines and 30% for the weaker ones. In the case of NGC 3516-UP the errors may be larger, up to 50%.

$^\diamond$ Letters in parentheses refer to regions defined in Table 1 of Pogge (1988b).

Pogge. For the region located to the NE, the best fit is obtained for a black hole mass of $10^6 M_\odot$ with $r_{out} \sim 740 r_g$ and $U_t \sim 8.4 \times 10^{-2}$. For a black hole mass of $10^7 M_\odot$ the best fit is for $r_{out} \sim 175 r_g$ and $U_t \sim 4.2 \times 10^{-2}$. The estimated densities from the two fits are 4 and 90 cm^{-3}, and the clouds are located at $D = 1.88$ kpc. The region located to the SW, at the same distance from the nucleus, gives the best fits for $r_{out} \sim 655$ and 155 r_g and $U_t \sim 5.6 \times 10^{-2}$ and 3.1×10^{-2} with $M = 10^6$ and $10^7 M_\odot$, respectively. The corresponding values for the density are 6 and 110 cm^{-3}. For $M = 10^8 M_\odot$, r_{out} is not well determined and $U_t \sim 6 \times 10^{-3}$, so the estimated n_H is ~ 9500 cm^{-3}. The SW region almost corresponds to the observations presented by UP and indeed the line ratios are quite similar. The fits obtained for the two regions are in good agreement, the calculated values for the disk size coincide, and only slight differences are found for the ionization parameter.

It is possible to estimate the number of ionizing photons present in the continuum from the measured Hα flux (Pogge 1989a). We assume a covering fraction of 0.6 (Pogge 1989a) and then the number of ionizing photons derived from the Hα luminosity is $N_l/4\pi \sim 2.2 \times 10^{52}$ *photons* sr^{-1} s^{-1}, which is very close to the value derived for NGC 1068.

5.4 DISCUSSION

Several consequences may be deduced from the previous calculations. An important one, concerning the accretion disk models we used, is that for a range of black hole masses $10^6 - 10^7 M_\odot$ the fits constrain both the ionization parameter and the accretion disk size. However, in order to select effectively between different spectral shapes, variations in the ionization parameter should not compensate for changes in the spectral shape due to different masses or disk sizes. In this respect, the values for the density of ENLR's, as estimated above, strongly depend on the value of U_t, which varies accordingly to the shape of the considered ionizing continuum. The best fit value for the ionization parameter decreases in the sequence $M = 10^6, 10^7$ and $10^8 M_\odot$ which, when taken together with the increase in N_i with increasing M, leads to a rapid increase in n_H along this sequence.

On the other hand, we find that the ionizing spectra we have used do not satisfactorily reproduce some of the observed line ratios, especially those corresponding to low excitation species (see Table 5.3). This effect could be attributed to the lack of an X–ray component in our ionizing spectra. The addition of a hard X–ray component will produce an increase in the strengths of the low excitation lines but will not affect appreciably the lines produced in the fully ionized region. As a test, we added a power law component ($F_X \propto \nu^{-0.7}$) to our ionizing continuum with an optical to X-ray spectral index $\alpha_{oX} = 1$. The index α_{oX} refers to a power law which connects the fluxes at 2500 Å (1.2×10^{15} Hz) in the optical/UV band and that at 2 keV in the soft X–ray part. This value is relatively high compared to the observed ones (Zamorani *et al.*, 1981; Marshall *et al.*, 1984), so our computations will tend to overestimate the importance of the X–ray component. We have considered two cases: $M = 10^6$ and $10^8 M_\odot$, in both we take $r_{out} = 1000 r_g$. We have adopted a large value of r_{out} because the importance of the X–ray power law component scales with the flux at $\sim 10^{15}$ Hz, and for the models we have considered here the flux at such frequency comes from the outer parts of the disks, as it can be seen from Fig. 5.1. Therefore the large is the disk size the high is the X–ray component, and then it affects more the emission line spec-

trum. The results for $10^6 M_\odot$ show an increase in the line ratio [SII] $\lambda\lambda 6716, 6731/\mathrm{H}\alpha$ by a factor of ~ 2 and a more moderate increase for the line [NII] $\lambda 6584$. The rest of the line ratios remain almost constant (see Fig. 5.6.a). However the addition of the X–ray component emission when $M = 10^8 M_\odot$ modifies the ionizing continuum more appreciably than when $M = 10^6 M_\odot$, since the continuum emission at 10^{15} Hz is larger in the former case. Hence the largest modification of the line spectrum will be expected for $M = 10^8 M_\odot$. The line ratio [SII] $\lambda\lambda 6716, 6731/\mathrm{H}\alpha$ increases by a factor of ~ 10 to 100 when U_t increases from $\sim 10^{-2}$, to 10^{-1}. The other lines, which are at least in a large part produced in the partially ionized zone are less affected by the presence of the additional X–ray component; thus [OI] $\lambda 6300/\mathrm{H}\alpha$ and [NII] $\lambda 6584/\mathrm{H}\alpha$ increase by a factor ~ 4 and ~ 2, respectively, when $U_t = 10^{-2}$. The rest of the lines we are considering, vary less than a factor of 2 in the considered range of U_t (see Fig. 5.6.b). We conclude that, except for extreme cases, the predictions of the emission lines are not changed with the inclusion of the X-ray power law. In fact, Binette, Robinson and Courvisier (1988; hereafter BRC) pointed out that the relative contribution of the hard X–ray component to a thermal component which peaks in the extreme UV (according to the observed α_{oX}) may be insufficient to affect significantly the low ionization lines.

The ionizing continua produced by our radiation supported torus are more similar in spectral form to blackbodies than to power laws particularly for low values of r_{out} (see BRC). The spectra we have considered tend, however, to be much more energetic (the mean energy ranges from 70 eV to 150 eV) than the black body considered by BRC (the mean energy in their case is around 35 eV). BRC noticed that a major drawback of using a black body as a photoionization source is the predicted weakness of the [SII]$\lambda\lambda 6716, 6731$ lines in comparison with power law models. Moreover, they found that both black body and power law spectra produce a very intense [OI] $\lambda 6300$ line. We have encountered the same problems: the theoretical curves in the diagnostic diagrams seem to be shifted to the right with respect to the observational points, owing to the high predicted value for [OI] $\lambda 6300/$[OIII] $\lambda 5007$ (see Fig. 5.2). This problem would be alleviated if some of the clouds were *matter bounded*; the partially ionized H^0 region would then be less extended and the intensity of the lines from OI, SII and NII would be lower, but this worsens the sulfur and nitrogen problem.

A more severe constraint may come from the line ratio HeII $\lambda 4686/\mathrm{H}\beta$. The predicted value of this line ratio is always larger than the observed one, possibly indicating that the contribution at energies between 4 and 7 *ryd* in the continuum is too large in our model compared with that at 1 *ryd*. The ionizing spectrum should be depressed at those energies, as concluded by Binette, Courvoisier and Robinson (1989). The predicted values for the line ratio [NeV] $\lambda 3426/\mathrm{H}\beta$ are larger than those observed in NGC 3516 by Pogge (1989a), although the predictions do not reach the high values found by Bergeron, Petitjean and Durret (1989) for NGC 1068. Photoelectric absorption of the soft X-ray part of the spectrum due to the presence of gas between the nucleus and the emission line clouds could alleviate this problem. Moreover this may also account for the observed high [NeV] $\lambda 3426/\mathrm{H}\beta$ ratio, in contrast with the moderate HeII $\lambda 4686/\mathrm{H}\beta$ ratio and in some cases low [OIII] $\lambda 5007/\mathrm{H}\beta$ ratio, found in the ENLR of NGC 1068 (Bergeron, Petitjean and Durret, 1989; Evans and Dopita, 1986). The low ionization lines produced in the partially ionized region will increase its luminosity relative to H recombination lines, since the importance of the X–ray component raises relative to the low energy part of the ionizing continuum.

A further modification of the spectrum will be to consider the reflection of the pho-

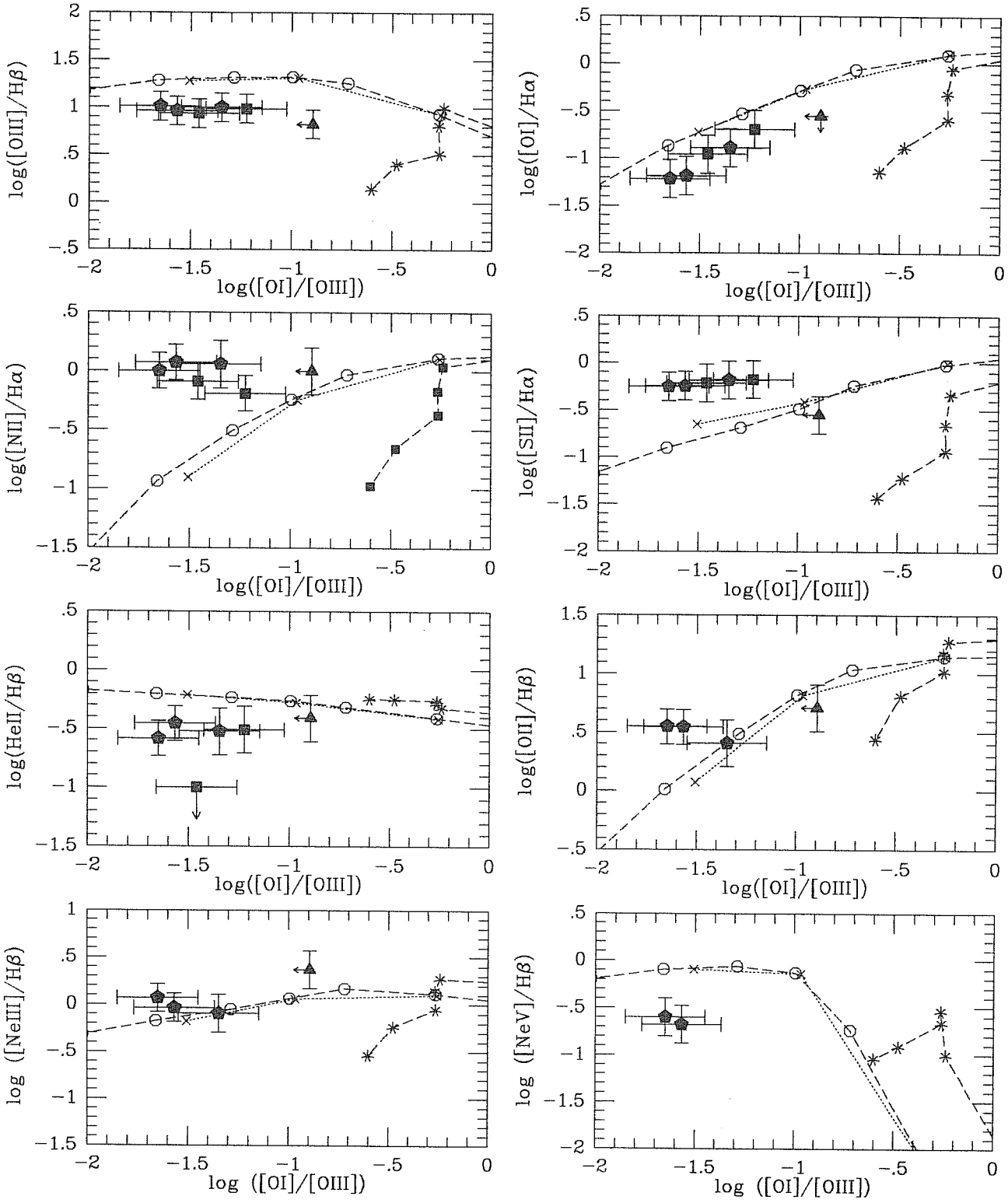

Figure 5.6: Diagnostic diagrams for $M = 10^6$ and $10^8 M_\odot$ and disk sizes $r_{out} = 50,\ 1000\, r_g$. We present the predictions for the emission lines calculated with only the ionizing continuum from the accretion disk (open circles for $r_{out} = 1000\, r_g$ and asterisks for $r_{out} = 50 r_g$) and with the addition of a power law component in the X–ray (crosses) [see text for details of this component]. Fig. 5.6.a, b correspond to $M = 10^6, 10^8\, M_\odot$, respectively. The joined points correspond to $logU_t = -1, -2, -3$ when the power law is included, whereas the same values as in Fig. 5.2 when the pure accretion disk emission is considered. The observed line ratios are the same as presented in Fig. 5.2.

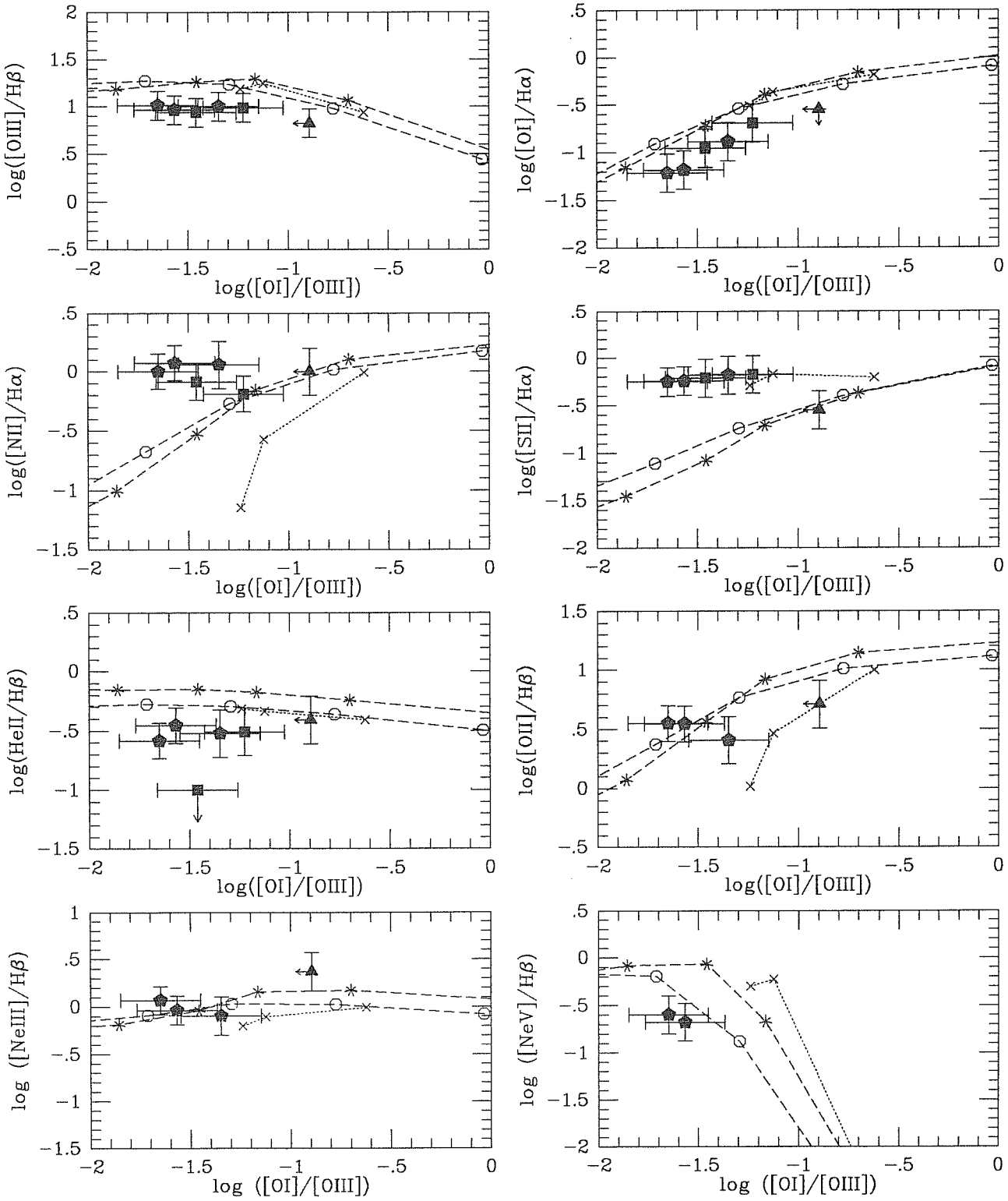
log([OIII]/Hβ)
log([OI]/[OIII])
log([OI]/Hα)
log([NII]/Hα)
log([SII]/Hα)
log(HeII/Hβ)
log([OII]/Hβ)
log ([NeIII]/Hβ)
log ([NeV]/Hβ)

tons in the walls of the funnel, as described in Madau (1988). The spectrum becomes harder and more strongly peaked in the *soft-X* and *UV* when $M = 10^6$ and $10^8\, M_\odot$, respectively. Note that we are only considering the changes operated upon the continuum including the reflection effect, when the disk is observed along the rotation axis; the angular dependence of the disk emission will be also affected, we will mention the effects on the emission lines in the next chapter. Therefore we expect for $M = 10^6\, M_\odot$ further increasing of the low ionization lines produced in the partially ionized region as well as those species with high ionization potential produced in the H^+ region, as Ne V, when compared with the current calculations. For $M = 10^8\, M_\odot$ we will expect more intense high ionization lines relative to low ionization lines for the species present in the fully ionized region, in particular HeII $\lambda 4686/\mathrm{H}\beta$ will have certainly higher values than the current ones. The lines coming from the partially ionized region will be increased as well.

5.5 CLOSING REMARKS

In this chapter we have studied the photoionization of Extended Narrow Line Regions in Seyfert galaxies by the radiation produced in a thick accretion disk, at the pole–on view of the disk.

We have calculated the emission line spectrum for three black hole masses ($10^6, 10^7$ and $10^8\ M_\odot$), under the assumption that the clouds are located close to the rotation axis. We varied the values of both the ionization parameter (which determines the ionization level of the nebula) and the disk size (which produces a variation in the continuum shape). An interesting feature of the ionizing spectra used is that by changing the accretion disk size and fixing the ionization parameter there are significant changes in the emission line spectrum, especially for the forbidden lines of O III and O II.

We have found that models with $M = 10^6 M_\odot$ fit the observations for very large accretion disk sizes ($\sim 500 r_g$), whereas models with $M = 10^7 M_\odot$ fit them better with smaller disks. The latter models would be preferable since they have less super–Eddington accretion rates than the former, in better agreement with the results for Seyfert 1 galaxies as derived from other methods 4.2.3. Models with $M = 10^8\ M_\odot$ do not predict different line ratios when r_{out} is varied.

There are discrepancies between our predicted lines ratios and the observed ones. The predicted ratios of the low ionization lines, *e. g.* [SII] $\lambda\lambda 6716, 6731/\mathrm{H}\alpha$, [NII] $\lambda 6584/\mathrm{H}\alpha$ are always smaller than the observed values. This suggests that the ionizing spectrum we used should be supplemented by an X-ray extension (Comptonization or a non-thermal component could increase the X-ray flux), although simply adding a power law at X-ray frequencies does not solve the problem, as we shown in Section 5.4. On the other hand the predicted HeII $\lambda 4686/\mathrm{H}\beta$ ratio is high compared with the observed values; this implies that the intensity of the continuum should be lower at energies larger than 4 *ryd.*

In conclusion, we see from Table 5.2 that models of the ENLR based on photoionization by accretion disk emissions can give some interesting constraints on the mass of the hole and on the size of the accretion disk. However, some of the line ratios deduced from the model are not in good agreement with observations and therefore the deduced values for the disk size and the ionization parameter are not very reliable. Nevertheless, we do believe that this kind of investigation is worthwhile mainly because it allows us to obtain more information on the central engine of AGN's from their ex-

Chapter 6

PHOTOIONIZATION OF THE ENLR BY THE THICK ACRETION DISK EMISSION: ANGULAR VARIATION OF THE EMISSION LINES

6.1 WHAT IS THE GEOMETRY TO STUDY THE ANGULAR DEPENDENCE IN THE ELNR?

The spatial distribution of the emitting gas is usually investigated by imaging with narrow-band filters, which are centered on certain intense emission lines, particularly [OIII]λ5007 and Hα. These studies show in several cases that highly ionized gas delineates a wide cone, pointing towards the nucleus and whose axis almost coincides with the radio structure. The opening angles of these structures are of several tens of degrees [1] (Pogge, 1989b), *e.g.* in NGC 5252 it is observed to be $\sim 75°$ (Tadhunter and Tsvetanov, 1989), in NGC 4388 it is $\sim 92°$ (Pogge, 1988b). In most of the cases the distribution of the line emitting gas is very filamentary and the surface brightness is quite low to allow to measure the angular dependence of the emission line spectrum.

We have assumed that the line emitting gas is photoionized by the radiation emerging from a geometrically thick accretion disk. In Chapter 5 we present the predictions for the emission lines only at viewing angles close to the disk axis. However the most appealing aspect of the thick disk model – the collimation of the radiation field – was not explored. In this chapter we will study if this ionizing continuum is able to reproduce the observed structure for the ENLR. Now we consider the angular dependence of the thick disk emission and we make predictions for the behaviour of various emission lines at different separation angles from the rotation axis. We consider two simplified geometries for the distribution of the ionized gas (see Fig. 6.1):

- The gas is distributed in the disk of the galaxy and the torus axis is contained in such plane (Fig. 6.1.a). In the case that the torus axis is slightly inclined with respect to this plane, this geometry is still valid with the inclusion of projection

[1] The value of the opening angle is usually given from edge to edge, instead when we refer to the opening angle of the funnel later on this Chapter it will correspond to the value from the axis to the edge.

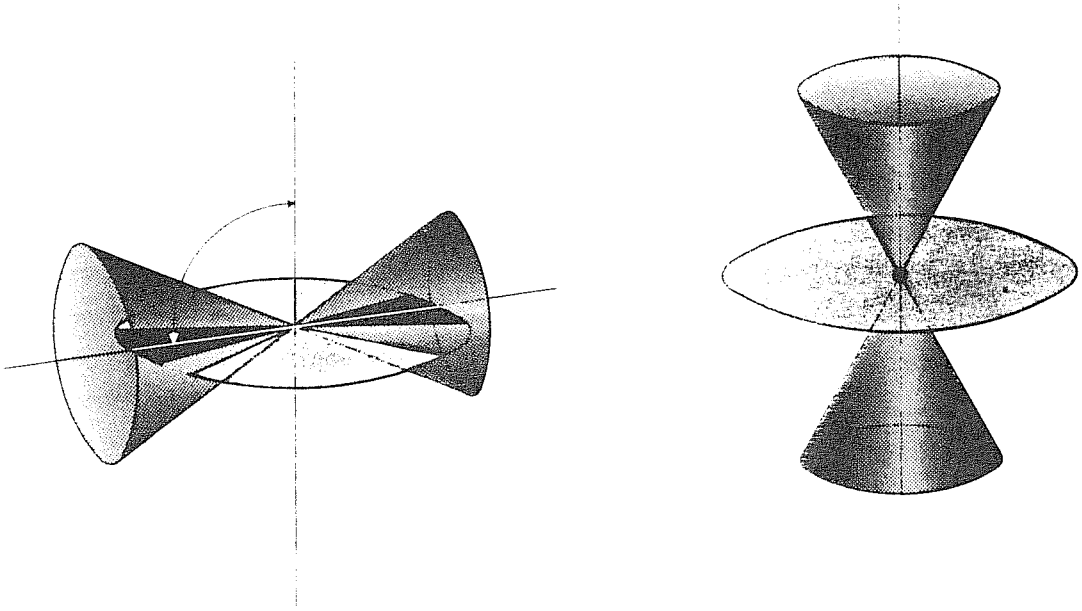

Figure 6.1: Two possible geometries for the study of the angular dependence of the emission line in ENLR, regarding to the line emitting gas distribution and the orientation of the source of the ionizing continuum (in our case the accretion torus). In case *a* the gas is distributed in the plane of an spiral galaxy, instead in case *b* we require the presence of gas outside the disk of the galaxy or either the situation is more appropiate for an elliptical galaxy. (Adapted from Meurs [1989]).

effects. In such conditions the emission that we associated with the torus axis is actually shifted to a small viewing angle separated from this.

- The gas is distributed uniformly in the halo of the galaxy, and the torus axis is oriented far from the plane of the galaxy disk (Fig. 6.1.b). In this geometry the cone which we observed is the projection in the plane of the sky of a whole volume of emitting gas. The line emission observed at a certain inclination angle with respect to the cone axis results as contribution from several inclination angles through the line of sight.

There are observational evidences which suggest that these two geometries are good descriptions. The disk distribution of the emitting gas is adequate in the galaxies observed by Unger *et al.* (1987) and NGC 4151 (Schulz, 1988), in which the gas shares the rotational motions of the galaxy disk. However a tridimensional cone projected in the plane of the sky seems to be a more appropiate description in the case of the nearly edge–on Seyfert 2 galaxy NGC 4388 (Pogge, 1988b).

In any of these geometries the simplest assumption is to consider an uniform distribution of gas which extends far from the active nucleus and is lit up by the anisotropic nuclear continuum source. Most of the radiation emitted by the accretion torus is produced in the funnel, at large separation angles from the disk axis it is occulted and the

ionizing flux is greatly decreased. In section 6.2 we present quantitatively the decrease of the number of ionizing photons with the viewing angle and the dependence on the disk model parameters, *i.e.* M and r_{out}. Moreover the spectral shape of the ionizing continuum changes with the viewing angle because the emission at different viewing angles is dominated by radiation from different temperature zones on the disk surface. We will study how this affects the predictions for the emission lines in Section 6.3. In Section 6.4 we include the variation of both the ionizing flux and the spectral shape to study how the luminosity of the emission lines will vary with the viewing angle in the geometry described in Fig. 6.1.a. In Section 6.5 we will discuss the results from the previous section and analyze the problems with this model. In order to test the conclusions about the angular dependence of the emission lines on the ionizing continuum, we have also computed a model in which the disk emission is calculated assuming the continuum as a sum of blackbodies and the same disk model. In Section 6.6 we present summary and conclusions of the Chapter.

6.2 ANGULAR DEPENDENCE OF THE IONIZING FLUX

Let us qualitatively examine how the emission coming from the disk changes with the viewing angle. When the disk is observed along the rotation axis the radiation coming from the funnel dominates the continuum emission at high energies. As one moves away from the axis, the farthest outer part of the torus is progressively occulted but the radiation coming from there contributes only to the lowest frequency part of the spectrum and with a small fraction to the absolute luminosity, except when the disk size is large enough. The most abrupt variation occurs when the viewing angle just exceeds the opening angle of the funnel (hereafter θ_{open}) and its walls start to be occulted. Thus θ_{open} will be the critical quantity which measures the collimation of the disk emission. The continuum emitted at large inclination angles will be affected in two ways: 1) the number of photons which are seen is progressively diminished; 2) the hottest parts of the funnel are occulted and the spectrum lacks its high energy tail and softens considerably since the temperature of the outer parts of the disk is lower than in the funnel (see Chapter 4). The first effect will decrease the luminosity of the lines and the global ionization level of the clouds at large viewing angles; this will be studied in the rest of this Section, while the qualitative change of the ionizing continuum will be presented in Section 6.3.

We can predict how the emission line spectrum of a low density isotropic nebula located far from the central source (the ENLR) is affected by the variation of the ionizing flux. A good indication of the degree of ionization of the nebula is given by the value of the ionization parameter U_i (U_i is defined in Section 5.2). The number of ionizing photons present in the continuum when varying the viewing angle θ is the quantity which governs the variation of U_i, at fixed n_H and D. Moreover the value of N_i depends on the disk model for a given inclination angle. The relevant parameters which make N_i to change considerably in the accretion disk model are the mass of the black hole and the size of the disk. Other parameters of the disk model, such as the ratio of gas pressure to total pressure (β) and the value of the internal radius (r_{in}), introduce only slight variations on the emitted spectrum.

The continuum emitted by the accretion disk is calculated as described by Madau

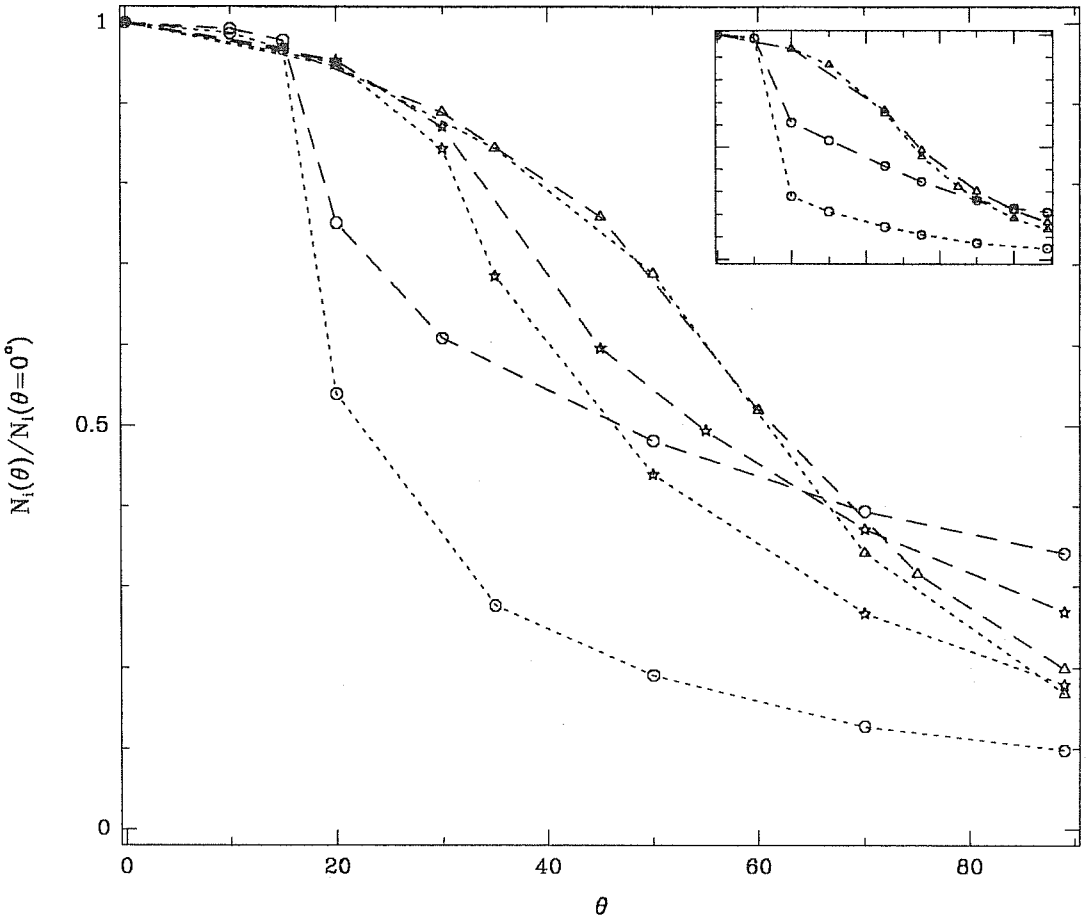

Figure 6.2: Variation of N_i [$\epsilon \geq$ 1ryd] with the viewing angle, normalized to the value at the rotation axis. The dashed and dotted lines correspond to models with $M = 10^6\,M_\odot$ and $M = 10^8\,M_\odot$, respectively. The meaning of the symbols is as follows: empty circles correspond to models with $r_{out} = 1000\,r_g$, stars to $r_{out} = 200\,r_g$ and triangles to $r_{out} = 50\,r_g$. For comparison, we present in the upper right box the same results from a disk model with the Jaroszyński *amd*. The meaning of the lines and symbols are the same as described above.

(1988) (see Chap. 4). We present in Fig. 6.2 the dependence of N_i on the inclination angle for different values of the black hole mass and disk size. From inspection of Fig. 6.2 it is clear that the greatest collimation of the ionizing continuum is obtained at large disk sizes and black hole masses. For comparison we present the results adopting the Jaroszynski *amd* (Abramowicz, Calvani and Nobili 1980 [ACN]; or see Sect. 4.5.2), but using the same assumptions for the rest of the model parameters (ratio of gaseous pressure to total pressure, and the opacity being dominated by electron scattering). Fortunately the choice of the *amd* is not a drastic assumption for our photoionization problem when calculating the emission at viewing angles close to the rotation axis (Section 4.5.2). Differences arise at viewing angles far from the disk axis, because the geometrical shape is strongly dependent on the *amd* used. The funnel is very steep when the Jaroszynski *amd* is used: this fact favours the shadowing of the inner parts of the disk and leads to a large collimation of the emitted continuum at high frequencies.

The variation of the disk size changes the profile of the disk, which becomes more inflated when the disk is larger. This fact modifies the geometry of the funnel, which becomes steeper as the disk size increases and therefore provides a narrower beam of

TABLE 6.1: OPENING ANGLE OF THE FUNNEL

r_{out}	θ_{open}	
r_g	MADAU	ACN
50	45°	30°
200	30°	20°
500	20°	10°
1000	15°	8°

Table 6.1: Opening angle of the funnel for various values of r_{out} and two angular momentum distributions (see text and Sect. 4.5.2 for details). The funnel becomes narrower when the disk size is increasing. Notice the large collimation which can be achieved.

radiation. In the model we are considering here the opening angle of the funnel is $\sim 45°$ for a disk size $\sim 50\ r_g$ and it becomes as narrow as $\sim 15°$ when the disk size increases up to $r_{out} \sim 1000 r_g$. We present in Table 6.1 the opening angles of the funnel at different disk sizes; for comparison we also present the values for a different thick accretion disk model (ACN). It is important to notice that the opening angle of the funnels critically depends on the *amd*. Here we have considered two *amd* which are close to be extreme cases (Jaroszynski, Abramowicz and Paczynski, 1980). The Jaroszynski *amd* produces the steepest funnels, therefore it can be taken qualitatively as a lower limit to the needed value for the accretion disk size, and consequently to the accretion rate. At first glance it seems that collimation of the radiation in cones with opening angles similar to those observed can be obtained without requiring the presence of a very thick accretion disk. This feature is somehow relieving if we recall that Seyfert galaxies seems to have sub-Eddington accretion rates (Padovani and Rafanelli, 1988). It is worth mentioning here that the reflection effect of the radiation in the funnel walls could shallow the collimation (Madau, 1988). Other mechanisms like electron scattering in a pair–plasma corona (Svensson, 1986), or in the broad line region itself (Kallman and Krolik, 1986) could affect as well the collimation of the disk emission.

The increase of the black hole mass shifts the frequency where the maximum of the spectrum is found (the surface temperature depends on the black hole mass as $M^{-4/15}$). In particular for $M = 10^6\ M_\odot$ the spectrum extends up to energies of few keV, instead for $M = 10^8\ M_\odot$ the spectrum extends only up to frequencies of hundreds of eV. This shift in frequency of the energy distribution with M produces an interesting effect when calculating the number of ionizing photons. The variation of N_i for small disk sizes (we refer to $r_{out} \sim 50\ r_g$) is quite similar for the two black hole masses mentioned above; however when the disk size is increased ($r_{out} \gtrsim 200 r_g$) the collimation is noticeably larger for $10^8\ M_\odot$ than for $10^6\ M_\odot$. The reason for this particular behaviour resides in the origin of photons with energies $\gtrsim 1\ ryd$ (see Fig. 6.3.a). The fraction of photons which comes from inside the funnel is similar in the two cases (10^6 and $10^8 M_\odot$). The continua emitted at $\theta = 0°$ and $90°$ are similar hence the angular variation of N_i reflects uniquely the effect of the obscuration by the funnel walls. However when the disk is large the outer parts contribute more to the low energy part of the spectrum: in the case of $M = 10^6 M_\odot$, the low energy tail lies substantially in the range of energies above 1 *ryd*, unlike the case of $M = 10^8 M_\odot$ where the outer parts contribute mostly at energies lower than 1 ryd (see Figs. 6.3.b and 6.3.c). Consequently, occultation of the funnel does not affect much the flux of ionizing photons when $M = 10^6\ M_\odot$ but it

is prominent when $M = 10^8\, M_\odot$.

6.3 ANGULAR DEPENDENCE OF THE SPECTRAL SHAPE OF THE DISK EMISSION

Up to now we have only considered the changes verified in the absolute ionizing flux by varying the inclination angle. In this section we study the variations of the emission lines corresponding purely to changes in the spectral shape of the ionizing continuum as seen at different values of θ. The photoionization code MAPPINGS (Binette, Dopita and Tuohy, 1985) was used to compute the line intensities. At each angle we assume a plane parallel slab which is photoionized by the disk emission. This slab is taken to be uniform, with a constant density of 100 cm^{-3}. The clouds are assumed to be optically thick and therefore radiation bounded (the clouds extend until the fraction of ionized hydrogen dropped below 1%). The fact that we are considering at each viewing angle a plane parallel geometry, instead of a global spherical geometry, is plausible only if the physical extension of the clouds in the radial direction is negligible in comparison with the scale of the observed features (Robinson [1989]; see also Binette, Robinson and Courvoisier [1988] for a discussion on the influence of the geometry).

We have constructed a grid of models for two values of the black hole mass ($M = 10^6$ and $10^8 M_\odot$) and three disk sizes ($r_{out} = 50$, 200 and $1000\, r_g$). We adopt the same values for the internal radius of the disk ($r_{in} = 2.7$), and for the ratio of gaseous to total pressure ($\beta = 10^{-4}$) as in Chapter 5. For each disk model (M and r_{out} fixed) we compute the emission at several inclination angles, and then for each continuum the emission line spectrum is calculated at different values of the ionization parameter.

In order to make an analysis of the variation of the spectral shape of the ionizing continuum with the viewing angle and the effect on the emision lines one has to look at the predictions for several line ratios by various models at a given value of U_t.[2] It is worth to keep in mind that in this section we make a comparison of different ionizing continua at fixed U_t. When we normalize each ionizing continua to this value, the self-shadowing of the surface of the disk determines only the spectral shape but not the value of N_i which is fixed a priori. The line ratios we have investigated are the same as considered in Chapter 5. They include the most commonly observed optical emission lines and have shown useful to distinguish among different ionizing continua (Baldwin, Phillips and Terlevich, 1981; Stasińska, 1984; Veilleux and Osterbrock, 1987).

The spectral shape of the continuum depends moreover on the parameters which model the accretion disk – we study the different angular dependence for various values of the disk parameters ($M = 10^6, 10^8 M_\odot$ and $r_{out} = 50$, 200 and $1000\, r_g$). Variation of the black hole mass and the disk size produce the most relevant changes in the shape of the continuum. Other disk parameters, such as the internal radius (r_{in}) and the ratio of gaseous to total pressure (β), produce minor variations (see Chapter 5) and will not be considered here.

[2] Comparison of line ratios at the same value of U_t is not a precise method to discriminate among different spectral shapes. Variations of U_t may compensate for variations of the spectral shape. It will be more correct to use a parameter which preserves the general excitation level of the line spectrum, as proposed by Binette, Robinson and Courvoisier (1988). However the advantage to use U_t is that it is directly related to the flux of ionizing photons N_i and then it can be easily related to the variation of the flux with θ because of obscuration.

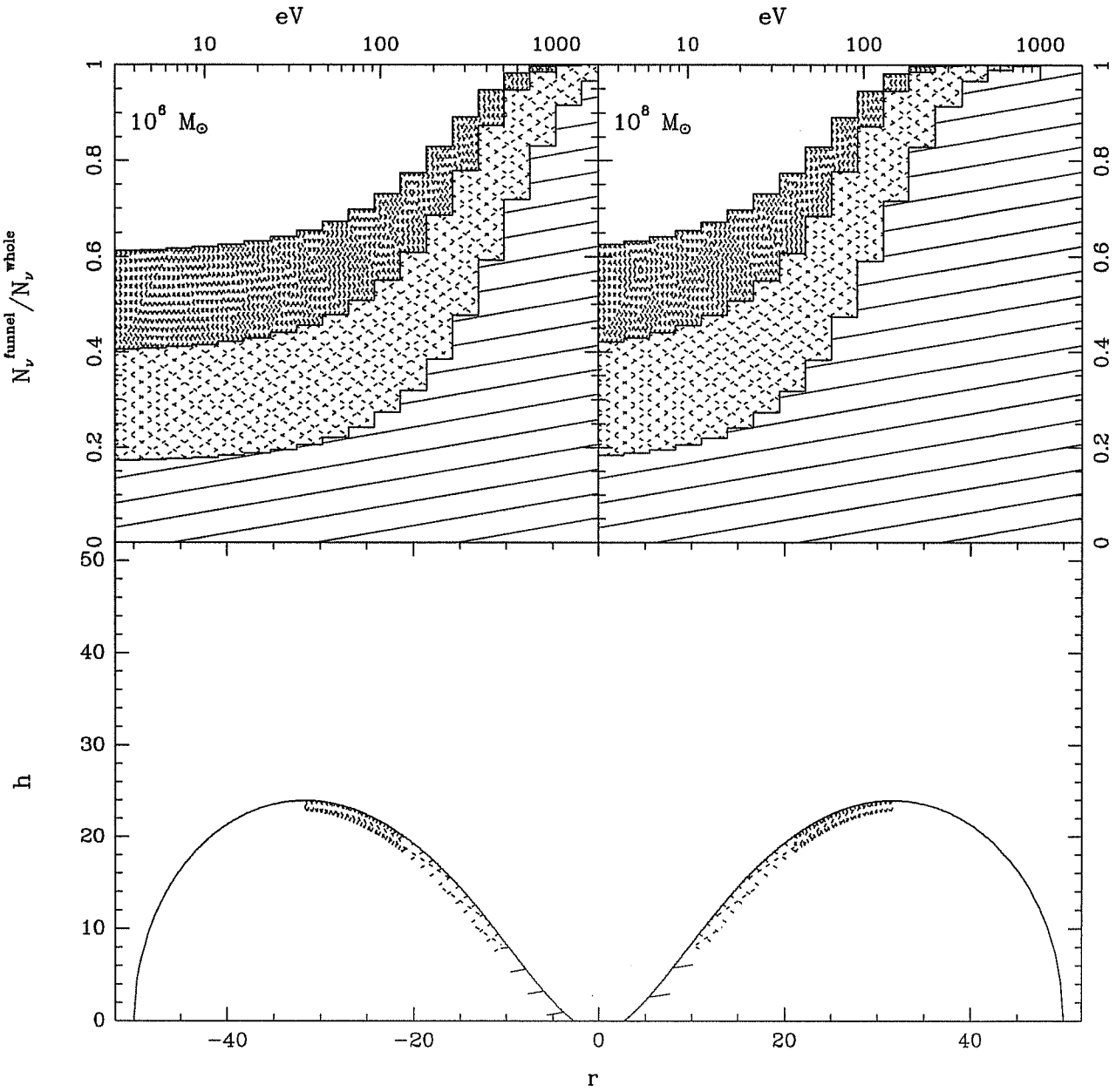

Figure 6.3: In the bottom panel we present the meridional cross section of the thick disk. The funnel is divided into three parts (indicated by the different shaded zones), each one corresponds to one third of the radial distance corresponding to the maximum height. In the upper panels the fraction of photons of the total disk emission which comes from each region is specified as a function of their energy, for two values of M (10^6 and $10^8\,M_\odot$). Figures 6.3.a,6.3.b and 6.3.c correspond to different disk sizes, 50, 200 and 1000 r_{out}, respectively. Note that for small disks ($r_{out} \sim 50\ r_g$) the fraction of ionizing photons ($\varepsilon \geq 13.6$ eV) which comes from the funnel is comparable for any value of M (see Fig. 6.3.a). However for large disks ($r_{out} \sim 1000\ r_g$) this fraction is smaller for $M = 10^6\,M_\odot$ than for $M = 10^8\,M_\odot$ (see Fig. 6.3.c).

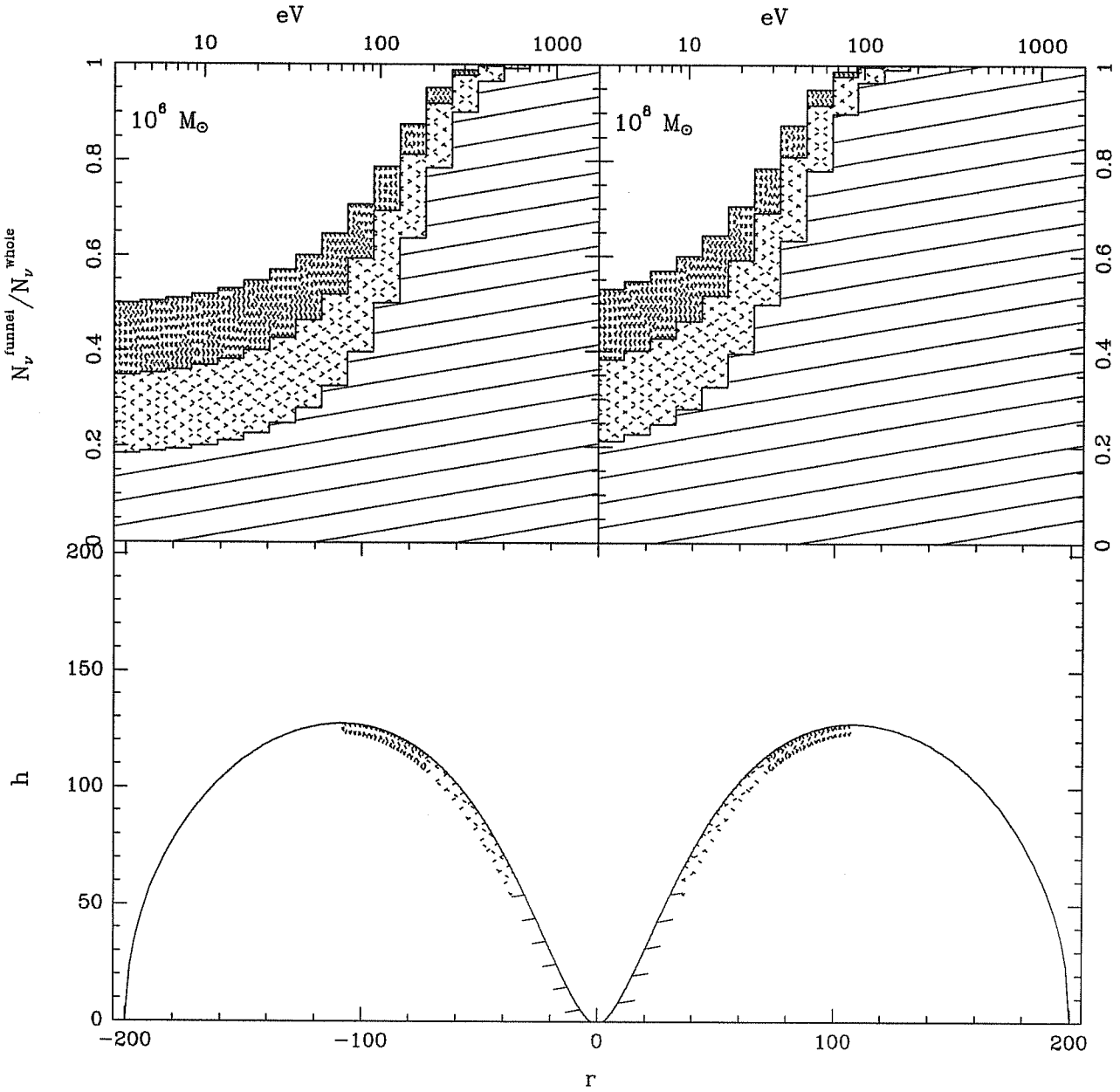
eV
10
100
1000
10^6 $M_\odot$
10^8 $M_\odot$
$N_\nu^{funnel}/N_\nu^{whole}$
0
0.2
0.4
0.6
0.8
1
h
150
100
50
0
−200
−100
0
100
200
r

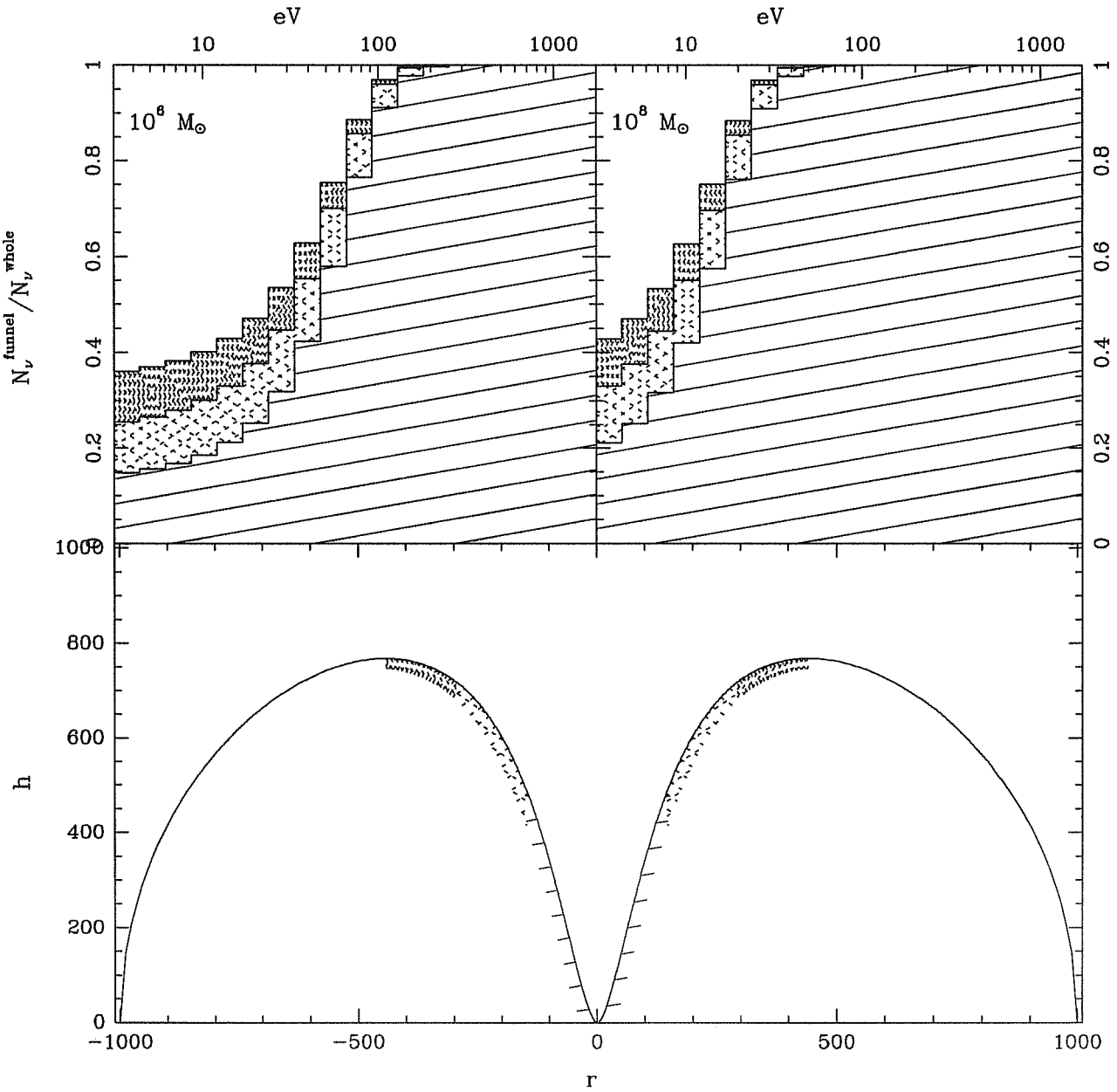
eV
10
100
1000
10^8 $M_\odot$
$N_\nu^{funnel}/N_\nu^{whole}$
0
0.2
0.4
0.6
0.8
1
h
800
600
400
200
0
−1000
−500
0
500
1000
r

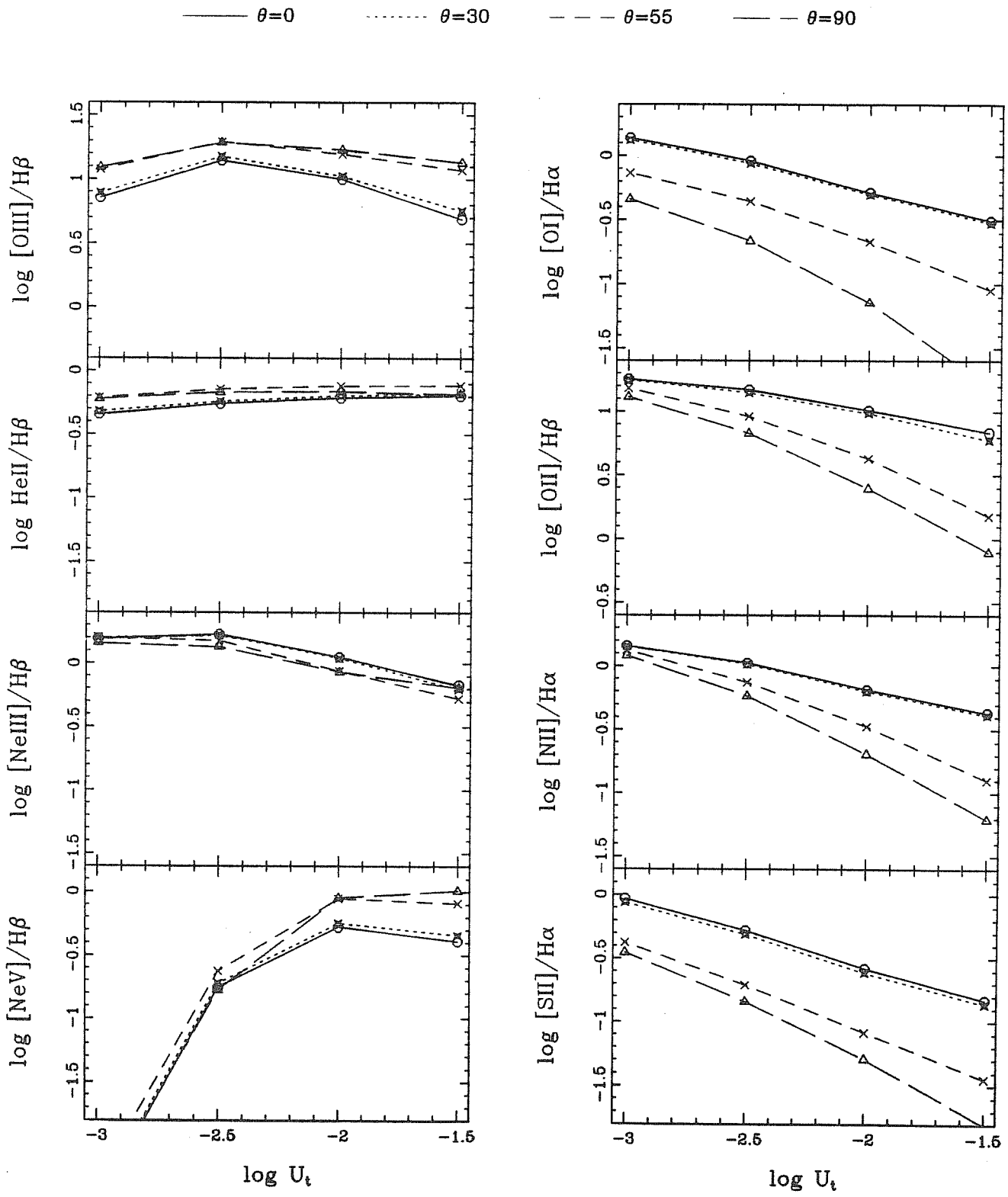

Figure 6.4: Different line intensities , normalized to H recombination lines, vs. U_t at different separation angles from the disk axis. We computed the angular variation of the line ratios for two values of M (10^6 and $10^8\,M_\odot$) and three value of r_{out} ($50, 200$ and $1000 r_g$).

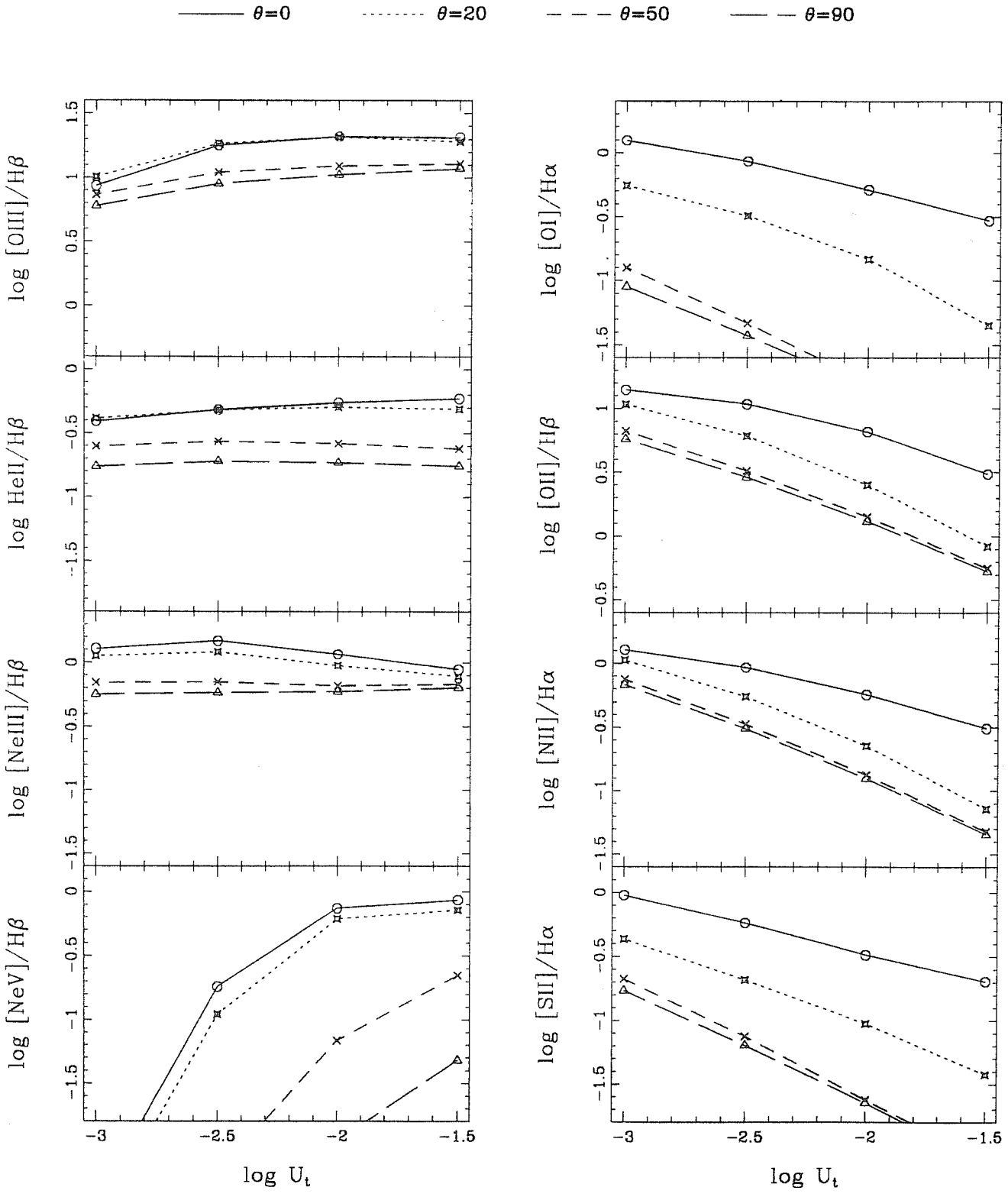
θ=0
θ=20
θ=50
θ=90
log [OIII]/Hβ
log HeII/Hβ
log [NeIII]/Hβ
log [NeV]/Hβ
log [OI]/Hα
log [OII]/Hβ
log [NII]/Hα
log [SII]/Hα
log U_t
log U_t

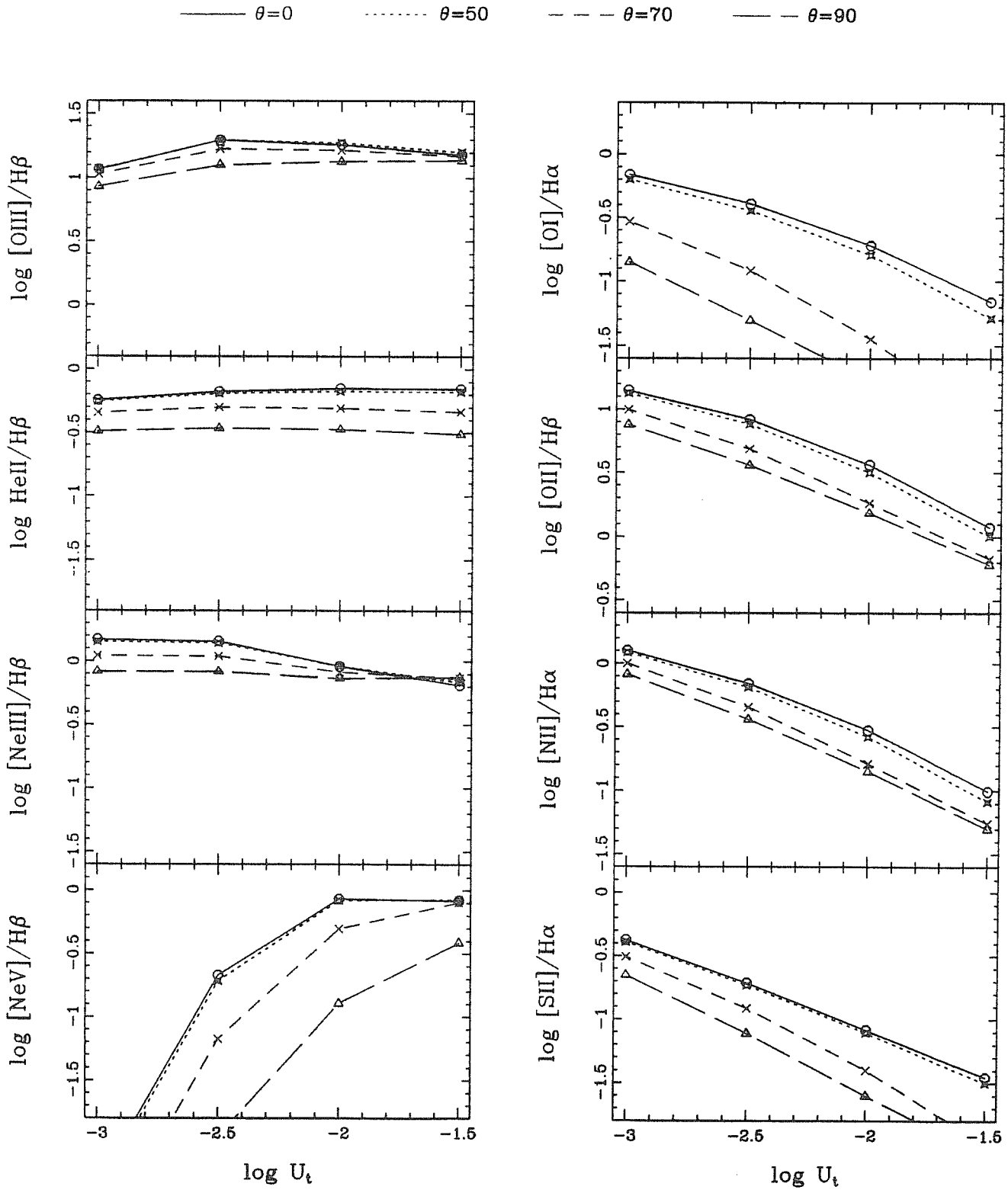
θ=0
θ=50
θ=70
θ=90
log [OIII]/Hβ
log HeII/Hβ
log [NeIII]/Hβ
log [NeV]/Hβ
log [OI]/Hα
log [OII]/Hβ
log [NII]/Hα
log [SII]/Hα
log U_t
log U_t

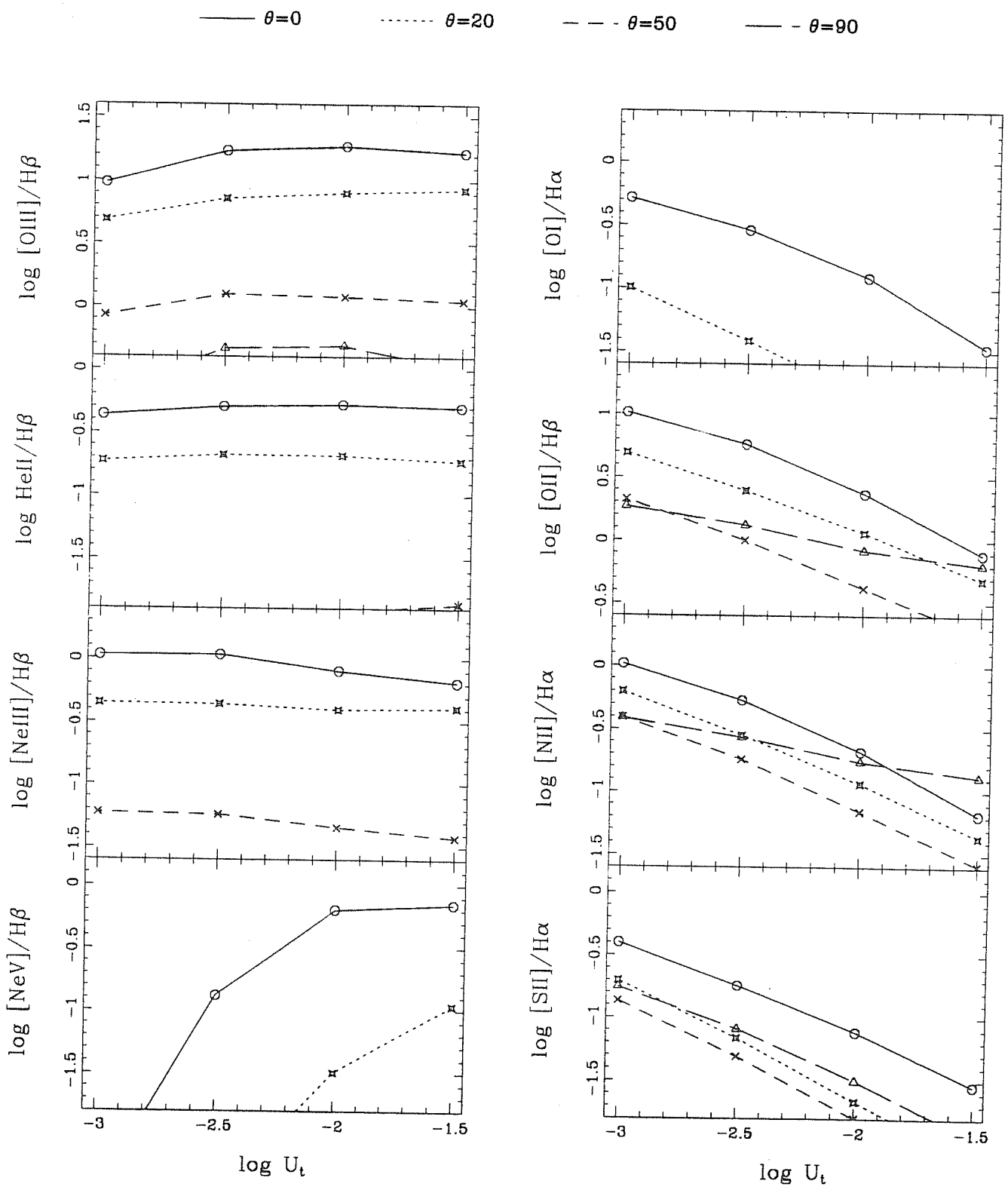
θ=0
θ=20
θ=50
θ=90
log [OIII]/Hβ
log HeII/Hβ
log [NeIII]/Hβ
log [NeV]/Hβ
log [OI]/Hα
log [OII]/Hβ
log [NII]/Hα
log [SII]/Hα
log U_t
log U_t

6.3.1 Black hole mass

The variation of the black hole mass produces not only a variation of the total luminosity but a shift towards low frequencies of the emitted continuum as the black hole mass increases. This feature revealed important in Chapter 5 for fairly large values of U_t ($U_t \gtrsim 10^{-2.5}$), especially for $M \lesssim 10^7 M_\odot$. The shift of the spectrum will be however more critical in the study of the angular dependence.

For $M \sim 10^6 M_\odot$ when θ increases the soft X–ray part ($\gtrsim 1$ keV) lacks in the spectrum. The partly ionized region, which is maintained by the X–ray emission becomes less extended, and the lines produced there ([OI] λ6300, [SII] $\lambda\lambda$6716, 6731) decrease appreciably. The lines which are produced in the fully ionized region are affected depending on the value of r_{out}. For relatively small disk sizes ($r_{out} \sim 200 r_g$) certain line ratios (*e.g.* [OIII] λ5007/Hβ , HeII λ4686/Hβ and [NeV] λ3426/Hβ) increase with θ, although by small factors. However when the disk is sufficiently large to have considerable emission at energies $\sim$ 30 eV all these lines decrease, whereas the lines from species with very high ionization potential ($\sim 100\, eV$) vary appreciably, *e.g.* for $r_{out} = 1000\, r_g$ and $U_t \sim 10^{-2.5}$, the ratio [NeV] λ3426/Hβ (the ionization potential of Ne^{3+} is 97.11 eV) decreases by a factor of $\sim$ 100, whereas the ratio [OIII] λ5007/Hβ varies only by a factor 2.5, from $\theta = 0°$ to 90° (see Fig. 6.4.b).

For $M \sim 10^8 M_\odot$ the spectrum varies with θ at energies $\lesssim$ 100 eV for $r_{out} \gtrsim 50 r_g$. The high energy tail which maintains the partly ionized regions is not present at large θ and therefore the intensity of the lines [OI] λ6300 and [SII] $\lambda\lambda$ 6716, 6731 decreases rapidly (see Figs. 6.4.c and 6.4.d). The emission lines produced in the fully ionized region shows stronger variation with θ than for 10^6 $M_\odot$, in particular the line ratios [NeV] λ3426/Hβ and HeII λ4686/Hβ decreases noticeably. The rest of lines show a less marked trend, except when the disk size is large enough and the contribution of intermediate radius of the disk is at few tens of eV (see Figs. 6.4.c and 6.4.d).

Summarizing, the increase of black hole mass from 10^6 to $10^8 M_\odot$ makes that the high ionization lines, preferentially those with the highest ionization potentials, show a pronounced decrease with increasing θ at fixed U_t. The low ionization lines produced in the partially ionized region, particularly [SII]$\lambda\lambda$6716, 6731, show stronger angular dependence for $M = 10^6$ $M_\odot$ than for $M = 10^8$ $M_\odot$. This occurs because the continuum varies with θ in two different frequency regions, according to the black hole mass: for $M = 10^6$ $M_\odot$ the soft–X ray part of the spectrum is occulted, whereas for $M = 10^8$ $M_\odot$ the UV part is occulted.

6.3.2 Disk size

The variation of the disk size affects the angular dependence of the ionizing continuum in two ways. Firstly, the funnel is steeper for larger disks, and this makes that the high energy tail of the continuum shows larger collimation (Madau 1988). Secondly, the spectrum has a large contribution at low frequencies when the disk size increases, and moreover the effective temperature of the outer parts decreases as $r_{out}^{-1/2}$ at different disk sizes and hence the spectrum softens considerably for large disks.

The major change in the spectral shape of the ionizing continuum at fixed r_{out} with θ occurs when the funnel is occulted from the line of sight, and affects the highest frequency part of the emission. The results confirm that for $\theta \leq \theta_{open}$ the predicted line ratios do not change appreciably; however for $\theta > \theta_{open}$ the emission lines suffer noticeable changes. In the current accretion disk model this always occurs at the same

value of θ, depending essentially on the value of r_{out} but not on M. According to this, it is straightforward to associate the value of opening angle of the cone with an accretion disk size or, equivalently, with an accretion rate.

The suppression of the most energetic part of the continuum affects different ranges of frequency according to the value of M. The predicted emission lines are moreover affected by the changes of the ionizing continuum with r_{out}. Generally speaking, the emission line spectrum has a more pronounced angular variation for large disks. This is because for small disk sizes the difference between the surface temperature from the maximum value (reached in the funnel) and the value in the outer parts is small, however for large disks this difference is large and the spectral shape of the continuum changes much when viewing the disk from the axis or from the equatorial plane.

Let us consider first the case when $M = 10^6 M_\odot$. For relatively small disks ($r_{out} = 200 r_g$) the emission line ratios [OIII] $\lambda 5007/\mathrm{H}\beta$, [NeV] $\lambda 3426/\mathrm{H}\beta$ and HeII $\lambda 4686/\mathrm{H}\beta$ tend to increase slightly with θ. The reason for this behaviour arises from the fact that most of the ionizing photons are shifted from high energies to energies (50-80 eV) which are still above the ionization potential of Ne^{3+} and O^{2+}, increasing the emission from [NeV] $\lambda 3426$ and [OIII] $\lambda 5007$. However the fraction of He^{2+} decreases, but the luminosity of $\mathrm{H}\beta$ also decreases, which leads to a net increase of HeII $\lambda 4686/\mathrm{H}\beta$. The low ionization lines decrease firmly with θ (see Fig. 6.4.a). For $r_{out} = 1000 r_g$ all the considered line ratios tend to decrease with θ (see Fig. 6.4.b). The line ratio [NeV] $\lambda 3426/\mathrm{H}\beta$ decreases noticeably by a factor ~ 10 from $\theta = 0°$ to $50°$, [SII] $\lambda\lambda 6716, 6731/\mathrm{H}\alpha$ and [OI] $\lambda 6300/\mathrm{H}\alpha$ decrease in a similar way; although the variation is smoother for the latter ratios. The rest of line ratios decreases moderately with θ, *e.g.* [OIII] $\lambda 5007/\mathrm{H}\beta$ decreases only a factor of 2.5 from $\theta = 0°$ to $90°$. For large disks ($r_{out} \sim 1000 r_g$ the continuum changes with θ at energies $\gtrsim 70$ eV. The angular variations in this range of energies affect the ionization of O^{2+} and Ne^{4+}, although for the two disk sizes the changes in the continuum operate in opposite directions: in the former (low r_{out}) increasing the ionization level in the latter (high r_{out}) decreasing it. The rather poor collimation predicted for the line ratio [OIII] $\lambda 5007/\mathrm{H}\beta$ and mainly its increase with θ at low values of r_{out} make models with $M \approx 10^6 M_\odot$ not appropiate to explain the ionization cones.

The results for $M = 10^8 M_\odot$ are much more promising in this sense. For a disk size 50 r_g all the line ratios decrease with θ increasing, although the variation is not enormous (see Fig. 6.4.c). Instead, for a disk size 1000 r_g the angular dependence of the emission line spectrum is remarkably strong (see Fig. 6.4.a), at a separation angle 20° the value of the line ratio [OIII] $\lambda 5007/\mathrm{H}\beta$ has reduced by a factor of ~ 3, HeII $\lambda 4686/\mathrm{H}\beta$ by a factor of ~ 2, [OI] $\lambda 6300/\mathrm{H}\alpha$ by a factor of ~ 5 and [NeV] $\lambda 3426/\mathrm{H}\beta$ by a factor of ~ 100. The variation of the spectral shape for low values of r_{out} affects energies $\gtrsim 60$ eV and the lines in the partially ionized zone, [NeV]$\lambda 3426$ and HeII $\lambda 4686$ suffer the strongest changes. However for large disks ($r_{out} \sim 1000 r_g$) the continuum varies with θ at energies ~ 20 eV. This leads to a strong variation of all the line ratios. In this case the partly ionized region is little extend and the low ionization lines rather come from the outer parts of the H^+ region. The continuum becomes very soft at large values of θ, the S^+ region extends down in the fully ionized region as well as the N^+ and O^+ regions at the expense of S^{2+}, N^{2+} and O^{2+}, respectively. Therefore the line ratios [SII] $\lambda\lambda 6716, 6731/\mathrm{H}\alpha$, [NII] $\lambda 6584/\mathrm{H}\alpha$ and [OII] $\lambda 3727/\mathrm{H}\beta$ will tend to increase instead of decreasing, when θ is increasing.

The line ratios HeII $\lambda 4686/\mathrm{H}\beta$ and to a lesser extent [NeIII] $\lambda 3869/\mathrm{H}\beta$ and [OIII] $\lambda 5007/\mathrm{H}\beta$

show an interesting behaviour: their values do not depend critically (less than 0.4 dex) on the value of U_t in the range $10^{-3} - 10^{-1.5}$, but they are rather sensitive to changes in spectral shape at different values of θ. Hence these lines could be adopted as good indicators of the anisotropy of the ionizing continuum. It is worth to notice that these lines adopt different values depending on the accretion disk parameters (see Fig. 5.3). There is a technical problem when using these lines as indicators of the anisotropy of the ionizing continuum, since the observational errors could be as large as the angular variation –in particular the line HeIIλ4686 is rather weak and therefore difficult to measure.

6.4 ANGULAR VARIATION OF THE EMISSION LINE SPECTRUM

In this section we compute the actual angular dependence of the emission lines considering both the change of the spectral shape and the decrease in the number of ionizing photons at large θ. We consider the gas distributed uniformly in the disk of the galaxy (see Fig. 6.1.a). The ionizing source is located at fixed distance from the gas clouds and the rotation axis of the torus lies in the galaxy disk. In practice the results which will be obtained in this Section combine the effects discussed in Sections 6.2 and 6.3. We are assuming an uniform distribution of gas, although the density may depend on the inclination angle from the disk axis, and so it influences the angular variation of U_t. If we have a more rarified medium at large θ then U_t will decrease slower than in an uniform medium, however if the medium becomes denser U_t will decrease faster. When higher quality observations off–axis will be available and the density can be measured then the behaviour of U_t will be well determined.

The distance of the ENLR clouds from the nucleus is assumed constant, as well as the hydrogen density. The fact that the product $n_H D^2$ is constant makes these calculations valid for a range of densities (always at the low density limit) and distances with the condition that such product is kept constant. The change of U_t with θ is due to the different value of N_i arising from the anisotropic disk emission. At each value of θ the value of N_i is fixed by the disk model, the product $n_H D^2$ is constant and therefore the value of U_t can be determined. The value of the product $n_H\, D^2$ is determined in the following way: we fix a value of U_t at $\theta = 0°$ and then the value of $n_H D^2$ is obtained from the expression $n_H D^2 = N_i(\theta = 0°)/4\pi c U_t(\theta = 0°)$, since we know the value of $N_i(\theta = 0°)$ for the selected disk model. Hence the value of U_t at any value of θ can be calculated as a function of N_i. We choose that value of U_t at $\theta = 0°$ which gives a best fit to the observed line ratios for a set of disk parameters, similar as it is done in Chapter 5. To make the fit we have used the same line ratios, except that now we give preferential weighting to the line ratios containing [OIII] λ5007 and [OII] λ3727 lines. We do not give preferential weighting to the line [OI] λ6300 because it depends on geometrical factors and on the presence of an additional X–ray component, furthermore its inclusion produces fits with rather large values of U_t. It will be come clear below that higher values of U_t imply less collimation of relevant line ratios (*e.g.* [OIII] λ5007/Hβ), hence if we want to obtain the maximum degree of collimation it is reasonable to choose a low value of U_t. We notice that the 90% confidence levels are well defined for U_t but not for r_{out}. This means that giving preferential weight only to the lines [OIII] λ5007 and [OII] λ3727 is not a good method to discriminate among the ionizing

continua, but it is efficient to constrain the value of U_t.

We study now the angular variation of the emission line luminosity. It is important to look at the line luminosity together with the line ratios when θ is varied, because it may happen that the detector sensitivity is not sufficient to detect any flux from large values of θ. In such case the predicted line ratios should be convolved with the detector sensitivity. The observations suggest that the spatial distribution of the line emission should be concentrated in a cone, particularly for the lines [OIII] λ5007 and Hα. The intensity of any line is computed by adding the contributions to such a line at each location in the cloud and so it is proportional to the column density $N(X^i)$[3]. The luminosity of the lines produced in the H^+ region depends strongly on the value of U_t, which determines the extension of the cloud. In particular the recombination lines Hα, Hβ and HeIIλ4686 are proportional to the value of U_t, therefore they vary with θ in the same fashion as U_t, *i.e.* as N_i decreases (see Figs. 6.2 and 6.5). The line HeII λ4686 shows a stronger decline than U_t for $M = 10^8\ M_\odot$, particularly for large values of r_{out}, since the changes in the ionizing spectrum affect the energy range around 50 eV. The forbidden lines, which are produced in the H^+ region, like [OIII] λ5007, [OII] λ3727, [NeIII] λ3869 and [NeV] λ3426 do not depend linearly on U_t, because U_t determines the ionization level of the atoms and a more complex dependence on U_t than linear is generally expected.

The line [NeV] λ3426 shows by far the strongest angular variation among the considered lines, meanwhile it presents a much more pronounced decrease for $M = 10^8 M_\odot$ than for $M = 10^6 M_\odot$. It shows a general trend: a constant value for $\theta \leq \theta_{open}$ and then it drops abruptly when $\theta \geq \theta_{open}$. This line is affected by the variation of U_t (it has a maximum for $U_t \sim 10^{-2}$) and by the suppression of the energetic parts in the continuum, therefore it is very appropriate to reveal any angular variation of the ionizing continuum.

The luminosity of [OIII] λ5007 shows a very slow decline for $M = 10^6\ M_\odot$, in particular for $r_{out} = 200\ r_g$ the luminosity decreases by only a factor of 1.2 and for $r_{out} = 1000\ r_g$ it decreases by a factor ~ 7 from $\theta = 0°$ to 90°. On the contrary, for $M = 10^8\ M_\odot$ the variation with θ of the [OIII] λ5007 luminosity is very strong, *e.g.* for a disk size of 50 r_g it decreases slowly until 50° where a turndown occurs, and at 90° the luminosity has decreased by a factor 10. For the same value of M and $r_{out} = 1000\ r_g$ there is a small plateau up to $\sim 15°$, and then it decreases rapidly at 30°, by a factor of 25. The angular variation of the ratio [OIII] λ5007/Hβ is very relevant in the comparison with the observations. This ratio involves the most intense and best studied line, in which the cones of ionizing radiation have been observed. It also gives indications about the degree of ionization if only spectroscopic measurements are available. For $M = 10^6 M_\odot$ this ratio increases with θ, because at the considered value of U_t O^{3+} is dominant over O^{2+} and then when U_t decreases with θ the O^{2+} fraction grows. For $M = 10^8 M_\odot$ this line ratio is constant at small values of θ and then it falls down at the opening angle of the funnel. The line ratios HeII λ4686/Hβ , [NeIII] λ3869/Hβ and [NeV] λ3426/Hβ show a similar behaviour to [OIII] λ5007/Hβ . When $M = 10^6 M_\odot$ these line ratios do not vary strongly with θ, except [NeV] λ3426/Hβ for large values of r_{out}; for $M = 10^8 M_\odot$ they decrease at the opening angle of the funnel.

The luminosity of the lines produced in the partially ionized H region, [OI] λ6300, [SII] $\lambda\lambda$6716, 6731 and a fraction of [NII] $\lambda\lambda$6548, 6584, does not depend basically on U_t,

[3] $N(X^i) = \int n(X^i) dl$, $n(X^i)$ is the number density of the X^i element and l is the distance through the cloud.

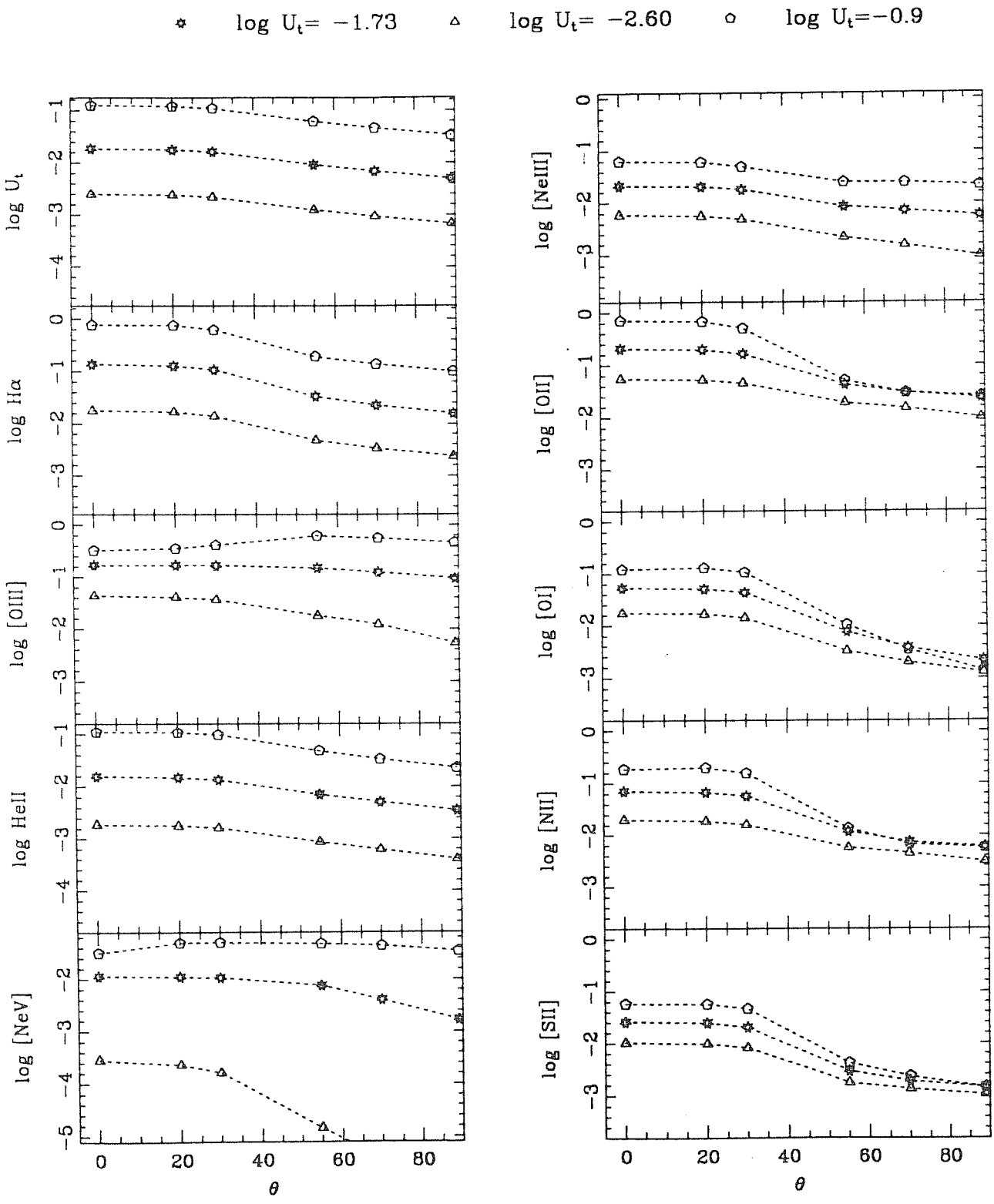

Figure 6.5: Angular variation of the luminosity for several emission lines, assuming the ionized gas is uniformly distributed in a disk. We present the results for three values of U_t, the intermediate value is the best fit and the other two are the 90% confidence levels for our particular χ^2 fitting. The units for the luminosity are $ergs\ s^{-1}\ cm^{-2}$, which corresponding to luminosity per unit area, since we are assuming a plane parallel slab. Figures 6.5.a and 6.5.b correspond to models for $M = 10^6 M_\odot$ with $r_{out} = 200$ and $1000\, r_g$, respectively; Figures 6.5.c and 6.5.d to models for $M = 10^8 M_\odot$ with $r_{out} = 50$ and $1000\, r_g$, respectively.

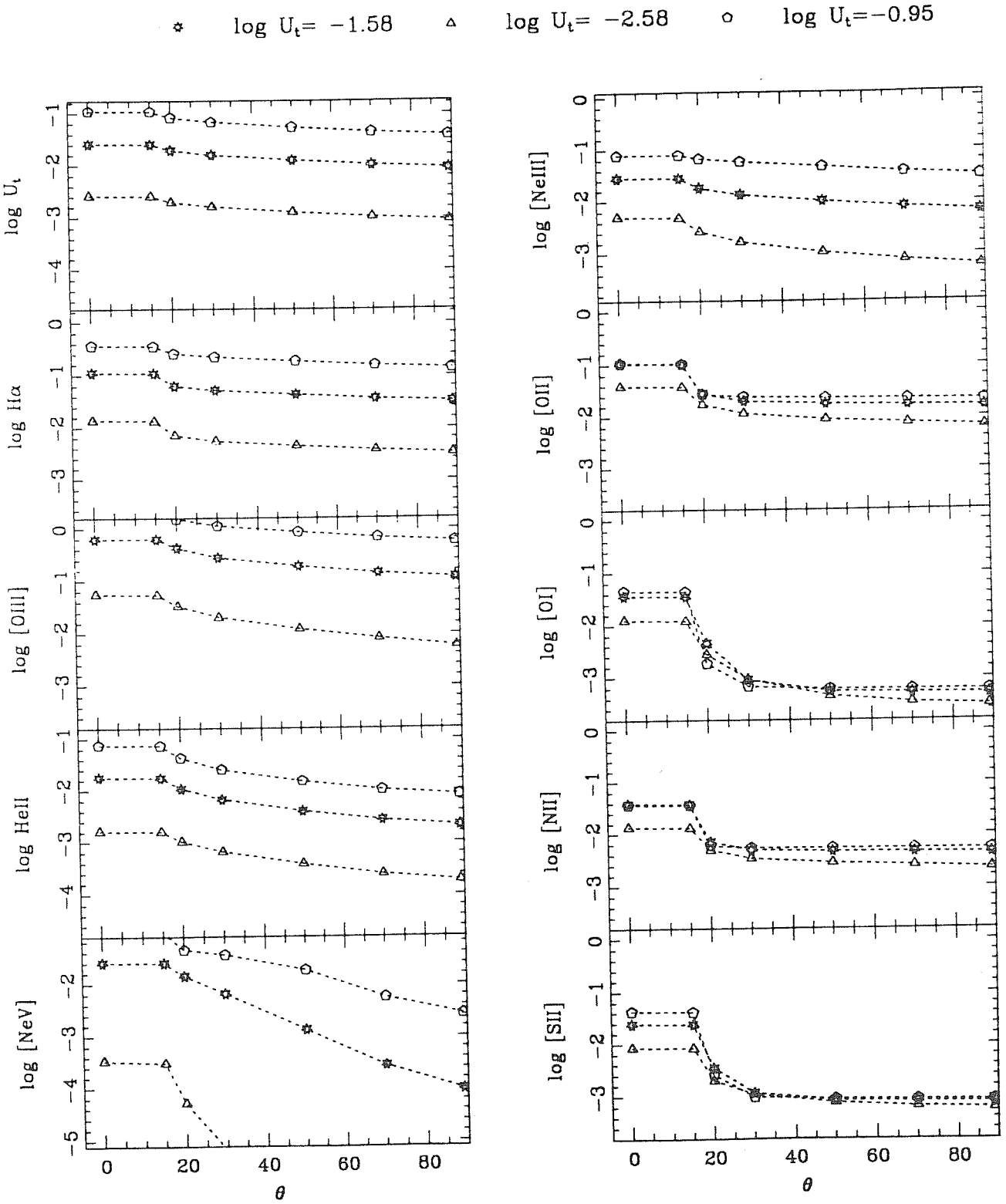
log U_t= −1.58
log U_t= −2.58
log U_t=−0.95
log U_t
log Hα
log [OIII]
log HeII
log [NeV]
log [NeIII]
log [OII]
log [OI]
log [NII]
log [SII]
θ
θ

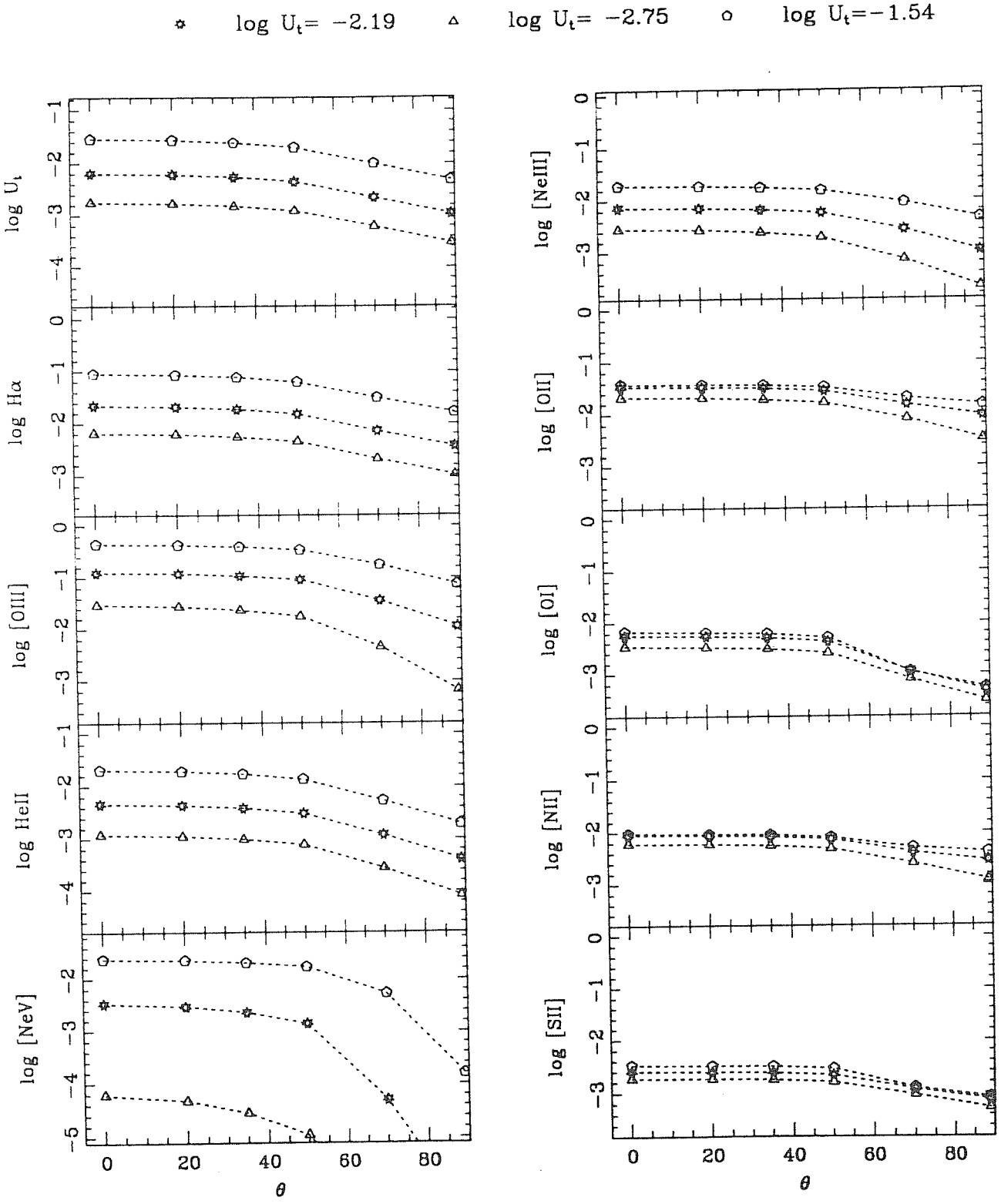
log U_t= −2.19
log U_t= −2.75
log U_t=−1.54
log U_t
log Hα
log [OIII]
log HeII
log [NeV]
log [NeIII]
log [OII]
log [OI]
log [NII]
log [SII]
θ
θ

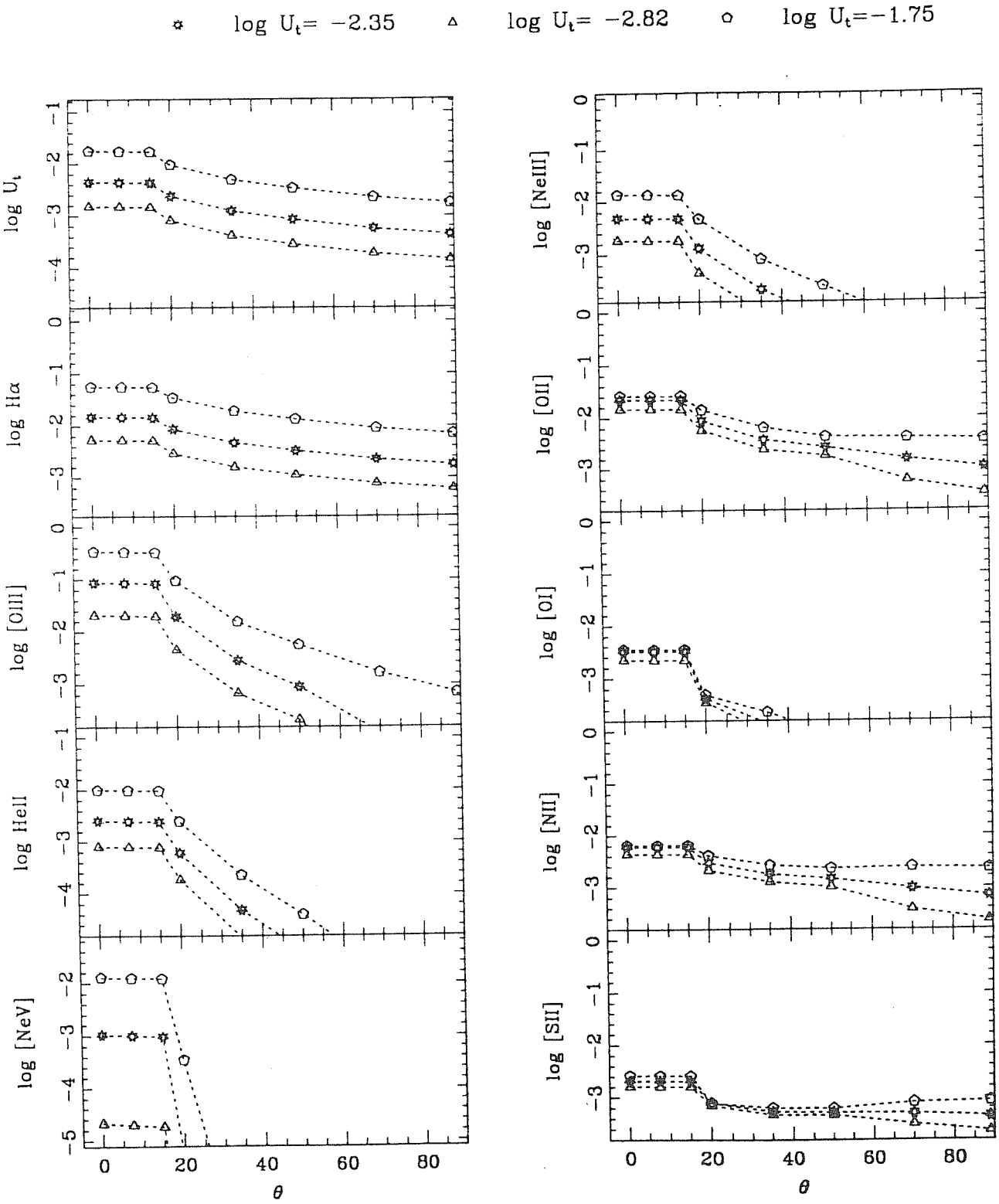
log U_t= −2.35
log U_t= −2.82
log U_t=−1.75
log U_t
log Hα
log [OIII]
log HeII
log [NeV]
log [NeIII]
log [OII]
log [OI]
log [NII]
log [SII]
θ
θ

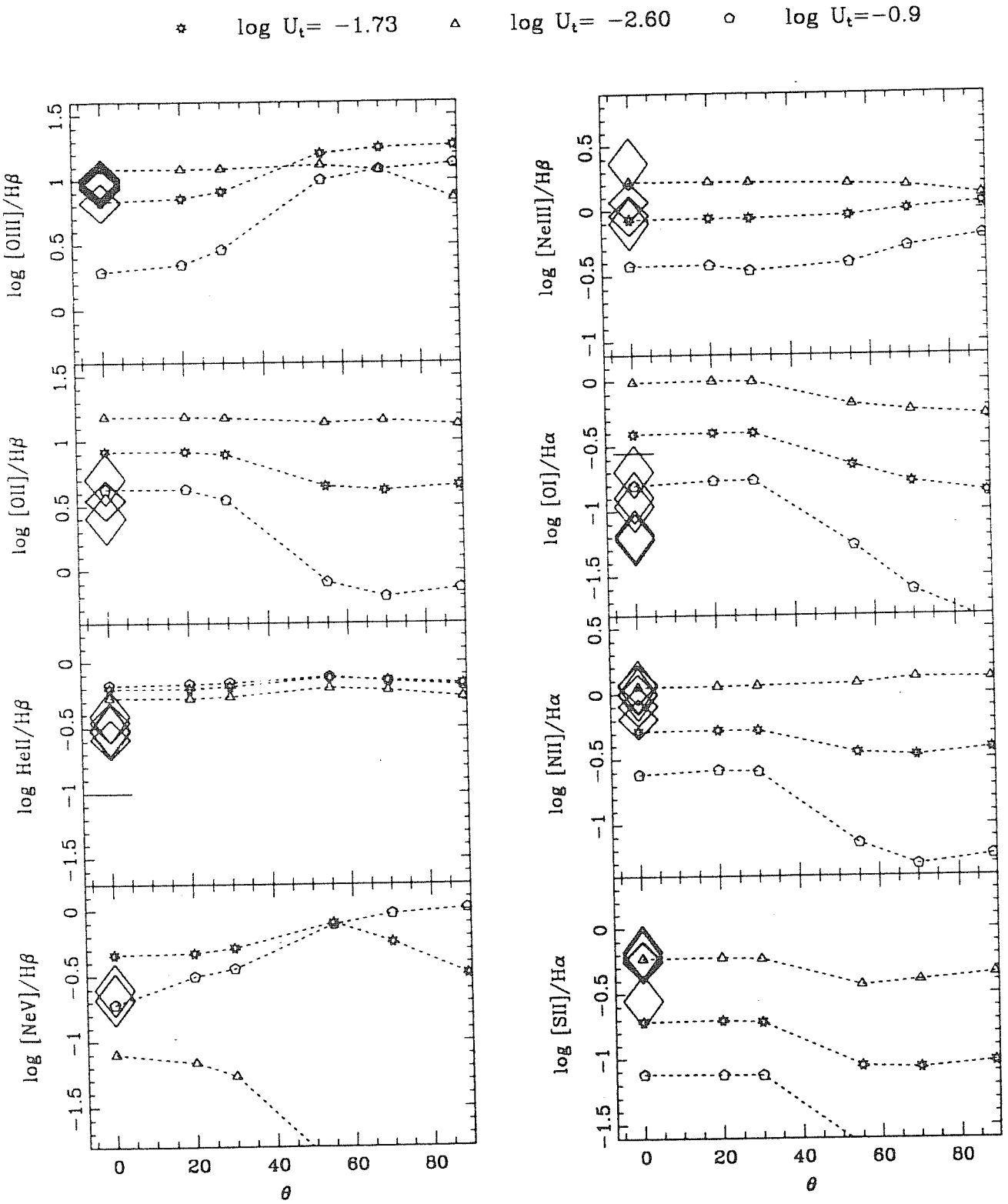

Figure 6.6: Angular variation of several line ratios (The same ratios as used in Chapter 5). The predictions are the same as in Figs. 6.5. The observational data are indicated by diamonds at $\theta = 0°$ with the estimated error, and correspond to NGC 1068 (Baldwin, Wilson and Whittle, 1987), NGC 3516 (Pogge, 1989a) and NGC 4388 (Pogge, 1988b).

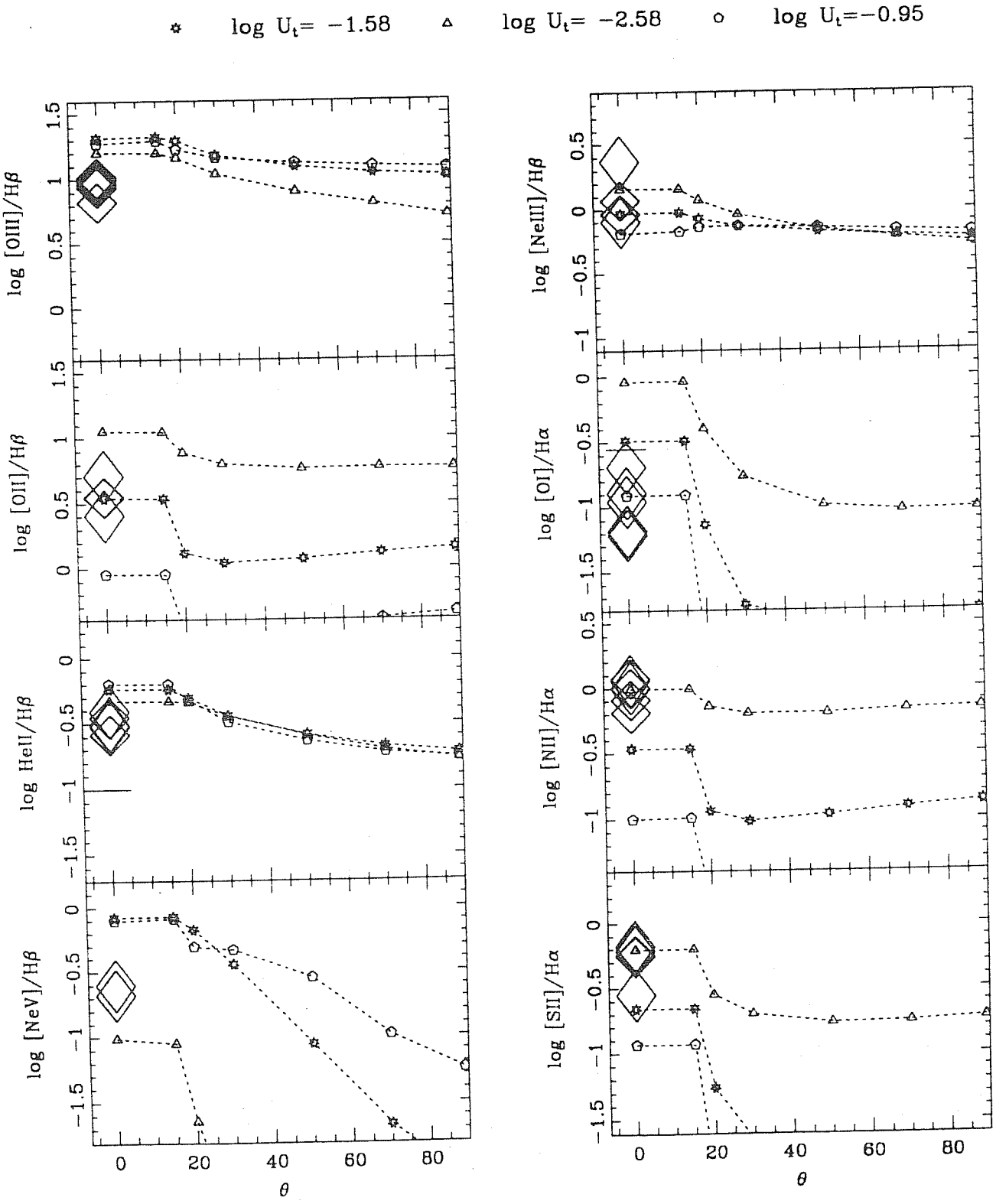
log U$_t$= −1.58
log U$_t$= −2.58
log U$_t$=−0.95
log [OIII]/Hβ
log [OII]/Hβ
log HeII/Hβ
log [NeV]/Hβ
log [NeIII]/Hβ
log [OI]/Hα
log [NII]/Hα
log [SII]/Hα
θ
θ

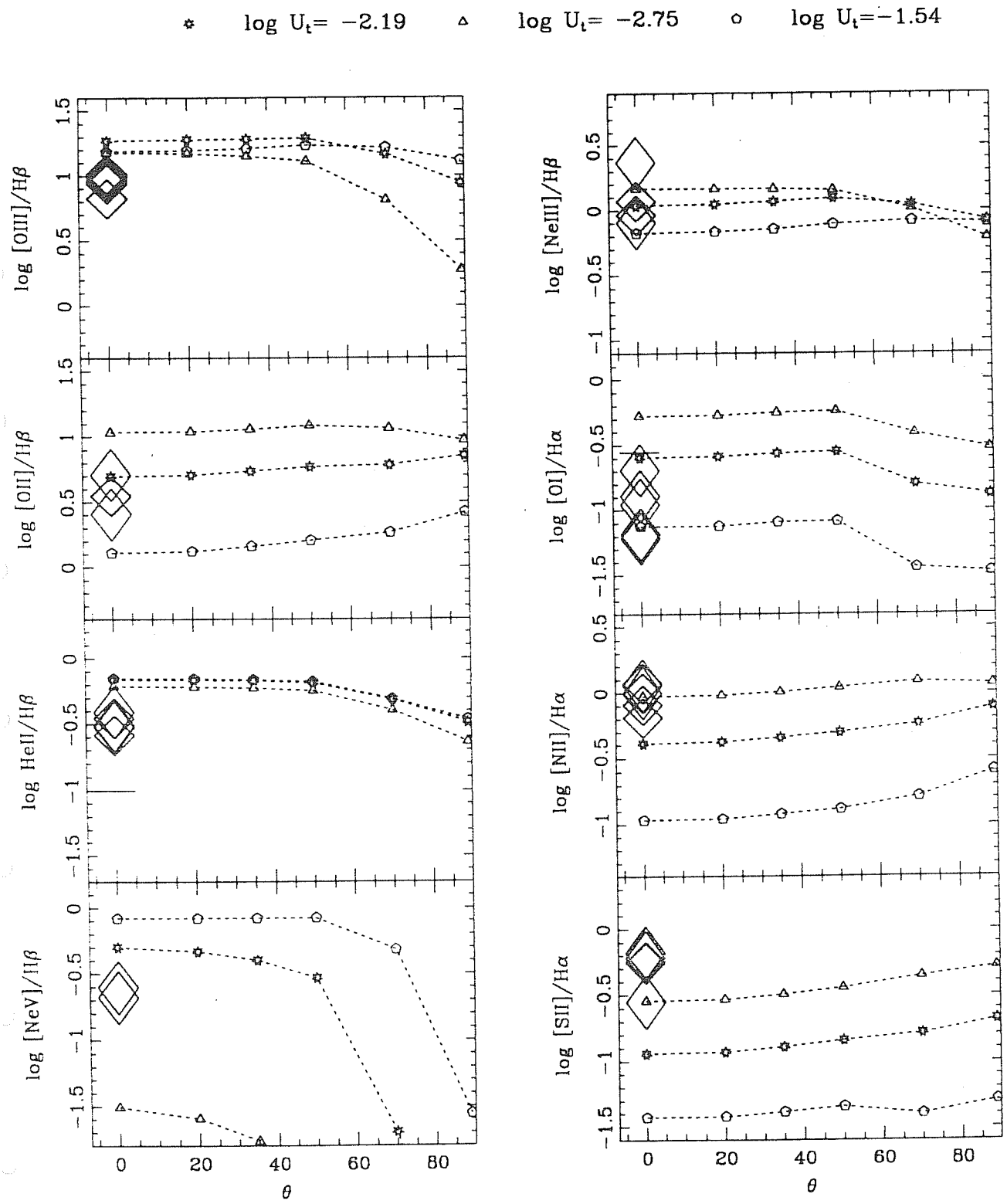
log U$_t$= −2.19
log U$_t$= −2.75
log U$_t$=−1.54
log [OIII]/Hβ
log [OII]/Hβ
log HeII/Hβ
log [NeV]/Hβ
log [NeIII]/Hβ
log [OI]/Hα
log [NII]/Hα
log [SII]/Hα
θ
θ

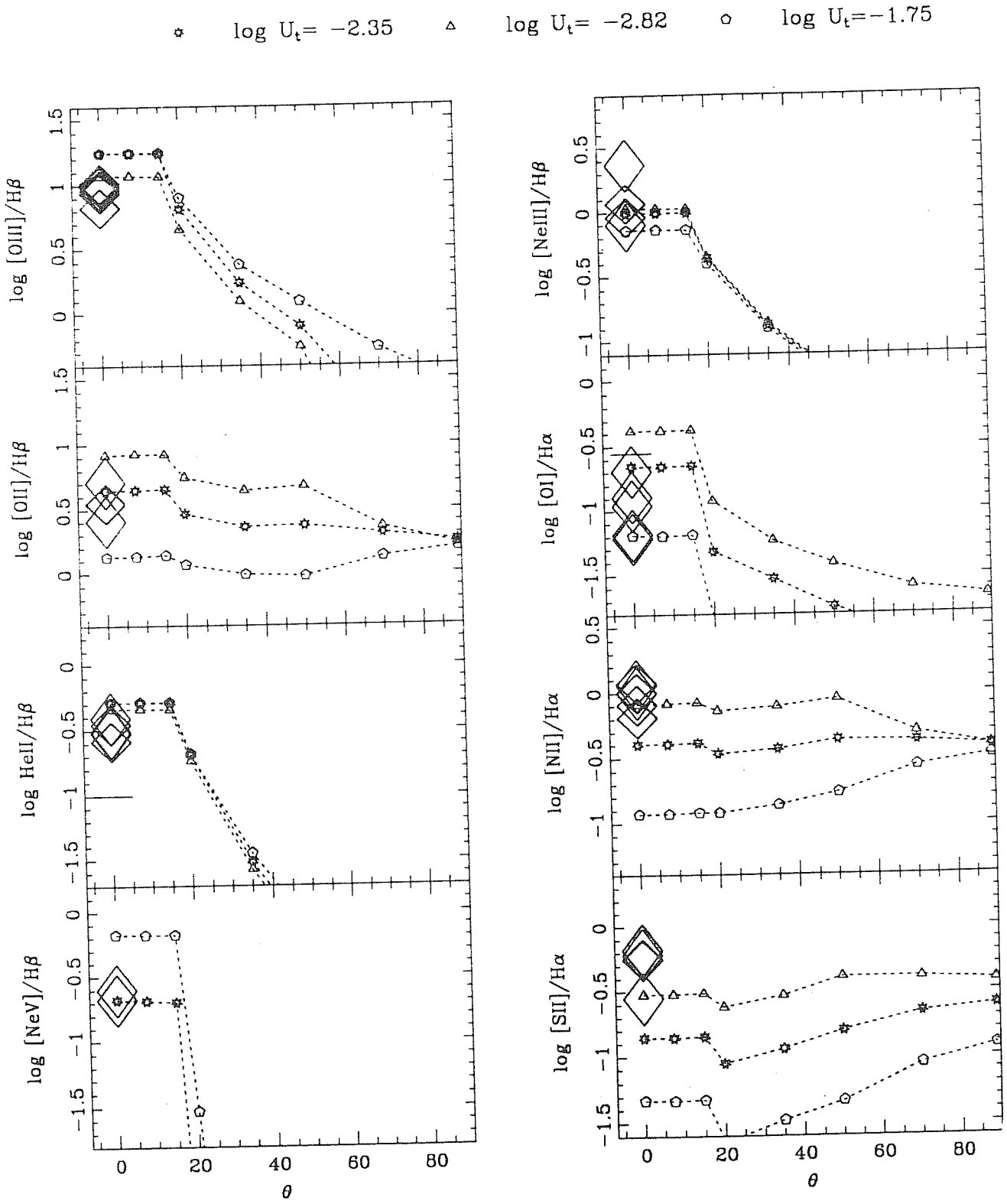
log U_t= −2.35
log U_t= −2.82
log U_t=−1.75
log [OIII]/Hβ
log [OII]/Hβ
log HeII/Hβ
log [NeV]/Hβ
log [NeIII]/Hβ
log [OI]/Hα
log [NII]/Hα
log [SII]/Hα
θ
θ

but rather on the extension of the ionizing continuum into the X–ray. The luminosity of these lines decrease when the X–ray part of the continuum is occulted by the funnel, furthermore the effect will be more important when the ionizing continuum is more extended to the X–ray. In fact for $M = 10^6\ M_\odot$ these lines suddenly decrease at a value of θ which corresponds to θ_{open}. However for $M = 10^8 M_\odot$ these lines vary slowly with θ, only the line [OI] λ6300 decreases noticeably with θ, but in this case O^+ is the dominant ionization level, and the partially ionized zone is greatly reduced. The low ionization line ratios [SII] $\lambda\lambda 6716, 6731/\mathrm{H}\alpha$ and [NII] $\lambda 6584/\mathrm{H}\alpha$ decrease with θ for $M = 10^6\ M_\odot$, but remain almost constant for $M = 10^8\ M_\odot$. This occurs because there are two effects operating in opposite direction. When the angle θ increases, the ionizing spectrum looses the X–ray part of the continuum and these line ratios decrease, on the other hand U_t decreases with θ and these line ratios should increase. The first effect dominates for $M = 10^6 M_\odot$ but for $M = 10^8 M_\odot$ both effects compensate, even at large θ the second effect dominates (see Section 6.3).

The luminosity of the line [OII] λ3727 shows a moderate decrease, which is more pronounced in the case of $M = 10^6\ M_\odot$. The line ratio [OII] $\lambda 3727/\mathrm{H}\beta$ decreases with θ for $M = 10^6 M_\odot$, but it remains almost constant for $M = 10^8 M_\odot$. The reason for such behaviour is that a high fraction of this line is produced in the partly ionized region when the continuum has a large X–ray contribution as it happens for $10^6 M_\odot$, and at large θ this region is much less extended. However for $10^8 M_\odot$ the fraction of [OII] λ3727 which comes from the mentioned region is smaller than in the former case, and tends equally to decrease when θ increases, on the contrary the fraction which comes from the H^+ region increases due the decrease of U_t, which makes the ionizing level of O^{2+} to decrease at the benefit of O^+.

It is important to investigate whether the predicted angular dependence of the line ratios is very sensitive to the precise value of U_t. The angular dependence of the line luminosities and their ratios was considered for values of U_t at 90% confidence level, using our particular χ^2 fitting. This indicates about the relevance of the adopted value for U_t at $\theta = 0°$ concerning the predictions of the angular behaviour of the line ratios. The line ratios HeII $\lambda 4686/\mathrm{H}\beta$, and to some extent [NeIII] $\lambda 3869/\mathrm{H}\beta$ and [OIII] $\lambda 5007/\mathrm{H}\beta$ do not depend on the precise value of U_t, for the restricted range of U_t we are considering as we mention above. The line ratio HeII $\lambda 4686/\mathrm{H}\beta$ shows the same behaviour with θ, at different values of U_t. Generally, after an initial plateau up to θ_{open} the predictions for different U_t run down together according to the variation of the spectral shape of the continuum. The rest of the considered line ratios depends strongly on the value of U_t adopted at the axis. Nevertheless they show similar trends with θ at different U_t, within the 90% confidence level. On the contrary, for $M = 10^6 M_\odot$ and $r_{out} \lesssim 500\ r_g$ the predicted angular variation of [OIII] $\lambda 5007/\mathrm{H}\beta$ and [NeV] $\lambda 3426/\mathrm{H}\beta$ depends critically on the value of U_t. For the best fit value of U_t and its upper bound of the confidence level these line ratios show a slight trend to increase from $\theta = 0°$ to 90°, however at the lower bound of the confidence level for U_t, the trend is to decrease at large θ. This is not the case for $M = 10^8\ M_\odot$ in which the predictions for different U_t show the same trend (Note that the best fits for $10^8 M_\odot$ are achieved with lower values of U_t than for $10^6 M_\odot$). Furthermore, the line ratio [OIII] $\lambda 5007/\mathrm{H}\beta$ shows a slight trend to decrease faster at large θ for the low values of U_t. The predictions for the line ratios [OI] $\lambda 6300/\mathrm{H}\alpha$, [SII] $\lambda\lambda 6716, 6731/\mathrm{H}\alpha$ and [NII] $\lambda 6584/\mathrm{H}\alpha$ for different values of U_t run almost parallel varying θ, although displaced since only Hα varies with U_t. However when comparing to the observed values only certain values of U_t are allowed.

It is important to notice that two line ratios, HeII $\lambda 4686/\mathrm{H}\beta$ and [NeIII] $\lambda 3869/\mathrm{H}\beta$ are rather insensitive to the value of U_t. These line ratios do show collimation, indicating that the variation of the spectral shape of the continuum with θ provides enough change in the emission line spectrum, and the variation of line ratio does not arise uniquely from the variation of U_t.

6.5 DISCUSSION

The angular dependence of the emission line spectrum calculated above can be described in simple terms as follows: at values of $\theta \leq \theta_{open}$ the emission lines do not change appreciably, and a small plateau is seen; when $\theta > \theta_{open}$ the emission lines start to change. In the frame of this model the aperture of the observed emission line cone indicates the value of the opening angle of the funnel. The steepening of the funnel increases with the outer radius of the disk, and is independent of the value of M. On the other hand, the geometry of the funnel is determined by the *amd*; the derived value for r_{out} by using the *Madau* and *Jaroszynski amd* can be taken as an upper and lower limit, respectively. Hence a range of possible values for the size of the disk can be constrained from the observations of the extended conical structure. There is certainly a variety of effects which may complicate this simple relation. The inclusion of the reflection effect when calculating the emission from the disk will make that high energy photons produced in the innermost regions of the funnel, which are shadowed for large θ will scattered in the funnel walls and will emerge even at large values of θ. Therefore the collimation of the most energetic part of the continuum is diluted and the value of r_{out} needed to obtain the observed angle is increased (see Fig. 7 of Madau [1988]).

On the other hand, the nmature of the ionizing continuum affects the collimation of the emission line luminosities. As it is shown in Section 6.4, only at certain values of M and r_{out} the ionizing continuum varies with θ in an adequate fashion to produce firm decrease of the emission lines. We will base our discussion on the emission line [OIII] $\lambda 5007$ and the ratio [OIII] $\lambda 5007/\mathrm{H}\beta$, since it is the only line where the presence of ionization cones is well established by now. The disk models built with $M = 10^6 M_\odot$ emit a large number of photons at very high energies (larger than 100 eV) and the angular variation do not produce any collimation of [OIII] $\lambda 5007/\mathrm{H}\beta$. When the disk size is increased a low energy contribution arises and the angular variation of the continuum occurs in an energy range where the ionization of O^{2+} is affected in an appropriate sense. Extrapolating our results we estimate that only disks with $r_{out} \gtrsim 600 r_g$ ($M = 10^6 M_\odot$) emit a continuum able to produce a decrease in the [OIII] $\lambda 5007$ luminosity with θ. However in such case the opening angle of the cones predicted by this model can not exceed 25°. Disks around more massive black holes ($M = 10^8 M_\odot$) emit an ionizing continuum whose variation with θ allows the line [OIII] $\lambda 5007$ to decrease towards large θ for any value of r_{out}. We find that the requirement that a certain line emission is decreasing at large inclination angles restricts the parameter space for this particular model of thick accretion disk. The models which are compatible with the observed behaviour are constrained to have $r_{out} \gtrsim 600 r_g$ if $M = 10^6 M_\odot$, $r_{out} \gtrsim 200 r_g$ if $M = 10^7 M_\odot$ and almost any value if $M = 10^8 M_\odot$. When the *Jaroszynski amd* is used, the continuum has a similar spectral shape, and hence it will not affect the emission line spectrum. The variations of the disk emission with θ are more abrupt in the latter case than in the previous case, although the trends will be similar regarding the change in the spectral shape of the continuum. We expect that M and r_{out} are restricted in a

similar way as described above.

The above calculations limit the ability of the thick accretion disk as being responsible for the observed structure in ENLRs to a certain disk configurations (M and r_{out}). In Chapter 5 it is found that models with $M = 10^6 M_\odot$ produce the best fit to the observations when $r_{out} \sim 600 r_g$, models with $M = 10^7 M_\odot$ when $r_{out} \sim 100 r_g$ and those with $M = 10^8 M_\odot$ do not predict essentially different emission line spectra varying r_{out}. There is a relation between those results and the ones discussed here, since we are in both cases limiting the hardness of the spectrum in two different ways. In Chapter 5 we constrain the model parameters by preferentially fitting oxygen lines, including [OI] λ6300 which is very dependent on the extension of the continuum to X–ray frequencies. In this case the continuum is required to vary with θ in the energy range $\sim 40 - 60\ eV$ to affect the line spectrum and moreover this should be the high energy tail. Therefore we guess that the continua responsible to ionize the ENLR should anyhow be less hard than the ones we have used here, *i.e.* the actual shape of the ionizing continua will look like more the one predicted for $10^8 M_\odot$ than that for $10^6 M_\odot$. It is important to notice that the emission line spectrum predicted for $M = 10^8 M_\odot$ and different r_{out} at $\theta = 0°$ do not permit to distinguish among different models (Fig. 5.2.c), however when the angular dependence is taken into account, different values of r_{out} produce distinguishable angular behaviour.

We have shown that the the thick accretion disk emission is able to produce the cones of [OIII] λ5007 emission, although additional requirements to the models must be imposed. Our argumentation was based purely on the energy distribution of the disk emission. The inconvenience of small r_{out} at low values of M ($M \lesssim 10^7 M_\odot$) arises from the fact that changes with θ of the continuum take place in a energy range such that the fraction of O^{2+} increases in going away from the disk axis. The high degree of ionization produced by our continuum could be attributed to the high U_t[4]. A possible solution to this problem is to adopt a sufficiently low value of U_t at $\theta = 0°$, in such case the decrease of U_t due to the obscuration at large value of θ leads to decrease the fraction of O^{2+}. Although this may help in some cases, the calculations presented in Sect. 6.4 at different values of U_t indicates that the collimation of [OIII]λ5007 is difficult to improve. In addition, there are line ratios, *e.g.* [OII] λ3727/Hβ , [NeV] λ3426/Hβ which depend critically on the value of U_t, and with low values of U_t the predictions will be out the range of the observed values. We therefore conclude that variation of the spectral shape of the ionizing continuum with M actually constrains the range of M while variations of U_t can not be advocated to compensate the angular dependence of the predicted emission line spectrum, without deteriorating the agreement of other predicted lines with the observations.

The relation between the opening angle of the funnel and that of the ionization cone restricts the values of r_{out}. Nevertheless various effects which are not considered here (*e.g.* the reflection effect, scattering in a hot corona) will enlarge the angle in which the radiation is collimated to values larger than θ_{open}. In an ideal situation, large aperture cones require small disks, hence a lower limit on the black hole mass should be imposed according to the above guesses. The fact of having a lower bound to the value of M gives a strong prediction for the luminosity of the active nucleus,

[4] The line ratio [OIII] λ5007/Hβ is at maximum when $U_t \sim 10^{-2.5}$ for this kind of ionizing continua (see Fig 5.3 in Chapter 5). In principle, there are two possible values of U_t which predict the same ratio [OIII] λ5007/Hβ if this is below the maximum of this ratio. Our fitting procedure normally selects the largest value because it predicts better agreement for the rest of the line ratios.

which should emit at least the Eddington value. In the case that the observed value of the luminosity is lower than that expected from the above considerations, there are two alternatives: either the model should be rule out or a strong obscuration of the nuclear continuum should be invoked. The latter possibility is very interesting since Seyfert 2 galaxies where the cones of ionization have been mostly detected, do not exhibit a strong non-stellar continuum. Also when the counting of ionizing photons from the Hβ luminosity at the ENLR location is done, the observed nuclear continuum seems to be only marginally sufficient to power the line emission (Wilson, Ward and Haniff, 1988). This feature precludes a very strong obscuration and favours models with low values of M, and suggests that the ionizing continuum of the ENLR comes from accretion disks around black holes with $M \lesssim 10^7 M_\odot$.

On the other hand the comparison of the predicted line ratios with the observed values suggests that the ionizing continuum we are using has an excess of energetic photons (see also Chapter 5). A strong indication comes from the high value of the line ratio HeII $\lambda 4686/\mathrm{H}\beta$, which means that the ratio between photons with energies in the range between 4 and $6ryd$ and those in the range between 1 and 4 ryd is high (Binette, Courvoisier and Robinson, 1988). Another indication comes from the high predicted values for [OII] $\lambda 3727/\mathrm{H}\beta$ and the low values for [OIII] $\lambda 5007/\mathrm{H}\beta$ in comparison (at the same value of U_t) with the values obtained using other more *successful* continua, namely a power law with $\alpha = -1.5$ and a blackbody with $T = 130000K$ (Robinson *et al.*, 1987). This fact makes that large values of U_t are needed to fit those line ratios with the observed values. A large amount of [OII] $\lambda 3727$ is produced in the partly ionized H region because there is a large fraction of high energy photons[5].

Photoionization modelling of the BLR shows that the nuclear emission from Seyfert galaxies is peaked at energies lower than $1ryd$, whereas in the case of radio-quiet QSO's the peak is shifted to larger energies (Clavel and Santos-Lléo, 1990; Binette *et al.*, 1989). However our ionizing continua are peaked at energies much larger than these values. These features suggest that relevant assumptions about the way in which the continuum is emitted (*e.g.* the opacity source in the atmosphere of the disk) should be changed in order to have the thick accretion disk emission being able to photoionize ENLR and produce collimation of the emission lines with reasonable disk parameters. We have therefore investigated a continuum in which the opacity in the disk photosphere is dominated by free–free absorptions. The ionizing continuum is now calculated as a sum of blackbodies and becomes softer than the one calculated with electron scattering (see Fig. 8 in Madau [1988]). We have repeated the calculations for the angular dependence of the line luminosity in order to investigate how such a change of ionizing continuum affects its behaviour. We consider a low value for $M = 10^6 M_\odot$, since the lower the black hole mass, the harder the continuum. We present in Fig. 6.7 the predictions for the line ratios using the blackbody approach and $r_{out} = 200$, and $1000\, r_g$; for comparison we include the same calculations but with the modified blackbody approximation. Let us first examine how the different spectral shape affect the predictions of the line ratios relative to the previous model. The first thing to notice from Figure 6.7 is the insensitivity of the predictions for the different line ratios to the value of r_{out}. This is really expected because modifications of the continuum when r_{out} is increasing, occur only at energies lower than 1 ryd, even in the case of $M = 10^6 M_\odot$. Since this ionizing continuum is less extended to X–ray energies the lines produced in the

[5]The ionization potential of O^0 is very similar to that of hydrogen and therefore can be collisionally ionized in the partially ionized region if the temperature is high enough.

TABLE 6.2: PREDICTED LINE RATIOS SUM OF BLACKBODIES

	$M = 10^6\ M_\odot$					
	$U_t = 10^{-3.5}$		$U_t = 10^{-2}$		$U_t = 10^{-1.5}$	
Ratio	$200r_g$	$1000r_g$	$200r_g$	$1000r_g$	$200r_g$	$1000r_g$
[OIII] λ5007/Hβ	3.10 (1.44)	2.83 (2.01)	19.7 (10.0)	18.8 (20.9)	16.3 (4.88)	15.8 (20.6)
[OII] λ3727/Hβ	16.4 (16.8)	14.0 (14.6)	3.09 (10.2)	2.64 (6.60)	0.95 (6.88)	0.83 (3.07)
[OI] λ6300/Hα	0.98 (1.87)	0.90 (1.61)	0.15 (0.51)	0.13 (0.51)	0.04 (0.31)	0.04 (0.30)
[NII] λ6584/Hα	1.70 (1.57)	1.54 (1.47)	0.25 (0.65)	0.23 (0.57)	0.08 (0.43)	0.07 (0.31)
[SII] $\lambda\lambda$6716, 6731/Hα	0.83 (1.50)	0.82 (1.46)	0.07 (0.26)	0.07 (0.33)	0.03 (0.15)	0.03 (0.20)
HeII λ4686/Hβ	0.39 (0.34)	0.35 (0.28)	0.65 (0.61)	0.59 (0.55)	0.65 (0.64)	0.79 (0.59)
[NeIII] λ3869/Hβ	1.09 (1.09)	0.91 (0.89)	0.91 (1.13)	0.80 (1.16)	0.67 (0.68)	0.61 (0.89)
[NeV] λ3426/Hβ	0.00 (0.00)	0.00 (0.00)	0.81 (0.53)	0.74 (0.74)	0.79 (0.41)	0.74 (0.86)

Table 6.2: Predicted values of several line ratios using as ionizing continuum the thick disk emission in the sum of blackbodies approximation. The same predictions but calculated in the modified blackbody approach are shown between parentheses.

partially ionized region will be considerably weaker than in the previous model, *e.g.* [SII] $\lambda\lambda$6716, 6731/Hα and [OI] λ6300/Hα (see Table 6.2), the ratio [NII] λ6584/Hα is also affected partially by this fact. The ratio [OIII] λ5007/Hβ is now slightly increased and the ratio [OII] λ3727/Hβ considerably decreased, the reason for such behaviour is that the present continuum is less effective ionizing O^{2+} to O^{3+} than the previous one, and on the other hand the fraction of [OII] λ3727 which comes from the partially ionized region now is greatly reduced. The rest of line ratios does not change much although there is a trend for HeII λ4686/Hβ and [NeV] λ3426/Hβ to increase relative to the previous model (see Table 6.2), which is basically explained as a decrease of Hβ and Hα. The predicted line ratio HeII λ4686/Hβ is slightly high compared to the observed values, which means that the ionizing continuum has still a large fraction of photons with energies in the range 4-6 ryd relative to those close to 1 ryd. If models with $M > 10^6\ M_\odot$ are considered these line ratios will certainly decrease and the agreement with the observations will improve. The observed line ratios are fitted now with $U_t \sim 5 \times 10^{-3}$, for a model with $M = 10^6 M_\odot$ and $r_{out} = 200 r_g$. These values of U_t are almost a factor 10 lower than those obtained in the case of modified blackbody continuum (see Table 5.2). We have repeated the calculations of the angular dependence of the line emission, as described in Section 6.4. The results are presented in Figures 6.8.a and 6.8.b. We find that the luminosity of the relevant line [OIII] λ5007 decreases with θ. However we recall that using the modified blackbody approach for the same disk parameters this line was increasing with θ. This feature reveals the sensitivity of the angular dependence of the line luminosities to the spectral shape of the ionizing continuum.

The presence of an isotropic source of X–ray emission will change the angular dependence of lines produced in the partially ionized region (Netzer, 1987). These lines will be emitted equally at large values of θ, however the Balmer lines will be emitted preferentially at low values of θ, although a small contribution from the partially ionized region still will be present. Therefore the line ratios such as [SII] $\lambda\lambda$6716, 6731/Hα , [OI] λ6300/Hα and probably [NII] λ6584/Hα will vary with θ in the following way: at

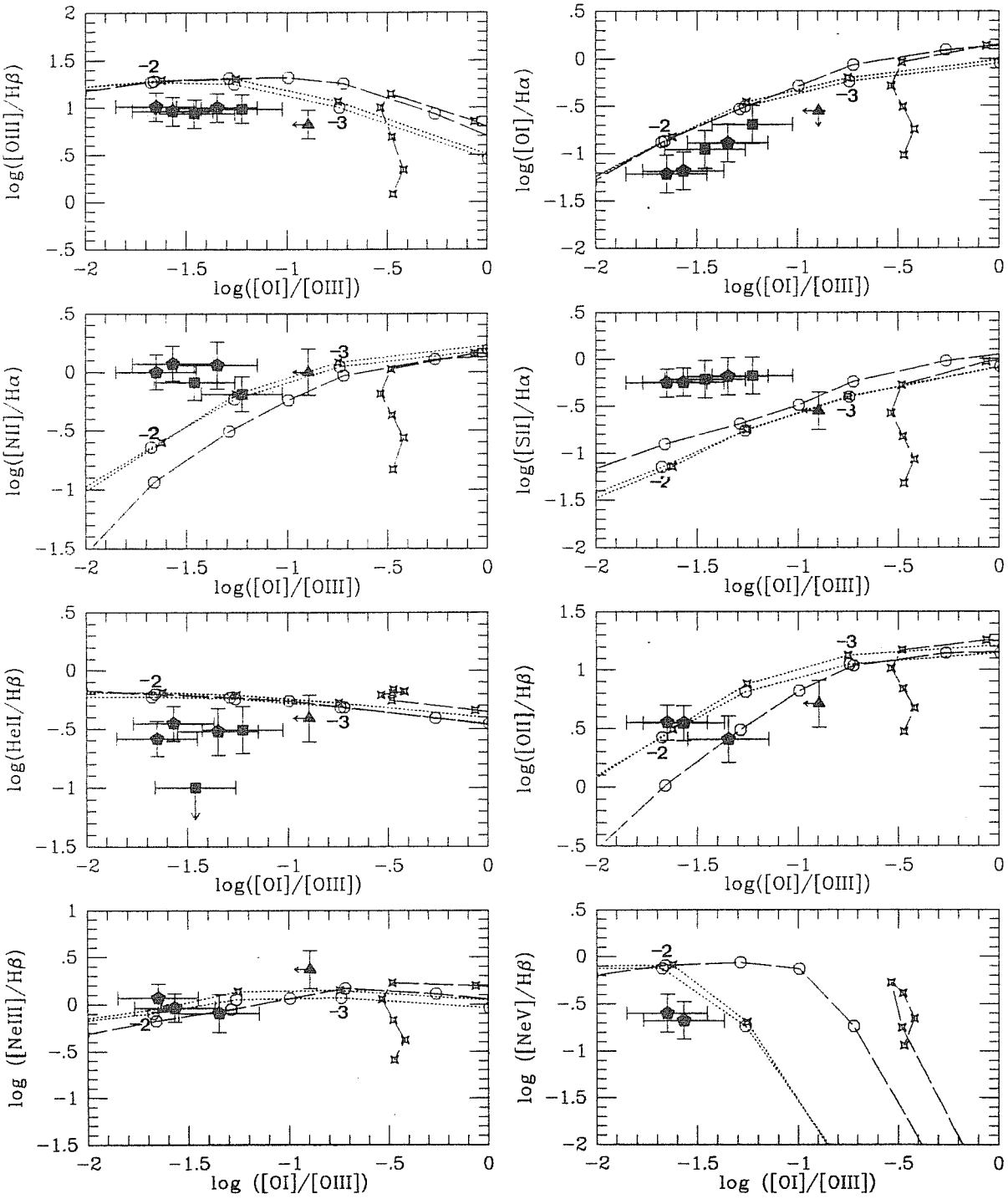

Figure 6.7: Diagnostic diagrams using the disk emission calculated in the sum of blackbodies approach, as ionizing continuum for a model with $M = 10^{9} M_{\odot}$ and two values of r_{out}. The disk emission is calculated along the rotation axis. We present the predictions for the same line ratios and the same observed ratios as in Fig. 5.2. For comparison we present also the predictions for a disk model in the modified blackbody approach. The lines join theoretical points corresponding to different values of U_t (the logarithmic value is indicated). The meaning of the symbols, which are joined by lines, is as follows: stars corresponds to a $r_{out} = 200\, r_g$, open circles to $r_{out} = 1000\, r_g$. The dotted lines join model calculated under the blackbody approach, instead the long-dashed lines join the models calculated with the electron scattering opacity.

● log U_t= −2.27 ○ log U_t= −2.73 ☆ log U_t=−1.73

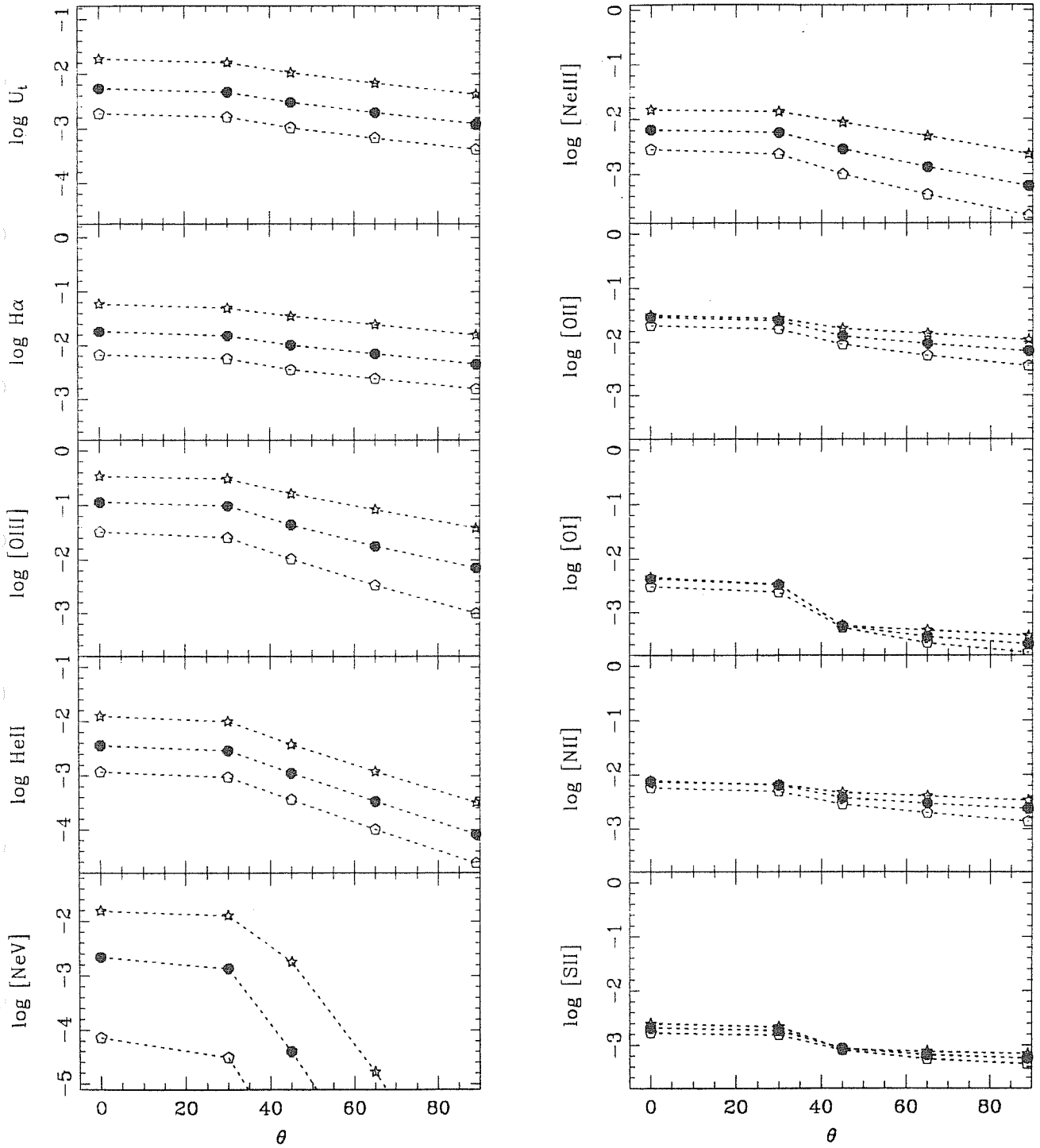

Figure 6.8: Angular variation of the luminosity of several lines (Fig. 6.8.a) and line ratios (Fig. 6.8.b), assuming that the gas is distributed uniformly in a disk. The ionizing continuum is calculated from the thick disk emission in the sum of blackbodies approximation. We present results for $M = 10^6 M_\odot$ and $r_{out} = 200 r_g$, at the best fit value for U_t ($\approx 5 \times 10^{-3}$, at the axis) and 90% confidence level ($U_t \approx 2 \times 10^{-3}$ and 2×10^{-2}). Notice that the collimation of the continuum provides a firm decrease of the luminosity of the line [OIII] λ5007 with θ.

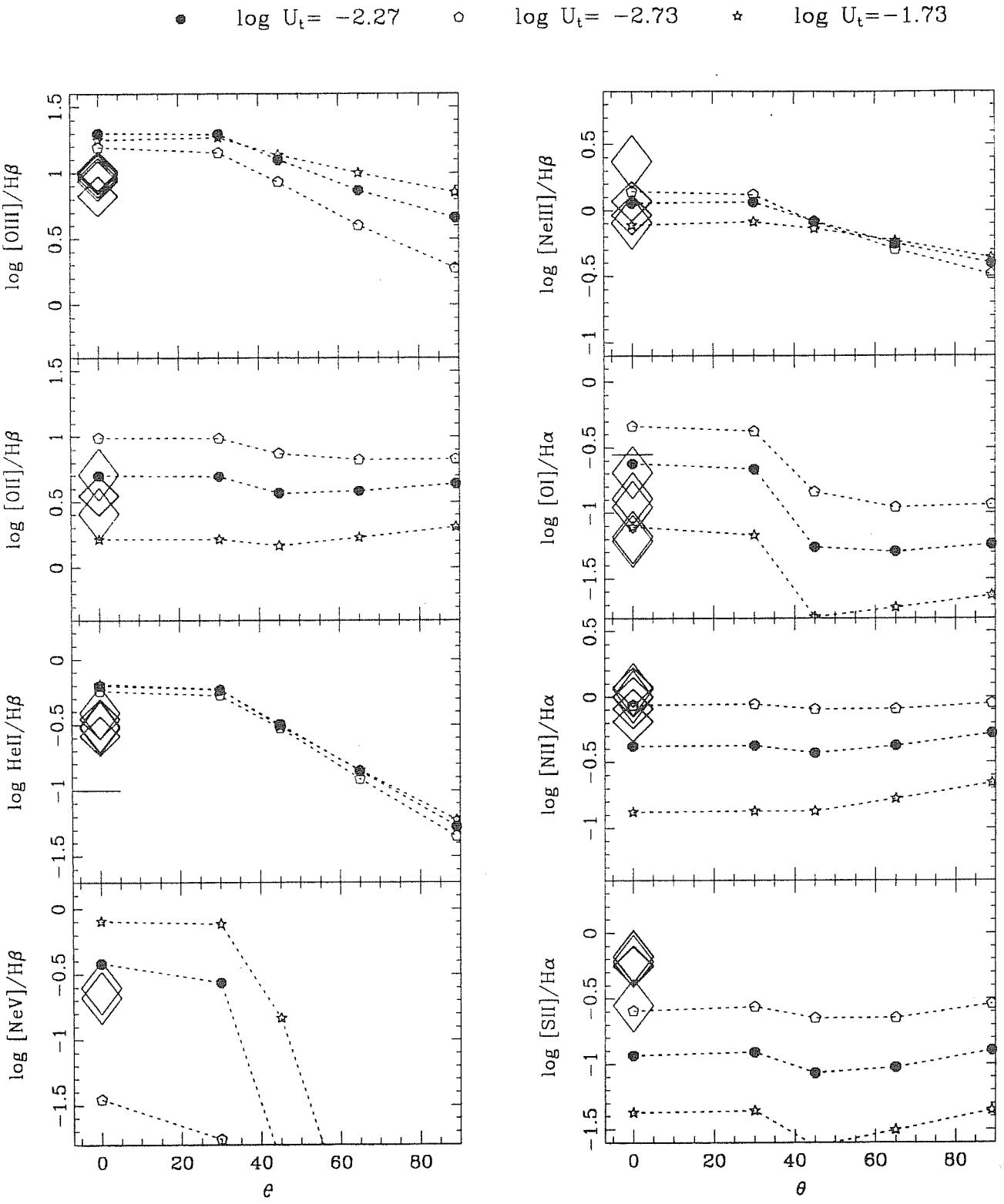
log U$_t$= −2.27
log U$_t$= −2.73
log U$_t$=−1.73
log [OIII]/Hβ
log [OII]/Hβ
log HeII/Hβ
log [NeV]/Hβ
log [NeIII]/Hβ
log [OI]/Hα
log [NII]/Hα
log [SII]/Hα
θ
θ

viewing angles close to the disk axis those line ratios will not change appreciably as we have shown above; at values of θ similar to the opening angle of the funnel they will start to increase because the X-ray component will dominate upon the anisotropic UV /soft X–ray component and Balmer–lines tend to decrease; at large values of θ those line ratio will remain at a constant value as corresponding to an isotropic ionizing source.

We have seen that the predicted angular variation for the emission lines (we refer only to those produced in the H^+ region) is more accentuated at larger M and r_{out}. We may speculate that if QSO's are powered by radiation pressure supported tori around black holes with $M = 10^8 M_\odot$, their emission line regions will be illuminated by a very collimated radiation field. In this respect we may notice that emission from the NLR is not normally observed in these objects, a possible explanation will be a NLR concentrated in two narrow cones and therefore the emitted luminosity is reduced with respect to a spherical configuration by an amount of $(1 - \cos\theta_{open})$. An obvious problem with this scenario is that the BLR will be equally affected by the collimation of the ionizing radiation, unless a different geometry is advocated for this region (Fabian *et al.* [1986], Betchold *et al.* [1987], see also Collin-Souffrin [1987]). In addition, observational evidences that low luminosity objects have a harder continuum than the high luminosity ones should be found in order that this scheme works.

6.6 CONCLUSIONS

We have considered the photoionization of the Extended Narrow Line Regions by the continuum emitted by an accreting radiation supported torus. In these regions highly ionized gas is concentrated in a cone whose axis coincides with the radio emission axis and the vertex points directly to the nucleus. The attractive feature of our model concerns the anisotropy of the radiation field. Geometrically thick disks possesses a characteristic funnel in the inner edge, where most of the radiation is emitted. This particular geometrical shape of the radiation source leads to a natural collimation of the radiation field which may be held responsible for the excitation of the ENLR gas and its spatial distribution.

We have calculated the angular variation of the emission line spectrum using the disk emission as the ionizing continuum. The angular variation of the emission line spectrum induced by the anisotropic continuum can be separated in two parts:

- The number of ionizing photons $N_i/4\pi$ which reaches the clouds is strongly decreased at large viewing angles. This will affect the general ionization level of the clouds and the total luminosity they will emit.

- The spectral shape of the ionizing continuum changes and softens at large separation angles from the rotation axis.

In addition, the disk emission depends on the value of the black hole mass M and the disk size r_{out}: an increase of M produces a shift of the whole emission towards low frequencies; the increase of the disk size broadens the range of frequency where most of the energy is emitted, at the same time the funnel steepenes and consequently the radiation is collimated in a narrower beam. The dependence of the emission on the disk parameters will affect in a different way the ionizing continuum at different θ. The decrease of $N_i/4\pi$ with θ is found to be more pronounced when M is high and when r_{out} is large. The changes in the spectral shape with θ has also a strong effect in the

emission line spectrum. The emission from a disk around a black hole with $M = 10^6 M_\odot$ is extended up to fairly large frequencies. This feature makes that several lines line ratios [OIII] λ5007/Hβ , [NeV] λ3426/Hβ and HeII λ4686/Hβ increases with θ which may be in apparent contradiction with the observations, particularly when the disk size is rather small ($r_{out} \sim 200 r_g$). However when the disk is large enough the emission in the low energy part of the continuum is increased. Hence the continuum softens and the excitation produced in the clouds is not so high, leading to a decrease with θ of the above mentioned line ratios. When $M = 10^8 M_\odot$ the change of the ionizing continuum with θ yields to a noticeable variation in the line ratios. In particular the ratio [OIII] λ5007/Hβ , [NeV] λ3426/Hβ and HeII λ4686/Hβ has a remarkable decrease for almost any value of r_{out}.

In order to investigate the actual variation of the line emission due to the anisotropy of the current ionizing source we have to assume a geometry for the emitting gas. We have assumed the gas distributed in a uniform disk with constant density and the rotation axis of the accretion torus contained in the disk plane. The luminosity and ratio of several lines is calculated at several inclinations angles, and a fixed distance from the nucleus to the clouds. The line luminosity does not show any variation at $\theta \leq \theta_{open}$ and it varies only at $\theta > \theta_{open}$. Then it becomes clear that in this particular model there is a direct association between the opening angle of the cone observed in the emission lines and that of the funnel, and hence on the outer radius of the disk, or equivalently on the accretion rate. The emission lines show different behaviour depending on the value of the disk parameters. We have found that a decrease in the luminosity of the line [OIII] λ 5007 by a factor $\gtrsim$ 10 is only obtained for a certain range of values of M and r_{out}.[6]

For $M = 10^6\ M_\odot$ only for rather large disk sizes this decrease will be achieved. Instead when $M = 10^8\ M_\odot$ even for $r_{out} \sim 50\ r_g$ this line decreases by a factor of 10 from $\theta = 0°$ to 90°. The line [NeV] λ3426 shows the strongest variation with θ and will be a good indicator of the edge of the cone. The line ratio HeII λ4686/Hβ and to some extent [NeIII] λ3869/Hβ depend weakly on U_t and therefore any change with θ will reflect mostly the change of the spectral shape of the ionizing continuum. The lines [OII] λ3727, [SII] $\lambda\lambda$ 6716, 6731 and [NII] λ 6583 show a larger decrease with $M = 10^6 M_\odot$ than when $M = 10^8 M_\odot$, because of the different fraction of the line luminosity which is produced in the partially ionized H region in the two cases. Instead the line [O I] λ 6300 is mainly produced in the partially ionized H region and hence it will decrease in both cases, in the absence of the X–ray part of the continuum.

We can conclude that the cones observed in the emission line [O III] λ 5007 could be explained in terms of photoionization by the anisotropic radiation field coming from an accreting radiation supported torus. However in the frame of our simple model not all the configurations are appropriate to reproduce the observed trends, namely those with low M ($10^6 M_\odot$) in combination with low r_{out} ($\sim$ 200 r_g). This trend to favour high black hole mass models is a serious problem for this model. The objects of our interest have rather low bolometric luminosity and black hole masses of the order $10^6 - 10^7\ M_\odot$ are expected. This fact together with the comparison of observed and predicted line ratios suggest that in order to make this model compatible with the observed excitation in the emission line cones the disk emission should be much less energetic than actually

[6] We are implicitly assuming that the emission of the line [OIII] λ 5007 is extended in the whole galaxy disk, except that when the surface brightness has decreased by a factor $\gtrsim$ 10 it is not seen by our detectors.

is.

We will conclude saying that in the light of the present results more work should be done in modelling the disk emission, if the disk emission is retained to be responsible for the anisotropy of the nuclear radiation field. On the other hand the actual angular dependence of the different emission lines should be firmly established observationally as well as measurements of the physical conditions in the clouds, *i.e.* density and temperature. Only then, modelling of the ionizing continuum could be done in a very detailed way.

We feel that it is very difficult to distinguish between the pattern of angular variation for the emission lines predicted by our model and the expected from the presence of a large molecular torus (Antonucci and Miller 1985; Krolik and Begelman 1986). Our models predict a "plateau" for most of the lines at viewing angles close to the cone axis, and then an abrupt decrease at large θ. This behaviour is similar to what expected in the case of a blocking structure, as the molecular torus. We further predict that the luminosity of the low ionization lines [OII] λ 3727, [SII] $\lambda\lambda$ 6716, 6731 and [NII] λ 6583 tends to remain constant or vary slightly with θ. The constancy of the line luminosity arises from the decrease of U_t with θ, therefore the ionization level is decreased and those lines are mainly produced in the outer part of the nebula. It has been found that the [NII] λ 6583 emission in NGC 1068 is rather diffuse and filamentary extending out to a $\sim$ 5 kpc radius (Bland, Sokolowski and Cecil, 1990). An explanation similar to ours is proposed by Bland, Sokolowski and Cecil (1990) in the frame of the molecular torus to explain this diffuse component. This model predicts the existence of a warm scattering medium which fills the torus hole and extends some way above its top. This medium allows us to observe the BLR light which comes from inside the obscuring structure. In the same way this medium will redirect nuclear photons outside the opening angle of the torus, and these regions will received a dilute nuclear radiation field. This makes that U_t is lowered which leads to a diffuse [NII] λ 6583 emission and to large values of the ratio [NII] λ6584/Hα .

Most of the contents of this chapter is taken from (Acosta-Pulido, Wilson and Perez-Fournon, 1991), in preparation.

FINAL CONCLUSIONS AND REMARKS

We have considered the photoionization of the Extended Narrow Line Regions in Seyfert galaxies by the continuum emitted by an accreting, radiation–supported torus. In these regions highly ionized gas is concentrated in a cone whose axis coincides with the radio emission axis and the vertex points directly to the nucleus. The attractive feature of our model concerns the anisotropy of the radiation field. Geometrically thick disks possess a characteristic funnel in the inner edge, where most of the radiation is emitted. This particular geometrical shape of the radiation source leads to a natural collimation of the radiation field which may be held responsible for the excitation of the ENLR gas and its spatial distribution.

The absolute luminosity emitted by an accretion disk is a linear function of the mass of the black hole. There is a way to estimate the absolute luminosity of the continuum which is ionizing the ENLR: counting the number of photons emitted in the Hydrogen recombination lines. If we compare the number of ionizing photons required to produce the observed luminosity in the ENLR (Table 1.1) with those present in the disk emission (Table 4.1), it is found that accretion disks around black holes with $M \gtrsim 10^6 M_\odot$ emit enough ionizing photons[1]. A number of ionizing photons larger than the derived from the line luminosity is allowed if the absorbing efficiency of the clouds is low (see Section 1.3).

In Chapter 5 we have studied the photoionization of the ENLR by the thick accretion disk emission,when the disk is seen pole-on. Initially we were mostly interested on the ability of the disk emission to reproduce the emission line spectrum observed in the ENLR. We have calculated the emission line spectrum for three black hole masses ($10^6, 10^7$ and 10^8 $M_\odot$), under the assumption that the clouds are located close to the rotation axis at a distance far from the nucleus. We varied the values of both the ionization parameter (which determines the ionization level of the nebula) and the disk size (which produces a variation in the continuum shape). An interesting feature of the ionizing spectra used is that by changing the accretion disk size and fixing the ionization parameter there are significant changes in the emission line spectrum, especially for the forbidden lines of O III and O II.

We have found that models with $M = 10^6 M_\odot$ fit the observations for very large accretion disk sizes ($\sim 500 r_g$), whereas models with $M = 10^7 M_\odot$ fit them better with smaller disks. The latter models would be preferable since they have less super–Eddington accretion rates than the former, in better agreement with the estimations for Seyfert 1 galaxies derived from other methods (Sect. 4.2.3). Models with $M = 10^8$ $M_\odot$

[1] Using a thin accretion disk model the number of ionizing photons present in the continuum is similar to the one in the thick disk emission for the same black hole mass.

do not predict different line ratios when r_{out} is varied.

There are discrepancies between our predicted lines ratios and the observed ones. The predicted ratios of the low ionization lines, *e. g.* [SII] $\lambda\lambda 6716, 6731/\mathrm{H}\alpha$, [NII] $\lambda 6584/\mathrm{H}\alpha$ are always smaller than the observed values. This suggests that the ionizing spectrum we used should be supplemented by an X-ray extension (Comptonization or a non-thermal component could increase the X-ray flux), although simply adding a power law at X-ray frequencies does not solve the problem, as we shown in Section 5.4.

The predicted HeII $\lambda 4686/\mathrm{H}\beta$ ratio is high compared with the observed values; this implies that the intensity of the continuum should be lower at energies larger than 4 *ryd.* Photoelectric absorption of the soft X-ray part of the spectrum due to the presence of gas between the nucleus and the emission line clouds could alleviate this problem. Moreover this may also account for the observed high [NeV] $\lambda 3426/\mathrm{H}\beta$ ratio, in contrast with the moderate HeII $\lambda 4686/\mathrm{H}\beta$ ratio and in some cases low [OIII] $\lambda 5007/\mathrm{H}\beta$ ratio, found in the ENLR of NGC 1068 (Bergeron, Petitjean and Durret, 1989; Evans and Dopita, 1986).

Summarizing, we found that models of the ENLR based on photoionization by accretion disk emissions can give some interesting constraints on the mass of the hole and on the size of the accretion disk. However, some of the line ratios deduced from the model are not in good agreement with observations and therefore the deduced values for the disk size and the ionization parameter are not very reliable.

We have calculated the angular variation of the emission line spectrum using the disk emission as an orientation depending ionizing continuum. The angular variation of the emission line spectrum induced by the anisotropic continuum can be separated in two parts:

- The number of ionizing photons $N_i/4\pi$ which reaches the clouds is strongly decreased at large viewing angles. This will affect the general ionization level of the clouds and the total luminosity they will emit.

- The spectral shape of the ionizing continuum changes and softens at large separation angles from the rotation axis.

In addition, the disk emission depends on the value of the black hole mass M and the disk size r_{out}: an increase of M produces a shift of the whole emission towards low frequencies; the increase of the disk size broadens the range of frequency where most of the energy is emitted, at the same time the funnel steepens and consequently the radiation is collimated in a narrower beam. The dependence of the emission on the disk parameters will affect in a different way the ionizing continuum at different θ. The decrease of $N_i/4\pi$ with θ is found to be more pronounced when M is high and when r_{out} is large. The changes in the spectral shape with θ has also a strong effect in the emission line spectrum. The emission from a disk around a black hole with $M = 10^6 M_\odot$ is extended up to fairly large frequencies. This feature makes that several lines line ratios [OIII] $\lambda 5007/\mathrm{H}\beta$, [NeV] $\lambda 3426/\mathrm{H}\beta$ and HeII $\lambda 4686/\mathrm{H}\beta$ increases with θ which may be in apparent contradiction with the observations, particularly when the disk size is rather small ($r_{out} \sim 200 r_g$). However when the disk is large enough the emission in the low energy part of the continuum is increased. Hence the continuum softens and the excitation produced in the clouds is not so high, leading to a decrease with θ of the above mentioned line ratios. When $M = 10^8 M_\odot$ the change of the ionizing continuum with θ yields to a noticeable variation in the line ratios. In particular the

ratio [OIII] λ5007/Hβ , [NeV] λ3426/Hβ and HeII λ4686/Hβ has a remarkable decrease with θ for almost any value of r_{out}.

In order to investigate the actual variation of the line emission due to the anisotropy of the current ionizing source we have to assume a geometry for the emitting gas. We have assumed the gas distributed in a uniform disk with constant density and the rotation axis of the accretion torus contained in the disk plane. The luminosity and ratio of several lines is calculated at several inclinations angles, and a fixed distance from the nucleus to the clouds. The line luminosity does not show any variation at $\theta \leq \theta_{open}$, like a plateau and it varies only at $\theta > \theta_{open}$. Then it becomes clear that in this particular model there is a direct association between the opening angle of the cone observed in the emission lines and that of the funnel, and hence on the outer radius of the disk, or equivalently on the accretion rate. The emission lines show different behaviour depending on the value of the disk parameters. We have found that a decrease in the luminosity of the line [OIII] λ 5007 by a factor $\gtrsim$ 10 is only obtained for a certain range of values of M and r_{out}.[5] When $M = 10^6\ M_\odot$ only for rather large disk sizes this decrease will be achieved. Instead when $M = 10^8\ M_\odot$ even for $r_{out} \sim 50\ r_g$ this line decreases by a factor of 10 from $\theta = 0°$ to 90°. The line [NeV] λ3426 shows the strongest variation with θ and will be a good indicator of the edge of the cone. The line ratio HeII λ4686/Hβ and to some extent [NeIII] λ3869/Hβ depend weakly on U_l and therefore any change with θ will reflect mostly the change of the spectral shape of the ionizing continuum. The lines [OII] λ3727, [SII] $\lambda\lambda$ 6716, 6731 and [NII] λ 6583 show a larger decrease with $M = 10^6\ M_\odot$ than when $M = 10^8\ M_\odot$, because of the different fraction of the line luminosity which is produced in the partially ionized H region in the two cases. Instead the line [O I] λ 6300 is mainly produced in the partially ionized H region and hence it will decrease in both cases, due to the absence of the X–ray part of the continuum.

We can conclude that the cones observed in the emission line [O III] λ 5007 could be explained in terms of photoionization by the anisotropic radiation field coming from an accreting radiation supported torus. However in the frame of our simple model not all the configurations are appropriate to reproduce the observed trends, namely those with low M ($10^6\ M_\odot$) in combination with low r_{out} ($\sim 200\ r_g$). This trend to favour high black hole mass models is a serious problem for this model. The objects of our interest have rather low bolometric luminosity and black hole masses of the order $10^6 - 10^7\ M_\odot$ are expected. This fact together with the comparison of observed and predicted line ratios suggest that in order to make this model compatible with the observed excitation in the emission line cones the disk emission should be much less energetic than actually is.

We will conclude saying that in the light of the present results more work should be done in modelling the disk emission, if the disk emission is retained to be responsible for the anisotropy of the nuclear radiation field. On the other hand the actual angular dependence of the different emission lines should be firmly established observationally as well as measurements of the physical conditions in the clouds, *i.e.* density and temperature. Only then, modelling of the ionizing continuum could be done in a very detailed way.

Thick accretion disks can not explain the obscuration of the BLR, which is observed

[5] We are implicitly assuming that the emission of the line [OIII] λ 5007 is extended in the whole galaxy disk, except that when the surface brightness has decreased by a factor $\gtrsim$ 10 it is confused with the galaxy light continuum.

in several objects (Antonucci and Miller 1985; Goodrich and Miller 1990). The thick accretion disks are located much closer to the nucleus than BLR is. The presence of a large obscuring torus (1 *pc*) is probably needed in those cases, however a close relationship between the obscuring torus and the inner accretion disk may exist.

We feel that it is very difficult to distinguish between the pattern of angular variation for the emission lines predicted by our model and the expected from the presence of a large molecular torus (Antonucci and Miller 1985; Krolik and Begelman 1986). Our models predict a "plateau" for most of the lines at viewing angles close to the cone axis, and then an abrupt decrease at large θ. This behaviour is similar to what is expected in the case of a blocking structure, as the molecular torus. We further predict that the luminosity of the low ionization lines [OII] λ 3727, [SII] $\lambda\lambda$ 6716, 6731 and [NII] λ 6583 tends to remain constant or vary slightly with θ. The constancy of the line luminosity arises from the decrease of U_t with θ, therefore the ionization level is decreased and those lines are mainly produced in the outer part of the nebula. It has been found that the [NII] λ 6583 emission in NGC 1068 is rather diffuse and filamentary extending out to a $\sim$ 5 kpc radius (Bland, Sokolowski and Cecil, 1990). An explanation similar to ours is proposed by Bland, Sokolowski and Cecil (1990) in the frame of the molecular torus. This model predicts the existence of a warm scattering medium which fills the torus hole and extends some way above its top. The scattering medium will redirect nuclear photons outside the opening angle of the torus, and these regions will received a dilute nuclear radiation field. This makes that U_t is lowered which leads to a diffuse [NII] λ 6583 emission and to large values of the ratio [NII] λ6584/Hα .

In spite of the difficulties, we do believe that this kind of investigation is worthwhile mainly because it allows us to obtain more information on the central engine of AGN's from their extranuclear activity. Our understanding of the ENLRs and NLRs may be improved in the future using better quality spectroscopic data, in particular high spatial resolution observations of the ionized gas and including the UV band with the Hubble Space Telescope will be crucial. The importance of determining the ionizing spectrum of ENLR arises from the privileged location of these regions. The continuum illuminating the ENLR clouds may be only partially absorbed by interstellar matter in the path from the nucleus. It should be remind that the range of frequencies of the continuum intervening in the photoionization of ENLR is not directly accessible from the Earth because of the photoelectric absorption in Our Galaxy. There is a strong dependence of the ionization level of the clouds and the continuum reaching them. Thus we will have the possibility to extract information about the energy distribution of the nuclear continuum from the emission line spectrum. A loose association between the band of energy which is absorbed and the energy emitted in the line can be found by studying the response of the emission line intensities to variations of the ionizing continuum shape. Therefore one will be able to reconstruct the shape of the ionizing continuum from the emission line spectrum. This has been attempted for Broad Line Regions (Krolik and Kallman 1988), although the results are undetermined. ENLRs are probably the most suitable laboratory to make this experiment because of their low density.

REFERENCES

Abramowicz M.A. 1985. *Pub. Astr. Soc. Japan*, **37**, 727.

Abramowicz M.A., Calvani M., and Madau P. 1987. *Comments on Astrophysics*, **122**, 67.

Abramowicz M.A., Calvani M., and Nobili L. 1980. *Ap. J.*, **242**, 772.

Abramowicz M.A., Czerny B., Lasota J.P., and Szuszkiewicz E. 1988. *Ap. J.*, **332**, 646.

Abramowicz M.A., Henderson P.F., and Ghosh P. 1983. *M.N.R.A.S.*, **203**, 323.

Abramowicz M.A., Jaroszyński, and Sikora M. 1978. *Astr. Ap.*, **63**, 221.

Acosta-Pulido J.A., Pérez-Fournon I., Calvani M., and Wilson A.S. 1990. *Ap. J.*, **365**. (Paper I).

Acosta-Pulido J.A., Wilson A.S., and Perez-Fournon I. 1991. (In preparation).

Adams T.F. 1977. *Ap J. Suppl.*, **33**, 19.

Aldrovandi S.M.V. 1981. *Astr. Ap.*, **97**, 122.

Antonucci R.R.J. 1983. *Nature*, **303**, 158.

Antonucci R.R.J. 1988. in *Supermassive Black Holes*, ed. M. Kafatos (Cambridge: Cambridge University Press), p. 26.

Antonucci R.R.J. and Miller J.S. 1985. *Ap. J.*, **297**, 621.

Appenzeller I. and Wagner S. 1990. *El Mensajero*, **60**, 40.

Ayani K. and Iye M. 1989. *A. J.*, **97**, 686.

Baldwin J.A., Phillips M.M., and Terlevich R. 1981. *Pub. A. S. P.*, **93**, 5.

Baldwin J.A., Wilson A.S., and Whittle M. 1987. *Ap. J.*, **319**, 84. (BWW).

Balick B. and Heckman T.M. 1985. *A. J.*, **90**, 197.

Baum S.A. and Heckman T. 1988a. *Ap. J.*, **336**, 681.

Baum S.A. and Heckman T. 1988b. *Ap. J.*, **336**, 702.

Baum S.A., Heckman T., Bridle A., van Breugel W., and Miley G. 1988. *Ap J. Suppl.*, **68**, 643.

Bechtold J., Czerny B., Elvis M., Fabbiano G., and Green R.F. 1987. *Ap. J.*, **314**, 699.

Begelman M.C. 1985. in *Astrophysics of Active Galaxies and QSOs*, ed. J.S. Miller (Mill Valley, CA: University Science Books), p. 411.

Begelman M.C. 1989. in *IAU Symposium 134, Active Galactic Nuclei*, ed. D.E. Osterbrock and J.S. Miller (Dordrecht: Kluwer Academic), p. 141.

Begelman M.C. and Meier D.L 1982. *Ap. J.*, **253**, 873.

Bergeron J., Petitjean P., and Durret F. 1989. *Astr. Ap.*, **213**, 61.

Binette L., Courvoisier T-L, and Robinson A. 1988. *Astr. Ap.*, **190**, 29.

Binette L., Dopita M.A., and Tuohy I.R. 1985. *Ap. J.*, **297**, 476.

Binette L., Prieto A., Szuskiewicz E., and Zheng W. 1989. *Ap. J.*, **343**, 135.

Binette L. and Raga A. 1990. *A. J.* (In press).

Binette L., Robinson A., and Courvoisier T-L 1988. *Astr. Ap.*, **194**, 65. (BRC).

Blaes O.M. 1987. *M.N.R.A.S.*, **227**, 975.

Bland J., Sokolowski J.K., and Cecil G.N. 1990. Preprint.

Blandford R.D. 1985a. in *Numerical Astrophysics*, ed. J. Centrella, J. LeBlanc, and R.L. Bowers (Boston: Jones and Bartlett), p. 6.

Blandford R.D. 1985b. in *Active Galactic Nuclei*, ed. J.E. Dyson (Manchester: University Press), p. 281.

Bruhweiler F.C. and Smith A.M. 1988. *Ap. J.*, **327**, 664.

Cecil G. 1989. in *Extranuclear Activity in Galaxies*, ed. E. Meurs and R. Fosbury, volume 32 (Munich: ESO Conference and Workshop Proceedings), p. 363.

Cecil G., Bland J., and Tully R.B. 1990. *Ap. J.*, **355**, 70.

Clavel J. et al. 1990. *Ap. J.* Preprint.

Clavel J. and Santos-Lléo M. 1990. *Astr. Ap.*, **230**, 3.

Cohen R.D. and Osterbrock D.E. 1981. *Ap. J.*, **243**, 81.

Coleman H.H. and Shields G.A. 1990. *Ap. J.* (In press).

Colina L., Fricke K.J., Kollatschny W., and Perryman M.A.C. 1987. *Astr. Ap.*, **186**, 39.

Collin-Souffrin S. 1987. *Astr. Ap.*, **179**, 60.

Corbin M.R., Baldwin J.A., and Wilson A.S. 1988. *Ap. J.*, **334**, 584.

Czerny B. and Elvis M. 1987. *Ap. J.*, **321**, 305.

Danziger I.J., Fosbury R.A.E., Goss W.M., Bland J., and Boksenberg A. 1984. *M.N.R.A.S.*, **208**, 589.

de Bruyn A.G. and Wilson A.S. 1978. *Astr. Ap.*, **64**, 433.

DeRobertis M.M. and Osterbrock D.E. 1984. *Ap. J.*, **286**, 171.

di Serego Alighieri S., Binette L., Courvoisier T.J.-L., Fosbury R.A.E., and Tadhunter C.N. 1988. *Nature*, **334**, 591.

Durret F. 1990. *Astr. Ap.*, **229**, 351.

Durret F. and Bergeron J. 1986. *Astr. Ap.*, **156**, 51.

Elvis M. 1989. *Comments on Astrophysics*, **143**, 177.

Elvis M., Briel U.G., and Henry J.P. 1983. *Ap. J.*, **268**, 105.

Elvis M., Fassnacht C., Wilson A.S., and Briel U. 1990. Preprint.

Elvis M. and Lawrence A. 1988. *Ap. J.*, **331**, 161.

Elvis M., Wilkes B.J., and Tananbaum H. 1985. *Ap. J.*, **292**, 357.

Evans I.N. and Dopita M.A. 1986. *Ap. J. (Letters)*, **310**, L15.

Fabian A.C., Guilbert P.W., Arnaud K.A., Shafer R.A., Tennant A.F., and Ward M.J. 1986. *M.N.R.A.S.*, **218**, 457.

Fabian A.C., Nulsen P.E.J., and Canizares C.R. 1984. *Nature*, **310**, 733.

Fabian A.C., Rees M.J., Stella L., and White N.E. 1989. *M.N.R.A.S.*, **238**, 729.

Ferland G.J. and Mushotzky R.F. 1982. *Ap. J.*, **262**, 564.

Ferland G.J. and Netzer H. 1983. *Ap. J.*, **264**, 105.

Ferland G.J. and Osterbrock D.E. 1986. *Ap. J.*, **300**, 658.

Filippenko A.V. 1986. in *IAU Symposium 119, Quasars*, ed. G. Swarup and V.K. Kapahi (Dordrecht: Reidel), p. 289.

Forman W., Jones C., and Tucker W. 1985. *Ap. J.*, **293**, 102.

Fosbury R.A.E. 1986. in *Structure and Evolution of AGN*, ed. G. Giuricin, F. Mardirossian, M. Mezzetti, and M. Ramella (Dordrecht: Reidel), p. 297.

Fosbury R.A.E. 1989. in *Extranuclear Activity in Galaxies*, ed. E.J.A. Meurs and R.A.E. Fosbury, volume 32 (Munich: ESO Conference and Workshop Proceedings), p. 169.

Fosbury R.A.E., Boksenberg A., Snijders M.A.J., Danziger I.J., Disney M.J., Goos W.M., Penston M.V., Wamsteker W., Wellington K.J., and Wilson A.S. 1982. *M.N.R.A.S.*, **201**, 991.

Fosbury R.A.E., Tadhunter C.N., Bland J., and Danziger I.J. 1984. *M.N.R.A.S.*, **208**, 955.

Frank J., King A.R., and Raine D.J. 1985. *Accretion Power in Astrophysics* (Cambridge: Cambridge University Press.

Ghisellini G., Maraschi L., and Treves A. 1985. *Astr. Ap.*, **146**, 204.

Goldreich P. and Tremaine S. 1978. *Icarus*, **34**, 227.

Halpern J.P. 1990. *Nature*, **344**, 713.

Halpern J.P. and Steiner J. 1983. *Ap. J. (Letters)*, **269**, L37.

Haniff C.A., Wilson A.S., and Ward M.J. 1988. *Ap. J.*, **334**, 104.

Hansen L. 1989. in *Extranuclear Activity in Galaxies*, ed. E.J.A. Meurs and R.A.E. Fosbury, volume 32 (Munich: ESO Conference and Workshop Proceedings), p. 363.

Hanson C.G., Skinner G.K., Eyles C.J., and Willmore A.P. 1990. *M.N.R.A.S.*, **242**, 262.

Heckman T.M. and Balick B. 1983. *Ap. J.*, **268**, 102.

Heckman T.M., Miley G.K., van Breugel W.J.M., and Butcher H.R. 1981. *Ap. J.*, **247**, 403.

Jaroszynski M., Abramowicz M.A., and Paczynski B. 1980. *Acta Astr.*, **30**, 1.

Joly M., Collin-Souffrin S., Masnou J.L., and Nottale L. 1985. *Astr. Ap.*, **152**, 282.

Kaastra J.S. and Barr P. 1989. *Astr. Ap.*, **226**, 59.

Kallman T. and White N.E. 1989. *Ap. J.*, **341**, 955.

Kallman T.R. and Krolik J.H. 1986. *Ap. J.*, **308**, 805.

Kartje J.F. and Königl A. 1990. *Preprint.*

Kolykhalov P.I. and Sunyaev R.A. 1984. *Adv. Space Res.*, **3**, 249.

Königl A. 1981. *Ap. J.*, **243**, 700.

Koyama K., Inoue H., Tanaka Y., Awaki H., Takano S., Ohashi T., and Matsuoka M. 1989. *Pub. Ast. Soc. Japan*, **41**, 731.

Kozlowski M., Jaroszyński M., and Abramowicz M.A. 1978. *Astr. Ap.*, **63**, 209.

Krolik J.H. 1988. in *The Physics of Neutron Stars and Black Holes*, ed. Y. Tanaka (Tokyo: Universal Academy Press), p. 317.

Krolik J.H. 1989a. in *The Interstellar Medium in External Galaxies*, ed. H.A. Thronson and J.M. Shull.

Krolik J.H. 1989b. in *23rd ESLAB Symposium: Two topics in X-ray Astronomy*, ed. J. Hunt and B. Battrick, volume 2 (Paris: ESA), p. 777.

Krolik J.H. and Begelman M.C. 1986. *Ap. J. (Letters)*, **308**, L55.

Krolik J.H. and Begelman M.C. 1988. *Ap. J.*, **329**, 702.

Krolik J.H. and Kallman T.R. 1988. *Ap. J.*, **324**, 714.

Krolik J.H. and Lepp S. 1989. *Ap. J.*, **347**, 179.

Krolik J.H., MacKee C.F., and Tarter C.B. 1981. *Ap. J.*, **249**, 422.

Krolik J.H. and Vrtilek J.M. 1984. *Ap. J.*, **279**, 521.

Kunieda H., Turner T.J., Awaki H., Koyama K., Mushtotzky R., and Tsusaka Y. 1990. *Nature*, **345**, 786.

Lawrence A. 1987. *Pub. A. S. P.*, **99**, 309.

Lawrence A. and Elvis M. 1982. *Ap. J.*, **256**, 410.

Lawrence A., Walker D., Rowan-Robinson M., Leech K.J., and Penston M.V. 1986. *M.N.R.A.S.*, **219**, 687.

MacAlpine G.M. 1972. *Ap. J.*, **175**, 11.

Macchetto F., Colina L., Golombek D., Perryman M.A.C., and di Serego Alighieri S. 1990. *Ap. J.*, **356**, 389.

Madau P. 1987. PhD thesis, SISSA, Trieste.

Madau P. 1988. *Ap. J.*, **327**, 116.

Malkan M.A. 1983. *Ap. J.*, **582**, 268.

Malkan M.A. and Sargent W.L.W. 1982. *Ap. J.*, **22**, 254.

Maraschi L. and Molendi S. 1990. *Ap. J.*, **353**, 452.

Marshall H., Avni Y., Braccesi A., Huchra J.P., Tanambaum H., Zamorani G., and Zitelli V 1984. *Ap. J.*, **283**, 50.

Mathews W.G. and Capriotti E.R 1985. in *Astrophysics of Active Galaxies and QSO*, ed. J.S. Miller (Mill Valley, CA: University Science Books), p. 185.

Mathews W.G. and Ferland G.J. 1987. *Ap. J.*, **323**, 456.

McHardy I.M. 1989. in *23rd ESLAB Symposium: Two topics in X-ray Astronomy*, ed. J. Hunt and B. Battrick, volume 2 (Paris: ESA), p. 1111.

Meaburn J., Morgan B., Vine H., Pedlar A., and Spencer R. 1982. *Nature*, **296**, 331.

Meaburn J., Whitehead M.J., and Pedlar A. 1989. *M.N.R.A.S.*, **241**, 1p.

Mendoza C. 1983. in *IAU Symposium 103, Planetary Nebulae*, ed. D.R. Flower (Reidel: Dordrecht), p. 143.

Meurs E.A.J. and Wilson A.S. 1984. *Astr. Ap.*, **136**, 206.

Meurs E.J.A. 1989. in *Extranuclear Activity in Galaxies*, ed. E. Meurs and R. Fosbury, volume 32 (Munich: ESO Conference and Workshop Proceedings), p. 405.

Miller J.S. 1989. in *IAU Symposium 134, Active Galactic Nuclei*, ed. D.E. Osterbrock and J.S. Miller (Dordrecht: Kluwer Academic), p. 273.

Miller J.S. and Goodrich R.W. 1990. *Ap. J.*, **355**, 456.

Netzer H. 1987. *M.N.R.A.S.*, **225**, 55.

Netzer H. 1989. *Comments on Astrophys.*, **143**, 137.

Netzer H., Maoz D., Laor A., Mendelson H., Brosch N., Leibowitz E., Almoznino E., Beck S., and Mazeh T. 1990. *Ap. J.*, **353**, 108.

Osterbrock D.E. 1974. *Astrophysics of gaseous nebulae* (San Francisco: Freeman and Company.

Osterbrock D.E. 1984. *Quart. J.R.A.S.*, **25**, 1.

Osterbrock D.E. and Shaw R.A. 1988. *Ap. J.*, **327**, 89.

Paczyński B. 1980. *Acta Astron.*, **30**, 347.

Paczyński B. and Abramowicz M.A. 1982. *Ap. J.*, **253**, 897.

Paczynski B. and Wiita P.J. 1980. *Astr. Ap.*, **88**, 23.

Padovani P. and Rafanelli P. 1988. *Astr. Ap.*, **205**, 53.

Papaloizou J.C.B. and Pringle J.E. 1984. *M.N.R.A.S.*, **208**, 721.

Pedlar A., Meaburn J., Axon D.J., Unger S.W., Whittle M., Meurs E.J.A., Guerrine N., and Ward M.J. 1989. *M.N.R.A.S.*, **238**, 863.

Penston M.V. et al. 1990. *Astr. Ap.*, **236**, 53.

Péquignot D. 1986. in *Workshop in Model Nebulae*, ed. D. Péquignot (Paris), p. 363.

Pérez E., González-Delgado R., Tadhunter C., and Tsvetanov Z. 1989. *M.N.R.A.S.*, **241**, 31p.

Pérez-Fournon I. and Wilson A.S. 1990. *Ap. J.*, **356**, 462.

Phillips M. and Malin D.F. 1982. *M.N.R.A.S.*, **199**, 905.

Pogge R.W. 1988a. *Ap. J.*, **328**, 519.

Pogge R.W. 1988b. *Ap. J.*, **332**, 702.

Pogge R.W. 1989a. *A. J.*, **98**, 124.

Pogge R.W. 1989b. *Ap. J.*, **345**, 730.

Pounds K.A. 1989. in *23rd ESLAB Symposium: Two topics in X–ray Astronomy*, ed. J. Hunt and B. Battrick, volume 2 (Paris: ESA), p. 753.

Pounds K.A., Stanger V.J., Turner T.J., King A.R., and Czerny B. 1986. *M.N.R.A.S.*, **224**, 443.

Prieto A., di Serego-Alighieri S., and Fosbury R.A.E. 1989. in *Extranuclear Activity in Galaxies*, ed. E.J.A. Meurs and R.A.E. Fosbury, volume 32 (Munich: ESO Conference and Workshop Proceedings), p. 31.

Pringle J. 1981. *Ann. Rev. Astr. and Ap.*, **19**, 137.

Robinson A. 1989. in *Extranuclear Activity in Galaxies*, ed. E. J. A. Meurs and R. A. E. Fosbury, volume 32 (Munich: ESO Conference and Workshop Proceedings), p. 259.

Robinson A., Binette L., Fosbury R.A.E., and Tadhunter C.N. 1987. *M.N.R.A.S.*, **97**, 227.

Rybicki G.B. and Lightman A.P. 1979. *Radiative Processes in Astrophysics* (New York: Wiley.

Sandage A. and Tamman G.R. 1984. *Nature*, **307**, 326.

Sandage A. and Tammann 1981. Washington, DC: Carnegie Institution of Washington.

Schommer R.A., Caldwell N., Wilson A.S., Baldwin J.A., Phillips M.M., Williams T.B., and Turtle A.J. 1988. *Ap. J.*, **324**, 154.

Schulz H. 1988. *Astr. Ap.*, **203**, 233.

Scoville N.Z., Young J., and Lucy L.B. 1983. *Ap. J.*, **270**, 443.

Seguin F.M. 1975. *Ap. J.*, **197**, 745.

Shakura N.I. and Sunyaev R.A. 1973. *Astr. Ap.*, **24**, 337.

Shields G.A. 1978. *Nature*, **272**, 70.

Shields J.C. and Filippenko A.V. 1988. *Ap. J. (Letters)*, **332**, L55.

Sikora M. 1981. *M.N.R.A.S.*, **196**, 257.

Singh K.P., Garmire G.P., and Nousek J. 1985. *Ap. J.*, **297**, 633.

Stasińska G. 1984. *Astr. Ap.*, **135**, 341.

Stella L. 1990. *Nature*, **344**, 747.

Stockman H.S., Moore R.L., and Angel J.R.P. 1984. *Ap. J.*, **279**, 289.

Stockton A. and MacKenty J.W. 1987. *Ap. J.*, **316**, 584.

Stone J.L.Jr., Wilson A.S., and Ward M.J. 1988. *Ap. J.*, **330**, 105.

Su H.J. and Simkin S.M. 1980. *Ap. J. (Letters)*, **238**, L1.

Sun W-H. and Malkan M.A. 1989. *Ap. J.*, **346**, 68.

Svensson R. 1986. Radiation hydrodynamics in stars and compact objects. in *IAU Colloquium 89*, ed. D. Mihalas and K-H. Winkler, p. 325. Springer–Verlag, NY.

Tadhunter C.N., Fosbury R.A.E., and Quinn P.J. 1989. *M.N.R.A.S.*, **240**, 225.

Tadhunter C.N., Robinson A., and Morganti R. 1989. in *Extranuclear Activity in Galaxies*, ed. E. Meurs and R. Fosbury, volume 32 (Munich: ESO Conference and Workshop Proceedings), p. 293.

Tadhunter C.V. 1987. PhD thesis, University of Sussex, England.

Tadhunter C.V., di Serego Alighieri S., Bland J., Danziger I.J., Goss W.M., McAdam W.B., and Snijders M.A. 1988. *M.N.R.A.S.*, **235**, 403.

Tadhunter C.V., Fosbury R.A., and di Serego Alighieri S. 1988. in *BL Lac Objects*, ed. L. Maraschi, T. Maccacaro, and M.-H. Ulrich, volume 334 of *Lectures Notes in Physics*, p. 79. Springer Verlag, Berlin.

Tadhunter C.V. and Tsvetanov Z. 1989. *Nature*, **341**, 422.

Tarter C.B. and Salpeter E.E. 1969. *Ap. J.*, **156**, 953.

Tarter C.B., Tucker W.H., and Salpeter E.E. 1969. *Ap. J.*, **156**, 943.

Tohline J.E. and Osterbrock D.E. 1982. *Ap. J. (Letters)*, **252**, L49.

Treves A., Maraschi L., and Abramowicz M.A. 1988. *Pub. A. S. P.*, **100**, 427.

Tsvetanov Z. 1989. in *Extranuclear Activity in Galaxies*, ed. E.J.A. Meurs and R.A.E. Fosbury, volume 32 (Munich: ESO Conference and Workshop Proceedings), p. 251.

Ulrich M-H and Péquignot D. 1980. *Ap. J.*, **238**, 45. (UP).

Ulvestad J.S. and Wilson A.S. 1984. *Ap. J.*, **278**, 544.

Ulvestad J.S. and Wilson A.S. 1989. *Ap. J.*, **343**, 659.

Unger S.W., Pedlar A., Axon D.J., Whittle M., Meurs E.J.A., and Ward M.J. 1987. *M.N.R.A.S.*, **228**, 671.

Veilleux S. and Osterbrock D.E. 1987. *Ap J. Suppl.*, **68**, 643.

Viegas-Aldrovandi S.M. 1988. *Ap. J. (Letters)*, **330**, L9.

Viegas-Aldrovandi S.M. and Contini M. 1989. *Ap. J.*, **339**, 689.

Viegas-Aldrovandi S.M. and Gruenwald R.B. 1988. *Ap. J.*, **324**, 683.

Voit G.M., Shull J.M., and Begelman M.C. 1987. *Ap. J.*, **316**, 573.

Walker M.F. 1968. *Ap. J.*, **151**, 71.

Wandel A. and Petrosian V. 1988. *Ap. J. (Letters)*, **329**, L11.

Wandel A. and Yahil A. 1985. *Ap. J. (Letters)*, **295**, L1.

Warwick R.S., Koyama K., Inoue H., Takano S., Awaki H., and Hoshi R. 1989. *Pub. Ast. Soc. Japan*, **41**, 739.

Wasilewski A.J. 1983. *Ap. J.*, **272**, 68.

Webb W. and Malkan M.A. 1986. in *The physics of Accretion onto Compact Objects*, ed. K.O. Mason, M.G. Watson, and N.E. White (Berlin: Springer-Verlag), p. 15.

Whittle M. 1985. *M.N.R.A.S.*, **213**, 33.

Whittle M., Haniff C.A., Ward M.J., Meurs E.J.A., Pedlar A., Unger S.W., Axon D.J., and Harrison B.A. 1986. *M.N.R.A.S.*, **222**, 189.

Whittle M., Pedlar A., Meurs E.J.A., Unger S.W., Axon D.J., and Ward M.J. 1988. *Ap. J.*, **326**, 125.

Wiita P.J. 1982. *Ap. J.*, **256**, 666.

Wills B.J., Netzer H., and Wills D. 1985. *Ap. J.*, **288**, 94.

Wilson A.S. and Heckman T.M. 1985. in *Astrophysics of Active Galaxies and QSO*, ed. J.S. Miller (Mill Valley, CA: University Science Books), p. 39.

Wilson A.S. and Ulvestad J.S. 1987. *Ap. J.*, **319**, 105.

Wilson A.S., Ward M., and Haniff C.A. 1988. *Ap. J.*, **334**, 121.

Wilson A.S. and Willis A. 1980. *Ap. J.*, **240**, 420.

Wilson A.S., Wu X., Heckman T.M., Baldwin J.A., and Balick B. 1989. *Ap. J.*, **339**, 729.

Wrobel J. and Heeschen D.S. 1988. *Ap. J.*, **335**, 677.

Zamorani G., Henry J.P., Maccacaro T., Tanambaum H., Soltan A., Avni Y., Liebert J., Stocke J., Strittmatter P.A., Weymann R.J., Smith M.G., and Condon J.J. 1981. *Ap. J.*, **245**, 357.